

Isocyanide Complexes of Technetium and Rhenium:  
Steric and Electronic Factors

Inaugural-Dissertation

to obtain the academic degree

Doctor rerum naturalium (Dr. rer. nat.)

submitted to the Department of Biology, Chemistry, Pharmacy  
of Freie Universität Berlin

by

Guilhem Claude

2023



The work for the present dissertation has been conducted between June 2019 and January 2023 under the guidance of Prof. Dr. Ulrich Abram at the Institute of Chemistry and Biochemistry (Department of Biology, Chemistry, Pharmacy) of the Freie Universität Berlin and Prof. Dr. Joshua Figueroa at the Department of Chemistry and Biochemistry, University of California, San Diego.

I hereby declare that the dissertation submitted is my own work. All direct or indirect sources used are acknowledged as references.

Intellectual property of other authors has been marked accordingly. I also declare that I have not applied for an examination procedure at any other institution and that I have not submitted the dissertation in this or any other form to any other faculty as a dissertation.

1<sup>st</sup> reviewer: Prof. Dr. Ulrich Abram

2<sup>nd</sup> reviewer: Prof. Dr. Christian Müller

Date of defense: 28/08/2023



## Acknowledgment

This doctoral thesis has been a tremendous personal and intellectual adventure and I want to express my sincere gratitude to my supervisor Prof. Dr. Ulrich Abram for allowing this project to happen. Throughout the years - most of which excessively straining due to the circumstances we all lived in - he provided an infallible support both scientifically as well as humanely. His advice on how to structure our reasoning while remaining open for out-of-the-box ideas were key for the success of this project and will keep guiding me in my further endeavors. Thank you!

Both during my stay in his San Diegan lab in 2019 and our numerous Zoom calls, Prof. Dr. Joshua Figueroa provided a reliable outside perspective on my chemistry. His enthusiasm for new reactions and chemistry in general was very contagious. I would like to extend my gratitude to Dr. Michael Neville and other members of the Figueroa lab for our regular personal and scientific exchanges and their help during my stay in San Diego.

Prof. Dr. Winfried Brenner as well as Dr. Sarah Spreckelmeyer also provided a regular and valuable external perspective on my thesis and were keen for me to share my work at conferences. They helped guide the chemistry towards future potential clinical applications.

Dr. Adelheid Hagenbach has been of a great help with crystallography and shared her extensive experience and knowledge of radioprotection through the years.

Both the infallible technical support and the great care and warmth as well as the shared interest for arts of Jacqueline Grewe will be fondly remembered.

Students who worked with me during those years also played a valuable role and I would like to thank Jonas Genz, Dominik Weh, Denis Puccio, Erika Kulitzki, Laura Zeh as well as Anna-Maria Tsirigoni for their efforts. They all brought enthusiasm and a willingness to learn and work to the table and helped translate my ideas into this work.

I want to thank Dr. Friedrich Wossidlo, Dr. Simon Steinhauer as well as Dr. Julia Bader for sharing their extensive NMR knowledge and taking care of our spectrometers and I would also like to acknowledge the work of the core facility BioSupraMol.

This work was financed by the graduate school BioQic and the DFG as well as the DAAD.



I would like to deeply thank my friends and family, especially my parents. Those lines are for me a unique opportunity to show them my gratitude and my admiration for their patience and steadiness. At this point, I would like to mention Dr. Maximilian Roca-Jungfer who incited me to pursue my own ideas and contributed greatly to this work. We shared a hood and became friends. Most chemists reading those lines will know the improbability of it to happen.

Several very dear persons had wished to see the end of this work and believed in me all along. Their hope and support were essential in those formative years. They are deeply missed and will not be forgotten.





# Table of Content

1.	Introduction.....	11
1.1.	Technetium and Rhenium as Elements.....	11
1.2.	The Chemistry of Technetium and Rhenium.....	12
1.3.	Radioactive Metals in Nuclear Medicine.....	13
1.3.1.	General Overview.....	13
1.3.2.	Technetium and Rhenium in Nuclear Medicine.....	15
1.4.	Isocyanides.....	18
1.4.1.	Ligand Properties and Synthesis.....	18
1.4.2.	m, m'-Terphenylic Isocyanides.....	20
1.4.3.	Isocyanide Chemistry in this Work.....	22
2.	Summary.....	27
3.	Zusammenfassung.....	29
4.	References.....	31
5.	Publications.....	37
5.1.	Rhenium Complexes with p-Fluorophenylisocyanide.....	37
5.2.	Mixed-Isocyanide Complexes of Technetium under Steric and Electronic Control.....	61
5.3.	Phenylimido Complexes of Rhenium: Fluorine Substituents Provide Protection, Reactivity and Solubility.....	103
5.4.	The Chemistry of Phenylimidotechnetium(V) Complexes with Isocyanides: Steric and Electronic Factors.....	163
5.5.	Technetium Complexes with an Isocyano-Alkyne Ligand and its Reaction Products.....	209
6.	List of all Publications.....	245
6.1.	Full Papers and Communications.....	245
6.2.	Contribution to Conferences.....	245



# 1. Introduction

## 1.1. Technetium and Rhenium as Elements

As the first artificially made element - hence its name - and by being the lightest element without stable isotopes, technetium presents unique characteristics and challenges. It was discovered as late as 1937 by Emilio Segrè and Carlo Perrier from an irradiated molybdenum foil.<sup>1</sup> The metastable  $^{95m}\text{Tc}$  and  $^{97m}\text{Tc}$  had been produced during the irradiation of the probe with deuterons and the chemical properties of the obtained products were compared to those of manganese and rhenium.<sup>2,3</sup> The discovery had been claimed previously by the discoverers of rhenium but their results could not be reproduced.<sup>4</sup> The most common isotope,  $^{99}\text{Tc}$ , which has a half-life of  $2.10 \cdot 10^5$  years, is a major fission product of  $^{235}\text{U}$  with a yield of 6%.<sup>5</sup> As such, it is responsible for a large amount of the long-term radioactive emissions of high-level nuclear waste.  $^{99}\text{Tc}$  compounds can be synthesized in macroscopic quantities and characterized by conventional methods such as nuclear magnetic resonance spectroscopy, infrared spectroscopy, or X-ray diffraction.<sup>2</sup> The natural occurrence of technetium is limited to trace amounts due to spontaneous fission reactions. However, atomic weapons, reprocessing facilities (e.g. Sellafield) using the PUREX cycle (Plutonium-Uranium Recovery by Extraction) as well as accidental releases led to the presence of several tons of this element in the environment.<sup>6</sup>

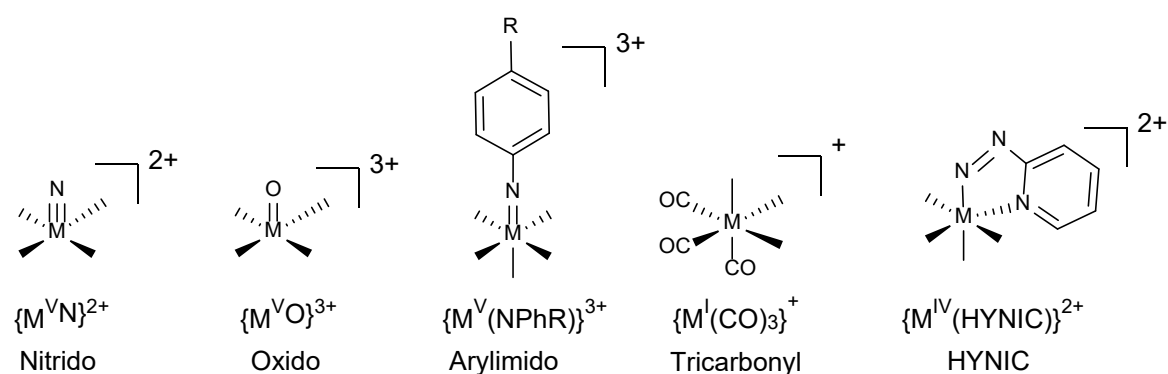
While long-lived Tc isotopes have no commercial applications, the short-lived nuclear isomer  $^{99m}\text{Tc}$  with its 6 h half-life and high availability (*vide infra*) has become one of the workhorses of nuclear medicine. The low concentration and high specific activity of  $^{99m}\text{Tc}$  precludes structural studies with this nuclide.

Rhenium was discovered in 1925 by Walter Noddack, Ida Tacke and Otto Berg and it was the last stable element to be discovered.<sup>7,8</sup> Its discovery by German researchers led to its name coming from the river Rhine. It was first isolated in small quantities from platinum ores and the first gram could be isolated a few years later from minerals like gadolinite and columbite.<sup>9</sup> Besides few minerals like molybdenite, which can be made up of 1-2% of rhenium, the concentration of rhenium is extremely low in the earth crust. Natural rhenium consists of two isotopes,  $^{185}\text{Re}$  and  $^{187}\text{Re}$ , from which  $^{187}\text{Re}$  is a very long-lived  $\beta^-$  emitter ( $>10^{10}$  a).<sup>7</sup> Rhenium is the higher homologue of technetium and, subsequently, structural studies have been performed on rhenium complexes to avoid the radiation protection issues caused by the long-lived  $^{99}\text{Tc}$ .

## 1.2. The Chemistry of Technetium and Rhenium

Technetium and rhenium have very similar atomic radii, which arises from the lanthanide contraction and technetium tends to react more like rhenium than like its lower homologue manganese. However, ligand exchange reactions can be hundreds of times slower with rhenium than with technetium, thus precluding a direct transposition of reaction conditions from one element to the other.<sup>10</sup> Only the oxidation states +VII (mostly as  $\text{MO}_4^-$ ), +IV (mostly as  $\text{MO}_2$ ) or 0 as a metal are stable without being part of metal complexes.<sup>10</sup> Also, both elements differ in their oxidation potential, as technetium ( $\text{TcO}_4^-/\text{TcO}_2$  at +0.747 V) is more readily reduced than rhenium ( $\text{ReO}_4^-/\text{ReO}_2$  at +0.510 V) but significantly less so than manganese ( $\text{MnO}_4^-/\text{MnO}_2$  at +1.679 V).

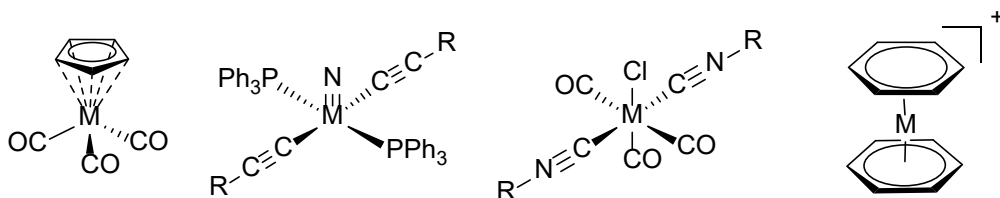
At least eight oxidation states of technetium and rhenium are known ranging from +VII to -I with every single oxidation state characterized by spectroscopic methods and X-ray diffraction. The oxidation state of the metal depends on the type of ligands used. Donor ligands such as amines, thiols, but also oxido, nitrido or imido units tend to stabilize the metal in higher oxidation states (+III and above), whereas accepting ligands such as nitrosyls, carbonyls, some phosphines as well as isocyanides are more suited to stabilize lower oxidation states.<sup>2,11</sup> The chemistry of rhenium and technetium complexes can be categorized in so-called “cores” where one ligand or one group of ligands stabilize the metal center in one oxidation state and are mostly impervious to ligand exchanges (see Fig. 1). “Core-stabilized” units, thus, have a comparable reactivity between technetium and rhenium.



**Figure 1:** Common cores of rhenium and technetium.

The nitrido core contains formally a  $\text{N}^{3-}$  ligand and stabilizes the metal in the oxidation states +V, +VI or +VII. The nitrogen atom can also act as a Lewis base. The nitrido core of rhenium and technetium is significantly more impervious to hydrolysis than its manganese equivalent. The phenylimido core stabilizes the metal center in the oxidation +V, +VI or +VII and contains a formally  $\{\text{NPhR}\}^{2-}$  ligand. The residue R on the aryl moiety can be changed, which can profoundly affect the solubility and reactivity of the metal ion.<sup>12,13</sup> The oxido core is isoelectronic to the phenylimido core and also stabilizes the

metal center in the oxidation state +V to +VII. A technetium oxo core is, however, more prone to be reduced than its rhenium equivalent.<sup>14</sup> The tricarbonyl core contains three facially arranged carbonyl ligands, which are strong  $\pi$ -acceptors, and, thus, stabilize the metal center in the oxidation state +I and exert a strong *trans* effect and influence on other ligands. The HYNIC core stabilizes both technetium and rhenium in high oxidation states and shows remarkable *in-vivo* stability even with bioconjugates.<sup>15</sup>



**Figure 2:** Examples of technetium and rhenium organometallic compounds.<sup>16</sup>

Organometallic compounds are known for both metals and under certain circumstances remarkably air- and water-stable (see Fig. 2). Complexes are known with many types of ligands. Cyclopentadienyl (Cp)-ligands usually form piano-stool like complexes and can be made in an aqueous environment. The obtained complexes, thus, only contain metal-carbon bonds.<sup>17-21</sup> Arene complexes can also be made in an aqueous environment and can be easily functionalized. Aryl, alkenyl as well as alkynyl complexes on the other hand usually require a synthesis under inert conditions to avoid the protonation of the ligands prior to the coordination.<sup>22</sup> Isocyanide and N-heterocyclic carbenes ligands are further examples of carbon-based ligands (*vide infra* for isocyanides).<sup>2,23</sup> The stability and ease of synthesis of some of those complexes as well as the possible modifications on the organic residues attached motivated significant efforts to transpose the chemistry to <sup>99m</sup>Tc for potential applications in nuclear medicine.

### 1.3. Radioactive Metals in Nuclear Medicine

#### 1.3.1. General Overview

An ideal isotope for medical application needs to fulfill a number of physical and chemical criteria. It needs to be available with a high specific activity (ideally several GBq). Moreover, an ideal isotope should be readily available on site, at best without requiring a complex setup such as a cyclotron or a nuclear reactor. Very few isotopes are available using a generator system (see Table 1). In addition, an ideal isotope needs to have a half-life sufficiently long to allow the binding to a biovector and measure the biodistribution after the intravenous injection.<sup>24</sup> As a counter example, the short half-life of <sup>15</sup>O

(2.0 min) limits the clinical use of this isotope.<sup>25</sup> An overview of common isotopes used in diagnostics is given in Table 1.

**Table 1:** Overview of isotopes used for diagnostic purposes.<sup>26</sup>

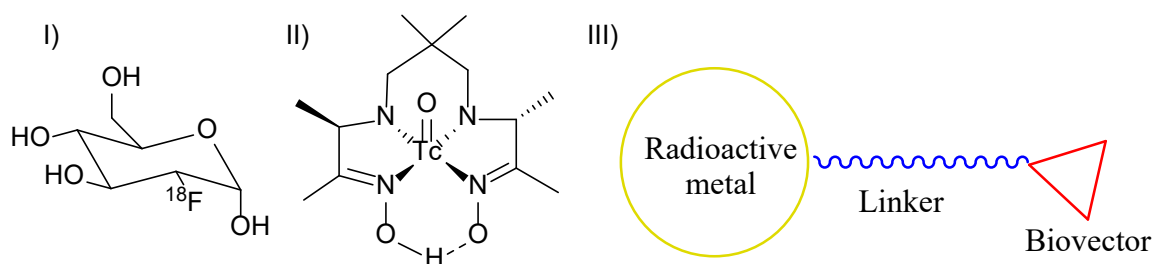
Isotope	Half-life	Radiation	Production
<sup>11</sup> C	20 min	$\beta^+$	Cyclotron
<sup>13</sup> N	10 min	$\beta^+$	Cyclotron
<sup>15</sup> O	2 min	$\beta^+$	Cyclotron
<sup>18</sup> F	110 min	$\beta^+$	Cyclotron
<sup>64</sup> Cu	12.7 h	$\beta^+$	Cyclotron or reactor
<sup>67</sup> Cu	2.58 d	$\gamma$ (93/185 keV)	Cyclotron
<sup>68</sup> Ga	68 min	$\beta^+$	Generator
<sup>89</sup> Zr	78.4 h	$\beta^+$	Cyclotron
<sup>99m</sup> Tc	6 h	$\gamma$ (140 keV)	Generator
<sup>111</sup> In	2.8 d	$\gamma$ (171.3/245.4 keV)	Cyclotron
<sup>123</sup> I	13.2 h	$\gamma$ (159 keV)	Cyclotron

Nuclear medicine can fulfill both diagnostic and therapeutic goals. Short-lived gamma emitters (e.g. <sup>111</sup>In) for single photon emission computer tomography (SPECT) or positron emitters (e.g. <sup>68</sup>Ga) for positron emission tomography (PET) can provide information about physiological functions such as blood flow or bind to overexpressed proteins in tumor tissues. Both techniques can be used conjointly with computed tomography (CT) and magnetic resonance imaging (MRI), which provide anatomical information on the targeted tissues.

Three approaches are possible to bring the radioactive isotope to the desired tissue. The first is to introduce a radioactive isotope directly in the scaffold of a biologically active molecule such as <sup>18</sup>F replacing a hydroxylic group in D-glucose. Such an approach seems to be ideal at a first glance since it uses already existing biomolecules with known biological distributions. However, most isotopes present in small organic molecules (e.g. <sup>13</sup>N or <sup>11</sup>C see Table 1) have extremely short half-lives. Furthermore, the introduction of such isotopes in the organic scaffold requires multi-step syntheses, which can be incompatible with the very short half-lives and requires the manipulation of highly radioactive solutions with so-called synthesis modules.<sup>27</sup>

A second approach is to synthesize *de-novo* small pharmaceutically active molecules, which contain a radioisotope (see Fig. 3). Such an approach faces the same hurdles as the development of non-radioactive small-molecule pharmaceutical compounds, but several commercially successful <sup>99m</sup>Tc-radiopharmaceuticals have been obtained using this approach.

A third approach is to bind a metal using a chelator system which is connected to a biovector (e.g. a peptide or an antibody) via a linker. This approach can lead to very high uptake specificity such as for  $^{68}\text{Ga}$ -PSMA-11, but it requires to find an appropriate biovector which is highly overexpressed in the desired tissue to obtain a good contrast. Furthermore, both the metal chelator and the linker to the biovector can negatively affect the biodistribution of the resulting compound.



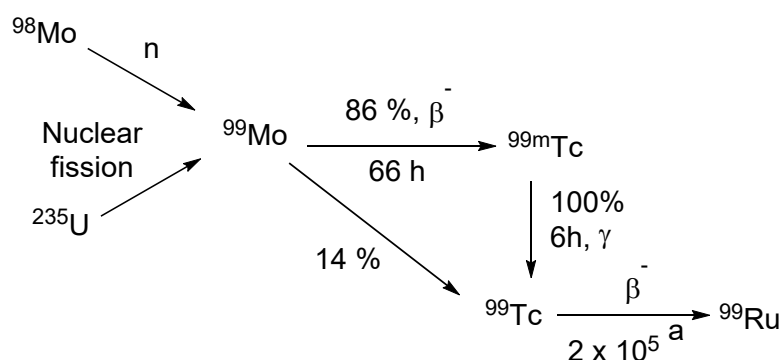
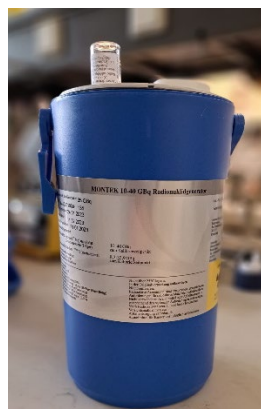
**Figure 3:** Three different approaches for binding a radioisotope. I) Radioisotope introduced in a biologically active molecule. II) *De-novo* molecule. III) Chelated metal linked to a biovector.

### 1.3.2. Technetium and Rhenium in Nuclear Medicine

While the long-lived, low-energy  $\beta^-$  emitter  $^{99}\text{Tc}$  has virtually no commercial use, its short-lived metastable nuclear isomer  $^{99\text{m}}\text{Tc}$  has experienced a tremendous success in nuclear medicine.<sup>28</sup>

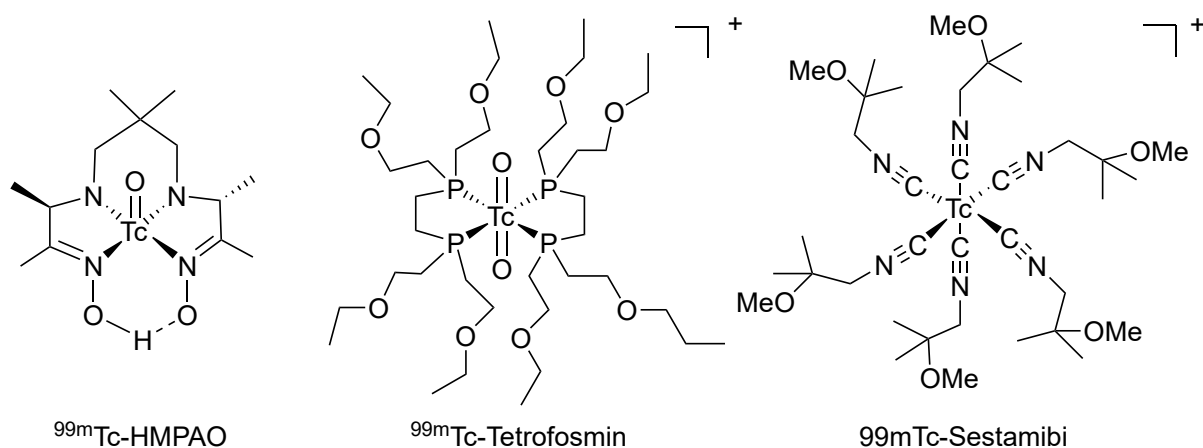
$^{99\text{m}}\text{Tc}$  possesses an ideal half-life of 6 h as well as a  $\gamma$  energy of 140 keV, which is not accompanied by any particle emission. This energy is high enough to penetrate biological tissues such as the human body but low enough to be collimated in SPECT scanners.  $^{99\text{m}}\text{Tc}$  can be conveniently produced by nuclear fission of  $^{235}\text{U}$  (see Scheme 1) in a nuclear reactor which leads to the formation of  $^{99}\text{Mo}$ . Once separated from the target material,  $^{99}\text{Mo}$  can be loaded as  $\text{MoO}_4^{2-}$  on an alumina column. It decays with a half-life of 66 h to  $^{99\text{m}}\text{Tc}$  which is obtained as  $\text{TcO}_4^-$ .<sup>29</sup> Pertechnetate is only singly charged and therefore less tightly bonded to the alumina column. An isotonic saline solution can elute the pertechnetate anion from the column in pure form. The obtained aqueous solution containing  $^{99\text{m}}\text{TcO}_4^-$  has the high specific activity required for nuclear imaging without requiring any further concentrating steps. The solution obtained from such a  $^{99}\text{Mo}/^{99\text{m}}\text{Tc}$  isotope generator can either be used as it is or mixed with so-called kits which contain several chemicals such as ligands, reducing agents and stabilizers. Besides a short heating step and standardized quality control, no chemical expertise is required to use such kits. The combination of a generator-based  $^{99\text{m}}\text{Tc}$  supply and kit chemistry explains

the role of this isotope as workhorse of nuclear medicine (19 x 10<sup>6</sup> injections in 2007 in the United States alone with 85% market share).<sup>29</sup>



**Scheme 1:** <sup>99</sup>Mo/<sup>99m</sup>Tc generator and the production of <sup>99</sup>Mo and its decay chain.<sup>5</sup>

Several cores at different oxidation states (*vide supra*) are used for nuclear medicine and the diversity of oxidation states is reflected in commercially available kits with <sup>99m</sup>Tc-HMPAO, which is for brain imaging, having an oxido core and <sup>99m</sup>Tc-Tetrofosmin used for myocardial imaging having a bis-oxido core, whereas <sup>99m</sup>Tc-sestamibi, mostly used for myocardial imaging as well, is an air- and water-stable organometallic compound (see Fig. 4). The technetium metal center is in the low oxidation state +I in the latter case.

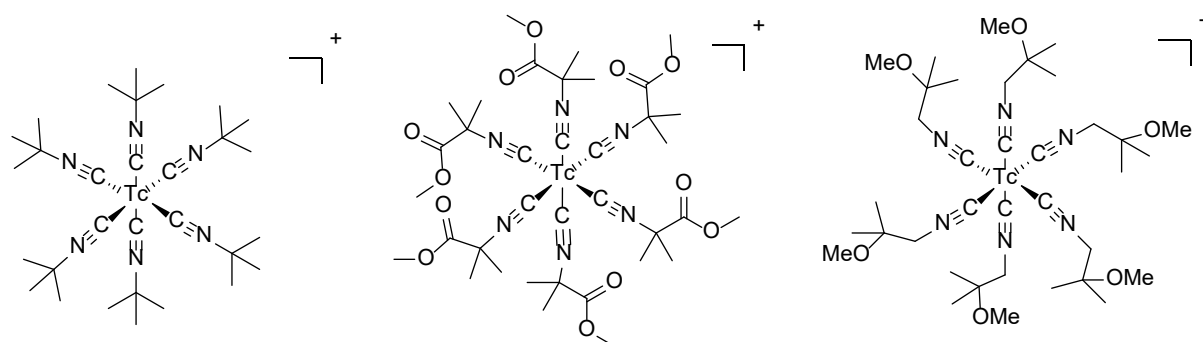


**Figure 4:** Three commercially successful <sup>99m</sup>Tc radiopharmaceuticals.

Small variations in the molecular structure of a potential radiopharmaceutical agent can lead to profound changes in its biological distribution. An example of structural studies which permitted the development of the successful imaging agent Cardiolite® (see Fig. 5) is the evolution of the residue on the isocyanide ligand. It started with the very lipophilic CN<sup>t</sup>Bu, which led to a significant uptake in the myocardium but also in the liver, thus, impairing a clear view of the heart. Furthermore, this compound suffered from a rapid washout in the targeted tissues. The lipophilicity of the compound was lowered by introducing ester groups on the isocyanides.<sup>30</sup> The ester groups were however cleaved very rapidly



*in-vivo*. This led to the development of Sestamibi (Cardiolite®) with ether groups.<sup>31</sup> A kit suitable for clinical routine was then formulated. It contained tin chloride as a reducing agent and cysteine as a stabilizer for intermediate oxidation states formed during the reduction from Tc(+VII) to Tc(+I). The isocyanide ligand had to be formulated as a copper(I) complex as small isocyanides tend to be liquid with a pungent smell and cannot be lyophilized.



**Figure 5:** Structural evolution of hexakis(isocyanide)technetium(I) complexes towards the myocardial imaging agent <sup>99m</sup>Tc-methoxyisobutylisocyanide.

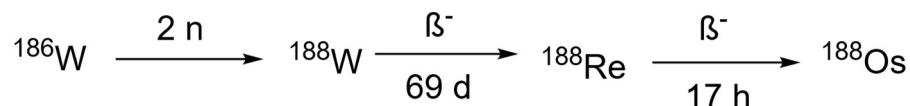
The constraints described above for diagnostic isotopes also apply for their therapeutic counterparts, which need to emit  $\beta^-$  or  $\alpha$  radiation with a significantly higher ionization potential than  $\gamma$ -rays and can, therefore, locally (within a few mm) destroy tumor tissues. An ideal isotope should be either long-lived enough to be transported from a central production site or made locally using a generator system. Furthermore, the chemistry of the therapeutic isotope should “match” well with that of a diagnostic isotope to have a comparable biological distribution without the need to develop a completely new chemistry for therapeutic isotopes. As an example, <sup>68</sup>Ga-PSMA-11 and <sup>177</sup>Lu-PSMA-617 require different chelators and linkers to cover both diagnostic and therapeutic purposes.<sup>32</sup> Furthermore, <sup>177</sup>Lu is made in nuclear reactors, thus, requiring the transport of large doses of radioactivity (see Table 2).

**Table 2:** Overview of isotopes used for therapeutic purposes.<sup>26</sup>

Isotope	Half-life	Radiation	Production
<sup>64</sup> Cu	12.7 h	$\beta^-$ (0.57 MeV)	Cyclotron or reactor
<sup>90</sup> Y	64.6 h	$\beta^-$ (2.28 MeV)	Reactor
<sup>177</sup> Lu	6.7 d	$\beta^-$ (0.49 MeV)	Reactor
<sup>188</sup> Re	16.9 h	$\beta^-$ (2.12 MeV)	Generator
<sup>225</sup> Ac	9.9 d	$\alpha$ (5.93 MeV)	Generator or cyclotron

<sup>99m</sup>Tc can form such a “matched-pair” with <sup>186</sup>Re and <sup>188</sup>Re to cover both diagnostic and therapeutic applications. Both rhenium isotopes are  $\beta^-$  emitters.<sup>33</sup> <sup>186</sup>Re has a half-life of 3.7 d and an intermediate  $\beta^-$  energy ( $E_{\beta_{\max}} = 1.07$  MeV), while <sup>188</sup>Re has a half-life of 16.9 h and emits highly energetic beta particles ( $E_{\beta_{\max}} = 2.12$  MeV) that can penetrate deeper in tissues than the particles emitted by <sup>186</sup>Re. While both isotopes possess interesting radiation properties, the availability of <sup>186</sup>Re is very limited as

it is mostly produced in nuclear reactors whereas  $^{188}\text{Re}$  can be obtained from a generator system similarly to that shown in Scheme 2. In such a generator,  $^{188}\text{W}$ , which can be synthesized by exposing  $^{186}\text{W}$  to a very high neutron flux, is loaded on an alumina column which can then be eluted with normal saline to obtain  $^{188}\text{Re}$  (see Scheme 2).<sup>34</sup> Such a generator can be eluted once daily and produces carrier free  $^{188}\text{Re}$  at high specific activity.



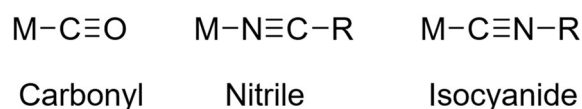
**Scheme 2:**  $^{188}\text{W}/^{188}\text{Re}$  generator and production and decay scheme of  $^{188}\text{Re}$ .

Though rhenium and technetium differ in their reaction kinetics and their redox potentials, structurally identical compounds can be synthesized in corresponding kits e.g.  $^{188}\text{Re}$ -DMSA (meso-2,3-dimercaptosuccinic acid) which has been proposed for oncological treatment.<sup>35</sup> Recent works showed that new synthetic pathways towards nitrido cores (*vide supra*) can be developed to overcome the differences between rhenium and technetium.<sup>36,37</sup> However, more fundamental coordination chemistry studies are required to obtain other cores.

## 1.4. Isocyanides

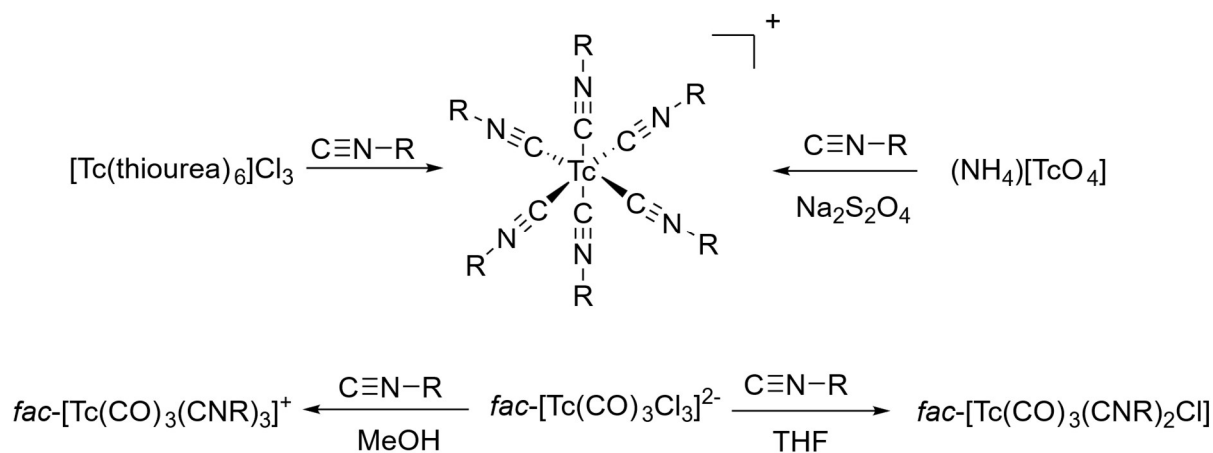
### 1.4.1. Ligand Properties and Synthesis

Isocyanides, also described as isonitriles, are ligands with a carbon-nitrogen triple bond. The coordination to a metal ion takes place via the carbon atom. Isocyanides are, therefore, frequently considered isolobal, though not isoelectronic, to carbonyl ligands (see Fig. 6). Both carbonyls and isocyanides are regarded as suitable ligands for metals in their low oxidation states due to their  $\pi$ -backbonding abilities.<sup>38</sup>



**Figure 6:** Comparison of carbonyl, nitrile and isocyanide ligands.

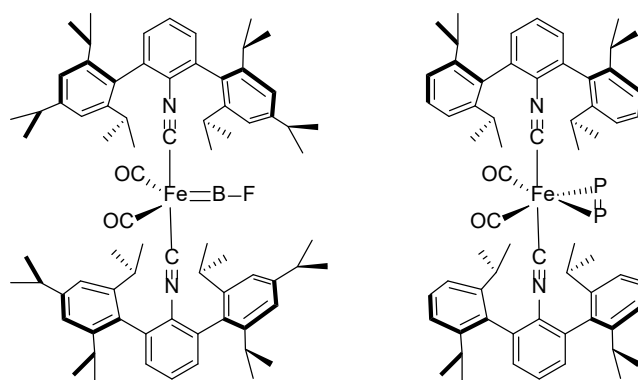
The isocyanide chemistry of technetium, while clinically successful, is limited to a few complexes (see Scheme 3). Hexakis(isocyanide)technetium(I) complexes can be synthesized from a Tc(III) thiourea complex or from pertechnetate using a reducing agent such as sodium dithionite.<sup>39-41</sup> Heteroleptic complexes could be obtained using such pathways but the products were only obtained as mixtures depending on the ligand ratio used.<sup>42</sup> Complexes have been obtained both with alkyl and aryl isocyanides and could be reacted with either nitric acid to form  $[\text{Tc}(\text{NO})(\text{CNR})_5]^{2+}$  complexes or with elemental halogens to form heptacoordinate Tc(III) complexes.<sup>43,44</sup> Mixed carbonyl-isocyanide complexes could be obtained from a *fac*- $[\text{Tc}(\text{CO})_3]^+$  starting material.<sup>45,46</sup> Depending on the solvent or the use of a halide scavenger bis- or tris-substituted complexes could be isolated, but the *fac*- $[\text{Tc}(\text{CO})_3]^+$  core was not further substituted. Mixed phosphine-isocyanide complexes with the formula  $[\text{Tc}(\text{PMe}_2\text{Ph})_{6-x}(\text{CN}^t\text{Bu})_x]^+$  were also reported.<sup>47</sup>



**Scheme 3:** Synthesis of hexakis(isocyanide)technetium(I) complexes and mixed carbonyl-isocyanide complexes of technetium.

### 1.4.2. *m, m'*-Terphenylic Isocyanides

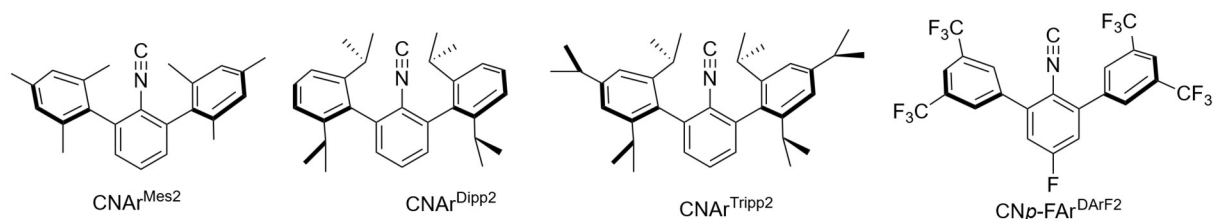
Most Tc isocyanide complexes studied so far have been prepared with commercially available isocyanides, which limited the information about the influence of the electrical and sterical factors of the organic residues attached to the nitrogen atom.<sup>48</sup> To overcome this limitation, Figueroa *et al.* developed several isocyanides with a *m, m'*-terphenyl scaffold, which lead to “well-behaved” ligands, which can coordinate metal centers in very low oxidation states by providing a steric protection. This precludes polymerization reactions of the very reactive metal centers.<sup>49</sup> The sterical protection also allowed the synthesis of unprecedented P<sub>2</sub> and BF compounds (see Fig. 7).<sup>50, 51</sup>



**Figure 7:** Recent examples of stabilized species thanks to sterical protection by *m, m'*-terphenyl isocyanides.<sup>50, 51</sup>

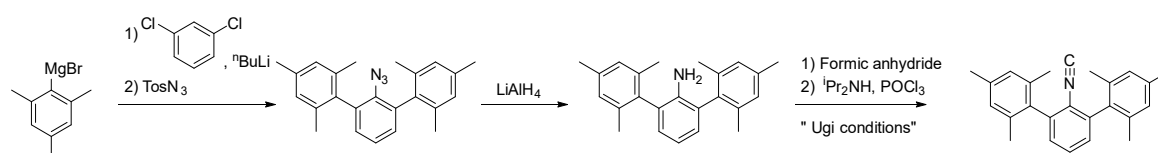
Remarkable results were also obtained with manganese, where very reactive Mn(0) complexes could be isolated.<sup>49,52,53</sup> Surprisingly, the same type of ligands was also found to stabilize metal centers in higher oxidation states such as Tc(V) or Re(V), whereas the isocyanide ligand acted as a  $\sigma$ -donor and not as a  $\pi$ -acceptor.<sup>54,55</sup> As only few reactions were attempted with group VII metals, further investigations were deemed necessary and are part of the present work.

The fluorine functionalized sterically hindered terphenyl isocyanide CN*p*-FAR<sup>DArF2</sup> has also been shown to replace carbonyl ligands.<sup>56</sup> While it has been reported as early as the 1950s that isocyanides can replace carbonyls, the exact electronic influence of the organic residue bonded to the nitrogen atom has not yet been systematically studied.<sup>57,58</sup> It is, thus, also necessary to better understand the reactivity of electron-poor isocyanides. The four *m, m'*-terphenyl isocyanides depicted in Figure 8 were used in this work to compare both electronic and steric influences of the substituents on the coordination chemistry with technetium and rhenium.



**Figure 8:** *m,m'*-Terphenyl isocyanides used in this work.

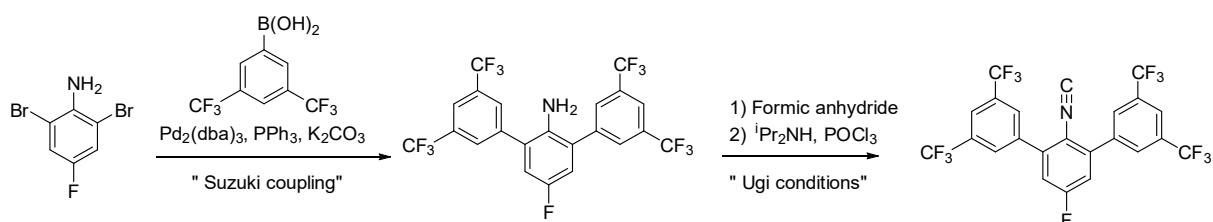
While several routes exist to introduce the isocyanato functional group, the dehydration of a formamide is by far the most reported in the literature. Dehydrating agents such as tosyl chloride, phosgene,  $\text{PPh}_3/\text{I}_2$ , Burgess reagent or  $\text{POCl}_3$  in presence of an amine have been reported in the literature.<sup>48</sup> The latter reagent was proposed by Ugi *et al.* in the late fifties and remains the easiest and cheapest synthetic pathway towards isocyanides and shows a good functional group tolerance.<sup>59</sup> Some limitations of this procedure, e.g. a lengthy aqueous work-up, have been resolved by Patil *et al.* by using a dry silica gel column eluted with diethyl ether.<sup>48</sup>



**Scheme 4:** Synthesis of  $\text{CNAr}^{\text{Mes}2}$  via the “aryne” route.

The terphenyl backbone used in  $\text{CNAr}^{\text{Tripp}2}$ ,  $\text{CNAr}^{\text{Mes}2}$  and  $\text{CNAr}^{\text{Dipp}2}$  can be made as depicted in Scheme 4. A lithiated 1,3-dichlorobenzene is added slowly to a solution containing the Grignard reagent of the desired flanking ring (see Scheme 4). The reaction proceeds via an “aryne” intermediate. The reaction is then quenched with tosyl azide. The obtained terphenyl azide is then reduced to an amine using  $\text{LiAlH}_4$ , which is subsequently reacted with formic anhydride to form a formamide. The latter is then dehydrated using “Ugi conditions”.<sup>60</sup>

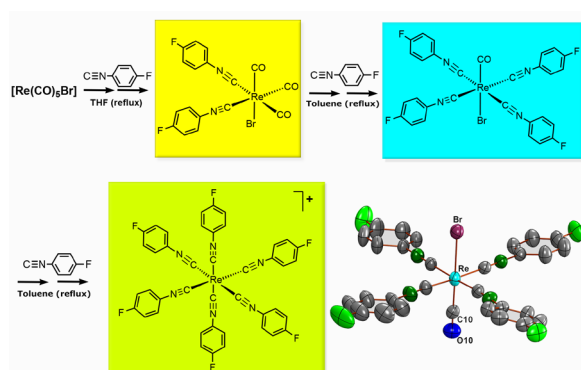
$\text{CNp-FAr}^{\text{DArF}2}$  can be synthesized via a different pathway. Both the boronic acid required for the flanking rings as well as the fluorinated aniline for the central ring are commercially available (see Scheme 5).<sup>61</sup> The target molecule can be made from the terphenyl aniline obtained after the Suzuki coupling using the same procedure as for the aforementioned ligands.



**Scheme 5:** Synthesis of  $\text{CNp-FAr}^{\text{DArF}2}$  via a Suzuki coupling.

### 1.4.3. Isocyanide Chemistry in this Work

The approach to the widely used compound Tc-Sestamibi is only suitable for the synthesis of homoleptic complexes. It is as such particularly relevant to gain a better control on the coordination sphere of hexakis(isocyanide) complexes. Previous studies with fluorinated isocyanides and the rhenium core  $\{\text{Re}(\text{CO})_3\}^+$  showed a remarkable reactivity.<sup>62</sup> The monitoring of ligand exchange on rhenium compounds with spectroscopic methods can be performed without the need of extensive radioprotection. As such, the substitution chemistry of rhenium carbonyls with a mono-fluorinated isocyanide ligand was studied in publication 1 (*Z. Anorg. Allg. Chem.*, **2023**, 649, e202200320.)



*Z. Anorg. Allg. Chem.*, **2023**, 649, e202200320

structures of  $[\text{Re}(\text{CO})\text{Br}(\text{CNPh}^{\text{pF}})_4]$  and  $[\text{Re}(\text{CNPh}^{\text{pF}})_6](\text{BPh}_4)$  have been elucidated by X-ray diffraction.

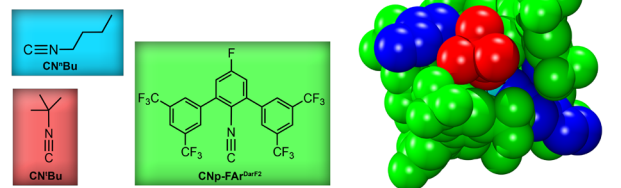
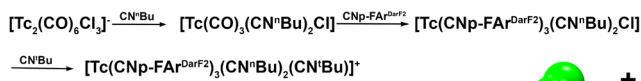
$p$ -Fluorophenylisocyanide ( $\text{CNPh}^{\text{pF}}$ ) reacts with  $[\text{Re}(\text{CO})_5\text{Br}]$  under stepwise exchange of the carbonyl ligands depending on the conditions applied. The reaction stops with the formation of  $\text{fac-}[\text{Re}(\text{CO})_3\text{Br}(\text{CNPh}^{\text{pF}})_2]$  in boiling THF. An ongoing carbonyl exchange is observed at higher temperatures, e. g. in refluxing toluene, with the final formation of the  $[\text{Re}(\text{CNPh}^{\text{pF}})_6]^+$  cation. The progress of the reactions has been studied by  $^{19}\text{F}$  NMR spectroscopy and the

The fluorine atom proved to have a large influence on the reaction kinetic compared to non-fluorinated ligands reported in the literature.<sup>63</sup> Furthermore, the NMR-active nuclei  $^{19}\text{F}$  proved useful to observe *in situ* the stepwise substitution of carbonyl ligands. It was, thus, possible to observe a strong dependence of the substitution rate on the temperature. The choice of temperature changed the outcome of the reaction. Lower temperatures lead to the exclusive formation of  $\text{fac-}\{\text{Re}(\text{CO})_3\}^+$  products. Higher temperatures lead to the isomerization and substitution of the remaining carbonyl ligands.

The reaction kinetic of technetium is known to be faster than that of rhenium, which was indeed observed when fluorinated isocyanides were reacted with a  $\text{fac-}\{\text{Tc}(\text{CO})_3\}^+$  starting material. Homoleptic hexakis(isocyanide)technetium(I) complexes could be obtained within one hour and the reaction patterns could be followed by both  $^{19}\text{F}$  and  $^{99}\text{Tc}$  NMR spectroscopy, which proved to be a powerful combination to observe the ligand and the metal at the same time. The stepwise substitution could be stopped at the pentakis(isocyanide) intermediate  $[\text{Tc}(\text{CNR})_2(\text{CN}p\text{-FAr}^{\text{DArF}_2})_3\text{Cl}]$  ( $\text{R} = {}^t\text{Bu}$  or  ${}^n\text{Bu}$ ) by introducing bulky  $m,m'$ -terphenyl isocyanides, which allowed the synthesis of the first defined

isocyanide complex with three different isocyanides. Thus, a better understanding of the reactivity pattern of isocyanides depending on their electronic characteristics or steric hinderance allowed a better control of the coordination sphere. The corresponding results are reported in publication 2 (*Inorg. Chem.*, **2022**, *61*, 16163–16176.)

Reactions of the alkyl isocyanide *fac*-[Tc(CO)<sub>3</sub>(CNR)<sub>2</sub>Cl] complexes (**2**) (CNR = CN<sup>n</sup>Bu or CN<sup>t</sup>Bu) with the sterically encumbered isocyanide CN*p*-FAR<sup>DarF2</sup> [DarF = 3,5-(CF<sub>3</sub>)<sub>2</sub>C<sub>6</sub>H<sub>3</sub>] allow a selective exchange of the carbonyl ligands of **2** and the isolation of the mixed-isocyanide complexes *mer,trans*-[Tc(CN*p*-FAR<sup>DarF2</sup>)<sub>3</sub>(CNR)<sub>2</sub>Cl] (**3**). Depending on the steric requirements of the



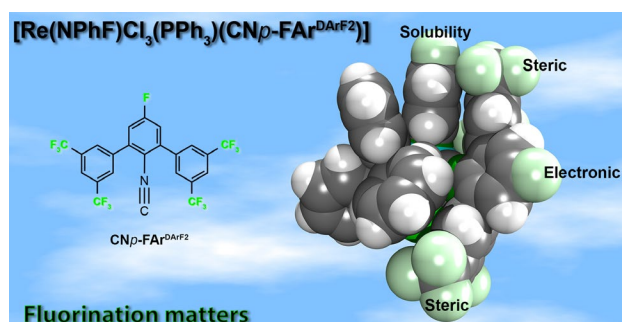
*One Technetium atom with three different isocyanide ligands*

*Inorg. Chem.*, **2022**, *61*, 16163–16176

residues *R*, the remaining chlorido ligand can be replaced by another isocyanide ligand. Cationic complexes such as *mer*-[Tc(CN*p*-FAR<sup>DarF2</sup>)<sub>3</sub>(CN<sup>n</sup>Bu)<sub>3</sub>]<sup>+</sup> (**4a**) or *mer,trans*-[Tc(CN*p*-FAR<sup>DarF2</sup>)<sub>3</sub>(CN<sup>n</sup>Bu)<sub>2</sub>(CN<sup>t</sup>Bu)]<sup>+</sup> (**6**) have been prepared in this way and isolated as their PF<sub>6</sub><sup>-</sup> salts. *mer,trans*-[Tc(CN*p*-FAR<sup>DarF2</sup>)<sub>3</sub>(CN<sup>n</sup>Bu)<sub>2</sub>(CN<sup>t</sup>Bu)](PF<sub>6</sub>) represents to the best of our knowledge the first transition-metal complex with three different isocyanides in its coordination sphere. Since the degree of the ligand exchange seems to be controlled both by the electronic and steric measures of the incoming isocyanides, we undertook similar reactions with the sterically less demanding *p*-fluorophenyl isocyanide, CNPh<sup>PF</sup>, which indeed readily led to the hexakis(isocyanide)technetium(I) cation through an exchange of all ligands in the starting materials [Tc<sub>2</sub>(CO)<sub>6</sub>(μ-Cl)<sub>3</sub>]<sup>-</sup> or *fac*-[Tc(CO)<sub>3</sub>(CNR)<sub>2</sub>Cl]. The influence of the substituents at the isocyanide ligands in such reactions has been reasoned with the density functional theory-derived electrostatic potential at the accessible surface of the corresponding isocyanide carbon atoms.

Surprisingly, even the most electron-withdrawing isocyanides used in the aforementioned publications were found to act as σ-donor ligands as soon as stronger π-acidic carbonyl ligands were still present. This contradicts the expected behavior of isocyanides which have been described as carbonyl analogs in the literature. Due to this comparison, the reactivity of isocyanides with metal centers in formally higher oxidation states has been only sparingly investigated. As mentioned above, rhenium offers a convenient starting point for spectroscopical studies. We, thus, investigated the reactivity of aryl and alkylisocyanides with [Re(NPhF)Cl<sub>3</sub>(PPh<sub>3</sub>)<sub>2</sub>] as a Re(V) starting material. The fluorine atom on the phenylimido ligand provides an enhanced solubility of the starting material which allowed reactions with delicate isocyanides leading to the formation of complexes of the formula [Re(NPhF)Cl<sub>3</sub>(PPh<sub>3</sub>)(CNR)] with alkyl, small aryl as well as with the strongly electron-deficient terphenyl isocyanide CN*p*-FAR<sup>DarF2</sup>. Attempts to synthesize complexes with more isocyanide ligands using a larger excess of ligands and prolonged reaction times lead to the decomposition of both the metal complex

and the free isocyanide ligands. On the other hand, electron-rich terphenyl isocyanides lead to bis isocyanide complexes, thus, highlighting the strong influence of substituents on the reactivity pattern of isocyanide ligands even with a high-oxidation-state metal ion.  $^{19}\text{F}$  NMR proved to be suitable to observe the reaction *in situ*. A survey of the observed reactivity was reported in publication 3 (*Dalton Trans.*, **2023**, 52, 4768-4778).



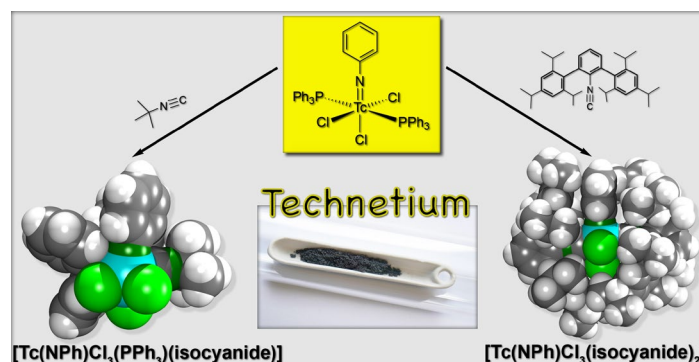
*Dalton Trans.*, **2023**, 52, 4768-4778

Reactions of  $[\text{Re}(\text{NPhF})\text{Cl}_3(\text{PPh}_3)_2]$  ( $\{\text{NPhF}\}^2-\text{=}$  p-fluorophenylimide) with a variety of alkyl and aryl isocyanides have been studied. Different reactivity patterns and products have been obtained depending on the steric and electronic properties of the individual ligands. This involves the formation of 1:1 and 1:2 exchange products of Re(V) with the general formulae *cis*- $[\text{Re}(\text{NPhF})\text{Cl}_3(\text{PPh}_3)(\text{isocyanide})]$  and *cis*- or *trans*- $[\text{Re}(\text{NPhF})\text{Cl}_3(\text{isocyanide})_2]$ . The stability of the obtained products is correlated with the substitution pattern of the isocyanide ligands. The products have been studied by single-crystal X-ray diffraction and spectroscopic methods, including IR and multinuclear NMR spectroscopy as well as mass spectrometry. The use of partially fluorinated starting materials and ligands allows the modulation of the solubilities of the starting materials and the products as well as the monitoring of the reactions by means of  $^{19}\text{F}$  NMR. The attachment of  $\text{CF}_3$  or F substitutions on the isocyanides gives control over the steric bulk and the electronic properties of the ligands and, thus, their reactivity.

Analogous reactions were attempted with the technetium(V) starting material  $[\text{Tc}(\text{NPh})\text{Cl}_3(\text{PPh}_3)_2]$ . The faster reaction kinetic of technetium allowed the reactions with small alkyl and aryl isocyanides to proceed at room temperature to form *cis*- $[\text{Tc}(\text{NPh})\text{Cl}_3(\text{PPh}_3)(\text{CNR})]$  complexes. On the other hand, terphenyl isocyanides form *cis*- or *trans*- $[\text{Tc}(\text{NPh})\text{Cl}_3(\text{CNR})_2]$  complexes depending on their steric bulk. Furthermore, a reaction at elevated temperature with the electron-poor isocyanide  $\text{CNPh}^{\text{pF}}$  led to the surprising isolation of a hexakis(isocyanide)technetium(I) complex, thus, highlighting the strong difference in reactivity depending on both steric and electronic factors. The obtained complexes were less stable than their rhenium equivalent, especially in solution. The results of this study are found in publication 4 (*Molecules*, **2022**, 27, 8546).



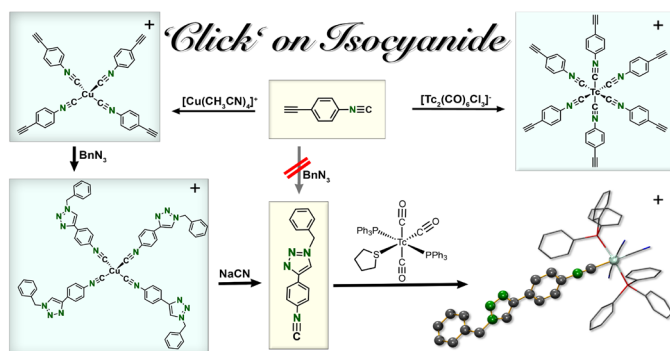
Organometallic approaches are of ongoing interest for the development of novel functional  $^{99m}\text{Tc}$  radiopharmaceuticals, while the basic organotechnetium chemistry seems frequently to be little explored. Thus, structural and reactivity studies with the long-lived isotope  $^{99}\text{Tc}$  are of permanent interest as the foundation for further



*Molecules*, **2022**, *27*, 8546

progress in the related radiopharmaceutical research with this artificial element. Particularly the knowledge about the organometallic chemistry of high-valent technetium compounds is scarcely developed. Here, phenylimido complexes of technetium(V) with different isocyanides are introduced. They have been synthesized by ligand-exchange procedures starting from  $[\text{Tc}(\text{NPh})\text{Cl}_3(\text{PPh}_3)_2]$ . Different reactivity patterns and products have been obtained depending on the steric and electronic properties of the individual ligands. This involves the formation of 1:1 and 1:2 exchange products of Tc(V) with the general formulae  $[\text{Tc}(\text{NPh})\text{Cl}_3(\text{PPh}_3)(\text{isocyanide})]$ , *cis*- or *trans*- $[\text{Tc}(\text{NPh})\text{Cl}_3(\text{isocyanide})_2]$ , but also the reduction in the metal and the formation of cationic technetium(I) complex of the formula  $[\text{Tc}(\text{isocyanide})_6]^+$  when *p*-fluorophenyl isocyanide is used. The products have been studied by single-crystal X-ray diffraction and spectroscopic methods, including IR and multinuclear NMR spectroscopy. DFT calculations on the different isocyanides allow the prediction of their reactivity towards electron-rich and electron-deficient metal centers by means of the empirical SADAP parameter, which has been derived from the potential energy surface of the electron density on their potentially coordinating carbon atoms.

A better understanding of the influence of steric and electronic properties of substituents on the reactivity of isocyanides was obtained from the publications mentioned above. The relationship between density functional theory derived Surface-Averaged Donor–Acceptor Potential (SADAP) parameters matched reliably with the observed reactivity patterns. A *para*-alkyne-functionalized aryl isocyanide ligand was found to have similar SADAP parameters to the fluorinated isocyanide ligands mentioned above and should, thus, be able to replace carbonyl ligands under thermal conditions. The introduction of an alkyne would allow the further functionalization of the isocyanide ligand with a potential biological vector. Indeed, a hexakis( $\text{CNPh}^{\text{pC}\equiv\text{CH}}$ )technetium(I) complex could be obtained from a Tc(I) carbonyl starting material. Benzyl azide was used as a model to assess the reactivity of an azide with the coordinated  $\text{CNPh}^{\text{pC}\equiv\text{CH}}$  ligand. Using Cu(I) catalysts, benzyl azide could be “clicked” on the alkyne once the isocyanide moiety was coordinated to the Tc metal center. As copper(I) complexes are used to deliver ligand by transmetalation in  $^{99m}\text{Tc}$ , a tetrakis( $\text{CNPh}^{\text{pC}\equiv\text{CH}}$ )copper(I) complex was also synthesized and could also be reacted with benzyl azide. The coordinated isocyano-triazole ligand was cleaved from the metal center and reacted with *mer,trans*- $[\text{Tc}(\text{CO})_3(\text{PPh}_3)_2(\text{tetrahydrothiophene})][\text{BF}_4]$ . The crystal structure of the resulting *mer,trans*- $[\text{Tc}(\text{CO})_3(\text{PPh}_3)_2(\text{CNPh}^{\text{azole}})][\text{BF}_4]$  complex could be obtained, which confirmed the formation of a C-bonded isocyano-triazole ligand.



*Inorg. Chem.*, **2023**, Submitted

The attachment of an ethyne substituent in *para* position of phenylisocyanide,  $\text{CNPh}^{\text{pC}\equiv\text{CH}}$ , enables the isocyanide to replace carbonyl ligands in the coordination sphere of common technetium(I) starting materials such as  $(\text{NBu}_4)[\text{Tc}_2(\mu\text{-Cl})_3(\text{CO})_6]$ . The ligand exchange proceeds under thermal conditions and finally forms the corresponding hexakis(isocyanide)technetium(I)

complex. The product undergoes a copper-catalyzed cycloaddition ('Click' reaction), e.g. with benzyl azide, which gives the  $[\text{Tc}(\text{CNPh}^{\text{azole}})_6]^+$  cation. The uncoordinated 'Click' product is obtained from a reaction of the corresponding tetrakis(isocyanide)copper(I) complex and NaCN. It readily reacts with *mer*- $[\text{Tc}(\text{CO})_3(\text{tht})(\text{PPh}_3)_2](\text{BF}_4)$  (tht = tetrahydrothiophene) under the exchange of the thioether ligand. Alternatively,  $[\text{Cu}(\text{CNPh}^{\text{azole}})_4]^+$  can be used as a transmetalation reagent for the synthesis of the hexakis(isocyanide)technetium(I) complex, which is the preferable approach for the synthesis of the technetium complex with the short-lived isotope  $^{99\text{m}}\text{Tc}$  and a corresponding protocol for  $^{99\text{m}}\text{Tc}(\text{CNPh}^{\text{azole}})_6]^+$  is reported. The  $^{99}\text{Tc}$  and copper complexes have been studied by single-crystal X-ray diffraction and/or spectroscopic methods including IR and multinuclear NMR spectroscopy.

## 2. Summary

Three aspects of group 7 isocyanide chemistry were considered in this thesis.

First, the reactivity of electron-poor isocyanides with *facial* tricarbonyl starting materials was investigated. As expected, the reactions with technetium were significantly faster than with rhenium and carbonyl ligands of *fac*-[Tc(CO)<sub>3</sub>(CNR)<sub>2</sub>Cl] (R = <sup>t</sup>Bu, <sup>n</sup>Bu) could be exchanged under thermal conditions forming the key intermediate *mer*-[Tc(CN*p*-FAR<sup>DArF2</sup>)<sub>3</sub>(CNR)<sub>2</sub>Cl]. The chlorido ligand in this compound can be abstracted using a halide scavenger and replaced by a sixth isocyanide ligand leading to the first defined heteroleptic hexakis(isocyanide)technetium(I) complex : [Tc(CN*p*-FAR<sup>DArF2</sup>)<sub>3</sub>(CN<sup>n</sup>Bu)<sub>2</sub>(CN<sup>t</sup>Bu)] [PF<sub>6</sub>].

CNPh<sup>PF</sup> was then used to assess the reactivity of electron-poor isocyanides without the sterical strain caused by the flanking rings of the *m,m'*-terphenyl isocyanide CN*p*-FAR<sup>DArF2</sup>. The reaction kinetics were even faster once the sterical strain was removed. In both cases, the combination of <sup>99</sup>Tc and <sup>19</sup>F NMR spectroscopy proved invaluable to monitor the progress of the reaction in solution. The use of <sup>19</sup>F NMR was even more important for reaction involving rhenium as the metal center cannot be observed by NMR. The slower reaction rates of the rhenium compounds allowed the facile isolation of intermediate compounds such as *fac*-[Re(CO)<sub>3</sub>(CNPh<sup>PF</sup>)<sub>2</sub>Br] or *trans*-[Re(CO)(CNPh<sup>PF</sup>)<sub>4</sub>Br], which could both only be spectroscopically observed for technetium.

In a second part of the thesis, the reactivity of isocyanides with high-valent phenylimido starting materials was studied. Both electronic and steric factors play a role in the outcomes of the reactions. The electron-deficient CNPh<sup>PF</sup> was able to cleave the technetium-nitrogen bond and replaced the entire coordination sphere to form a hexakis(isocyanide)technetium(I) complex. Such a high substitution degree was not observed for rhenium and only a [Re(NPhF)(PPh<sub>3</sub>)(CNPh<sup>PF</sup>)Cl<sub>3</sub>] complex could be obtained. On the other hand, the electron-rich *m,m'*-terphenyl isocyanides CNAr<sup>Dipp2</sup> and CNAr<sup>Tripp2</sup> were able to form bis(isocyanide) complexes with both metals.

The reactions with [Re(NPhF)Cl<sub>3</sub>(PPh<sub>3</sub>)<sub>2</sub>] also show, which role fluorine-substitution may have in the coordination chemistry. The non-fluorinated starting material [Re(NPh)Cl<sub>3</sub>(PPh<sub>3</sub>)<sub>2</sub>] is too little soluble for reactions with delicate isocyanides and the introduction of a fluorine atom on the phenylimido ring increases the solubility. Furthermore, this fluorine atom shows small, but significant shifts in <sup>19</sup>F NMR resonances, which were used to monitor the progress of such reactions. Moreover, the electron-deficient and highly fluorinated CN*p*-FAR<sup>DArF2</sup> only forms [M(NPhR)Cl<sub>3</sub>(PPh<sub>3</sub>)(CN*p*-FAR<sup>DArF2</sup>)], even though the sterical hinderance of the ligand does not preclude a higher substitution.

Remarkably, the IR stretches of all used isocyanides show hypsochromic shift upon coordination on Re(V) and Tc(V) centers. This means, they act exclusively as  $\sigma$ -donors.

In the last part of this thesis, the gained knowledge on the influence of steric and electronic parameters on the reactivity of isocyanide ligands was applied to synthesize a functionalizable isocyano ligand. Surface-Averaged Donor–Acceptor Potential (SADAP) parameters showed that the alkyne functionalized isocyanide  $\text{CNPh}^{\text{pC}\equiv\text{CH}}$  should have a similar reactivity to the  $\text{CNPh}^{\text{pF}}$  ligand, which replaces carbonyl ligands under thermal conditions. Indeed, the reaction of  $(\text{NBu}_4)[\text{Tc}_2(\mu\text{-Cl})_3(\text{CO})_6]$  with  $\text{CNPh}^{\text{pC}\equiv\text{CH}}$  lead to the (hexakis)isocyanide complex  $[\text{Tc}(\text{CNPh}^{\text{pC}\equiv\text{CH}})_6]^+$ . The latter complex could be “clicked” with benzyl azide using an appropriate copper catalyst. The reaction conditions to form the (hexakis)isocyanide complex were harsh and required an inert atmosphere which precluded equivalent reactions with aqueous  $^{99\text{m}}\text{Tc}$ . The Cu(I) complex  $[\text{Cu}(\text{CNPh}^{\text{pC}\equiv\text{CH}})_4](\text{BF}_4)$  could be readily synthesized and “clicked” under milder conditions. The resulting  $[\text{Cu}(\text{CNPh}^{\text{azole}})_4]^+$  can be used as a transmetalation reagent for the synthesis of the hexakis(isocyanide)technetium(I) complex, which is the preferable approach for the synthesis of the technetium complex with the short-lived isotope  $^{99\text{m}}\text{Tc}$ . Alternatively, the uncoordinated ‘Click’ product can be obtained by cleaving the  $[\text{Cu}(\text{CNPh}^{\text{azole}})_4](\text{BF}_4)$  complex with aqueous NaCN. It readily reacts with *mer*- $[\text{Tc}(\text{CO})_3(\text{tht})(\text{PPh}_3)_2](\text{BF}_4)$  (tht = tetrahydrothiophene) under the exchange of the thioether ligand.

### 3. Zusammenfassung

In dieser Arbeit wurden drei Aspekte der Isocyanidchemie der Gruppe 7 betrachtet.

Zunächst wurde die Reaktivität von elektronenarmen Isocyaniden mit *facialen* Tricarbonyl-Ausgangsmaterialien untersucht. Erwartungsgemäß waren die Reaktionen mit Technetium signifikant schneller als mit Rhenium, und die Carbonylliganden von *fac*-[Tc(CO)<sub>3</sub>(CNR)<sub>2</sub>Cl] (R = <sup>t</sup>Bu, <sup>n</sup>Bu) konnten unter thermischen Bedingungen ausgetauscht werden, wobei das Zwischenprodukt *mer*-[Tc(CN<sup>p</sup>-FAr<sup>DArF2</sup>)<sub>3</sub>(CNR)<sub>2</sub>Cl] gebildet wurde. Der Chlorid-Ligand in dieser Verbindung kann mit Hilfe eines Halogenidfängers abstrahiert und durch einen sechsten Isocyanid-Liganden ersetzt werden, was zum ersten definierten heteroleptischen Hexakis(isocyanid)technetium(I)-Komplex führt: [Tc(CN<sup>p</sup>-FAr<sup>DArF2</sup>)<sub>3</sub>(CN<sup>n</sup>Bu)<sub>2</sub>(CN<sup>t</sup>Bu)] [PF<sub>6</sub>].

CNPh<sup>PF</sup> wurde dann verwendet, um die Reaktivität von elektronenarmen Isocyaniden ohne die sterische Hinderung, die durch die flankierenden Ringe des *m,m'*-Terphenylisocyanids CN<sup>p</sup>-FAr<sup>DArF2</sup> verursacht wird, zu untersuchen. In beiden Fällen erwies sich die Kombination aus <sup>99</sup>Tc- und <sup>19</sup>F-NMR-Spektroskopie als unverzichtbar, um den Fortschritt der Reaktion in Lösung zu überwachen. Die Verwendung der <sup>19</sup>F-NMR war für die Reaktion mit Rhenium noch wichtiger, da das Metallzentrum durch NMR nicht beobachtet werden kann. Die langsameren Reaktionsgeschwindigkeiten der Rheniumverbindungen ermöglichten die einfache Isolierung von Zwischenprodukten wie *fac*-[Re(CO)<sub>3</sub>(CNPh<sup>PF</sup>)<sub>2</sub>Br] oder *trans*-[Re(CO)(CNPh<sup>PF</sup>)<sub>4</sub>Br], deren Analoga im Fall von Technetium nur spektroskopisch beobachtet werden konnten.

In einem zweiten Teil der Arbeit wurde die Reaktivität von Isocyaniden mit hochvalenten Phenylimid-Ausgangsstoffen untersucht. Sowohl elektronische als auch sterische Faktoren haben den Reaktionsausgang beeinflusst. Das elektronendefiziente CNPh<sup>PF</sup> war in der Lage, die Technetium-Stickstoff-Bindung zu spalten und ersetzte die gesamte Koordinationssphäre, unter Bildung eines Hexakis(isocyanid)technetium(I)-Komplexes. Ein derart hoher Substitutionsgrad wurde für Rhenium nicht beobachtet und es konnte nur ein [Re(NPhF)(PPh<sub>3</sub>)(CNPh<sup>PF</sup>)Cl<sub>3</sub>]-Komplex erhalten werden. Andererseits konnten die elektronenreichen *m,m'*-Terphenylisocyanide CNAr<sup>Dipp2</sup> und CNAr<sup>Tripp2</sup> mit beiden Metallen Bis(isocyanid)-Komplexe bilden.

Die Reaktionen mit [Re(NPhF)Cl<sub>3</sub>(PPh<sub>3</sub>)<sub>2</sub>] zeigen auch, welche Rolle Fluorsubstituenten in der Koordinationschemie spielen können. Das nicht-fluorierte Ausgangsmaterial [Re(NPh)Cl<sub>3</sub>(PPh<sub>3</sub>)<sub>2</sub>] ist zu unlöslich für Reaktionen mit empfindlichen Isocyaniden und die Einbringung eines Fluoratoms auf dem Phenylimid-Ring erhöht die Löslichkeit. Darüber hinaus zeigt dieses Fluoratom kleine, aber signifikante Verschiebungen in den <sup>19</sup>F-NMR-Resonanzen, die zur Überwachung des Verlaufs solcher Reaktionen

verwendet wurden. Darüber hinaus bildet das elektronenarme und hochfluorierte CN*p*-FAR<sup>DArF2</sup> nur [M(NPhR)(PPh<sub>3</sub>)(CN*p*-FAR<sup>DArF2</sup>)Cl<sub>3</sub>] – Komplexe (M = Tc, Re), obwohl die sterische Hinderung des Liganden eine höhere Substitution nicht ausschließt.

Bemerkenswert ist, dass die IR-Schwingungen aller verwendeten Isocyanide eine hypsochrome Verschiebung bei Koordination an Re(V)- und Tc(V)-Zentren zeigen, d.h. sie agieren ausschließlich als  $\sigma$ -Donor.

Im letzten Teil dieser Arbeit wurden die gewonnenen Erkenntnisse über den Einfluss sterischer und elektronischer Parameter auf die Reaktivität von Isocyanid-Liganden genutzt, um einen funktionalisierbaren Isocyano-Liganden zu synthetisieren. Surface-Averaged-Donor-Acceptor-Potential-Parameter (SADAP) zeigten, dass das Alkin-funktionalisierte Isocyanid CNPh<sup>pC≡CH</sup> eine ähnliche Reaktivität aufweisen sollte wie der CNPh<sup>pF</sup> Ligand, der unter thermischen Bedingungen Carbonyl-Liganden ersetzt. Tatsächlich führte die Reaktion von (NBu<sub>4</sub>)[Tc<sub>2</sub>( $\mu$ -Cl)<sub>3</sub>(CO)<sub>6</sub>] mit CNPh<sup>pC≡CH</sup> zum (Hexakis)Isocyanid-Komplex [Tc(CNPh<sup>pC≡CH</sup>)<sub>6</sub>]<sup>+</sup>. Letzterer Komplex konnte mit Benzylazid unter Verwendung eines geeigneten Kupferkatalysators "geklickt" werden. Vergleichbaren Reaktionen mit wässrigem <sup>99m</sup>Tc sind aber wegen der harschen und inerten Reaktionsbedingungen ausgeschlossen. Der Cu(I)-Komplex [Cu(CNPh<sup>pC≡CH</sup>)<sub>4</sub>](BF<sub>4</sub>) konnte unter mildereren Bedingungen leicht synthetisiert und "geklickt" werden. Das resultierende [Cu(CNPh<sup>azole</sup>)<sub>4</sub>]<sup>+</sup> kann als Transmetallierungsreagenz für die Synthese des <sup>99m</sup>Tc Hexakis(isocyanid)technetium(I)-Komplexes verwendet werden. Alternativ kann das unkoordinierte 'Click'-Produkt durch Spaltung des [Cu(CNPh<sup>azole</sup>)<sub>4</sub>](BF<sub>4</sub>)-Komplexes mit wässrigem NaCN erhalten werden. Es reagiert mit *mer*-[Tc(CO)<sub>3</sub>(tth)(PPh<sub>3</sub>)<sub>2</sub>](BF<sub>4</sub>) (tth = Tetrahydrothiophen) unter dem Austausch des Thioetherliganden.

## 4. References

- (1) Perrier, C.; Segrè, E. Some Chemical Properties of Element 43. *J. Chem. Phys.* **1937**, *5*, 712-716.
- (2) Schwochau, K. *Technetium: chemistry and radiopharmaceutical applications*; John Wiley & Sons, **2008**.
- (3) de Jonge, F. A. A.; Pauwels, E. K. J. Technetium, the missing element. *Eur. J. Nucl. Med.* **1996**, *23*, 336-344.
- (4) Zingales, R. From Masurium to Trinacrium: The Troubled Story of Element 43. *J. Chem. Educ.* **2005**, *82*, 221.
- (5) Ali, S. A.; Ache, H. J. Production Techniques of Fission Molybdenum-99. *Radiochimica Acta* **1987**, *41*, 65-72.
- (6) Ozawa, M.; Ishida, M.; Sano, Y. Strategic Separation of Technetium and Rare Metal Fission Products in Spent Nuclear Fuel: Solvent Extraction Behavior and Partitioning by Catalytic Electrolytic Extraction. *Radiochemistry* **2003**, *45*, 225-232.
- (7) Abram, U. Rhenium. *Comprehensive Coordination Chemistry II* **2003**.
- (8) Noddack, W. T., I. . Die Ekamangane. *Die Naturwissenschaften* **1925**, *13*, 567-574.
- (9) Noddack, J.; Noddack, W. Die Herstellung von einem Gramm Rhenium. *Z. Anorg. Allg. Chem.* **1929**, *183*, 353-375.
- (10) Helm, L.; Deutsch, K.; Deutsch, E. A.; Merbach, A. E. Multinuclear NMR Studies of Ligand-Exchange Reactions on Analogous Technetium(V) and Rhenium(V) Complexes. Relevance to nuclear medicine. *Helv. Chim. Acta* **1992**, *75*, 210-217.
- (11) Bandoli, G.; Dolmella, A.; Porchia, M.; Refosco, F.; Tisato, F. Structural overview of technetium compounds (1993–1999). *Coord. Chem. Rev.* **2001**, *214*, 43-90.
- (12) Scholtysik, C.; Roca-Jungfer, M.; Hagenbach, A.; Abram, U. Reactions of [ReOCl<sub>3</sub>(PPh<sub>3</sub>)<sub>2</sub>] with 4-Fluoroaniline. *Z. Anorg. Allg. Chem.* **2018**, *644*, 1451-1455.
- (13) Scholtysik, C.; Njiki Noufele, C.; Hagenbach, A.; Abram, U. Complexes of Technetium(V) and Rhenium(V) with  $\beta$ -Diketonates. *Inorg. Chem.* **2019**, *58*, 5241-5252.
- (14) Figueroa, J. S.; Abram, U. Oxidorhenium(V) and Rhenium(III) Complexes with *m*-Terphenyl Isocyanides. *Z. Anorg. Allg. Chem.* **2020**, 909-914.
- (15) Meszaros, L. K.; Dose, A.; Biagini, S. C. G.; Blower, P. J. Hydrazinonicotinic acid (HYNIC) – Coordination chemistry and applications in radiopharmaceutical chemistry. *Inorg. Chim. Acta* **2010**, *363*, 1059-1069.
- (16) Braband, H. 5.08 - Organometallic Complexes of Technetium. In *Comprehensive Organometallic Chemistry IV*, Parkin, G., Meyer, K., O'Hare, D. Eds.; Elsevier, **2022**; 547-586.

- (17) Alberto, R.; Schibli, R.; Egli, A.; Abram, U.; Abram, S.; Kaden, T. A.; August Schubiger, P. Steps towards  $[(C_5Me_5)TcO_3]$ : Novel synthesis of  $[(C_5Me_5)Tc(CO)_3]$  from  $[Tc(\mu_3-OH)(CO)_3]_4$  and oxidation of  $[(C_5Me_5)M(CO)_3]$  ( $M = Tc, Re$ ) with  $Br_2$ . *Polyhedron* **1998**, *17*, 1133-1140.
- (18) Alberto, R.; Schibli, R.; Waibel, R.; Abram, U.; Schubiger, A. P. Basic aqueous chemistry of  $[M(OH_2)_3(CO)_3]^+$  ( $M=Re, Tc$ ) directed towards radiopharmaceutical application. *Coord. Chem. Rev.* **1999**, *190-192*, 901-919.
- (19) Wald, J.; Alberto, R.; Ortner, K.; Candreia, L. Aqueous One-Pot Synthesis of Derivatized Cyclopentadienyl–Tricarbonyl Complexes of  $^{99m}Tc$  with an In Situ CO Source: Application to a Serotonergic Receptor Ligand. *Angew. Chem. Int. Ed.* **2001**, *40*, 3062-3066.
- (20) Bernard, J.; Ortner, K.; Spingler, B.; Pietzsch, H. J.; Alberto, R. Aqueous Synthesis of Derivatized Cyclopentadienyl Complexes of Technetium and Rhenium Directed toward Radiopharmaceutical Application. *Inorg. Chem.* **2003**, *42*, 1014-1022.
- (21) Meola, G.; Braband, H.; Jordi, S.; Fox, T.; Blacque, O.; Spingler, B.; Alberto, R. Structure and reactivities of rhenium and technetium bis-arene sandwich complexes  $[M(\eta_6\text{-arene})_2]^+$ . *Dalton Trans.* **2017**, *46*, 14631-14637.
- (22) Ernst, M. J.; Roca Jungfer, M.; Abram, U. Reactions of  $Tc^I(NO)$  and  $Tc^V N$  Complexes with Alkynes and Alkynides. *Organometallics* **2022**, *41*, 2011-2021.
- (23) Oehlke, E.; Kong, S.; Arciszewski, P.; Wiebalck, S.; Abram, U. Aryl and NHC Compounds of Technetium and Rhenium. *J. Am. Chem. Soc.* **2012**, *134*, 9118-9121.
- (24) Schwochau, K. Technetium Radiopharmaceuticals—Fundamentals, Synthesis, Structure, and Development. *Angew. Chem. Int. Ed.* **1994**, *33*, 2258-2267.
- (25) Schlyer, D. J. PET tracers and radiochemistry. *Ann. Acad. Med. Singapore* **2004**, *33*, 146-154.
- (26) <https://world-nuclear.org/information-library/non-power-nuclear-applications/radioisotopes-research/radioisotopes-in-medicine.aspx> (accessed on 18/05/2023).
- (27) Li, Z.; Conti, P. S. Radiopharmaceutical chemistry for positron emission tomography. *Advanced Drug Delivery Reviews* **2010**, *62*, 1031-1051.
- (28) Eckelman, W. C. Unparalleled contribution of technetium-99m to medicine over 5 decades. *JACC-Cardiovasc. Imag* **2009**, *2*, 364-368.
- (29) Bartholomä, M. D.; Louie, A. S.; Valliant, J. F.; Zubieta, J. Technetium and Gallium Derived Radiopharmaceuticals: Comparing and Contrasting the Chemistry of Two Important Radiometals for the Molecular Imaging Era. *Chem. Rev.* **2010**, *110*, 2903-2920.
- (30) Abram, U.; Knop, G. Hexakis(isocynoessigsäureethylester)technetium(I)-tetraphenylboranat,  $[Tc(EIN)_6]BPh_4$ . *Z. Chem.* **1988**, *28*, 106-106.
- (31) Kronauge, J. F.; Mindiola, D. J. The Value of Stable Metal–Carbon Bonds in Nuclear Medicine and the Cardiolite Story. *Organometallics* **2016**, *35*, 3432-3435.



- (32) Meyer, C.; Prasad, V.; Stuparu, A.; Kletting, P.; Glating, G.; Miksch, J.; Solbach, C.; Lueckerath, K.; Nyiranshuti, L.; Zhu, S.; et al. Comparison of PSMA-TO-1 and PSMA-617 labeled with gallium-68, lutetium-177 and actinium-225. *EJNMMI Research* **2022**, *12*, 65.
- (33) Lepareur, N.; Lacœuille, F.; Bouvry, C.; Hindré, F.; Garcion, E.; Chérel, M.; Noiret, N.; Garin, E.; Knapp Jr, F. R. Rhenium-188 labeled radiopharmaceuticals: current clinical applications in oncology and promising perspectives. *Front. Med.* **2019**, *6*, 132.
- (34) Argyrou, M.; Valassi, A.; Andreou, M.; Lyra, M. Rhenium-188 Production in Hospitals, by W-188/Re-188 Generator, for Easy Use in Radionuclide Therapy. *Int. J. Mol. Imaging.* **2013**, *2013*, 290750.
- (35) Seifert, S.; Heinrich, T.; Jentschel, C.; Smuda, C.; Bergmann, R.; Pietzsch, H.-J. Preparation and Biological Characterization of Isomeric  $^{188}\text{Re(V)}$  Oxocomplexes with Tetradentate  $\text{S}_4$  Ligands Derived from meso-Dimercaptosuccinic Acid for Labeling of Biomolecules. *Bioconjugate Chem.* **2006**, *17*, 1601-1606.
- (36) Boschi, A.; Bolzati, C.; Uccelli, L.; Duatti, A. High-yield synthesis of the terminal  $^{188}\text{Re}\equiv\text{N}$  multiple bond from generator-produced  $[\text{}^{188}\text{ReO}_4]^-$ . *Nucl. Med. Biol.* **2003**, *30*, 381-387.
- (37) Boschi, A.; Uccelli, L.; Pasquali, M.; Pasqualini, R.; Guerrini, R.; Duatti, A. Mixed Tridentate; -Donor and Monodentate ; -Acceptor Ligands as Chelating Systems for Rhenium-188 and Technetium-99m Nitrido Radiopharmaceuticals. *Curr. Radiopharm.* **2013**, *6*, 137-145.
- (38) Cotton, F. A.; Zingales, F. The donor-acceptor properties of isonitriles as estimated by infrared study. *J. Am. Chem. Soc.* **1961**, *83*, 351-355.
- (39) Jones, A. G.; Davison, A.; Abrams, M. J. A new class of water soluble low valent technetium unipositive cations: hexakisisonitrile technetium(I) salts. *J. Labelled Compd. Radiopharm.* **1982**, *19*, 1594-1595.
- (40) Abrams, M. J.; Davison, A.; Jones, A. G.; Costello, C. E.; Pang, H. Synthesis and characterization of hexakis (alkyl isocyanide) and hexakis (aryl isocyanide) complexes of technetium (I). *Inorg. Chem.* **1983**, *22*, 2798-2800.
- (41) Abrams, M. J.; Davison, A.; Faggiani, R.; Jones, A. G.; Lock, C. J. L. Chemistry and structure of hexakis(thiourea-S)technetium(III) trichloride tetrahydrate,  $[\text{Tc}(\text{SC}(\text{NH}_2)_2)_6]\text{Cl}_3 \cdot 4\text{H}_2\text{O}$ . *Inorg. Chem.* **1984**, *23*, 3284-3288.
- (42) Abram, U.; Beyer, R.; Münze, R.; Findeisen, M.; Lorenz, B. Mixed-ligand complexes of technetium. Iv. Cationic, hexa-coordinated Tc(I) complexes with two different isocyanide ligands in the coordination sphere,  $[\text{Tc}(\text{R}_1\text{NC})_k(\text{R}_2\text{NC})_{6-k}]^+$  ( $k = 0-6$ ). *Inorg. Chim. Acta* **1989**, *160*, 139-142.
- (43) Linder, K. E.; Davison, A.; Dewan, J. C.; Costello, C. E.; Maleknia, S. Nitrosyl complexes of technetium: synthesis and characterization of  $[\text{Tc}^{\text{I}}(\text{NO})(\text{CNCMe}_3)_5](\text{PF}_6)_2$  and  $\text{Tc}(\text{NO})\text{Br}_2(\text{CNCMe}_3)_3$  and the crystal structure of  $\text{Tc}(\text{NO})\text{Br}_2(\text{CNCMe}_3)_3$ . *Inorg. Chem.* **1986**, *25*, 2085-2089.

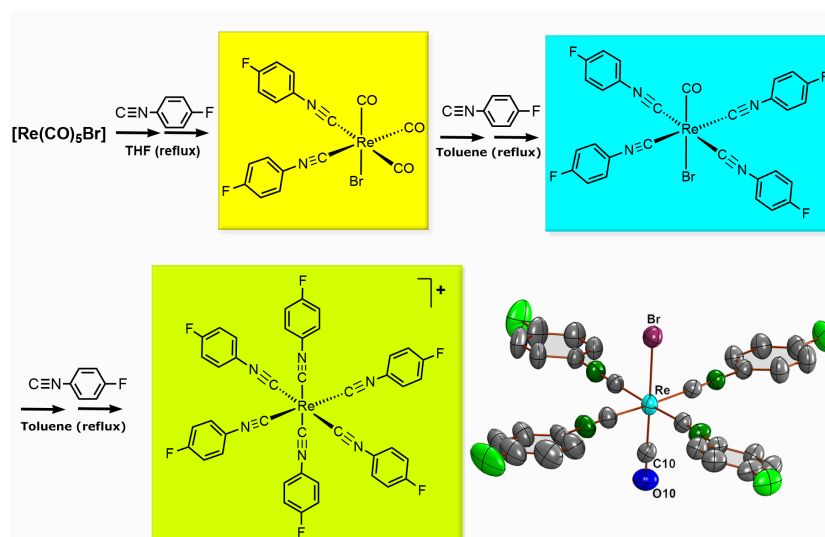
- (44) Farr, J. L.; Abrams, M. J.; Costello, C. E.; Davison, A.; Lippard, S. J.; Jones, A. G. Higher coordinate complexes. Part 22. Synthesis and reactions of seven-coordinate technetium and rhenium alkyl isocyanide complexes. *Organometallics* **1985**, *4*, 139-142.
- (45) Alberto, R.; Schibli, R.; Egli, A.; August Schubiger, P.; Herrmann, W. A.; Artus, G.; Abram, U.; Kaden, T. A. Metal carbonyl syntheses XXII. Low-pressure carbonylation of  $[\text{MOCl}_4]^-$  and  $[\text{MO}_4]^-$ . The technetium(I) and rhenium(I) complexes  $[\text{NEt}_4]_2[\text{MCl}_3(\text{CO})_3]$ . *J. Organomet. Chem.* **1995**, *492*, 217-224.
- (46) Alberto, R.; Schibli, R.; Schubiger, P. A.; Abram, U.; Kaden, T. A. Reactions with the technetium and rhenium carbonyl complexes  $(\text{NEt}_4)_2[\text{MX}_3(\text{CO})_3]$ . Synthesis and structure of  $[\text{Tc}(\text{CN-But})_3(\text{CO})_3](\text{NO}_3)$  and  $(\text{NEt}_4)[\text{Tc}_2(\mu\text{-SCH}_2\text{CH}_2\text{OH})_3(\text{CO})_6]$ . *Polyhedron* **1996**, *15*, 1079-1089.
- (47) Rochon, F. D.; Melanson, R.; Kong, P.-C. Synthesis and crystal structure of mixed-ligand Tc(I) complexes, with dimethylphenylphosphine and t-butylisonitrile. *Inorg. Chim. Acta* **1996**, *245*, 251-256.
- (48) Patil, P.; Ahmadian-Moghaddam, M.; Dömling, A. Isocyanide 2.0. *Green Chemistry* **2020**, *22*, 6902-6911.
- (49) Stewart, M. A.; Moore, C. E.; Ditre, T. B.; Labios, L. A.; Rheingold, A. L.; Figueroa, J. S. Electrophilic functionalization of well-behaved manganese monoanions supported by m-terphenyl isocyanides. *Chem. Commun.* **2011**, *47*, 406-408.
- (50) Drance, M. J.; Sears, J. D.; Mrse, A. M.; Moore, C. E.; Rheingold, A. L.; Neidig, M. L.; Figueroa, J. S. Terminal coordination of diatomic boron monofluoride to iron. *Science* **2019**, *363*, 1203-1205.
- (51) Wang, S.; Sears, J. D.; Moore, C. E.; Rheingold, A. L.; Neidig, M. L.; Figueroa, J. S. Side-on coordination of diphosphorus to a mononuclear iron center. *Science* **2022**, *375*, 1393-1397.
- (52) Agnew, D. W.; Moore, C. E.; Rheingold, A. L.; Figueroa, J. S. Kinetic Destabilization of Metal–Metal Single Bonds: Isolation of a Pentacoordinate Manganese(0) Monoradical. *Angew. Chem. Int. Ed.* **2015**, *54*, 12673-12677.
- (53) Agnew, D. W.; Moore, C. E.; Rheingold, A. L.; Figueroa, J. S. Controlled cis Labilization of CO from Manganese(I) Mixed Carbonyl/Isocyanide Complexes: An Entry Point to Coordinatively Unsaturated Metallo-Lewis Acids. *Organometallics* **2017**, *36*, 363-371.
- (54) Claude, G.; Salsi, F.; Hagenbach, A.; Gembicky, M.; Neville, M.; Chan, C.; Figueroa, J. S.; Abram, U. Structural and Redox Variations in Technetium Complexes Supported by m-Terphenyl Isocyanides. *Organometallics* **2020**, *39*, 2287-2294.
- (55) Salsi, F.; Shuai, W.; Teutloff, C.; Busse, M.; Neville, M. L.; Hagenbach, A.; Bittl, R.; Figueroa, J. S.; Abram, U. A Complete Triad of Zero-Valent 17-Electron Monoradicals of Group 7 Elements Stabilized by m-Terphenyl Isocyanides. *Angew. Chem. Int. Ed.* **2023**, *62*, e202300254,
- (56) Salsi, F.; Neville, M.; Drance, M.; Hagenbach, A.; Figueroa, J. S.; Abram, U.  $\{\text{M}^{\text{I}}(\text{CO})\text{X}(\text{CNAr}^{\text{DARF}2})_4\}$  (DARF = 3,5-(CF<sub>3</sub>)<sub>2</sub>C<sub>6</sub>H<sub>3</sub>; M = Re and Tc; X = Br and Cl) Complexes: Convenient Platforms for the Synthesis of Low-Valent Rhenium and Technetium Compounds. *Organometallics* **2021**, *40*, 1336-1343.

- (57) Lentz, D. Fluorinated Isocyanides—More than Ligands with Unusual Properties. *Angew. Chem. Int. Ed.* **1994**, *33*, 1315-1331,
- (58) Hieber, W.; Böckly, E. Über Metallcarbonyle. XLVIII. Neue Substitutionsreaktionen an Nickel- und Kobaltcarbonylen: Metallisonitrile. *Z. Anorg. Allg. Chem.* **1950**, *262*, 344-352.
- (59) Ugi, I.; Meyr, R. Neue Darstellungsmethode für Isonitrile. *Angew. Chem.* **1958**, *70*, 702-703.
- (60) Fox, B. J.; Sun, Q. Y.; DiPasquale, A. G.; Fox, A. R.; Rheingold, A. L.; Figueroa, J. S. Solution behavior and structural properties of Cu(I) complexes featuring *m*-terphenyl isocyanides. *Inorg. Chem.* **2008**, *47*, 9010-9020.
- (61) Claude, G.; Genz, J.; Weh, D.; Roca Jungfer, M.; Hagenbach, A.; Gembicky, M.; Figueroa, J. S.; Abram, U. Mixed-Isocyanide Complexes of Technetium under Steric and Electronic Control. *Inorg. Chem.* **2022**, *61*, 16163-16176.
- (62) Salsi, F.; Neville, M.; Drance, M.; Hagenbach, A.; Chan, C.; Figueroa, J. S.; Abram, U. A closed-shell monomeric rhenium(1-) anion provided by *m*-terphenyl isocyanide ligation. *Chem. Commun.* **2020**, *56*, 7009-7012.
- (63) Treichel, P. M.; Williams, J. P. Rhenium(I) isocyanide complexes. *J. Organomet. Chem.* **1977**, *135*, 39-51.



## 5. Publications

### 5.1. Rhenium Complexes with p-Fluorophenylisocyanide



Reproduced from Claude, G.; Weh, D.; Hagenbach, A.; Figueroa, J. S.; Abram, U. Rhenium Complexes with p-Fluorophenylisocyanide. *Z. Anorg. Allg. Chem.* **2022**, *649*, e202200320.

DOI: 10.1002/zaac.202200320

© 2022 The Authors. Zeitschrift für anorganische und allgemeine Chemie published by Wiley-VCH GmbH

#### Author Contributions:

Guilhem Claude, Ulrich Abram and Joshua Figueroa designed the project. Guilhem Claude performed the synthesis and characterization of the compounds. Guilhem Claude and Adelheid Hagenbach calculated the X-ray structures. Domenik Weh performed some of the experiments during a research internship under the supervision of Guilhem Claude. Ulrich Abram and Joshua Figueroa supervised the project, provided scientific guidance and suggestions, and wrote a draft of the manuscript.

DOI: 10.1002/zaac.202200320

## Rhenium Complexes with p-Fluorophenylisocyanide

Guilhem Claude,<sup>[a]</sup> Dominik Weh,<sup>[a]</sup> Adelheid Hagenbach,<sup>[a]</sup> Joshua S. Figueroa,<sup>[b]</sup> and Ulrich Abram<sup>\*[a]</sup>

p-Fluorophenylisocyanide (CNPh<sup>F</sup>) reacts with [Re(CO)<sub>5</sub>Br] under stepwise exchange of the carbonyl ligands depending on the conditions applied. The reaction stops with the formation of *fac*-[Re(CO)<sub>3</sub>Br(CNPh<sup>F</sup>)<sub>2</sub>] in boiling THF. An ongoing carbonyl exchange is observed at higher temperatures, e.g. in refluxing

toluene, with the final formation of the [Re(CNPh<sup>F</sup>)<sub>6</sub>]<sup>+</sup> cation. The progress of the reactions has been studied by <sup>19</sup>F NMR spectroscopy and the structures of [Re(CO)Br(CNPh<sup>F</sup>)<sub>4</sub>] and [Re(CNPh<sup>F</sup>)<sub>6</sub>](BPh<sub>4</sub>) have been elucidated by X-ray diffraction.

The frequent use of an hexakis(isocyanide) complex of technetium (<sup>99m</sup>Tc-Sestamibi or Cardiolite)<sup>[1–3]</sup> in diagnostic nuclear medicine has also stimulated the related chemistry of rhenium.<sup>[4–9]</sup> Rhenium complexes are frequently used as (almost) non-radioactive mimics for the corresponding technetium compounds, but there are also two beta-emitting nuclei (<sup>186</sup>Re: half-life 90 h, E<sub>βmax</sub> = 1.09 MeV and <sup>188</sup>Re: half-life 16.9 h, E<sub>βmax</sub> = 2.12 MeV),<sup>[10]</sup> which are under discussion for applications in nuclear medical therapy. Particularly <sup>188</sup>Re is readily available for the clinical sites from an alumina-based <sup>188</sup>W/<sup>188</sup>Re generator system, from which the isotope can be eluted when it is required.<sup>[11]</sup>

Mixed carbonyl/isocyanide complexes are under consideration for a long time not only as potential imaging agents, but also because of their interesting optical properties and as potential anticancer drugs.<sup>[12–16]</sup> For both fields, corresponding CO/CNR exchange reactions are of interest and for the most alkyl isocyanides reactions starting from [Re(CO)<sub>5</sub>Br] or [Re(CO)<sub>3</sub>(X)<sub>3</sub>]<sup>+2-</sup> complexes (X=solvent, halide) form products with the *fac*-tricarbonyl core.<sup>[17]</sup> Under mild conditions, frequently two isocyanides are introduced and products of the composition [Re(CO)<sub>3</sub>(X)(CNR)<sub>2</sub>]<sup>+0</sup> are formed,<sup>[5,13,17–19]</sup> while the introduction of a third isocyanide ligands usually requires a halide scavenger.<sup>[12,18]</sup> A slightly different behavior has been observed for aryl isocyanides, which may allow an ongoing

carbonyl exchange depending on their substitutions. First reports about this point can be found in an early paper of Treichel and Williams,<sup>[17]</sup> and during our experiments with technetium and rhenium complexes with sterically encumbered m-terphenyl isocyanides we found that particularly the p-fluorinated isocyanide CNp-FAR<sup>Darf2</sup> (see Scheme 1) does not stop with the replacement of three carbonyl ligands. Irrespective of its steric bulk it forms the tetrakis(isocyanide) complex [Re(CO)Br(CNp-FAR<sup>Darf2</sup>)<sub>4</sub>] (3) (Scheme 1).<sup>[20]</sup> The tris(isocyanide) complex 2 could be isolated as well for rhenium, while a similar reaction with the common technetium starting material (NBu<sub>4</sub>)[Tc<sub>2</sub>(CO)<sub>6</sub>(Cl)<sub>3</sub>] gives quantitatively the tetrakis compound. Such a difference in the reactivity is not unexpected keeping in mind the slower kinetics in exchange reactions of rhenium compared with technetium.<sup>[21]</sup>

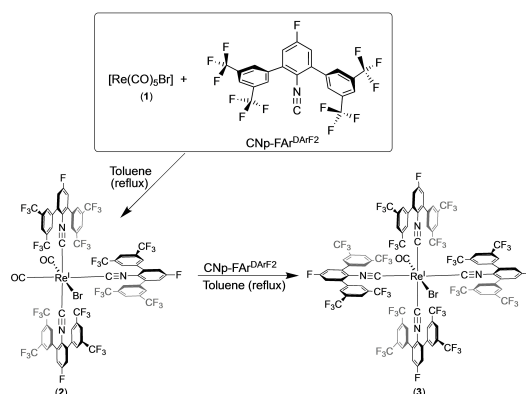
Very recently, we found that the bulky CNp-FAR<sup>Darf2</sup> shows a remarkable reactivity also with other synthons such as *fac*-[Tc(CO)<sub>3</sub>Cl(CN<sup>t</sup>Bu)<sub>2</sub>] (CN<sup>t</sup>Bu = t-butylisocyanide), where it replaced selectively the three carbonyl ligands and gave the mixed-isocyanide complex [Tc(CNp-FAR<sup>Darf2</sup>)<sub>3</sub>Cl(CN<sup>t</sup>Bu)<sub>2</sub>].<sup>[22]</sup> On the basis of DFT calculations,<sup>[22]</sup> we address the observed

[a] G. Claude, D. Weh, Dr. A. Hagenbach, Prof. U. Abram  
Institute of Chemistry and Biochemistry,  
Freie Universität Berlin,  
Fabeckstr. 34/36, D-14195 Berlin, Germany  
E-mail: Ulrich.Abram@fu-berlin.de

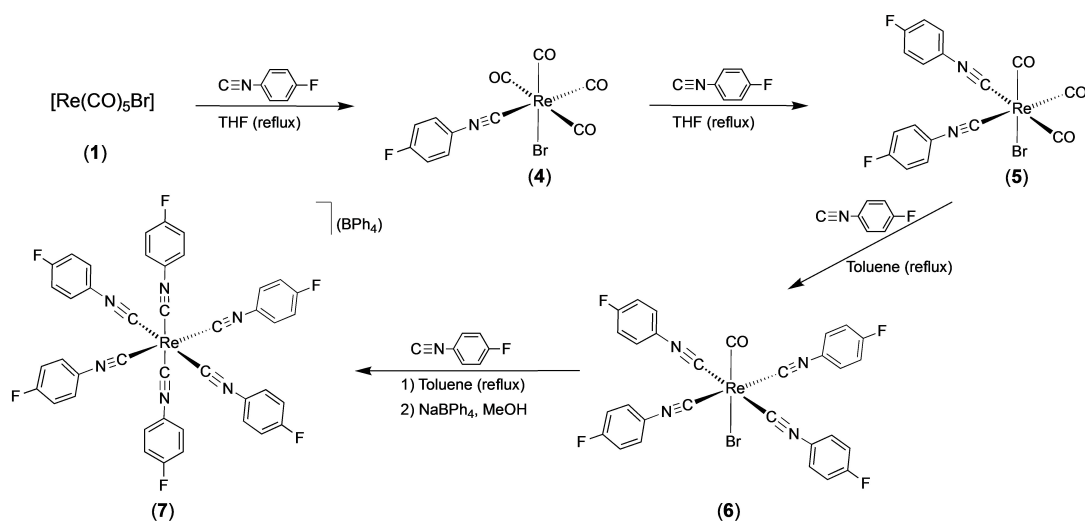
[b] Prof. J. S. Figueroa  
Department of Chemistry and Biochemistry  
University of California, San Diego, La Jolla,  
California 92093, United States

Supporting information for this article is available on the WWW under <https://doi.org/10.1002/zaac.202200320>

© 2022 The Authors. Zeitschrift für anorganische und allgemeine Chemie published by Wiley-VCH GmbH. This is an open access article under the terms of the Creative Commons Attribution License, which permits use, distribution and reproduction in any medium, provided the original work is properly cited.



Scheme 1. Reactions of [Re(CO)<sub>5</sub>Br] (1) with the sterically encumbered isocyanide CNp-FAR<sup>Darf2</sup>.<sup>[20]</sup>



Scheme 2. Stepwise ligand exchange with  $\text{CNPh}^{\text{PF}}$  starting from  $[\text{Re}(\text{CO})_5\text{Br}]$  (1).

reactivity to the fluorine substituent on the central phenyl ring, while the steric bulk of the ligands limits the extend of potential exchange reactions. For a further insight into the electronic and steric effects of such reactions, we performed reactions of  $(\text{NBu}_4)[\text{Tc}_2(\text{CO})_6\text{Cl}_3]$  and  $[\text{Tc}(\text{CO})_3\text{Cl}(\text{CN}^t\text{Bu})_2]$  with *p*-fluorophenylisocyanide ( $\text{CNPh}^{\text{PF}}$ ), during which the entire coordination sphere of technetium was replaced and the  $[\text{Tc}(\text{CNPh}^{\text{PF}})_6]^+$  cation was formed.<sup>[22]</sup> Having in mind the slower ligand exchange kinetics for the 'third transition row' elements, we decided to extend these experiments also to related rhenium complexes.

Attempted reactions of  $[\text{Re}(\text{CO})_3\text{Cl}(\text{CN}^t\text{Bu})_2]$  with  $\text{Cnp-FAr}^{\text{Darf2}}$  did not result in the replacement of carbonyl ligands as was observed for the technetium analog. Even after prolonged heating (3 days!) in toluene there was no evidence for the formation of defined mixed isocyanide complexes and an gradual decomposition of the ligand and intermediate products was observed by subsequently recorded  $^{19}\text{F}$  NMR spectra.

In contrast, reactions with  $\text{CNPh}^{\text{PF}}$  are more defined and the ligand exchange starting from  $[\text{Re}(\text{CO})_5\text{Br}]$  proceeds under a stepwise replacement of carbonyl ligands (Scheme 2). The rate of the exchange is generally slow, but can be controlled by the reaction temperature. In boiling THF, up to two CO ligands are replaced. The intermediate formation of the monosubstitution product  $[\text{Re}(\text{CO})_4\text{Br}(\text{CNPh}^{\text{PF}})]$  (4) is indicated by a  $^{19}\text{F}$  NMR signal at 109.3 ppm, which could be recorded in the reaction mixture during the early stages of the reaction. Subsequent recordings of  $^{19}\text{F}$  NMR spectra of the reaction mixture are shown in Figure 1, in which only the signals of two ligand exchange products could be detected. While no pure samples of the transient compound 4 could be isolated from such reactions, the final product *fac*- $[\text{Re}(\text{CO})_3\text{Br}(\text{CNPh}^{\text{PF}})_2]$  (5) was obtained as a colorless solid in good yields.

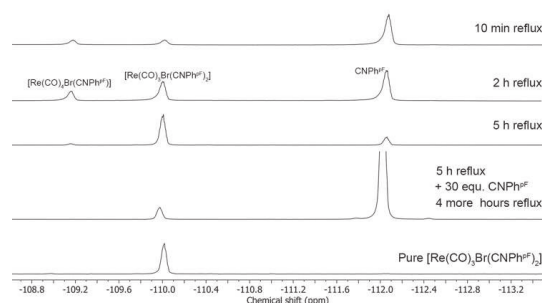


Figure 1.  $^{19}\text{F}$  NMR spectra of the stepwise CO/ $\text{CNPh}^{\text{PF}}$  exchange starting from  $[\text{Re}(\text{CO})_5\text{Br}]$  (1) in boiling THF and of pure  $[\text{Re}(\text{CO})_3\text{Br}(\text{CNPh}^{\text{PF}})_2]$  (5) in THF.

The IR spectrum of 5 shows the  $\nu_{(\text{CO})}$  stretches at 1916, 1973 and  $2026\text{ cm}^{-1}$ , while the  $\nu_{(\text{CN})}$  bands appear at 2153 and  $2183\text{ cm}^{-1}$ . The latter values are higher than that of the uncoordinated isocyanide ( $2129\text{ cm}^{-1}$ ), which suggests that the isocyanide does not act as  $\pi$ -acceptor in compound 5. This is in accord with other rhenium or technetium complexes of the general composition  $[\text{M}(\text{CO})_3\text{X}(\text{CNR})_2]$ .<sup>[12,13,17,18,23–28]</sup> The ESI + mass spectrum of 5 shows an intense signal at  $m/z = 614.914$  for the cluster ion  $\{\text{M} + \text{Na}\}^+$  with the expected isotopic pattern. Details are shown in the Supporting Information.

Prolonged heating of the above mentioned reaction mixture in THF did not give higher carbonyl/isocyanide exchange rates, even when additional  $\text{Ag}(\text{PF}_6)$  was added as  $\text{Br}^-$  scavenger.  $^{19}\text{F}$  NMR spectra of such reaction mixtures indicate a gradual decomposition of  $\text{CNPh}^{\text{PF}}$  in such solutions by the appearances of numerous  $^{19}\text{F}$  signals (see Supporting Information). All our

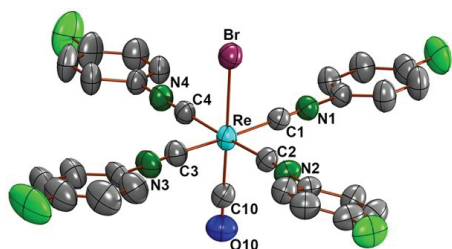
attempts to isolate the expected tris complex  $[\text{Re}(\text{CO})_3(\text{CNPh}^{\text{PF}})_3]^+$  from such solutions failed.

An ongoing ligand exchange, however, is observed at higher temperatures, e.g. in boiling toluene, and species such as  $[\text{Re}(\text{CO})\text{Br}(\text{CNPh}^{\text{PF}})_4]$  and  $[\text{Re}(\text{CNPh}^{\text{PF}})_6]^+$  could be assigned unambiguously in the  $^{19}\text{F}$  NMR spectra of such solutions. Two more signals with an intensity ratio of 4:1 can be assigned to  $[\text{ReBr}(\text{CNPh}^{\text{PF}})_5]$  or  $[\text{Re}(\text{CO})(\text{CNPh}^{\text{PF}})_5]^+$ . The spectra of such a reaction sequence are shown as Supporting Information. In the course of the reaction, the initially clear mixture became turbid and gradually a colorless solid precipitated. This solid contains charged species (mainly  $[\text{Re}(\text{CNPh}^{\text{PF}})_6]\text{Br}$ ) which are only sparingly soluble in toluene, while the neutral species (mainly  $[\text{Re}(\text{CO})\text{Br}(\text{CNPh}^{\text{PF}})_4]$  (**6**)) remain in solution.

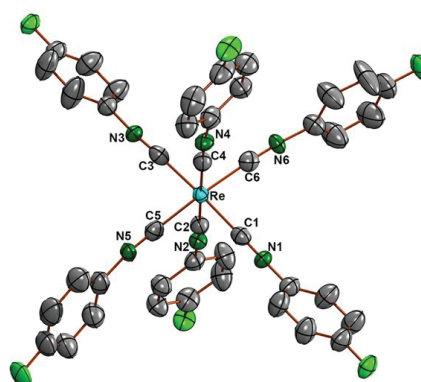
Yellow crystals of compound **6** can be obtained by concentration of the mother liquor, filtration from the precipitated salt(s) and crystallization from  $\text{CH}_2\text{Cl}_2/n$ -pentane in a yield of approximately 30%. The compound is readily soluble in polar solvents. The  $\nu_{(\text{CO})}$  band appears at a low value of  $1874\text{ cm}^{-1}$ , but unlike in compound **5** also the  $\nu_{(\text{CN})}$  frequency ( $2065\text{ cm}^{-1}$ ) is bathochromically shifted against the value in the uncoordinated isocyanide indicating that  $\text{CNPh}^{\text{PF}}$  participates in the withdrawal of electron density from the  $d^6$  ion by  $\pi$ -backbonding in the tetrakis complex.

The ESI+ mass spectrum of  $[\text{Re}(\text{CO})\text{Br}(\text{CNPh}^{\text{PF}})_4]$  (**6**) in acetonitrile shows an intense signal at  $m/z = 740.107$ , which can be assigned to the  $\{\text{M}-\text{Br} + \text{CH}_3\text{CN}\}^+$  ion, but also the molecular ion  $\{\text{M} + \text{Na}\}^+$  is visible with lower intensity at  $m/z = 800.986$ . Similar to the spectrum of compound **5**, also that of  $[\text{Re}(\text{CO})\text{Br}(\text{CNPh}^{\text{PF}})_4]$  (**6**) gives evidence for the formation of dimeric species in the mass spectrometer (for details see Experimental and Supporting Information).

Single crystals of **6** were obtained by slow diffusion of *n*-pentane into a solution of the complex in  $\text{CH}_2\text{Cl}_2$ . Figure 2 shows an ellipsoid representation of the molecular structure of the complex with an almost perfectly planar equatorial coordination sphere formed by the four  $\text{CNPh}^{\text{PF}}$  ligands. Minor deviations are only due to the  $\text{C}10\text{-Re-C}1/\text{C}4$  angles being slightly larger than  $90^\circ$  due to the bulk of the CO ligand. Selected bond lengths and angles can be found in the Supporting Information.



**Figure 2.** Molecular structure of  $[\text{Re}(\text{CO})\text{Br}(\text{CNPh}^{\text{PF}})_4]$  (**6**). Ellipsoids represent 50% probability. Hydrogen atoms have been omitted for clarity.



**Figure 3.** Ellipsoid representation of the  $[\text{Re}(\text{CNPh}^{\text{PF}})_6]^+$  cation in **7**. Ellipsoids represent 50% probability. Hydrogen atoms have been omitted for clarity.

The colorless solid removed from the reaction mixture in toluene dissolves in MeOH. Addition of  $\text{Na}(\text{BPh}_4)$  to such a solution gives a colorless precipitate, which is readily soluble in dichloromethane. Single crystals of  $[\text{Re}(\text{CNPh}^{\text{PF}})_6](\text{BPh}_4)$  were grown from  $\text{CH}_2\text{Cl}_2/n$ -pentane. Since there are hitherto only two examples of homoleptic hexakis(isocyanide)rhenium(I) cations are studied crystallographically, we undertook an X-ray diffraction study on compound **7**.<sup>[9,29]</sup> Figure 3 shows the structure of the  $[\text{Re}(\text{CNPh}^{\text{PF}})_6]^+$  cation. The coordination environment of the rhenium atom is an almost perfect octahedron with *cis*- $\text{C}-\text{Re}-\text{C}$  angles between  $87.2(2)$  and  $92.7(2)^\circ$ . Details about individual bond lengths and angles are contained in the Supporting Information.

The ESI+ mass spectrum of **7** is dominated by the molecular ion at  $m/z = 913.151$  and the  $\nu_{(\text{CN})}$  stretch appears at  $2074\text{ cm}^{-1}$  in its IR spectrum. The latter value confirms the expected back-donation to the isocyanide ligands in the homoleptic rhenium(I) complex.

Summarizing, it can be stated that the introduction of a fluorine atom in 4-position of the phenyl ring increases the reactivity of arylisocyanides with  $d^6$  metal centers such as Tc(I) or Re(I) carbonyl complexes and that depending on the reaction conditions applied a complete exchange of the coordination sphere of the metal ions and the formation of  $[\text{M}(\text{CNPh}^{\text{PF}})_6]^+$  cations ( $\text{M} = \text{Tc}, \text{Re}$ ) can be achieved. The exchange rate is faster with technetium, where only the final products could be obtained, while for rhenium intermediates such as  $[\text{Re}(\text{CO})_3\text{Br}(\text{CNPh}^{\text{PF}})_2]$  or  $[\text{Re}(\text{CO})\text{Br}(\text{CNPh}^{\text{PF}})_4]$  could be isolated. The results of the present communication can be regarded as another experimental proof of the old paradigm of Dieter Lentz that "fluorinated isocyanides are more than ligands with unusual properties".<sup>[30]</sup>



## Experimental Section

Details about the crystallographic studies and the spectroscopic instrumentation are given as Supporting Information. Unless otherwise stated, reagent-grade starting materials were purchased from commercial sources and either used as received or purified by standard procedures. Solvents were dried and deoxygenated according to standard procedures. The synthesis of CNPh<sup>PF</sup> was done by adapted literature procedures.<sup>[31]</sup>

*fac*-[Re(CO)<sub>3</sub>Br(CNPh<sup>PF</sup>)<sub>2</sub>] (**5**): [Re(CO)<sub>5</sub>Br] (40.6 mg, 0.1 mmol) was dissolved in 4 mL of THF. CNPh<sup>PF</sup> (120 μL, 1 mmol) was added and the mixture was heated on reflux for 8 h. The progress of the reaction was monitored by <sup>19</sup>F NMR spectroscopy. After completion of the reaction, all volatiles were removed and the obtained light brown residue was suspended in *n*-hexane, filtered and washed with several portions of *n*-hexane. The obtained colorless solid was dried under reduced pressure. Yield: 45 mg (0.076 mmol, 76%). Elemental analysis: Calcd. for: C<sub>17</sub>H<sub>6</sub>BrF<sub>2</sub>N<sub>2</sub>O<sub>3</sub>Re: C, 34.47, H, 1.36, N, 4.73, found: C, 34.90, H 1.62, N, 4.78. IR (ATR, cm<sup>-1</sup>): ν(CN) 2188 (sh), ν(CN) 2153 (s), ν(CO) 2026 (s). ν(CO) 1973 (s), ν(CO) 1916 (s). <sup>1</sup>H NMR (CD<sub>2</sub>Cl<sub>2</sub>, ppm): 7.53 (m<sub>c</sub>, 4H), 7.18 (m<sub>c</sub>, 4H). <sup>13</sup>C{<sup>1</sup>H} NMR (CD<sub>2</sub>Cl<sub>2</sub>, ppm): 186.6, 184.2, 163.4 (d, <sup>1</sup>J(<sup>19</sup>F-<sup>13</sup>C)=250 Hz), 143.9, 129.7 (d, <sup>3</sup>J(<sup>19</sup>F-<sup>13</sup>C)=9 Hz), 123.4, 117.5 (d, <sup>2</sup>J(<sup>19</sup>F-<sup>13</sup>C)=24 Hz). <sup>19</sup>F NMR (CD<sub>2</sub>Cl<sub>2</sub>, ppm): -107.48 (m<sub>c</sub>). ESI+ MS (acetonitrile): 614.914 ([M+Na]<sup>+</sup>; calcd 614.914), 630.887 ([M+K]<sup>+</sup>; calcd 630.888), 1206.835 ([2M+Na]<sup>+</sup>; calcd 1206.838).

*trans*-[Re(CO)Br(CNPh<sup>PF</sup>)<sub>2</sub>] (**6**): [Re(CO)<sub>5</sub>Br] (40.6 mg, 0.1 mmol) was dissolved in 6 mL of toluene. CNPh<sup>PF</sup> (120 μL, 1 mmol) was added and the reaction mixture was heated on reflux for 4 h. Another portion of CNPh<sup>PF</sup> (120 μL, 1 mmol) was added and the mixture was heated on reflux for another 14 h. The volatiles were removed in vacuum, methanol (5 mL) was added and the remaining solid was filtered off. It was washed with methanol (2 mL) and dissolved in CH<sub>2</sub>Cl<sub>2</sub>. Diffusion of *n*-pentane into this solution gave yellow crystals suitable for X-Ray diffraction. They were isolated by filtration and washed with MeOH (2 mL) and *n*-pentane (2 mL) and dried under reduced pressure. Yield: 24 mg (0.031 mmol, 31%). Elemental analysis: Calcd. for: C<sub>29</sub>H<sub>16</sub>BrF<sub>4</sub>N<sub>4</sub>ORe: C, 44.74; H, 2.07; N, 7.20. Found: C, 44.87; H, 2.40; N, 6.79. IR (ATR): ν(CN) 2065 (s), ν(CO) 1874 (s), ν(CO) 2040 (s). <sup>1</sup>H NMR (CD<sub>2</sub>Cl<sub>2</sub>, ppm): 7.43 (m<sub>c</sub>, 8H, m, aryl-H), 7.12 (m<sub>c</sub>, 8H, aryl-H). <sup>13</sup>C{<sup>1</sup>H} NMR (CD<sub>2</sub>Cl<sub>2</sub>, ppm): 190.71, 162.39 (d, <sup>1</sup>J(<sup>19</sup>F-<sup>13</sup>C)=250 Hz), 154.63, 129.02 (d, <sup>3</sup>J(<sup>19</sup>F-<sup>13</sup>C)=9 Hz), 125.40, 117.07 (d, <sup>2</sup>J(<sup>19</sup>F-<sup>13</sup>C)=24 Hz). <sup>19</sup>F NMR (CDCl<sub>3</sub>, ppm): -110.7 (m<sub>c</sub>). ESI+ MS (acetonitrile): 740.108 ([M-Br+MeCN]<sup>+</sup>; calcd 740.108), 800.986 ([M+Na]<sup>+</sup>; calcd 800.990), 1477.076 ([2M-Br]<sup>+</sup>; calcd 1477.082), 1578.985 ([2M+Na]<sup>+</sup>; calcd 1578.990), 1595.957 ([2M+K]<sup>+</sup>; calcd 1594.964).

[Re(CNPh<sup>PF</sup>)<sub>2</sub>](BPh<sub>4</sub>) (**7**): Na(BPh<sub>4</sub>) (340 mg, 1.00 mmol) was added to the filtrate obtained from the synthesis of compound **6**, which resulted in the precipitation of a colorless solid. The solid was filtered off and was washed with methanol (3 mL) and diethyl ether (3 mL). Recrystallization was performed from CH<sub>2</sub>Cl<sub>2</sub>/pentane. Colorless crystals suitable for X-ray diffraction were obtained. The crystals were washed with MeOH and diethyl ether and dried under reduced pressure. Yield: 37 mg (0.030 mmol, 30%). Elemental analysis: Calcd. for: C<sub>66</sub>H<sub>44</sub>BF<sub>6</sub>N<sub>4</sub>Re: C, 64.34; H, 3.60; N, 6.86. Found: C, 63.36; H, 3.48; N, 6.25. IR (ATR, cm<sup>-1</sup>): ν(CN) 2074 (s). <sup>1</sup>H NMR (CD<sub>2</sub>Cl<sub>2</sub>, ppm): 7.44–7.35 (12H, m, pF-aryl-H), 7.30 (8H, dt, J=7.1, 3.4 Hz, phenyl-H), 7.19–7.09 (12H, m, pF-aryl-H), 7.02 (8H, t, J=7.3 Hz, phenyl-H), 6.86 (4H, t, J=7.2 Hz, phenyl-H). <sup>13</sup>C{<sup>1</sup>H} NMR (CD<sub>2</sub>Cl<sub>2</sub>, ppm): 164.61 (q, <sup>1</sup>J(<sup>13</sup>B-<sup>13</sup>C)=50 Hz), 162.59 (d, <sup>1</sup>J(<sup>19</sup>F-<sup>13</sup>C)=250 Hz), 136.48 (s); 128.89 (d, <sup>3</sup>J(<sup>19</sup>F-<sup>13</sup>C)=9 Hz), 126.17 (q, <sup>2</sup>J(<sup>13</sup>B-<sup>13</sup>C)=3 Hz), 125.11, 122.24, 117.48 <sup>2</sup>J(<sup>19</sup>F-<sup>13</sup>C)=25 Hz), the isocyanide carbon was not observed, probably due to line broadening. <sup>19</sup>F

NMR (CD<sub>2</sub>Cl<sub>2</sub>, ppm): -109.54 (m<sub>c</sub>). ESI+ MS (acetonitrile): 913.151 ([M+H]<sup>+</sup>; calcd 913.152).

## Acknowledgements

We gratefully acknowledge financial support from the DFG (Deutsche Forschungsgemeinschaft: Graduate School BIOQIC), the U.S. National Science Foundation (International Supplement to CHE-1802646) and the Alexander von Humboldt Foundation (Fellowship to J.S.F.). We also acknowledge the assistance of the Core Facility BioSupraMol supported by the DFG. Open Access funding enabled and organized by Projekt DEAL.

## Conflict of Interest

The authors declare no conflict of interest.

## Data Availability Statement

The data that support the findings of this study are available in the supplementary material of this article.

**Keywords:** Rhenium · Isocyanides · Carbonyls · X-Ray Crystallography · Ligand Exchange

- [1] J. F. Kronauge, D. J. Mindiola, *Organometallics* **2016**, *35*, 3432–3435.
- [2] M. J. Abrams, A. Davison, A. G. Jones, C. Costello, H. Pang, *Inorg. Chem.* **1983**, *22*, 2798–2800.
- [3] D. Piwnica-Worms, J. F. Kronauge, B. L. Holman, A. Davison, A. G. Jones, *Invest. Radiol.* **1989**, *24*, 25–29.
- [4] N. Agorastos, L. Borsig, A. Renard, P. Antoni, G. Viola, B. Spingler, P. Kurz, R. Alberto, *Chem. Eur. J.* **2007**, *13*, 3842–3852.
- [5] E. Kottelat, V. Chabert, A. Crochet, K. M. Fromm, F. Zobi, *Eur. J. Inorg. Chem.* **2015**, 5628–5638.
- [6] A. E. Miroslavov, Y. S. Polotski, V. V. Guzhii, A. Y. Ivanov, A. A. Lumpov, M. Y. Tyupina, G. V. Sidorenko, P. M. Tolstoy, D. A. Maltsev, D. N. Suglobov, *Inorg. Chem.* **2014**, *53*, 7861–7869.
- [7] M. Sagnou, C. Tsoukalas, C. Triantis, C. P. Raptopoulou, A. Terzis, I. Pirmettis, M. Pelecanou, M. Papadopoulos, *Inorg. Chim. Acta* **2010**, *363*, 1649–1653.
- [8] R. Garcia, A. Paulo, A. Domingos, I. Santos, H.-J. Pietzsch, *Synth. React. Inorg. Met.-Org. Nano-Met. Chem.* **2005**, *35*, 35–42.
- [9] G. Meola, H. Braband, S. Jordi, T. Fox, O. Blacque, B. Spingler, R. Alberto, *Dalton Trans.* **2017**, *46*, 14631–14637.
- [10] F. F. Knapp Jr., A. L. Beets, J. Pinkert, J. Kropp, W. Y. Lin, S. Y. Wang, *Rhenium radioisotopes for therapeutic radiopharmaceutical development*, IAEA report, Vienna, **2001**, ISSN 1011–4289.
- [11] F. F. Knapp Jr., *Cancer Biother. Radiopharm.* **1998**, *13*, 337–349.
- [12] A. W.-Y. Cheung, L. T.-L. Lo, C.-C. Ko, S.-M. Yiu, *Inorg. Chem.* **2011**, *50*, 4798–4810.
- [13] C.-C. Ko, L. T.-L. Lo, C.-O. Ng, S.-M. Yiu, *Chem. Eur. J.* **2010**, *16*, 13773.
- [14] S. C. Marker, A. P. King, S. Granja, B. Vaughn, J. J. Woods, E. Boros, J. Wilson, *Inorg. Chem.* **2020**, *59*, 10285–10303.
- [15] K. Schindler, F. Zobi, *Molecules* **2022**, *27*, 539.

- [16] S. Ajay Sharma, N. Vaibhavi, B. Kar, U. Das, P. Paira, *RSC Adv.* **2022**, *12*, 20264–20295.
- [17] P. M. Treichel, J. P. Williams, *J. Organomet. Chem.* **1977**, *135*, 39–51.
- [18] R. Alberto, R. Schibli, P. A. Schubiger, U. Abram, T. A. Kaden, *Polyhedron* **1996**, *15*, 1079–1089.
- [19] C. C. Konkankit, J. Lovett, H. H. Harris, J. J. Wilson, *Chem. Commun.* **2020**, *56*, 6515–6518.
- [20] F. Salsi, M. Neville, M. Drance, A. Hagenbach, J. S. Figueroa, U. Abram, *Organometallics* **2021**, *40*, 1336–1343.
- [21] L. Helm, *Coord. Chem. Rev.* **2008**, *252*, 2346–2361.
- [22] G. Claude, J. Genz, D. Weh, A. Hagenbach, M. Roca Jungfer, M. Gembicky, J. S. Figueroa, U. Abram, *Inorg. Chem.* **2022**, *61*, 16163–16176.
- [23] J.-S. Fan, F.-Y. Lee, C.-C. Chiang, H.-C. Chen, S.-H. Liu, y.-S. Wen, C.-C. Chang, S.-Y. Li, K.-M. Chi, K.-L. Lu, *J. Organomet. Chem.* **1999**, *580*, 82–89.
- [24] L. Yang, K.-K. Cheung, A. Mayr, *J. Organomet. Chem.* **1999**, *585*, 26–34.
- [25] N. J. Coville, P. Johnston, A. E. Leins, A. J. Markwell, *J. Organomet. Chem.* **1989**, *378*, 401–420.
- [26] F. Salsi, M. Neville, M. Drance, A. Hagenbach, C. Chan, U. Abram, *Chem. Commun.* **2020**, *56*, 7009–7013.
- [27] R. Alberto, R. Schibli, A. Egli, P. A. Schubiger, W. A. Herrmann, G. Artus, U. Abram, T. A. Kaden, *J. Organomet. Chem.* **1995**, *492*, 217–224.
- [28] G. Claude, F. Salsi, A. Hagenbach, M. Gembicky, M. Neville, C. Chan, J. S. Figueroa, U. Abram, *Organometallics* **2020**, *39*, 2287–2294.
- [29] P. Schaffer, J. S. Britten, A. Davison, A. G. Jones, J. F. Vaillant, *J. Organomet. Chem.* **2003**, *680*, 323–328.
- [30] D. Lentz, *Angew. Chem.* **1994**, *33*, 1315–1331.
- [31] P. Patil, M. Ahmadian-Moghaddam, A. Dömling, *Green Chem.* **2020**, *22*, 6902–6911.

Manuscript received: September 27, 2022  
Accepted manuscript online: October 10, 2022

# Zeitschrift für anorganische und allgemeine Chemie

Supporting Information

## **Rhenium Complexes with p-Fluorophenylisocyanide**

Guilhem Claude, Dominik Weh, Adelheid Hagenbach, Joshua S. Figueroa, and Ulrich Abram\*

Supporting information for the paper entitled:

## **Rhenium Complexes with p-Fluorophenylisocyanide**

*Guilhem Claude,<sup>a</sup> Dominik Weh<sup>a</sup>, Adelheid Hagenbach,<sup>a</sup> Joshua S. Figueroa<sup>b</sup> and Ulrich Abram<sup>a\*</sup>*

<sup>a</sup>Freie Universität Berlin, Institute of Chemistry and Biochemistry, Fabeckstr. 34–36, 14195 Berlin, Germany

<sup>b</sup>Department of Chemistry and Biochemistry, University of California, San Diego, La Jolla, California 92093, United States

E-mail: [ulrich.abram@fu-berlin.de](mailto:ulrich.abram@fu-berlin.de)

## Table of content

Crystallographic data.....	4
<b>Table 1.</b> Crystallographic data and data collection parameters .....	4
Figure S1. Ellipsoid representation of <i>trans</i> -[Re(CO)Br(CNPh <sup>PF</sup> ) <sub>4</sub> ] ( <b>6</b> ). The thermal ellipsoids are set at a 50% probability level. Hydrogen atoms are omitted for clarity. A number of 14 reflections below theta <sub>min</sub> is missing due to the large unit cell and the data collection with the IPDS T2 measuring routine.....	5
<b>Table S2.</b> Selected bond lengths (Å) and angles (°) in <i>trans</i> -[Re(CO)Br(CNPh <sup>PF</sup> ) <sub>4</sub> ] ( <b>6</b> )....	5
<b>Figure S2.</b> Ellipsoid representation of [Re(CNPh <sup>PF</sup> ) <sub>6</sub> ](BPh <sub>4</sub> ) ( <b>7</b> ). The thermal ellipsoids are set at a 50% probability level. Hydrogen atoms are omitted for clarity. A number of 21 reflections below theta <sub>min</sub> is missing due to the large unit cell and the data collection with the IPDS T2 measuring routine.....	6
<b>Table S3.</b> Selected bond lengths (Å) and angles (°) in [Re(CNPh <sup>PF</sup> ) <sub>6</sub> ](BPh <sub>4</sub> ) ( <b>7</b> ) .....	6
Spectra.....	7
<i>fac</i> -[Re(CO) <sub>3</sub> Br(CNPh <sup>PF</sup> ) <sub>2</sub> ] ( <b>5</b> ).....	7
<b>Figure S3.</b> IR spectrum of <i>fac</i> -[Re(CO) <sub>3</sub> Br(CNPh <sup>PF</sup> ) <sub>2</sub> ]. .....	7
<b>Figure S4.</b> <sup>1</sup> H NMR spectrum of <i>fac</i> -[Re(CO) <sub>3</sub> Br(CNPh <sup>PF</sup> ) <sub>2</sub> ] in CD <sub>2</sub> Cl <sub>2</sub> . .....	7
<b>Figure S5.</b> <sup>19</sup> F NMR spectrum of <i>fac</i> -[Re(CO) <sub>3</sub> Br(CNPh <sup>PF</sup> ) <sub>2</sub> ] in CD <sub>2</sub> Cl <sub>2</sub> . .....	8
<b>Figure S6.</b> <sup>13</sup> C{ <sup>1</sup> H} NMR spectrum of <i>fac</i> -[Re(CO) <sub>3</sub> Br(CNPh <sup>PF</sup> ) <sub>2</sub> ] in CD <sub>2</sub> Cl <sub>2</sub> .....	8
<b>Figure S7.</b> <sup>13</sup> C, <sup>1</sup> H HMBC NMR spectrum of <i>fac</i> -[Re(CO) <sub>3</sub> Br(CNPh <sup>PF</sup> ) <sub>2</sub> ] in CD <sub>2</sub> Cl <sub>2</sub> . .....	9
<b>Figure S8.</b> ESI+ mass spectrum of <i>fac</i> -[Re(CO) <sub>3</sub> Br(CNPh <sup>PF</sup> ) <sub>2</sub> ] in acetonitrile. ....	9
<i>trans</i> -[Re(CO)Br(CNPh <sup>PF</sup> ) <sub>4</sub> ] ( <b>6</b> ).....	10
<b>Figure S9.</b> IR spectrum of <i>trans</i> -[Re(CO)Br(CNPh <sup>PF</sup> ) <sub>4</sub> ]. .....	10
<b>Figure S10.</b> <sup>1</sup> H NMR spectrum of <i>trans</i> -[Re(CO)(CNPh <sup>PF</sup> ) <sub>4</sub> Br] in CD <sub>2</sub> Cl <sub>2</sub> .....	10
<b>Figure S11.</b> <sup>13</sup> C{ <sup>1</sup> H} NMR spectrum of <i>trans</i> -[Re(CO)Br(CNPh <sup>PF</sup> ) <sub>4</sub> ] in CD <sub>2</sub> Cl <sub>2</sub> . .....	11
<b>Figure S12.</b> <sup>19</sup> F NMR spectrum of <i>trans</i> -[Re(CO)Br(CNPh <sup>PF</sup> ) <sub>4</sub> ] in CD <sub>2</sub> Cl <sub>2</sub> .....	11
<b>Figure S13.</b> ESI+ mass spectrum of <i>trans</i> -[Re(CO)Br(CNPh <sup>PF</sup> ) <sub>4</sub> ] in acetonitrile. The main peaks set (see above for comparison of experimental and calculated data) correspond to <i>trans</i> -[Re(CO)(CNPh <sup>PF</sup> ) <sub>4</sub> (MeCN)] <sup>+</sup> . Peaks with high masses e.g. at 14770.76 are attributed to a dimer of the product.....	12
[Re(CNPh <sup>PF</sup> ) <sub>6</sub> ](BPh <sub>4</sub> ) ( <b>7</b> ).....	13
<b>Figure S14.</b> IR spectrum of [Re(CNPh <sup>PF</sup> ) <sub>6</sub> ](BPh <sub>4</sub> ). .....	13
<b>Figure S15.</b> <sup>1</sup> H NMR spectrum of [Re(CNPh <sup>PF</sup> ) <sub>6</sub> ](BPh <sub>4</sub> ) in CD <sub>2</sub> Cl <sub>2</sub> . .....	13
<b>Figure S16.</b> <sup>13</sup> C{ <sup>1</sup> H} NMR spectrum of [Re(CNPh <sup>PF</sup> ) <sub>6</sub> ](BPh <sub>4</sub> ) in CD <sub>2</sub> Cl <sub>2</sub> .....	14
<b>Figure S17.</b> <sup>19</sup> F NMR spectrum of [Re(CNPh <sup>PF</sup> ) <sub>6</sub> ](BPh <sub>4</sub> ) in CD <sub>2</sub> Cl <sub>2</sub> . .....	14
<b>Figure S18.</b> ESI+ mass spectrum of [Re(CNPh <sup>PF</sup> ) <sub>6</sub> ](BPh <sub>4</sub> ) in acetonitrile. ....	15
<b>Figure S19.</b> Selected <sup>19</sup> F NMR of the stepwise substitution of [Re(CO) <sub>5</sub> Br] with CNPh <sup>PF</sup> in toluene. Spectrum 1 was recorded after one hour of heating in toluene. Spectrum 2 was recorded after 4 h at 110°C and after the addition of ten more equivalents of CNPh <sup>PF</sup> . Spectrum 3 was recorded after 7 h of heating. Spectrum 4 was recorded after	

18h of heating and addition of MeOH to dissolve the precipitated  $[\text{Re}(\text{CNPh}^{\text{pF}})_6]\text{Br}$ . Note the solvent-dependent chemical shift changes of up to 3 ppm in toluene vs. THF. .... 16

**Figure S20:**  $^{19}\text{F}$  NMR spectra of an attempted reaction of  $[\text{Re}(\text{CO})_3(\text{CNPh}^{\text{pF}})_2\text{Br}]$  with an excess of  $\text{CNPh}^{\text{pF}}$  illustrating the gradual decomposition of the isocyanide without formation of the  $[\text{Re}(\text{CO})_3(\text{CNPh}^{\text{pF}})_3]^+$  cation. Spectrum **1**: synthesis of  $[\text{Re}(\text{CO})_3(\text{CNPh}^{\text{pF}})_2\text{Br}]$  from  $[\text{Re}(\text{CO})_5\text{Br}]$  and a slight excess of  $\text{CNPh}^{\text{pF}}$  in THF. Spectrum **2**: isolated  $[\text{Re}(\text{CO})_3(\text{CNPh}^{\text{pF}})_2\text{Br}]$  in THF. Spectrum **3**:  $[\text{Re}(\text{CO})_3(\text{CNPh}^{\text{pF}})_2\text{Br}]$  in THF after the addition of two equivalents of  $\text{AgPF}_6$  and subsequent filtration. Spectrum **4**: the solution of spectrum **3** after the addition of two more equivalents of  $\text{CNPh}^{\text{pF}}$ . Spectrum **5**: the solution of spectrum **5** after heating in THF. Spectrum **6**: the solution of spectrum **5** after removal of the THF, dissolution in toluene and heating on reflux for 30 min. .... 17

## Crystallographic data

The intensities for the X-ray determinations were collected on a STOE IPDS II instrument with Mo K $\alpha$  radiation. The space groups were determined by the detection of systematic absences. Absorption corrections were carried out by integration methods. Structure solution and refinement were performed with the SHELX program package. Hydrogen atoms were derived from the final Fourier maps and refined or placed at calculated positions and treated with the 'riding model' option of SHELXL. The representation of molecular structures was done using the program DIAMOND 4.2.2.

Additional information on the structure determinations is contained in the Supporting Information and has been deposited with the Cambridge Crystallographic Data Centre.

**Table 1.** Crystallographic data and data collection parameters

	<i>trans</i> -[Re(CNPh <sup>PF</sup> ) <sub>4</sub> (CO)Br] (6)	[Re(CNPh <sup>PF</sup> ) <sub>6</sub> ](BPh <sub>4</sub> ) (7)
Empirical formula	C <sub>29</sub> H <sub>16</sub> BrF <sub>4</sub> N <sub>4</sub> ORe	C <sub>66</sub> H <sub>44</sub> BF <sub>6</sub> N <sub>6</sub> Re
Formula weight	778.57	1232.08
Temperature/K	240.0	200.0
Crystal system	monoclinic	monoclinic
Space group	P2 <sub>1</sub> /c	P2 <sub>1</sub> /n
a/Å	13.8916(14)	11.162(2)
b/Å	13.9445(10)	34.932(7)
c/Å	15.3715(12)	14.069(3)
$\alpha$ /°	90	90
$\beta$ /°	106.862(7)	94.06(3)
$\gamma$ /°	90	90
Volume/Å <sup>3</sup>	2849.6(4)	5471.7(19)
Z	4	4
$\rho_{\text{calc}}/\text{cm}^{-3}$	1.815	1.496
$\mu/\text{mm}^{-1}$	5.722	2.290
F(000)	1488.0	2464.0
Crystal size/mm <sup>3</sup>	0.35 × 0.19 × 0.07	0.36 × 0.22 × 0.14
Radiation	MoK $\alpha$ ( $\lambda$ = 0.71073)	MoK $\alpha$ ( $\lambda$ = 0.71073)
2 $\theta$ range for data collection/°	6.79 to 54.062	6.488 to 51.998
Index ranges	-15 ≤ h ≤ 17, -17 ≤ k ≤ 17, -19 ≤ l ≤ 19	-13 ≤ h ≤ 13, -43 ≤ k ≤ 43, -15 ≤ l ≤ 17
Reflections collected	18263	31289
Independent reflections	6196 [R <sub>int</sub> = 0.0477, R <sub>sigma</sub> = 0.0545]	10722 [R <sub>int</sub> = 0.0591, R <sub>sigma</sub> = 0.0559]
Data/restraints/parameters	6196/470/361	10722/852/722
Goodness-of-fit on F <sup>2</sup>	0.910	0.930
Final R indexes [ $I \geq 2\sigma(I)$ ]	R <sub>1</sub> = 0.0358, wR <sub>2</sub> = 0.0548	R <sub>1</sub> = 0.0333, wR <sub>2</sub> = 0.0711
Final R indexes [all data]	R <sub>1</sub> = 0.0805, wR <sub>2</sub> = 0.0632	R <sub>1</sub> = 0.0525, wR <sub>2</sub> = 0.0755
Largest diff. peak/hole / e Å <sup>-3</sup>	0.43/-0.71	0.67/-0.89
CCDC access code	2176655	2176656

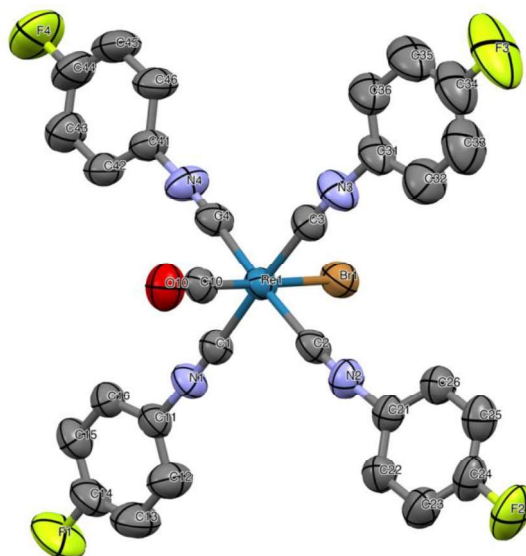
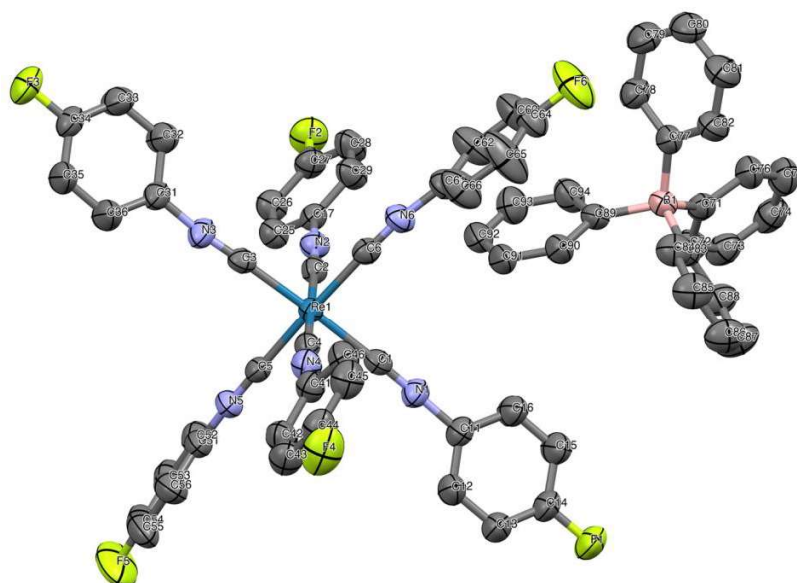


Figure S1. Ellipsoid representation of *trans*-[Re(CO)Br(CNPh<sup>PF</sup>)<sub>4</sub>] (**6**). The thermal ellipsoids are set at a 50% probability level. Hydrogen atoms are omitted for clarity. A number of 14 reflections below  $\theta_{\min}$  is missing due to the large unit cell and the data collection with the IPDS T2 measuring routine.

**Table S2.** Selected bond lengths (Å) and angles (°) in *trans*-[Re(CO)Br(CNPh<sup>PF</sup>)<sub>4</sub>] (**6**).

Re1-Br1	2.6539(7)	Re1-C2	2.032(5)	Re1-C4	2.015(5)
Re1-C1	2.038(5)	Re1-C3	2.012(5)	Re1-C10	1.919(6)
C1-N1	1.155(6)	C3-N3	1.157(6)	C10-O10	1.092(6)
C2-N2	1.162(6)	C4-N4	1.163(6)		
Br1-Re1-C1	85.9(1)	C1-Re1-C2	93.8(2)	C2-Re1-C4	175.5(2)
Br1-Re1-C2	89.8(2)	C1-Re1-C3	176.7(2)	C2-Re1-C10	93.1(2)
Br1-Re1-C3	90.9(2)	C1-Re1-C4	88.1(2)	C3-Re1-C4	92.7(2)
Br1-Re1-C4	86.3(2)	C1-Re1-C10	92.6(2)	C3-Re1-C10	90.6(2)
Br1-Re1-C10	176.9(1)	C2-Re1-C3	85.2(2)	C4-Re1-C10	90.9(2)
Re1-C1-N1	177.5(4)	Re1-C3-N3	175.8(5)	Re1-C10-O10	178.6(5)
Re1-C2-N2	175.2(4)	Re1-C4-N4	178.8(5)		





**Figure S2.** Ellipsoid representation of  $[\text{Re}(\text{CNPh}^{\text{PF}})_6](\text{BPh}_4)$  (**7**). The thermal ellipsoids are set at a 50% probability level. Hydrogen atoms are omitted for clarity. A number of 21 reflections below  $\theta_{\text{min}}$  is missing due to the large unit cell and the data collection with the IPDS T2 measuring routine.

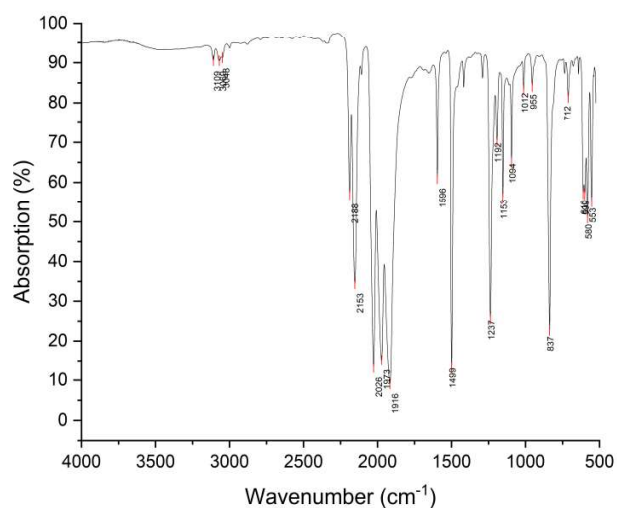
**Table S3.** Selected bond lengths (Å) and angles (°) in  $[\text{Re}(\text{CNPh}^{\text{PF}})_6](\text{BPh}_4)$  (**7**)

Re1-C1	2.047(4)	Re1-C3	2.022(4)	Re1-C5	2.029(4)
Re1-C2	2.044(4)	Re1-C4	2.029(4)	Re1-C6	2.027(4)
C1-N1	1.157(5)	C3-N3	1.161(5)	C5-N5	1.153(5)
C2-N2	1.154(5)	C4-N4	1.154(5)	C6-N6	1.149(5)
C1-Re1-C2	92.4(2)	C2-Re1-C3	87.2(2)	C3-Re1-C5	89.9(2)
C1-Re1-C3	177.5(1)	C2-Re1-C4	177.3(2)	C3-Re1-C6	88.2(2)
C1-Re1-C4	89.3(2)	C2-Re1-C5	89.6(2)	C4-Re1-C5	92.6(2)
C1-Re1-C5	87.6(2)	C2-Re1-C6	88.2(2)	C4-Re1-C6	89.7(2)
C1-Re1-C6	89.8(2)	C3-Re1-C4	91.1(2)	C5-Re1-C6	176.6(2)

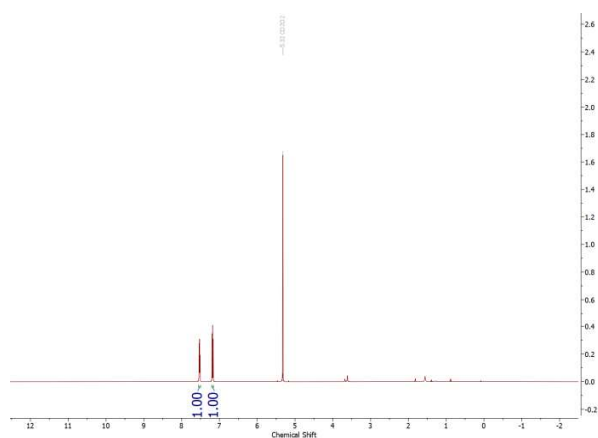
## Spectra

NMR spectra were recorded with JEOL 400 MHz ECS or ECZ or Bruker AV700 multinuclear spectrometers. IR spectra were recorded with a FT IR spectrometer (Nicolet iS10, Thermo Scientific). Intensities are classified as vs = very strong, s = strong, m = medium, w = weak, vw = very weak, sh = shoulder. The following abbreviations were used for the intensities and characteristics of IR absorption bands: vs = very strong, s = strong, m = medium, w = weak, sh = shoulder.

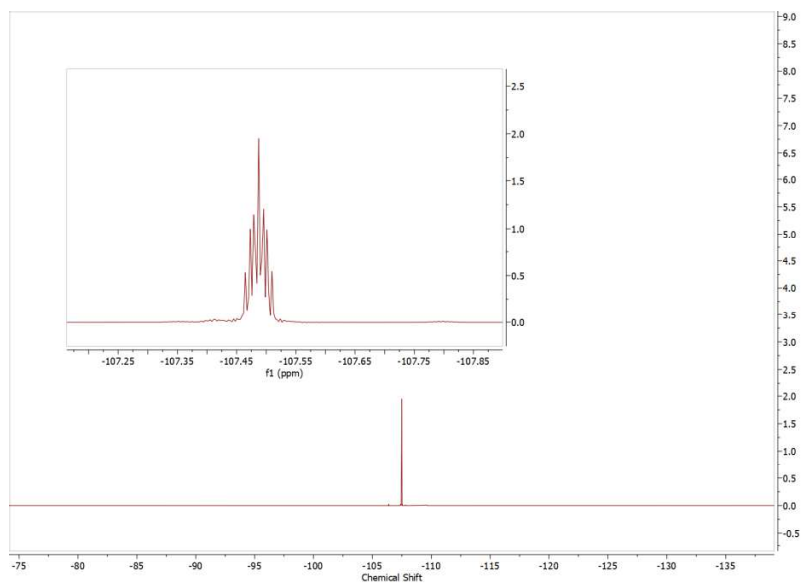
### *fac*-[Re(CO)<sub>3</sub>Br(CNPh<sup>PF</sup>)<sub>2</sub>] (5)



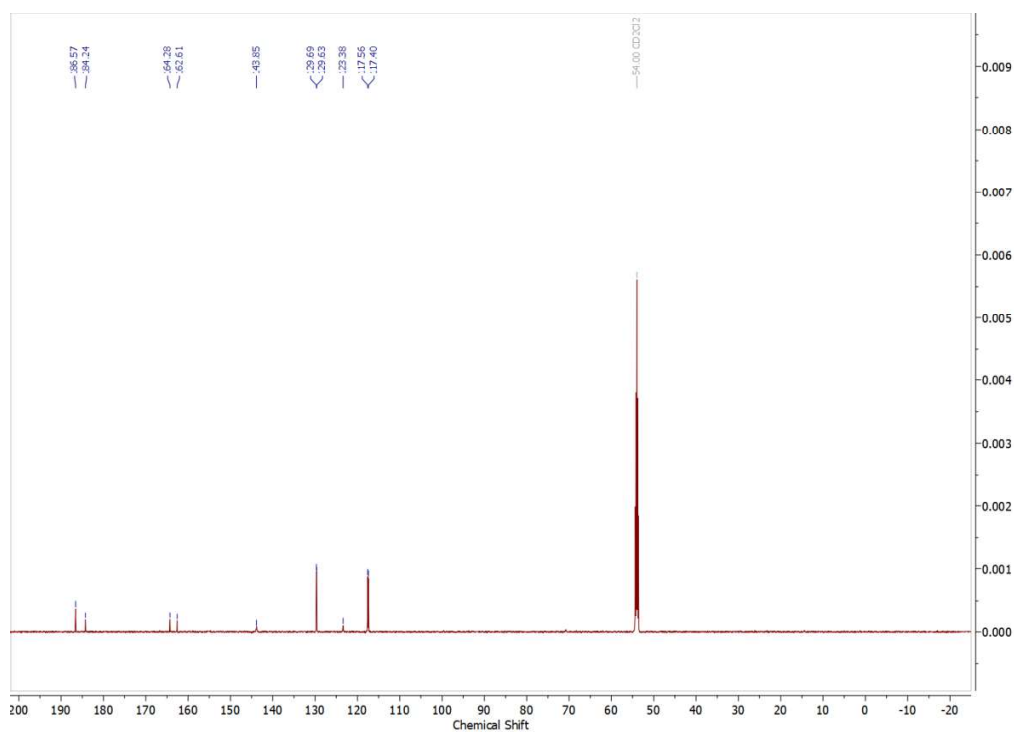
**Figure S3.** IR spectrum of *fac*-[Re(CO)<sub>3</sub>Br(CNPh<sup>PF</sup>)<sub>2</sub>].



**Figure S4.** <sup>1</sup>H NMR spectrum of *fac*-[Re(CO)<sub>3</sub>Br(CNPh<sup>PF</sup>)<sub>2</sub>] in CD<sub>2</sub>Cl<sub>2</sub>.



**Figure S5.**  $^{19}\text{F}$  NMR spectrum of *fac*-[Re(CO) $_3$ Br(CNPh $^{\text{PF}}$ ) $_2$ ] in CD $_2$ Cl $_2$ .



**Figure S6.**  $^{13}\text{C}\{^1\text{H}\}$  NMR spectrum of *fac*-[Re(CO) $_3$ Br(CNPh $^{\text{PF}}$ ) $_2$ ] in CD $_2$ Cl $_2$ .

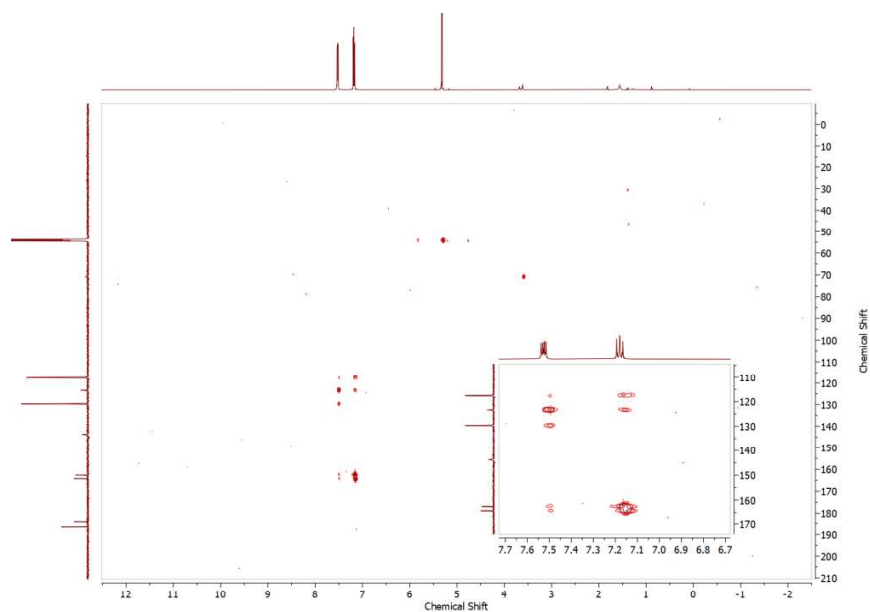


Figure S7.  $^{13}\text{C}$ ,  $^1\text{H}$  HMBC NMR spectrum of *fac*- $[\text{Re}(\text{CO})_3\text{Br}(\text{CNPh}^{\text{pF}})_2]$  in  $\text{CD}_2\text{Cl}_2$ .

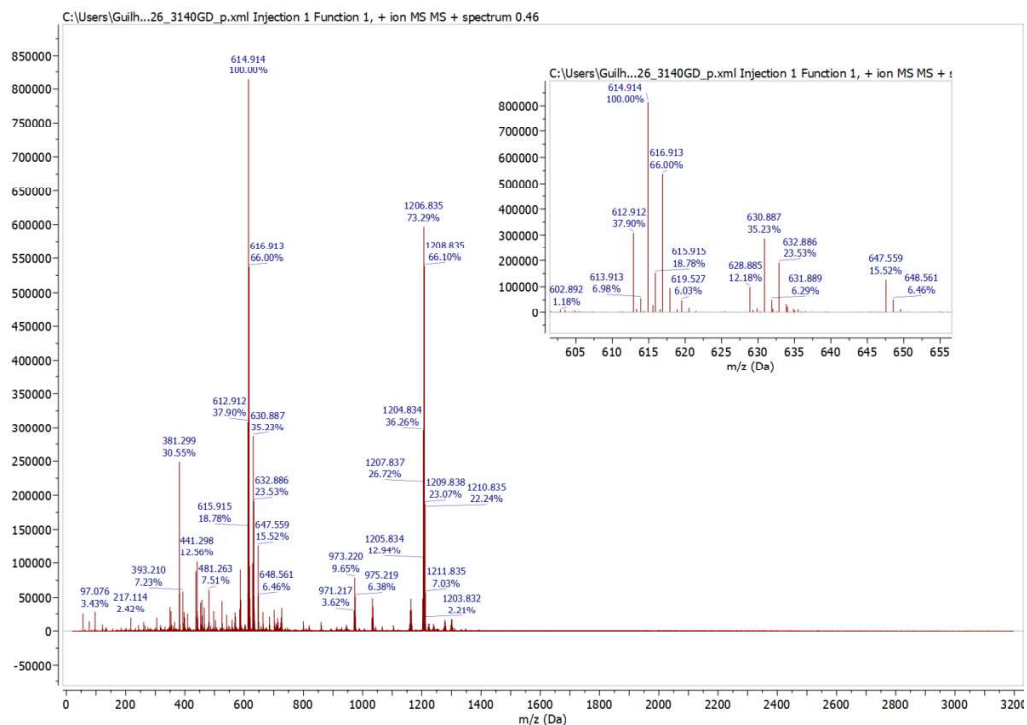
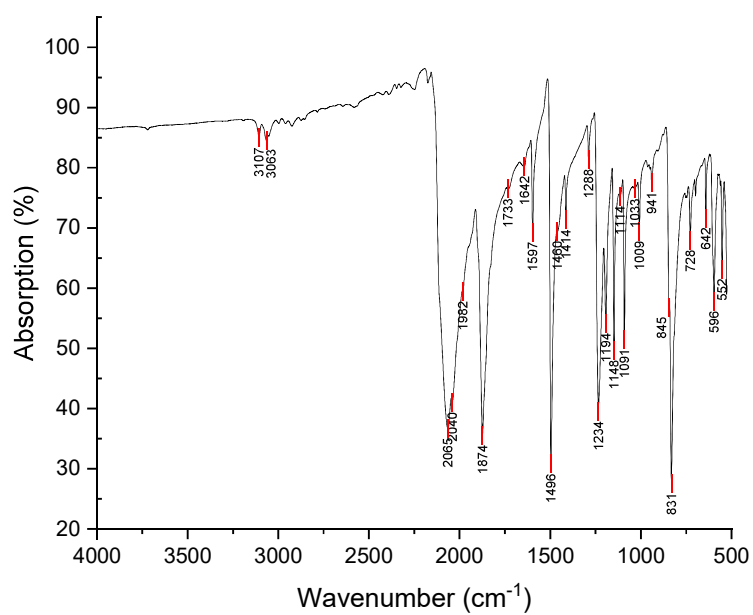
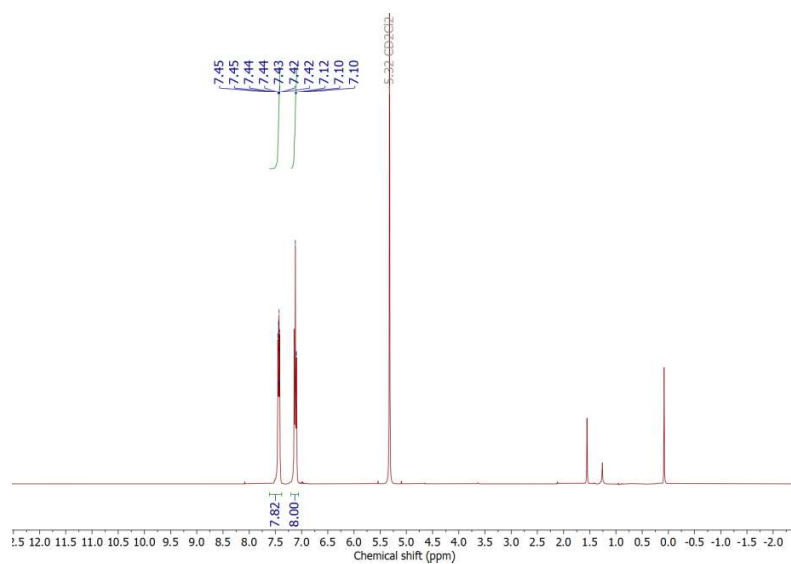


Figure S8. ESI+ mass spectrum of *fac*- $[\text{Re}(\text{CO})_3\text{Br}(\text{CNPh}^{\text{pF}})_2]$  in acetonitrile.

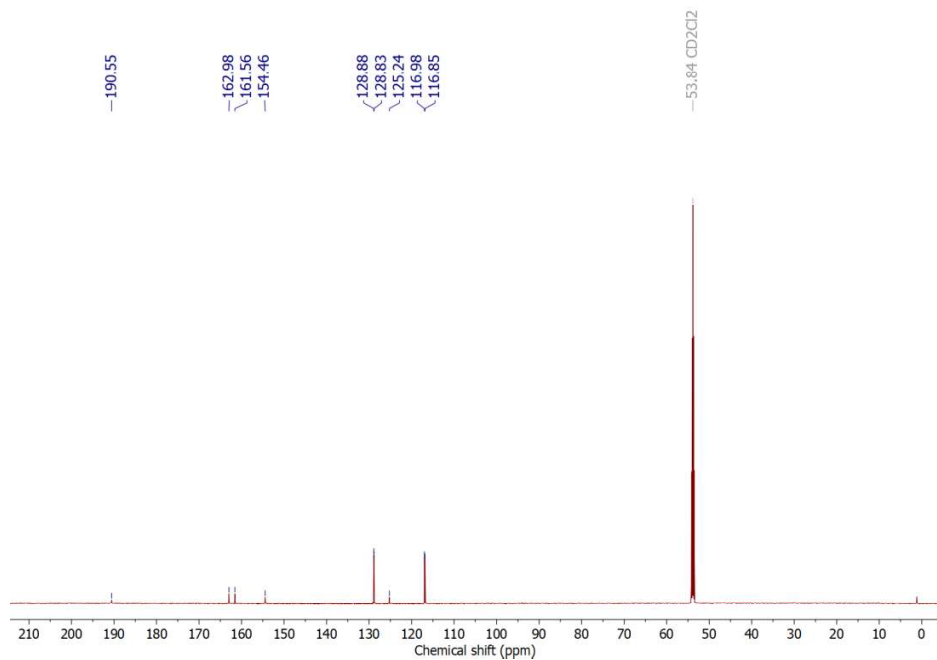
*trans*-[Re(CO)Br(CNPh<sup>P</sup>F)<sub>4</sub>] (**6**)



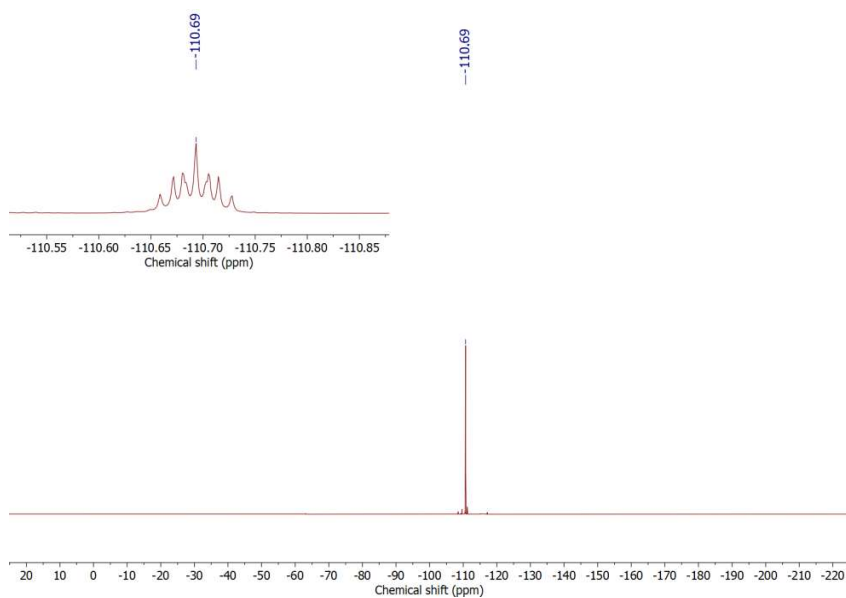
**Figure S9.** IR spectrum of *trans*-[Re(CO)Br(CNPh<sup>P</sup>F)<sub>4</sub>].



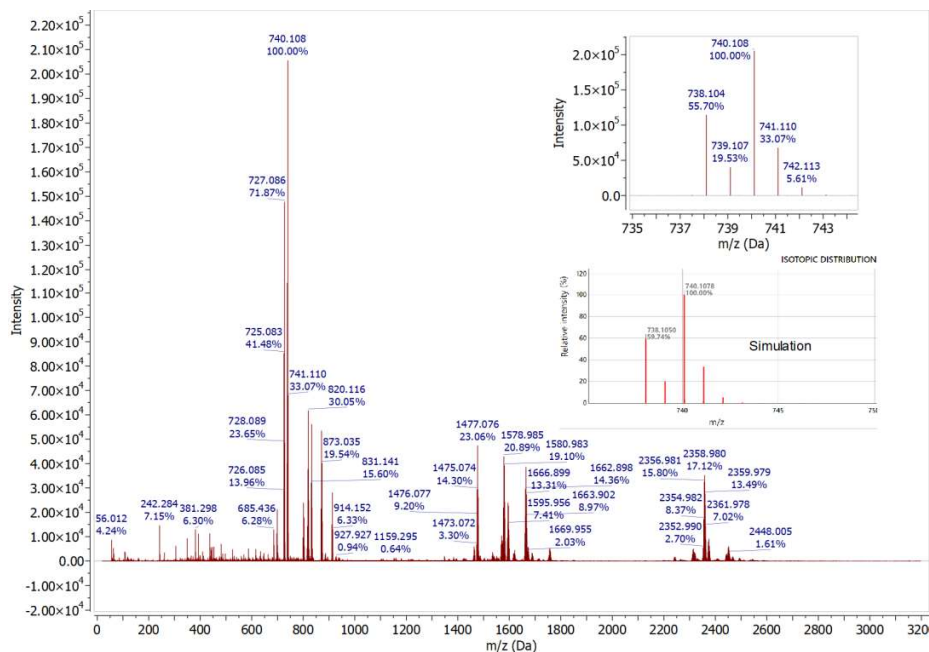
**Figure S10.** <sup>1</sup>H NMR spectrum of *trans*-[Re(CO)(CNPh<sup>P</sup>F)<sub>4</sub>Br] in CD<sub>2</sub>Cl<sub>2</sub>.



**Figure S11.**  $^{13}\text{C}\{^1\text{H}\}$  NMR spectrum of *trans*-[Re(CO)Br(CNPh<sup>PF</sup>)<sub>4</sub>] in CD<sub>2</sub>Cl<sub>2</sub>.



**Figure S12.**  $^{19}\text{F}$  NMR spectrum of *trans*-[Re(CO)Br(CNPh<sup>PF</sup>)<sub>4</sub>] in CD<sub>2</sub>Cl<sub>2</sub>.



**Figure S13.** ESI+ mass spectrum of  $trans\text{-}[\text{Re}(\text{CO})\text{Br}(\text{CNPh}^{\text{pF}})_4]$  in acetonitrile. The main peaks set (see above for comparison of experimental and calculated data) correspond to  $trans\text{-}[\text{Re}(\text{CO})(\text{CNPh}^{\text{pF}})_4(\text{MeCN})]^+$ . Peaks with high masses e.g. at 14770.76 are attributed to a dimer of the product.

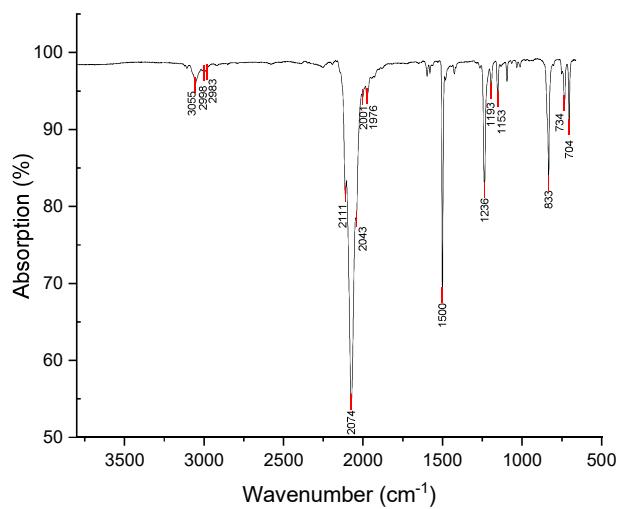
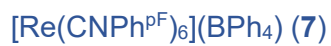


Figure S14. IR spectrum of  $[\text{Re}(\text{CNPh}^{\text{pF}})_6](\text{BPh}_4)$ .

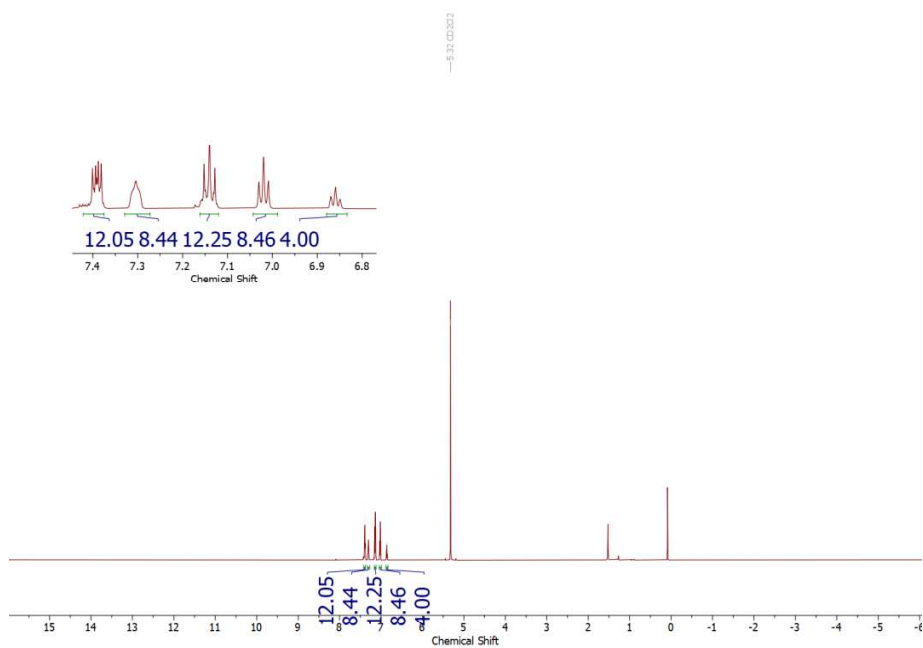
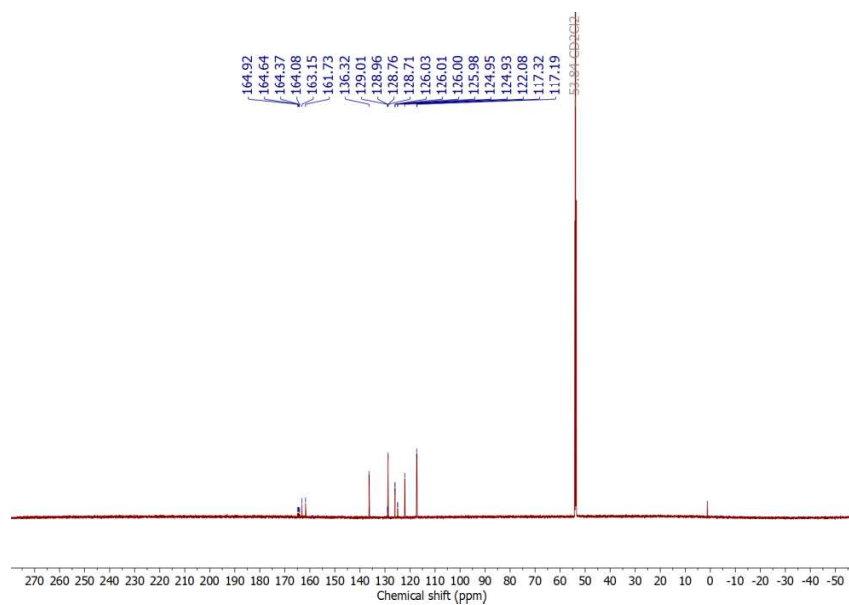
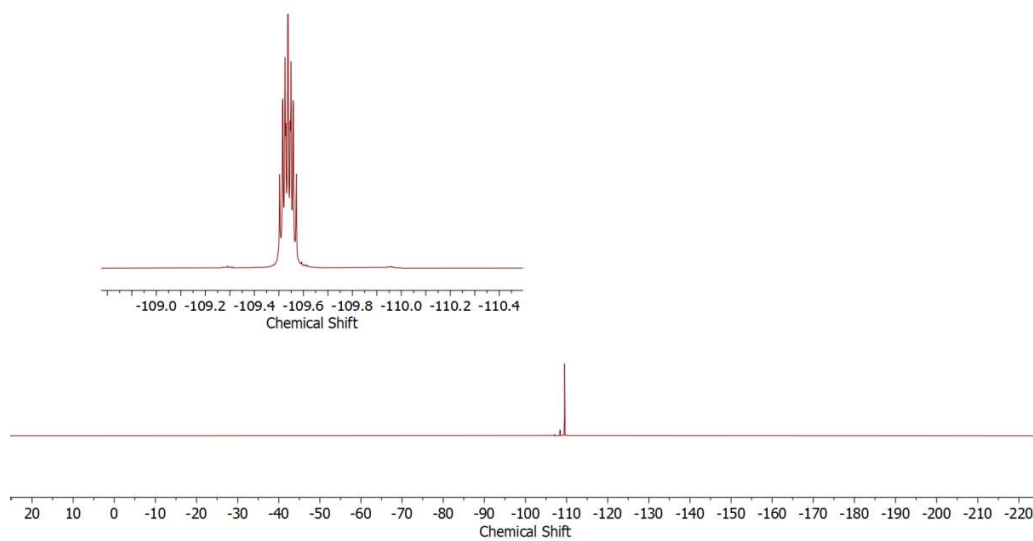


Figure S15. <sup>1</sup>H NMR spectrum of  $[\text{Re}(\text{CNPh}^{\text{pF}})_6](\text{BPh}_4)$  in  $\text{CD}_2\text{Cl}_2$ .





**Figure S16.**  $^{13}\text{C}\{^1\text{H}\}$  NMR spectrum of  $[\text{Re}(\text{CNPh}^{\text{PF}})_6](\text{BPh}_4)$  in  $\text{CD}_2\text{Cl}_2$ .



**Figure S17.**  $^{19}\text{F}$  NMR spectrum of  $[\text{Re}(\text{CNPh}^{\text{PF}})_6](\text{BPh}_4)$  in  $\text{CD}_2\text{Cl}_2$ .

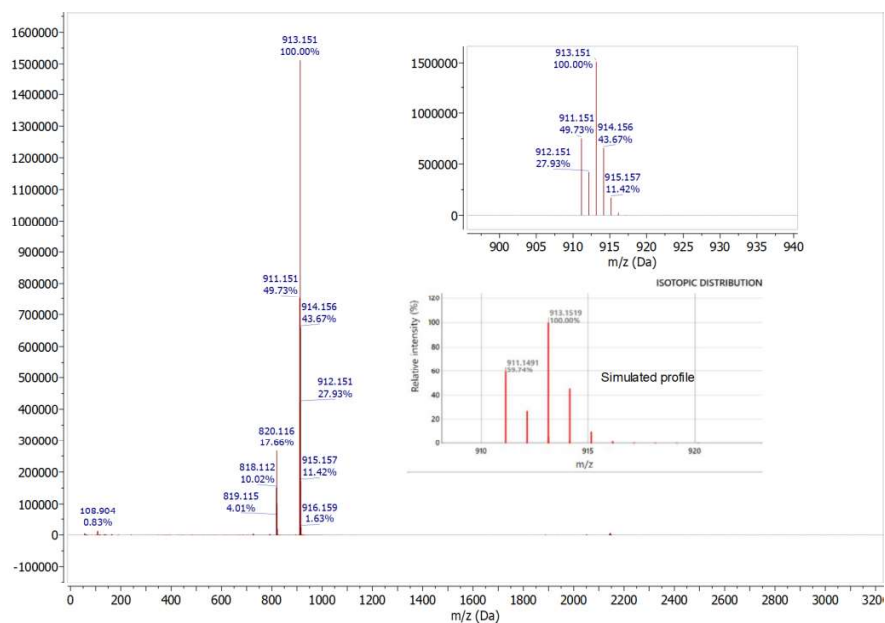
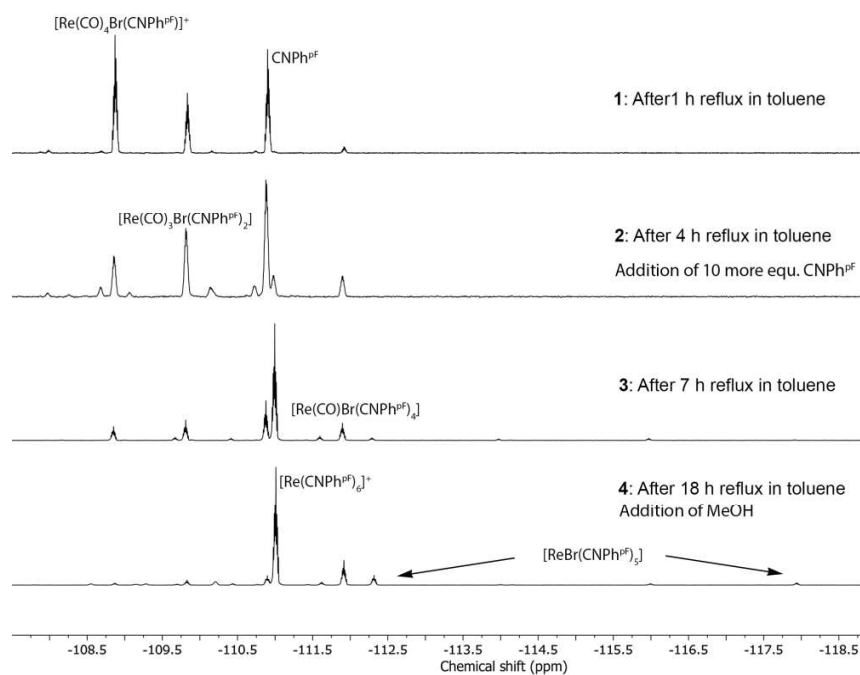
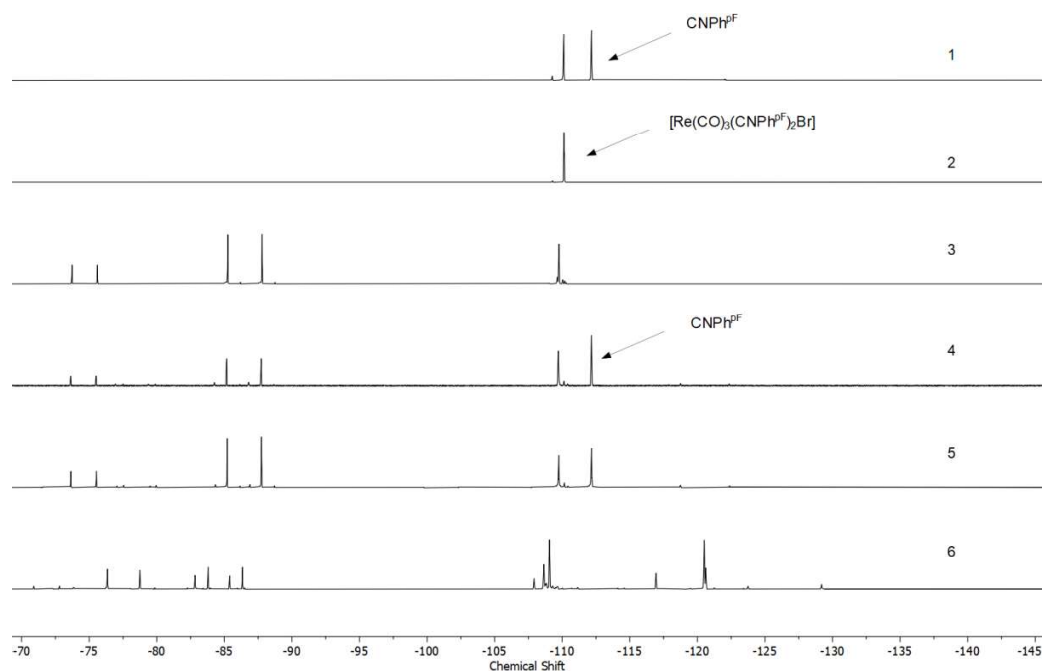


Figure S18. ESI+ mass spectrum of  $[\text{Re}(\text{CNPh}^{\text{PF}})_6](\text{BPh}_4)$  in acetonitrile.

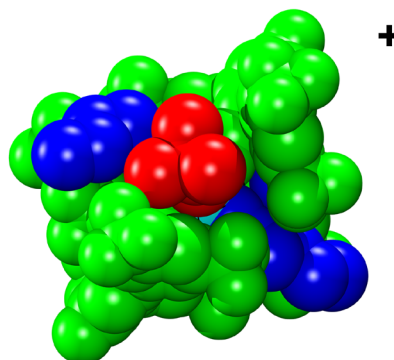
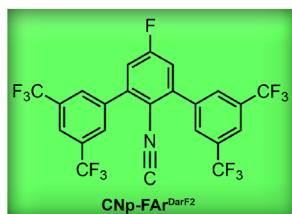
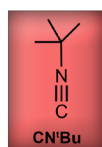
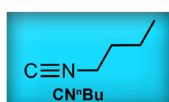
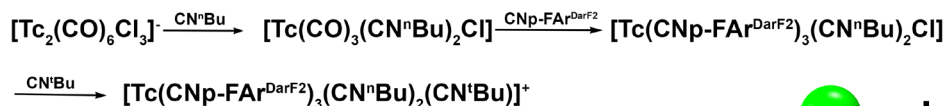


**Figure S19.** Selected  $^{19}\text{F}$  NMR of the stepwise substitution of  $[\text{Re}(\text{CO})_5\text{Br}]$  with  $\text{CNPh}^{\text{PF}}$  in toluene. Spectrum 1 was recorded after one hour of heating in toluene. Spectrum 2 was recorded after 4 h at  $110^\circ\text{C}$  and after the addition of ten more equivalents of  $\text{CNPh}^{\text{PF}}$ . Spectrum 3 was recorded after 7 h of heating. Spectrum 4 was recorded after 18h of heating and addition of MeOH to dissolve the precipitated  $[\text{Re}(\text{CNPh}^{\text{PF}})_6]\text{Br}$ . Note the solvent-dependent chemical shift changes of up to 3 ppm in toluene vs. THF.



**Figure S20:**  $^{19}\text{F}$  NMR spectra of an attempted reaction of  $[\text{Re}(\text{CO})_3(\text{CNPh}^{\text{pF}})_2\text{Br}]$  with an excess of  $\text{CNPh}^{\text{pF}}$  illustrating the gradual decomposition of the isocyanide without formation of the  $[\text{Re}(\text{CO})_3(\text{CNPh}^{\text{pF}})_3]^+$  cation. Spectrum 1: synthesis of  $[\text{Re}(\text{CO})_3(\text{CNPh}^{\text{pF}})_2\text{Br}]$  from  $[\text{Re}(\text{CO})_5\text{Br}]$  and a slight excess of  $\text{CNPh}^{\text{pF}}$  in THF. Spectrum 2: isolated  $[\text{Re}(\text{CO})_3(\text{CNPh}^{\text{pF}})_2\text{Br}]$  in THF. Spectrum 3:  $[\text{Re}(\text{CO})_3(\text{CNPh}^{\text{pF}})_2\text{Br}]$  in THF after the addition of two equivalents of  $\text{AgPF}_6$  and subsequent filtration. Spectrum 4: the solution of spectrum 3 after the addition of two more equivalents of  $\text{CNPh}^{\text{pF}}$ . Spectrum 5: the solution of spectrum 5 after heating in THF. Spectrum 6: the solution of spectrum 5 after removal of the THF, dissolution in toluene and heating on reflux for 30 min.

## 5.2. Mixed-Isocyanide Complexes of Technetium under Steric and Electronic Control



*One Technetium atom with three different isocyanide ligands*

Reproduced with permission from Claude, G.; Genz, J.; Weh, D.; Roca Jungfer, M.; Hagenbach, A.; Gembicky, M.; Figueroa, J. S.; Abram, U. Mixed-Isocyanide Complexes of Technetium under Steric and Electronic Control. *Inorg. Chem.* **2022**, *61*, 16163-16176.

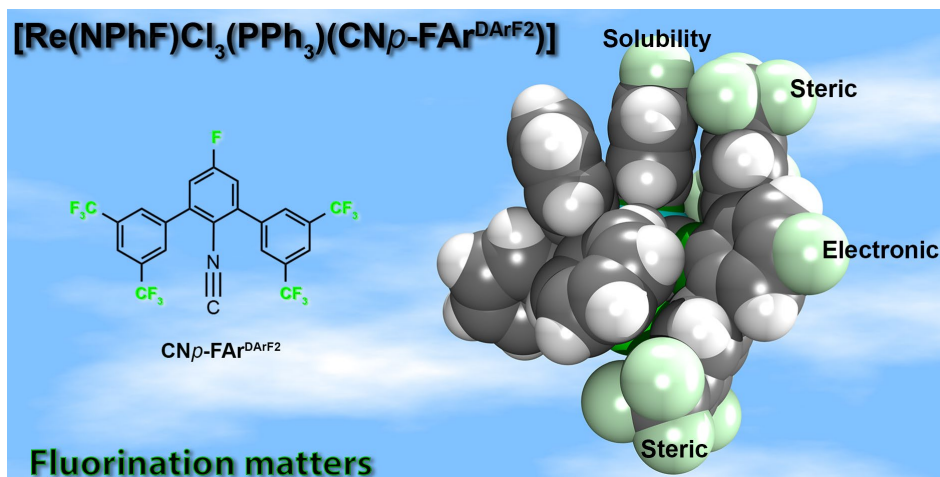
DOI: 10.1021/acs.inorgchem.2c02730

© 2021 American Chemical Society

### Author Contributions:

Guilhem Claude, Ulrich Abram and Joshua Figueroa designed the project. Guilhem Claude performed the synthesis and characterization of the compounds. Maximilian Roca Jungfer performed DFT calculations. Guilhem Claude, Adelheid Hagenbach and Milan Gembicky calculated the X-ray structures. Jonas Genz and Domenik Weh performed some of the experiments during a research internship under the supervision of Guilhem Claude. Ulrich Abram and Joshua Figueroa supervised the project, provided scientific guidance and suggestions, and wrote a draft of the manuscript.

### 5.3. Phenylimido Complexes of Rhenium: Fluorine Substituents Provide Protection, Reactivity and Solubility



Reproduced from Claude, G.; Kulitzki, E.; Hagenbach, A.; Roca Jungfer, M.; Figueroa, J. S.; Abram, U. Phenylimido Complexes of Rhenium: Fluorine Substituents Provide Protection, Reactivity and Solubility. *Dalton Trans.* **2023**,52, 4768-4778.

DOI: 10.1039/D3DT00446E

© 2023 by the authors. The Royal Society of Chemistry.

#### Author Contributions:

Guilhem Claude, Ulrich Abram and Joshua Figueroa designed the project. Guilhem Claude performed the synthesis and characterization of the compounds. Maximilian Roca Jungfer performed DFT calculations. Guilhem Claude and Adelheid Hagenbach calculated the X-ray structures. Erika Kulitzki performed some of the experiments during her bachelor thesis under the supervision of Guilhem Claude and Ulrich Abram. Ulrich Abram and Joshua Figueroa supervised the project, provided scientific guidance and suggestions, and wrote a draft of the manuscript.

Cite this: *Dalton Trans.*, 2023, **52**,  
4768

## Phenylimido complexes of rhenium: fluorine substituents provide protection, reactivity, and solubility†

Guilhem Claude,<sup>a</sup> Erika Kulitzki,<sup>a</sup> Adelheid Hagenbach,<sup>a</sup>  
Maximilian Roca Jungfer,<sup>a</sup> Joshua S. Figueroa<sup>b</sup> and Ulrich Abram<sup>b</sup>\*

Reactions of  $[\text{Re}(\text{NPhF})\text{Cl}_3(\text{PPh}_3)_2]$  ( $[\text{NPhF}]^{2-}$  = *p*-fluorophenylimido) with a variety of alkyl and aryl isocyanides have been studied. Different reactivity patterns and products have been obtained depending on the steric and electronic properties of the individual ligands. This involves the formation of 1:1 and 1:2 exchange products of Re(v) with the general formulae *mer*- $[\text{Re}(\text{NPhF})\text{Cl}_3(\text{PPh}_3)(\text{isocyanide})]$  and *cis*- or *trans*- $[\text{Re}(\text{NPhF})\text{Cl}_3(\text{isocyanide})_2]$ . The stability of the obtained products is correlated with the substitution pattern of the isocyanide ligands. The products have been studied by single-crystal X-ray diffraction and spectroscopic methods, including IR and multinuclear NMR spectroscopy as well as mass spectrometry. The use of partially fluorinated starting materials and ligands allows the modulation of the solubilities of the starting materials and the products as well as the monitoring of the reactions by means of  $^{19}\text{F}$  NMR. The attachment of the  $\text{CF}_3$  or F substituent on the isocyanides gives control over the steric bulk and the electronic properties of the ligands and, thus, their reactivity.

Received 11th February 2023,  
Accepted 7th March 2023

DOI: 10.1039/d3dt00446e

rsc.li/dalton

## Introduction

Fluorine possesses a series of peculiar properties. Its very high electronegativity (3.98 on the Pauling scale), as well as the strong hyperconjugation resulting from a low lying  $\sigma^*(\text{C}-\text{F})$  combined with its small atomic radius, has been shown to have profound structural and electronic effects on both organic and inorganic compounds.<sup>1,2</sup> Fluorine can therefore be introduced in biologically active molecules to increase their bioavailability and/or efficacy, which led to a significant growth of the number of small, fluorine-containing molecules considered for pharmaceutical applications. It was estimated that already in 2012 fluorinated compounds made 40% of all phase III drug candidates.<sup>3</sup>

In diagnostic nuclear medicine, the radioactive isotope  $^{18}\text{F}$  is a common tracer in positron-emission tomography (PET), *e.g.* by replacing a “cold” fluorine atom by  $^{18}\text{F}$  in an established pharmacologically active compound.<sup>4–6</sup> A hitherto relatively little considered option is the use of fluorine-substituted ligand systems for the modulation of the pharmacokinetic pro-

erties of metal-containing radiotracers, *e.g.* of the matched-pair  $^{99\text{m}}\text{Tc}/^{188}\text{Re}$ .<sup>6–8</sup> For the development of corresponding compounds, however, some fundamental work is required to learn more about the influence, which can be expected by partially fluorinated ligands in terms of the solubility and lipophilicity of the products, but also with regard to possible electronic effects. Such studies are commonly performed with natural rhenium and the long-lived technetium isotope  $^{99}\text{Tc}$  (weak  $\beta^-$  emitter with  $E_{\text{max}} = 0.3$  MeV,  $t_{1/2} = 2.1 \times 10^5$  years), which is available in macroscopic amounts and allows the use of conventional spectroscopic methods including  $^{19}\text{F}$  NMR spectroscopy, which is indicative of convenient monitoring of reactions.

Some recent work in our group with nuclear medically relevant metals such as indium, technetium or rhenium demonstrated that the structure and reactivity of metal complexes can markedly be influenced by (partial) fluorination of the ligands.<sup>2,9–12</sup> The observed changes in properties were found to be dependent on both the number of fluorine atoms and their exact position. The addition of sometimes even a single fluorine atom on a ligand also led to new reactivity patterns for both rhenium and technetium complexes. Thus, the use of *p*-fluorophenyl isocyanide instead of unsubstituted phenyl isocyanide resulted in completely different substitution patterns of *fac*-tricarbonyl complexes of these metals.<sup>10,11</sup>

Isocyanides are interesting ligands for nuclear medical procedures with  $^{99\text{m}}\text{Tc}$  and probably also for  $^{188}\text{Re}$ .  $^{99\text{m}}\text{Tc}$ -Sestamibi (Cardiolite), an octahedral technetium(i) complex

<sup>a</sup>Freie Universität Berlin, Institute of Chemistry and Biochemistry, Fabeckstr. 34/36, 14195 Berlin, Germany. E-mail: ulrich.abram@fu-berlin.de

<sup>b</sup>University of California San Diego, La Jolla, Department of Chemistry and Biochemistry, California 92093, USA. E-mail: jsfig@ucsd.edu

† Electronic supplementary information (ESI) available. CCDC 2236802–2236812. For ESI and crystallographic data in CIF or other electronic format see DOI: <https://doi.org/10.1039/d3dt00446e>

with six methoxy-substituted isocyanides, is one of the most used diagnostic radiopharmaceuticals worldwide.<sup>12–15</sup> Isocyanide complexes with high-valent rhenium and technetium centers are rare and only a few examples of oxidorhenium(v) complexes are known,<sup>16–18</sup> while the corresponding  $\{\text{TcO}\}^{3+}$  core is prone to reduction by isocyanides and no such compounds could be isolated until now.

More stable against reduction is the isoelectronic phenylimido core and some technetium isocyanide complexes with a central  $\{\text{Tc}(\text{NPh})\}^{3+}$  unit could be isolated.<sup>19,20</sup> A number of interesting reactivity features have been observed during this study, which makes it interesting to have a look at the related chemistry of rhenium.

The phenylimido complex  $[\text{Re}(\text{NPh})\text{Cl}_3(\text{PPh}_3)_2]$  is isoelectronic to the oxidorhenium(v) compound  $[\text{ReOCl}_3(\text{PPh}_3)_2]$ , which is frequently used as a common precursor for ligand exchange procedures.<sup>21</sup> A similar use of the phenylimido compound as the starting material may give access to a wide variety of phenylimido complexes. Unfortunately, the rhenium compound is significantly less soluble than its technetium analog. Thus, predominately reactions with strong chelators or with robust ligands,<sup>22–45</sup> which resist harsh reaction conditions, give pure products in good yields. The corresponding bromido complex  $[\text{Re}(\text{NPh})\text{Br}_3(\text{PPh}_3)_2]$  is slightly more soluble and is, thus, occasionally used as a better suitable starting material.<sup>37,40,44,45</sup> Alternatively, substitutions on the arylimido ligand with the carboxylic, hydroxylic or amine group provide an enhanced solubility.<sup>46–50</sup> Such residues, however, sometimes undergo undesired reactions with co-ligands and/or solvents (*e.g.* esterification, formation of Schiff bases, *etc.*), which frequently causes undesired side-reactions and/or lower yields. A modulation of the solubility of the phenylimido starting material without significant interference with the chemical behaviour of other ligands has recently been demonstrated with the use of *p*-fluoro-substituted phenylimido ligands in  $[\text{M}(\text{NPhF})\text{Cl}_3(\text{PPh}_3)_2]$  complexes,  $\text{M} = \text{Tc}$  or  $\text{Re}$  (**1**).<sup>51,52</sup>

In the present report, we present a series of (fluorinated) phenylimidorhenium(v) complexes with a variety of different alkyl and aryl isocyanides (Fig. 1).

## Results and discussion

The attachment of a fluorine atom to the phenylimido ligand of  $[\text{Re}(\text{NPh})\text{Cl}_3(\text{PPh}_3)_2]$  increases the room temperature-solubility by a factor of 5 in both dichloromethane and acetonitrile. This allows for milder reaction conditions and lower temperatures, which is particularly beneficial for sensitive isocyanides such as  $\text{CNPh}$ ,  $\text{CNMe}$  or  $\text{CNPh}^{\text{pNO}_2}$  of the present study. These ligands as well as other common isocyanides such as  $\text{CN}^t\text{Bu}$  or  $\text{CNPh}^{\text{t-propyl}}$  react with  $[\text{Re}(\text{NPhF})\text{Cl}_3(\text{PPh}_3)_2]$  (**1**) with the formation of mono-substituted complexes of the composition  $[\text{Re}(\text{NPhF})\text{Cl}_3(\text{PPh}_3)(\text{CNR})]$  (Scheme 1). The reactions have first been performed with an excess of ligands and for the more stable ligands ( $\text{CN}^t\text{Bu}$  and  $\text{CNPh}^{\text{t-propyl}}$ ) also prolonged reactions at higher temperatures have been tested. In

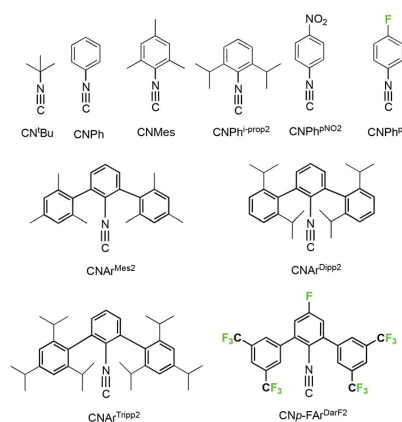
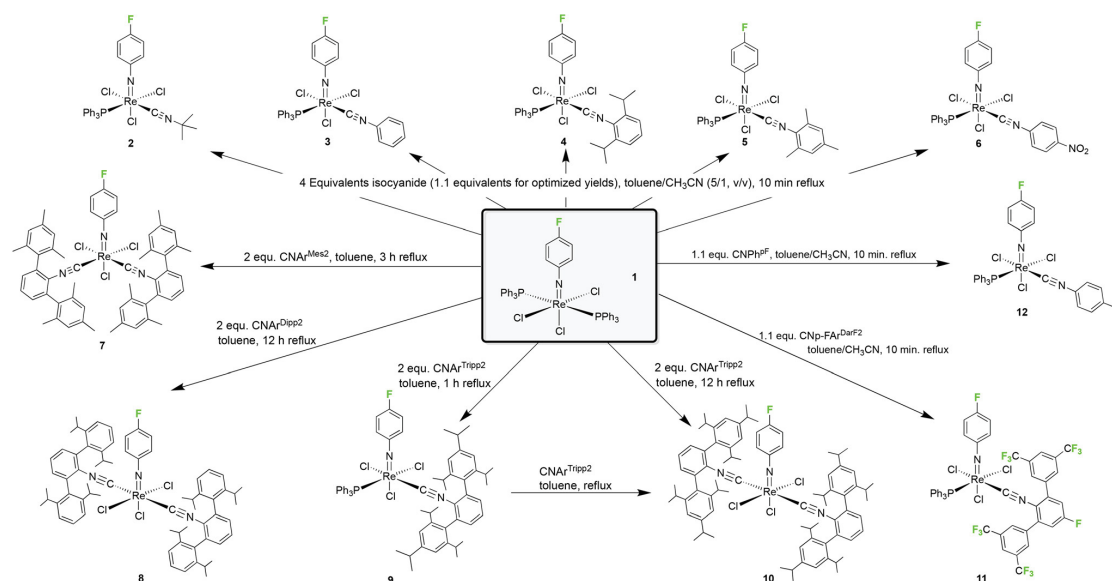


Fig. 1 Isocyanides used throughout this paper.

both cases, exclusively 1 : 1 ligand exchange products could be isolated. The gradual (not metal-driven) decomposition of the isocyanides, however, caused significant problems during the isolation of pure products in these cases. For this reason, relatively short reaction times and only a slight excess of the ligands have been used in optimized procedures. Even so, only a small amount of pure products could be obtained from some of the sensitive isocyanides.

The formation of 1 : 1 complexes with common isocyanides has also been observed for reactions of  $[\text{Tc}(\text{NPh})\text{Cl}_3(\text{PPh}_3)_2]$ ,<sup>20</sup> and for reactions of robust isocyanides with the corresponding phenyl- or tolyl- or xylylimido complexes.<sup>46,53–55</sup> These findings are not necessarily trivial since the ligand exchange behaviour of isocyanides has been found to be strongly dependent on steric and electronic factors. In particular, electronic effects due to electron withdrawing or electron donating substituents on (phenyl) isocyanides have been underestimated in the coordination chemistry of these compounds. Systematic studies about this point are rare, which is attributed to the preferred use of commercially available and stable ligands such as *e.g.* *tert*-butyl or cyclohexyl isocyanide in many papers about the related chemistry. Approximately 40 percent of all studies with isocyanides are done with these two representatives. A nice overview of this point is given in ref. 56. This, finally, resulted in a (not fully justified) generalization of their chemical behaviour for all isocyanides. After the exploration of the coordination chemistry of the bulky (but also electronically diverse) *m*-terphenyl isocyanides,<sup>57–69</sup> it became evident that isocyanides are more than bulky surrogates of carbonyl ligands. This also includes studies on group 7 elements, which have been stabilized in oxidation states ranging from ‘–1’ to ‘+5’.<sup>10,11,20–22,70,71</sup> A DFT-based sum parameter describing the electronic potential on the accessible VdW surface of the isocyanide carbon atom has recently been derived for a number of isocyanides.<sup>10</sup> The so-called SADAP (surface-averaged donor acceptor potential) parameter is a combined descriptor of the steric and electrostatic properties of the potential ligand.





Scheme 1 Reaction of  $[\text{Re}(\text{NPhF})\text{Cl}_3(\text{PPh}_3)_2]$  with various isocyanides.

Table 2 contains selected SADAP parameters for the isocyanides of the present study. Details of the calculations and the derived parameter comprising a large number of isocyanides are outlined in ref. 10. Such parameters nicely describe the reactivity of a number of carbonyltechnetium(I) complexes, where ligands with progressively electron-deficient properties readily replace carbonyl ligands, while those with a large negative potential at the carbon atoms are  $\sigma$ -donors with predominantly negligible back-donation properties.<sup>10</sup> Similar considerations have also been done for phenylimidotechnetium(V) compounds,  $d^2$  systems, where  $\pi$ -acceptor behaviour should be negligible.<sup>20</sup>

The formation of 1:1 complexes during reactions of  $[\text{Re}(\text{NPhF})\text{Cl}_3(\text{PPh}_3)_2]$  with the relatively electron-deficient isocyanides as shown in Fig. 1 is in line with such considerations. The  $\nu_{\text{C}=\text{N}}$  IR stretches of the complexes appear between 2158 and 2192  $\text{cm}^{-1}$ . These values are significantly higher (between 39 and 72  $\text{cm}^{-1}$ , for individual values see the Experimental section) than those in the spectra of uncoordinated isocya-

nides, which means that there is no sign for  $\pi$ -backdonation into anti-bonding orbitals of the ligands in the  $d^2$  complexes under study.

Ellipsoid plots of the molecular structures of the  $[\text{Re}(\text{NPhF})\text{Cl}_3(\text{PPh}_3)(\text{CNR})]$  complexes ( $R = ^i\text{Bu}$ , Ph,  $\text{Ph}^i\text{-prop}^2$ , Mes,  $\text{Ph}^{\text{pNO}_2}$ ) are depicted in Fig. 1. Selected bond lengths and angles are summarized in Table 1. The Re–N bonds are clearly in the range of double bonds and the slightly bent phenylimido units (Re–N–C angles between 164 and 173°) are a common feature of such compounds.<sup>22–45</sup> The replacement of one of the  $\text{PPh}_3$  ligands of  $[\text{Re}(\text{NPhF})\text{Cl}_3(\text{PPh}_3)_2]$  goes along with a rearrangement of the coordination sphere of rhenium. The incoming isocyanides are found in *cis* position to phosphine in all 1:1 complexes.

Two isocyanide ligands could be bonded to a  $\{\text{ReNPhF}\}^{3+}$  unit, when more electron-rich isocyanides such as  $\text{CNAr}^{\text{Mes}2}$ ,  $\text{CNAr}^{\text{Dipp}2}$  or  $\text{CNAr}^{\text{Tripp}2}$  were used. The steric bulk of the individual ligands, however, has an influence on the isomers formed. The reaction of the less bulky  $\text{CNAr}^{\text{Mes}2}$  gives the 1:2

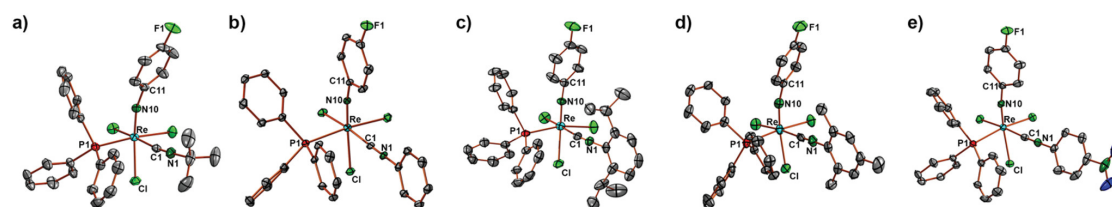


Fig. 2 Molecular structures of (a)  $[\text{Re}(\text{NPhF})\text{Cl}_3(\text{PPh}_3)(\text{CN}^i\text{Bu})]$  (2), (b)  $[\text{Re}(\text{NPhF})\text{Cl}_3(\text{PPh}_3)(\text{CNPh})]$  (3), (c)  $[\text{Re}(\text{NPhF})\text{Cl}_3(\text{PPh}_3)(\text{CNPh}^i\text{-prop}^2)]$  (4), (d)  $[\text{Re}(\text{NPhF})\text{Cl}_3(\text{PPh}_3)(\text{CNMes})]$  (5) and (e)  $[\text{Re}(\text{NPhF})\text{Cl}_3(\text{PPh}_3)(\text{CNPh}^{\text{pNO}_2})]$  (6).

**Table 1** Selected bond lengths and angles of [Re(NPhF)Cl<sub>3</sub>(PPh<sub>3</sub>)(CNR)] complexes

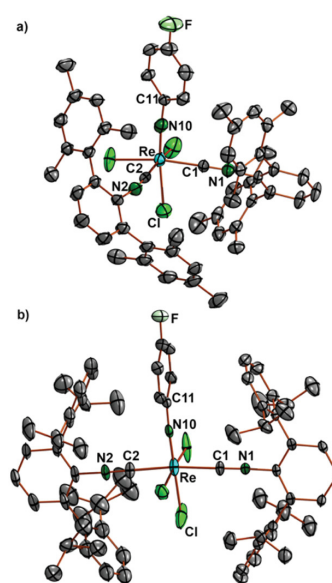
	2 <sup>a</sup>	3	4	5	6	11	12
Re–N10	1.715(3), 1.715(3)	1.731(3)	1.722(3)	1.712(3)	1.711(3)	1.721(3)	1.705(4)
N10–C11	1.391(4), 1.382(4)	1.377(4)	1.385(4)	1.399(5)	1.390(5)	1.380(4)	1.395(7)
Re–P1	2.4593(9), 2.4473(9)	2.4539(9)	2.4476(9)	2.463(1)	2.454(1)	2.4494(8)	2.470(2)
Re–C1	2.020(4), 2.045(4)	2.028(4)	2.023(3)	2.030(4)	2.020(5)	2.022(3)	2.024(6)
C1–N1	1.151(5), 1.146(5)	1.165(5)	1.147(4)	1.151(6)	1.162(6)	1.151(4)	1.156(7)
Re–N10–C11	164.4(3), 166.7(2)	168.7(3)	172.1(2)	166.0(3)	171.2(3)	170.4(2)	172.9(4)
Re–C1–N1	172.9(3), 173.8(8)	177.7(3)	170.6(3)	176.9(3)	176.6(4)	174.6(3)	176.9(4)
N10–Re–P1	93.1(1), 91.42(9)	89.99(9)	94.15(9)	92.0(1)	94.2(1)	91.96(8)	94.2(2)
N10–Re–C1	86.0(1), 88.1(1)	87.7(1)	88.1(1)	85.7(1)	89.4(2)	88.5(1)	91.8(2)

<sup>a</sup> Values of two crystallographically independent species.

complex *fac*-[Re(NPhF)Cl<sub>3</sub>(CNAr<sup>Mes2</sup>)<sub>2</sub>] (7) with the two isocyanide ligands in *cis* position to each other, while the corresponding *trans* complexes are formed by the sterically more encumbered ligands CNAr<sup>Dipp2</sup> and CNAr<sup>Tripp2</sup> (Scheme 1). The formation of *cis* complexes with CNAr<sup>Mes2</sup> is a common feature of this ligand and has also been observed for oxido and nitrido complexes of rhenium and technetium.<sup>18,19</sup> There are even some rare cases where three CNAr<sup>Mes2</sup> ligands are accommodated in octahedral complexes of cobalt,<sup>72</sup> molybdenum,<sup>58,73</sup> and manganese.<sup>62</sup> Such flexibility regarding the number of ligands and their coordination positions, however, is also the source of the appearance of a fluxional behaviour in solution, which could be detected preferably by <sup>19</sup>F NMR, with subsequent problems for the isolation of satisfactory amounts of the individual species in pure form. This is mainly due to the almost identical solubility of the formed species and also applies to the phenylimido compounds under study with the consequence that only a relatively small amount of complex 7 could be isolated in crystalline form. Although the isolated blue needles of 7 were identical as has been tested by X-ray diffraction on several species, they quickly isomerize in solution and again several <sup>19</sup>F NMR signals are detected. This behaviour is unlike that of the complexes with the more bulky CNAr<sup>Dipp2</sup> or CNAr<sup>Tripp2</sup> ligands, which form inert *mer*-[Re(NPhF)Cl<sub>3</sub>(isocyanide)] complexes that contain the isocyanides necessarily in *trans* position to each other.

Ellipsoid plots of the molecular structures of complex *fac*-[Re(NPhF)Cl<sub>3</sub>(CNAr<sup>Mes2</sup>)<sub>2</sub>] (7) and *mer*-[Re(NPhF)Cl<sub>3</sub>(CNAr<sup>Dipp2</sup>)<sub>2</sub>] (8) are shown in Fig. 3. All common features of the central {Re(NPhF)}<sup>3+</sup> unit discussed above for compounds 2–6 (Re–N double bond, slightly bent Re–N10–C11 axis) also apply for the bis complexes 7 and 8. The rhenium-carbon bonds in the *cis* isomer 7 (2.034–2.044 Å) are slightly shorter than in the *trans* isomer 8 (2.055–2.076 Å). This comes not unexpected with regard to the sterically favoured *trans* compound. Similar effects have been observed previously for the *cis* and *trans* isomers of [Re(CO)<sub>3</sub>Br(CNAr<sup>Dipp2</sup>)<sub>2</sub>], where the Re–C (isocyanide) bonds are elongated by approximately 0.02 Å in *trans* position to carbonyl ligands,<sup>70</sup> for which, however, mainly electronic effects shall be responsible.

The exchange of the PPh<sub>3</sub> ligands occurs stepwise and can nicely be monitored by <sup>19</sup>F NMR. Fig. 4 shows <sup>19</sup>F NMR spectra



**Fig. 3** Molecular structures of (a) *fac*-[Re(NPhF)Cl<sub>3</sub>(CNAr<sup>Mes2</sup>)<sub>2</sub>] (7) and (b) *mer*-[Re(NPhF)Cl<sub>3</sub>(CNAr<sup>Dipp2</sup>)<sub>2</sub>] (8) (selected bond lengths and angles of 7: Re–N10 1.724(3), Re–C1 2.043(4), Re–C2 2.034(4) Å, Re–N10–C11 173.0(3), Re–C1–N1 176.6(3), and Re–C2–N2 174.2(4)°; selected bond lengths and angles of 8: Re–N10 1.728(7) and 1.722(6), Re–C1 2.076(6) and 2.066(6), Re–C2 2.055(7) and 2.055(7) Å, Re–N10–C11 177.4(5) and 171.5(5), Re–C1–N1 179.1(7) and 178.2(6), and Re–C2–N2 176.6(7) and 178.3(6)°. The values of compound 8 refer to two independent molecular species.

recorded for a corresponding reaction of [Re(NPhF)Cl<sub>3</sub>(PPh<sub>3</sub>)<sub>2</sub>] (1) with CNAr<sup>Dipp2</sup> in toluene. The formation of two transient compounds can readily be detected by their <sup>19</sup>F NMR signals in addition to the signals of the (not yet consumed) starting material 1 in the initial phase (first hour) of the reaction. Upon subsequent heating, the intensities of these signals and of compound 1 decrease in favour of the formation of the final product of the reaction *mer*-[Re(NPhF)Cl<sub>3</sub>(CNAr<sup>Dipp2</sup>)<sub>2</sub>] (8). The tentative assignment of the transient signals A and B is possible in two ways: (1) to a mixture of *cis*- and *trans*-[Re(NPhF)

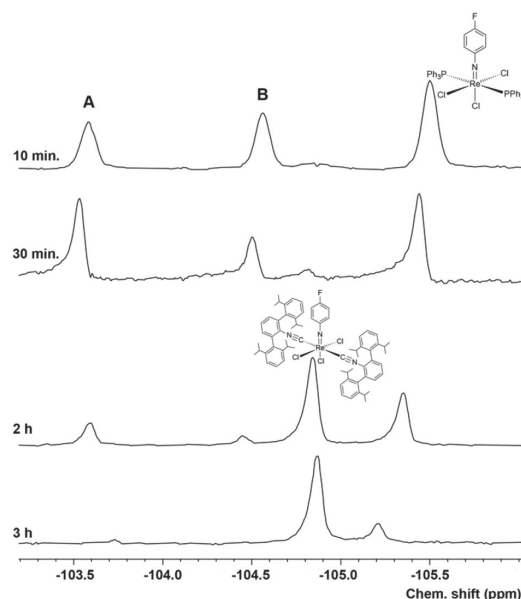


Fig. 4  $^{19}\text{F}$  NMR monitoring of a reaction mixture of  $[\text{Re}(\text{NPhF})\text{Cl}_3(\text{PPh}_3)_2]$  and two equivalents of  $\text{CNAr}^{\text{Dipp}2}$  in boiling toluene. Note the narrow chemical shift range depicted and that the chemical shifts slightly differ from the values given in the Experimental part due to solvent effects.

$\text{Cl}_3(\text{PPh}_3)(\text{CNAr}^{\text{Dipp}2})$  or (2) to a mixture of *cis*- $[\text{Re}(\text{NPhF})\text{Cl}_3(\text{PPh}_3)(\text{CNAr}^{\text{Dipp}2})]$  and  $[\text{Re}(\text{NPhF})\text{Cl}_3(\text{PPh}_3)(\text{CNAr}^{\text{Dipp}2})_2]$ . Evidence for the latter, seven-coordinate species is given with the detection of an intense peak at  $m/z = 1349.600$  (simulation: 1349.309) in the ESI + mass spectrum of the reaction mixture after 10 min. Up to now, we could not isolate these two or at least one of these complexes in crystalline form for an unambiguous proof of one of these assumptions. This, however, was possible for the corresponding reaction with  $\text{CNAr}^{\text{Tripp}2}$ .

The  $^{19}\text{F}$  NMR monitoring of the reaction of **1** with  $\text{CNAr}^{\text{Tripp}2}$  (see the ESI, Fig. S57†) shows that essentially only one major transient compound is formed. The concentration of this compound reaches a maximum after approximately 90 min and when the reaction is stopped at this point, a small amount of this intermediate can be separated from the bulk of the starting material **1** and crystallized. An X-ray diffraction study on these single crystals confirms the formation of *fac*- $[\text{Re}(\text{NPhF})\text{Cl}_3(\text{PPh}_3)(\text{CNAr}^{\text{Tripp}2})]$  (**9**) as the (isolated) intermediate of this reaction. Prolonged heating of the reaction mixtures gives the bis complex  $[\text{Re}(\text{NPhF})\text{Cl}_3(\text{CNAr}^{\text{Tripp}2})_2]$  (**10**) similar to the reaction with  $\text{CNAr}^{\text{Dipp}2}$ . The molecular structures of compounds **9** and **10** are depicted in Fig. 5. Bond lengths and angles in the products with the extremely sterically encumbered  $\text{CNAr}^{\text{Tripp}2}$  ligand are similar to those observed in the other 1:1 complexes or in the analogous bis complex with  $\text{CNAr}^{\text{Dipp}2}$  discussed above. Also in compound **10**, the Re–C bonds are slightly longer than in the complexes of the compo-

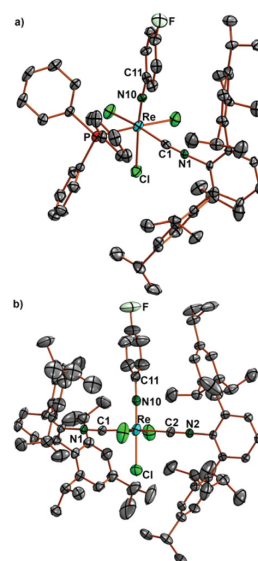


Fig. 5 Molecular structures of (a) *fac*- $[\text{Re}(\text{NPhF})\text{Cl}_3(\text{PPh}_3)(\text{CNAr}^{\text{Tripp}2})]$  (**9**) and (b) *mer*- $[\text{Re}(\text{NPhF})\text{Cl}_3(\text{CNAr}^{\text{Tripp}2})_2]$  (**10**). Selected bond lengths and angles of **9**: Re–N10 1.711(4), Re–P 2.460(2), Re–C1 2.027(5), C1–N1 1.167(5) Å; Re–N10–C11 168.7(3), and Re–C1–N1 170.4(4)°. Selected bond lengths and angles of **10**: Re–N10 1.698(6) and 1.711(5), Re–C1 2.093(6) and 2.090(6), Re–C2 2.084(6) and 2.076(6), C1–N1 1.135(7) and 1.139(7), C2–N2 1.135(7) and 1.148(7) Å; Re–N10–C11 177.1(5) and 178.7(5), Re–C1–N1 175.3(6) and 178.2(6), and Re–C2–N2 175.4(5) and 179.5(7)°. The values of compound **10** refer to two independent molecular species.

sition  $[\text{Re}(\text{NPhF})\text{Cl}_3(\text{PPh}_3)(\text{CNR})]$ , where the isocyanides are in *trans* positions to chlorido ligands.

$\text{CNAr}^{\text{Dipp}2}$  and  $\text{CNAr}^{\text{Tripp}2}$  are structurally distinguished by the presence of additional isopropyl substituents at the peripheral phenyl rings. At first glance this seems to be a minor difference, especially since this substitution is in the 4-position and, thus, relatively far away from the coordinating carbon atom. This means, that a similar electronic potential should be expected for both ligands, while  $\text{CNAr}^{\text{Tripp}2}$  should be slightly more sterically hindered, which is finally also reflected by the SADAP parameters in Table 2 and the formation of 1:2 complexes of the present study. Nevertheless, there is a striking difference between these two isocyanides

Table 2 Selected SADAP parameters of the isocyanides of the present study. Values are taken from ref. 10 and 20

Isocyanide	SADAP
$\text{CNAr}^{\text{Tripp}2}$	–3.33
$\text{CNAr}^{\text{Dipp}2}$	–3.28
$\text{CNPh}^{\text{t-Prop}2}$ , CNMes, CN <sup>t</sup> Bu	–2.38, –2.26, –2.15
CNPh, CNPh <sup>pNO2</sup>	–1.64, –0.95
CNPh <sup>BF</sup>	–1.25
CNp-FAR <sup>D<sup>+</sup>FP2</sup>	+2.73

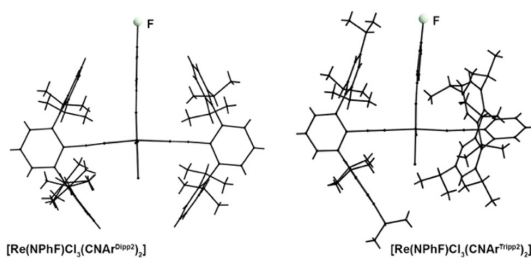


Fig. 6 Wire-frame presentation of the structures of *mer*-[Re(NPhF)Cl<sub>3</sub>(CNAr<sup>Dipp2</sup>)<sub>2</sub>] (**8**) and *mer*-[Re(NPhF)Cl<sub>3</sub>(CNAr<sup>Tripp2</sup>)<sub>2</sub>] (**10**) along the planes formed by their phenylimido ligands.

regarding their steric bulk. This can nicely be seen in Fig. 6, where the solid state structures of [Re(NPhF)Cl<sub>3</sub>(CNAr<sup>Dipp2</sup>)<sub>2</sub>] (**8**) and [Re(NPhF)Cl<sub>3</sub>(CNAr<sup>Tripp2</sup>)<sub>2</sub>] (**10**) are shown along the planes formed by their phenylimido ligands. The central phenyl rings of the two CNAr<sup>Dipp2</sup> ligands are almost perfectly co-planar (twisting angle: 7.1(6)°) in a perpendicular arrangement to the phenylimido ring. The larger bulk of CNAr<sup>Tripp2</sup> results in a torsion of 52.3(2)° of the isocyanide ligand around its coordination axis. This is a direct effect of the ‘outer-sphere’ substitution on this ligand and may underline the influence of such relatively small modifications in the ligand design on structural factors, but also on the reactivity of the respective metal ion. It shall be noted that the proton NMR resonances of CNAr<sup>Tripp2</sup> appear as one set of signals suggesting that a rotation is possible in solution.

The steric effects discussed above shall always be regarded together with potential electronic effects due to the introduced residues and the electronic configuration of the metal ion. An example of the complex interplay of such influences shall be discussed with the use of the fluorinated isocyanides CNp-FAr<sup>DarF2</sup> and CNPh<sup>Pf</sup>.

The steric bulk of CNp-FAr<sup>DarF2</sup> due to the CF<sub>3</sub> residues in *meta* positions of the terphenyl rings takes mainly effect in the outer sphere of the complex similar to CNAr<sup>Tripp2</sup>, but the fluorinated ligand is more flexible in terms of a spheric arrangement around the metal ions. Thus, it allows the coordination of up to four of the ligands around a metal ion. This has been demonstrated recently for carbonyl complexes of manganese, technetium and rhenium, where compounds of the compositions [M<sup>-1</sup>(CO)(CNp-FAr<sup>DarF2</sup>)<sub>4</sub>]<sup>-</sup> (M = Tc, Re), [M<sup>0</sup>(CO)(CNp-FAr<sup>DarF2</sup>)<sub>4</sub>] (M = Tc, Re) and [M<sup>1</sup>(CO)(CNp-FAr<sup>DarF2</sup>)<sub>4</sub>] (M = Tc, Re) have been isolated in crystalline form.<sup>71,74</sup> The replacement of carbonyl ligands from tricarbonylrhenium(i) or technetium(i) centers is not common and can be attributed to the special electronic situation on the donor carbon atom due to the strong electron withdrawing capacity of the fluorine atom at the central phenyl ring of CNp-FAr<sup>DarF2</sup>.

For isocyanides, it is reasonable to assume that electron-deficient regions on the surface of the coordinating carbon atom would enable improved π-back-donation, while electron-rich regions on the surface of the same carbon atom are

responsible for a better σ-donation. Steric restraints on the donor carbon atom can be partially included in such an approach by averaging the obtained potential energies over the accessible surface of the potential donor atoms.

Thus, sterically demanding isocyanides such as CNAr<sup>Dipp2</sup> or CNAr<sup>Tripp2</sup> show less overall accessible surface area, while the less encumbered isocyanides have a larger overall accessible carbon surface. A more comprehensive discussion of this approach is shown in ref. 10. In the sterically encumbered, but fluorine-substituted CNp-FAr<sup>DarF2</sup> ligand the steric effects are overruled by the electron withdrawing capacity of fluorine, which make this ligand a powerful π-acceptor when it reacts with electron rich metal ions such as rhenium(i) or technetium(i) and explains the reactivity with the corresponding carbonyl compounds.<sup>10,11,20</sup> In the electron-deficient rhenium(v) complexes of the present study, however, π-back-donation plays practically no role, which is supported by the blue-shift of the IR ν<sub>C=N</sub> frequencies. Consequently, the reactivity of CNp-FAr<sup>DarF2</sup> in such cases is identical with those isocyanides with predominantly σ-donor properties and [Re(NPhF)Cl<sub>3</sub>(PPh<sub>3</sub>)(CNp-FAr<sup>DarF2</sup>)] (**11**) is formed as the sole product in a reaction with **1**. The corresponding reactivity is well reflected by the SADAP parameters in Table 2.

A similar behavior is observed for CNPh<sup>Pf</sup>, where the fluorine substitution at the central ring is retained, but the steric bulk due to the peripheral residuals is removed. Indeed, it behaves with electron-rich metal ions as a powerful π-acceptor, as has been demonstrated by the complete replacement of carbonyl and halido ligands in [Tc<sub>2</sub>(CO)<sub>6</sub>Cl<sub>3</sub>]<sup>2-</sup> and the formation of a [Tc(CNPhpF)<sub>6</sub>]<sup>+</sup> cation.<sup>20</sup> Expectedly, this is not observed for the d<sup>2</sup> complexes of the present study and the 1 : 1 complex [Re(NPhF)Cl<sub>3</sub>(PPh<sub>3</sub>)(CNPh<sup>Pf</sup>)] (**12**) was isolated from a corresponding reaction with compound **1**.

The structures of compounds **11** and **12** are shown in Fig. 7. All main structural features are close to those of the other 1 : 1 complexes presented in Fig. 2 and Table 1 and shall not be discussed here in detail.

## Experimental

### General considerations

Unless otherwise stated, reagent-grade starting materials were purchased from commercial sources and either used as received or purified by standard procedures. Solvents were dried according to standard procedures. The reactions have been performed in air unless otherwise stated. [Re(NPh<sup>Pf</sup>)Cl<sub>3</sub>(PPh<sub>3</sub>)] (**1**) as well as CNAr<sup>Dipp2</sup>, CNAr<sup>Tripp2</sup>, CNp-FAr<sup>DarF2</sup>, CNPh<sup>Pf</sup>, and CNPh<sup>t-prop2</sup> were prepared according to literature procedures.<sup>10,51,56,58,59</sup>

### Physical measurements

NMR spectra were recorded with JEOL 400 MHz ECS or ECZ or JEOL ECZ 600 or Bruker AV700 multinuclear spectrometers. IR spectra were recorded with an ATR spectrometer (Nicolet iS10, Thermo Scientific). Intensities are classified as vs = very

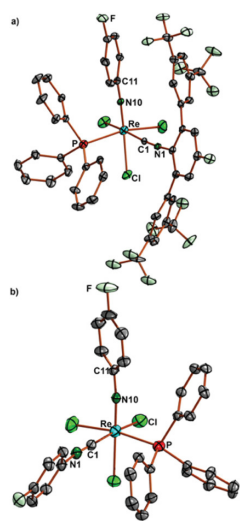


Fig. 7 Molecular structures of a) *fac*-[Re(NPh)Cl<sub>3</sub>(PPh<sub>3</sub>)(CNAr<sup>Dmf2</sup>)<sub>2</sub>] (**11**) and b) *mer*-[Re(NPh)Cl<sub>3</sub>(PPh<sub>3</sub>)(CNPh<sup>F</sup>)<sub>2</sub>] (**12**). Selected bond lengths and angles for **11**: Re–N10 1.721(43), Re–P 2.4494(9), Re–C1 2.022(3), C1–N1 1.151(4) Å; Re–N10–C11 170.4(2), and Re–C1–N1 174.6(43)°; selected bond lengths and angles for **12**: Re–N10 1.705(4), Re–P 2.470(2), Re–C1 2.024(6), C1–N1 1.156(7) Å; Re–N10–C11 172.9(4), and Re–C1–N1 176.9(5)°.

strong, s = strong, m = medium, w = weak, vw = very weak, and sh = shoulder. Electrospray ionization mass spectrometry (ESI MS) was carried out with the ESI MSD time-of-flight (TOF) unit of an Agilent 6210 TOF liquid chromatography/mass spectrometry system. Elemental analyses of carefully dried samples of the bulk were performed using a Vario MICRO cube CHNS elemental analyser.

#### X-ray crystallography

The intensities for X-ray determinations were collected on STOE IPDS II or Bruker D8 Venture instruments with Mo K $\alpha$  radiation. The space groups were determined by the detection of systematic absences. Absorption corrections were carried out by multi scan or integration methods.<sup>75,76</sup> Structure solution and refinement were performed with the SHELX program package using OLEX 2.<sup>77–79</sup> Hydrogen atoms were derived from the final Fourier maps and refined or placed at calculated positions and treated with the ‘riding model’ option of SHELXL. The representation of molecular structures was done using the program DIAMOND 4.2.2.<sup>80</sup>

Additional information on the structure determinations is presented in the ESI<sup>†</sup> and has been deposited with the Cambridge Crystallographic Data Centre.

#### Synthesis

**[Re(NPh)Cl<sub>3</sub>(PPh<sub>3</sub>)(CNR)] complexes.** [Re(NPh)Cl<sub>3</sub>(PPh<sub>3</sub>)<sub>2</sub>] (**1**) (92 mg, 0.1 mmol) was suspended in a 5 : 1 toluene/acetonitrile mixture (6 mL) and the corresponding isocyanide

(0.11 mmol) was added. The mixture was heated under reflux for 10 min in a pre-heated oil bath. The starting material dissolved and the solution turned blue or green. Volatiles were removed under reduced pressure and the residue was resuspended in diethyl ether (5 mL) and filtered. The obtained solid was washed with diethyl ether (3  $\times$  5 mL) and dried under reduced pressure.

***fac*-[Re(NPh)Cl<sub>3</sub>(PPh<sub>3</sub>)(CN<sup>t</sup>Bu)] (**2**).** Recrystallization from CH<sub>2</sub>Cl<sub>2</sub>/diethyl ether. Light blue plates. Yield: 36 mg, 48%. Elemental analysis: calc.: C: 46.6, H: 3.8, N: 3.7%. Found: C: 46.7, H: 3.8, N: 3.8%. IR (cm<sup>-1</sup>): 2192 (vs,  $\nu_{C=N}$ ), 1584 (vs). <sup>1</sup>H NMR (CD<sub>2</sub>Cl<sub>2</sub>, ppm):  $\delta$  = 7.75 (m<sub>c</sub>, 6H), 7.42 (m<sub>c</sub>, 9H), 7.02 (m<sub>c</sub>, 2H), 6.82 (t,  $J$  = 8.0 Hz, 2H), 1.43 (s, 9H). <sup>19</sup>F NMR (CD<sub>2</sub>Cl<sub>2</sub>, ppm):  $\delta$  = -101.9 (m<sub>c</sub>). <sup>13</sup>C{<sup>1</sup>H} NMR (CD<sub>2</sub>Cl<sub>2</sub>, ppm):  $\delta$  = 162.83 (d, <sup>1</sup> $J$ (<sup>13</sup>C–<sup>19</sup>F) = 260 Hz), 151.32, 135.01 (d, <sup>1</sup> $J$ (<sup>13</sup>C–<sup>31</sup>P) = 8 Hz), 133.73 (d, <sup>1</sup> $J$ (<sup>13</sup>C–<sup>31</sup>P) = 53 Hz), 131.74, 128.90 (d, <sup>1</sup> $J$ (<sup>13</sup>C–<sup>31</sup>P) = 10 Hz), 127.09 (d, <sup>3</sup> $J$ (<sup>13</sup>C–<sup>19</sup>F) = 10 Hz), 117.55 (d, <sup>2</sup> $J$ (<sup>13</sup>C–<sup>19</sup>F) = 25 Hz), 60.30, 31.24. ESI + MS:  $m/z$  = 628.0141 [M – CN<sup>t</sup>Bu – Cl]<sup>+</sup> (calc.: 628.0158), 711.0855 [M – Cl]<sup>+</sup> (calc.: 711.0894), 769.0463 [M + Na]<sup>+</sup> (calc.: 769.0494), 1517.069 [2M + Na]<sup>+</sup> (calc.: 1517.0999).

***fac*-[Re(NPh)Cl<sub>3</sub>(PPh<sub>3</sub>)(CNPh)] (**3**).** Single crystals were obtained directly from the reaction mixture at 5 °C. Green, sensitive blocks. Only a small amount of the compound could be isolated in this way, since it quickly decomposes in solution even at room temperature precluding the measurement of spectra of appropriate quality. Already the uncoordinated CNPh is significantly more unstable than other isocyanides in this study. IR (cm<sup>-1</sup>): 2171 (vs,  $\nu_{C=N}$ ). ESI + MS:  $m/z$  = 731.0669 [M – Cl]<sup>+</sup> (calc.: 731.0581), 789.0183 [M + Na]<sup>+</sup> (calc.: 789.01622), 804.9920 [M + K]<sup>+</sup> (calc.: 804.9901), 1557.0502 [2M + Na]<sup>+</sup> (calc.: 1557.0417).

***fac*-[Re(NPh)Cl<sub>3</sub>(PPh<sub>3</sub>)(CNPh<sup>i</sup>prop<sup>2</sup>)] (**4**).** Recrystallization from CH<sub>2</sub>Cl<sub>2</sub>. Blue crystals. Yield: 44 mg, 52%. Elemental analysis: calc.: C: 52.2, H: 4.3, N: 3.3%. Found: C: 52.2, H: 4.3, N: 3.5%. IR (cm<sup>-1</sup>): 2168 (vs,  $\nu_{N=C}$ ). <sup>1</sup>H NMR (CD<sub>2</sub>Cl<sub>2</sub>, ppm):  $\delta$  = 7.81 (m<sub>c</sub>, 6H), 7.39 (m<sub>c</sub>, 3H), 7.34 (m<sub>c</sub>, 6H), 7.26–7.19 (m, 3H), 7.03 (m<sub>c</sub>, 2H), 6.86 (m<sub>c</sub>, 2H), 2.71 (h, <sup>3</sup> $J$ (<sup>1</sup>H, <sup>1</sup>H) = 7 Hz, 2H), 1.00 (d, <sup>3</sup> $J$ (<sup>1</sup>H, <sup>1</sup>H) = 7 Hz, 6H), 0.92 (d, <sup>3</sup> $J$ (<sup>1</sup>H, <sup>1</sup>H) = 7 Hz, 6H). <sup>19</sup>F NMR (CD<sub>2</sub>Cl<sub>2</sub>, ppm):  $\delta$  = -101.9 (m<sub>c</sub>). <sup>13</sup>C{<sup>1</sup>H} NMR (CD<sub>2</sub>Cl<sub>2</sub>, ppm):  $\delta$  = 162.86 (d, <sup>1</sup> $J$ (<sup>13</sup>C, <sup>19</sup>F) = 260 Hz), 151.45 (t, <sup>1</sup> $J$ (<sup>13</sup>C, <sup>14</sup>N) = 3 Hz), 145.48, 135.02 (d, <sup>1</sup> $J$ (<sup>13</sup>C, <sup>31</sup>P) = 9 Hz), 133.45 (d, <sup>1</sup> $J$ (<sup>13</sup>C, <sup>31</sup>P) = 45 Hz), 131.87 (d, <sup>1</sup> $J$ (<sup>13</sup>C, <sup>31</sup>P) = 2 Hz), 131.30, 129.01 (d, <sup>1</sup> $J$ (<sup>13</sup>C, <sup>31</sup>P) = 11 Hz), 126.93 (d, <sup>3</sup> $J$ (<sup>13</sup>C, <sup>19</sup>F) = 10 Hz), 123.41, 117.58 (d, <sup>2</sup> $J$ (<sup>13</sup>C, <sup>19</sup>F) = 25 Hz), 29.74, 23.51, 22.86. ESI + MS:  $m/z$  = 873.109 [M + Na]<sup>+</sup> (calc.: 873.112), 889.084 [M + K]<sup>+</sup> (calc.: 889.086), 1725.233 [2M + Na]<sup>+</sup> (calc.: 1723.234), 1739.209 [2M + K]<sup>+</sup> (calc.: 1739.208).

***fac*-[Re(NPh)Cl<sub>3</sub>(PPh<sub>3</sub>)(CNMes)] (**5**).** A few single crystals were obtained upon cooling the reaction mixture. Green-blue, sensitive blocks. Only a small amount of the compound could be isolated in this way, since it quickly decomposes in solution even at room temperature precluding the measurement of spectra of appropriate quality. IR (cm<sup>-1</sup>): 2173 (vs,  $\nu_{N=C}$ ). <sup>1</sup>H NMR (CD<sub>2</sub>Cl<sub>2</sub>, ppm):  $\delta$  = 7.78 (m<sub>c</sub>, 6H), 7.34 (m<sub>c</sub>, 9H), 7.04 (m<sub>c</sub>, 2H), 6.92 (s, 2H), 6.83 (dd, <sup>3</sup> $J$ (<sup>1</sup>H, <sup>1</sup>H) = 8 Hz, 2H), 2.42 (s, 3H),

2.01 (s, 6H). ESI + MS:  $m/z = 773.098$  [M - Cl]<sup>+</sup> (calc.: 773.1051), 1656.115 [2M + K]<sup>+</sup> (calc.: 1656.1019), 1657.115 [2M + K]<sup>+</sup> (calc.: 1657.1097).

**fac-[Re(NPhF)Cl<sub>3</sub>(PPh<sub>3</sub>)(CNPh<sup>NO2</sup>)Cl<sub>3</sub>] (6).** Recrystallization from CH<sub>2</sub>Cl<sub>2</sub>/toluene. Green, very unstable plates. Yield: 28 mg, 40%. The compound quickly decomposes in solution, which goes along with a color change to brown and precludes the measurement of the solution spectra of reasonable quality. IR (cm<sup>-1</sup>): 2160 (s,  $\nu_{N=C}$ ), 1735 (m,  $\nu_{N=O}$ ). <sup>1</sup>H NMR (acetone-d<sub>6</sub>, ppm):  $\delta = 8.32$  (m<sub>c</sub>, 2H), 7.79 (m<sub>c</sub>, 6H), 7.42–7.32 (m, 9H), 7.12–7.05 (m, 4H), 6.88 (dd, <sup>3</sup>J(<sup>1</sup>H, <sup>1</sup>H) = 8 Hz, 6H). <sup>19</sup>F NMR (acetone-d<sub>6</sub>, ppm):  $\delta = -100.4$  (m<sub>c</sub>). ESI + MS:  $m/z = 834.003$  [M + Na]<sup>+</sup> (calc.: 834.003), 1647.013 [2M + Na]<sup>+</sup> (calc.: 1645.017).

**fac-[Re(NPhF)Cl<sub>3</sub>(PPh<sub>3</sub>)(CNp-FAr<sup>DppF2</sup>)] (11).** Recrystallization from acetonitrile. Blue blocks. Yield: 82 mg, 67%. Elemental analysis: calc.: C: 46.7, H: 2.3, N: 2.3%. Found: C: 47.2, H: 2.3, N: 2.2%. IR (cm<sup>-1</sup>): 2158 (s,  $\nu_{N=C}$ ). <sup>1</sup>H NMR (acetone-d<sub>6</sub>, ppm):  $\delta = 8.22$  (s, 4H), 7.76 (s, 2H), 7.73 (d, <sup>3</sup>J(<sup>1</sup>H, <sup>19</sup>F) = 8 Hz, 2H), 7.49 (m<sub>c</sub>, 9H), 7.35 (m<sub>c</sub>, 3H), 7.22 (m<sub>c</sub>, 6H), 6.75 (m<sub>c</sub>, 2H), 6.62 (m<sub>c</sub>, 2H). <sup>19</sup>F NMR (acetone-d<sub>6</sub>, ppm):  $\delta = -62.6$  (s, 12F), -103.1 (m<sub>c</sub>, 1F), -109.9 (t, <sup>3</sup>J(<sup>19</sup>F, <sup>1</sup>H) = 8 Hz, 1F). <sup>13</sup>C{<sup>1</sup>H} NMR (acetone-d<sub>6</sub>, ppm):  $\delta = 163.42$  (d, <sup>1</sup>J(<sup>13</sup>C, <sup>19</sup>F) = 260 Hz), 163.31 (d, <sup>1</sup>J(<sup>13</sup>C, <sup>19</sup>F) = 260 Hz), 150.41, 148.13, 139.71 (d, J = 10 Hz), 138.30, 135.12 (d, J(<sup>13</sup>C, <sup>31</sup>P) = 10 Hz), 133.88 (d, <sup>1</sup>J(<sup>13</sup>C, <sup>31</sup>P) = 52 Hz), 132.46 (q, <sup>2</sup>J(<sup>13</sup>C, <sup>19</sup>F) = 33 Hz), 131.78, 131.14, 128.92 (d, J(<sup>13</sup>C, <sup>31</sup>P) = 10 Hz), 128.62 (d, <sup>3</sup>J(<sup>13</sup>C, <sup>19</sup>F) = 10 Hz), 124.00 (q, <sup>1</sup>J(<sup>13</sup>C, <sup>19</sup>F) = 260 Hz), 123.77, 119.98, 119.04 (d, <sup>2</sup>J(<sup>13</sup>C, <sup>19</sup>F) = 26 Hz), 117.61 (d, <sup>2</sup>J(<sup>13</sup>C, <sup>19</sup>F) = 26 Hz). ESI + MS:  $m/z = 1231.015$  [M + Na]<sup>+</sup> (calc.: 1231.020), 1246.989 [M + K]<sup>+</sup> (calc.: 1246.995), 2441.037 [2M + Na]<sup>+</sup> (calc.: 2441.043), 2457.010 [2M + K]<sup>+</sup> (calc.: 2457.017).

**fac-[Re(NPhF)(PPh<sub>3</sub>)Cl<sub>3</sub>(CNPh<sup>Pf</sup>)] (12).** Recrystallization from CH<sub>2</sub>Cl<sub>2</sub>/*n*-pentane. Green trapezoids. Yield: 60 mg, 76%. Elemental analysis: calc.: C: 47.4, H: 3.0, N: 3.6%. Found: C: 47.5, H: 3.1, N: 3.6%. IR (cm<sup>-1</sup>): 2173 (vs,  $\nu_{N=C}$ ). <sup>1</sup>H NMR (CD<sub>2</sub>Cl<sub>2</sub>, ppm):  $\delta = 7.80$  (m<sub>c</sub>, 6H), 7.39 (m<sub>c</sub>, 9H), 7.18 (m<sub>c</sub>, 2H), 7.08 (m<sub>c</sub>, 2H), 7.03 (m<sub>c</sub>, 2H), 6.85 (m<sub>c</sub>, 2H). <sup>19</sup>F NMR (CD<sub>2</sub>Cl<sub>2</sub>, ppm):  $\delta = -101.4$  (m<sub>c</sub>, 1F), -106.9 (m<sub>c</sub>, 1F). <sup>13</sup>C{<sup>1</sup>H} NMR (CD<sub>2</sub>Cl<sub>2</sub>, ppm):  $\delta = 164.12$  (d, (<sup>1</sup>J(<sup>13</sup>C-<sup>19</sup>F) = 260 Hz), 163.17 (d, (<sup>1</sup>J(<sup>13</sup>C-<sup>19</sup>F) = 260 Hz), 150.98, 140.81, 134.93 (d, J(<sup>13</sup>C-<sup>31</sup>P) = 8 Hz), 133.16 (d, <sup>1</sup>J(<sup>13</sup>C-<sup>31</sup>P) = 54 Hz), 131.87, 129.49 (d, <sup>3</sup>J(<sup>13</sup>C-<sup>19</sup>F) = 10 Hz), 129.05 (d, J(<sup>13</sup>C-<sup>31</sup>P) = 10 Hz), 127.65 (d, <sup>3</sup>J(<sup>13</sup>C-<sup>19</sup>F) = 10 Hz), 122.79, 117.70 (d, <sup>2</sup>J(<sup>13</sup>C-<sup>19</sup>F) = 25 Hz), 117.17 (d, <sup>2</sup>J(<sup>13</sup>C-<sup>19</sup>F) = 25 Hz). ESI + MS:  $m/z = 806.990$  [M + Na]<sup>+</sup> (calc.: 807.008), 822.964 [M + K]<sup>+</sup> (calc.: 822.983), 1590.993 [2M + Na]<sup>+</sup> (calc.: 1591.028), 1607.002 [2M + K]<sup>+</sup> (calc.: 1606.966).

**fac-[Re(NPhF)Cl<sub>3</sub>(CNAr<sup>Mes2</sup>)<sub>2</sub>] (7).** [Re(NPhF)Cl<sub>3</sub>(PPh<sub>3</sub>)<sub>2</sub>] (1) (92 mg, 0.1 mmol) was suspended in toluene (10 mL) and CNAr<sup>Mes2</sup> (68 mg, 0.2 mmol) was added to it. The mixture was heated under reflux and the progress of the reaction was monitored by <sup>19</sup>F NMR. The solution became blue and homogeneous upon heating. After three hours, the complete starting material was consumed. Volatiles were removed under reduced pressure and the resulting blue solid was resuspended in *n*-pentane, filtered and washed with more *n*-pentane. Blue

needles suitable for X-ray diffraction were obtained by slow evaporation of the toluene solution at 5 °C. Yield: 18 mg, 17%. Elemental analysis: calc.: C: 62.2, H: 5.0, N: 3.9%. Found: C: 62.4, H: 5.1, N: 3.9%. IR (cm<sup>-1</sup>): 2192 (s,  $\nu_{C=N}$ ), 2163 (s,  $\nu_{C=N}$ ). <sup>1</sup>H NMR (CD<sub>2</sub>Cl<sub>2</sub>, ppm):  $\delta = 7.52$  (dd, <sup>3</sup>J(<sup>1</sup>H, <sup>1</sup>H) = 8 Hz, 2H), 7.27 (d, <sup>3</sup>J(<sup>1</sup>H, <sup>1</sup>H) = 8 Hz, 4H), 7.85 (dd, <sup>3</sup>J(<sup>1</sup>H, <sup>1</sup>H) = 8 Hz, 2H), 6.83 (s, 4H), 6.74 (s, 4H), 6.43 (m<sub>c</sub>, 2H), 2.22 (s, 12H), 2.01 (s, 12H), 1.98 (s, 12H). <sup>19</sup>F NMR (CD<sub>2</sub>Cl<sub>2</sub>, ppm):  $\delta = -101.1$  (m<sub>c</sub>). <sup>13</sup>C{<sup>1</sup>H} NMR (CD<sub>2</sub>Cl<sub>2</sub>, ppm):  $\delta = 163.39$  (d, <sup>1</sup>J(<sup>13</sup>C, <sup>19</sup>F) = 260 Hz), 150.20 (br. s), 140.13, 138.08, 136.17 (d, <sup>3</sup>J(<sup>13</sup>C, <sup>19</sup>F) = 14 Hz), 135.21, 133.13, 131.61, 130.27, 128.89, 128.72, 128.58 (d, <sup>4</sup>J(<sup>13</sup>C, <sup>19</sup>F) = 9 Hz), 125.03, 117.14 (d, <sup>2</sup>J(<sup>13</sup>C, <sup>19</sup>F) = 24 Hz), 21.38, 20.69, 20.29. ESI + MS:  $m/z = 1044.3266$  [M - Cl]<sup>+</sup> (calc.: 1044.3224), 1102.2871 [M + Na]<sup>+</sup> (calc.: 1102.2850), 2183.5903 [2M + Na]<sup>+</sup> (calc.: 2183.5718).

**mer-[Re(NPhF)Cl<sub>3</sub>(CNAr<sup>Dipp2</sup>)<sub>2</sub>] (8).** [Re(NPhF)Cl<sub>3</sub>(PPh<sub>3</sub>)<sub>2</sub>] (1) (92 mg, 0.1 mmol) was suspended in toluene (4 mL) and CNAr<sup>Dipp2</sup> (128 mg, 0.3 mmol) was added to it. The mixture was heated under reflux and the progress of the reaction was monitored by <sup>19</sup>F NMR. After 4 h, the starting complex was completely consumed. The volatiles were removed under reduced pressure and the obtained blue solid was suspended in *n*-pentane, filtered off, and washed with further *n*-pentane. Blue single crystals suitable for X-ray diffraction were obtained from CH<sub>2</sub>Cl<sub>2</sub>/toluene. Yield: 46 mg, 37%. Elemental analysis: calc.: C: 65.4, H: 6.3, N: 3.4%. Found: C: 65.4, H: 6.1, N: 3.1%. IR (cm<sup>-1</sup>): 2170 (vs,  $\nu_{N=C}$ ). <sup>1</sup>H NMR (CD<sub>2</sub>Cl<sub>2</sub>, ppm):  $\delta = 7.47$  (dd, <sup>3</sup>J(<sup>1</sup>H, <sup>1</sup>H) = 7 Hz), 7.28 (d, <sup>3</sup>J(<sup>1</sup>H, <sup>1</sup>H) = 8 Hz, 4H), 7.12 (dd, <sup>3</sup>J(<sup>1</sup>H, <sup>1</sup>H) = 8 Hz), 7.06 (m<sub>c</sub>, 2H), 7.02–6.98 (m, 10H), 2.42 (hept, <sup>3</sup>J(<sup>1</sup>H, <sup>1</sup>H) = 7 Hz), 1.05 (d, <sup>3</sup>J(<sup>1</sup>H, <sup>1</sup>H) = 8 Hz, 24H), 1.03 (d, <sup>3</sup>J(<sup>1</sup>H, <sup>1</sup>H) = 8 Hz, 24H). <sup>19</sup>F NMR (CD<sub>2</sub>Cl<sub>2</sub>, ppm):  $\delta = -103.4$  (m<sub>c</sub>). <sup>13</sup>C{<sup>1</sup>H} NMR (CD<sub>2</sub>Cl<sub>2</sub>, ppm):  $\delta = 160.43$  (d, <sup>1</sup>J(<sup>13</sup>C, <sup>19</sup>F) = 260 Hz), 153.48, 146.77, 140.32, 133.35, 130.83, 130.17, 129.57, 125.34, 124.25 (d, <sup>3</sup>J(<sup>13</sup>C, <sup>19</sup>F) = 10 Hz), 123.17, 117.84 (d, <sup>2</sup>J(<sup>13</sup>C, <sup>19</sup>F) = 25 Hz), 31.54, 24.57, 24.13. ESI + MS:  $m/z = 1270.4715$  [M + Na]<sup>+</sup> (calc.: 1270.46951).

**fac-[Re(NPhF)Cl<sub>3</sub>(PPh<sub>3</sub>)(CNAr<sup>Tripp2</sup>)] (9).** [Re(NPhF)Cl<sub>3</sub>(PPh<sub>3</sub>)<sub>2</sub>] (1) (92 mg, 0.1 mmol) was suspended in toluene (6 mL) and CNAr<sup>Tripp2</sup> (102 mg, 0.2 mmol) dissolved in toluene (2 mL) was added to it. The mixture was heated under reflux and the progress of the reaction was monitored by <sup>19</sup>F NMR. After one hour, only the resonances of the starting material and one other compound were observed. The heating was stopped and a few blue needles suitable for X-ray diffraction were obtained by slow evaporation of the crude reaction mixture at 5 °C.

**mer-[Re(NPhF)Cl<sub>3</sub>(CNAr<sup>Tripp2</sup>)<sub>2</sub>] (10).** [Re(NPhF)Cl<sub>3</sub>(PPh<sub>3</sub>)<sub>2</sub>] (1) (92 mg, 0.1 mmol) was suspended in toluene (6 mL) and CNAr<sup>Tripp2</sup> (102 mg, 0.2 mmol) dissolved in toluene (2 mL) was added to it. The mixture was heated under reflux and the progress of the reaction was monitored by <sup>19</sup>F NMR. After 12 h, complex 1 was nearly completely consumed. The volatiles were removed under reduced pressure and the residue was dissolved in diethyl ether and filtered. The solvent was removed under reduced pressure leading to a blue powder. Blue single crystals suitable for X-ray diffraction were obtained from diethyl ether/

*n*-hexane. Yield: 116 mg, 82%. Elemental analysis: calc.: C: 67.8, H: 7.3, N: 3.0%. Found: C: 67.9, H: 7.3, N: 3.0%. IR (cm<sup>-1</sup>): 2170 (vs,  $\nu_{\text{N}=\text{C}}$ ). <sup>1</sup>H NMR (CD<sub>2</sub>Cl<sub>2</sub>, ppm):  $\delta$  = 7.47 (dd, <sup>3</sup>*J*(<sup>1</sup>H,<sup>1</sup>H) = 8 Hz, 2H), 7.31 (d, <sup>3</sup>*J*(<sup>1</sup>H,<sup>1</sup>H) = 8 Hz, 4H), 7.07 (m<sub>c</sub>, 2H), 6.93 (s, 8H), 6.86 (m<sub>c</sub>, 2H), 2.82 (h, <sup>3</sup>*J*(<sup>1</sup>H,<sup>1</sup>H) = 7 Hz, 4H), 2.38 (h, <sup>3</sup>*J*(<sup>1</sup>H,<sup>1</sup>H) = 7 Hz, 8H), 1.28 (d, <sup>3</sup>*J*(<sup>1</sup>H,<sup>1</sup>H) = 8 Hz, 24H), 1.02 (d, <sup>3</sup>*J*(<sup>1</sup>H,<sup>1</sup>H) = 8 Hz, 24H), 0.95 (d, <sup>3</sup>*J*(<sup>1</sup>H,<sup>1</sup>H) = 8 Hz, 24H). <sup>19</sup>F NMR (CD<sub>2</sub>Cl<sub>2</sub>, ppm):  $\delta$  = -104.1 (m<sub>c</sub>). <sup>13</sup>C{<sup>1</sup>H} NMR (CD<sub>2</sub>Cl<sub>2</sub>, ppm):  $\delta$  = 160.43 (d, <sup>1</sup>*J*(<sup>13</sup>C,<sup>19</sup>F) = 260 Hz), 153.96, 149.74, 146.40, 141.49, 131.18, 130.76, 130.46, 126.09, 123.59 (d, <sup>3</sup>*J*(<sup>13</sup>C,<sup>19</sup>F) = 10 Hz), 121.75, 117.52 (d, <sup>2</sup>*J*(<sup>13</sup>C,<sup>19</sup>F) = 24 Hz), 34.99, 31.67, 24.91, 24.53, 24.09. ESI + MS: *m/z* = 1438.644 [M + Na]<sup>+</sup> (calc.: 1436.657), 1454.618 [M + K]<sup>+</sup> (calc.: 1454.631).

## Conclusions

The results of the present study may demonstrate that the use of fluorine-substituted ligand systems can have a number of benefits apart from their use in pharmaceutical approaches, but also for fundamental chemical studies. (1) The introduction of the fluorine or CF<sub>3</sub> substituent modulates the solubility *e.g.* of the starting materials, (2) reactions with diamagnetic compounds can readily be monitored (and thus optimized) by means of <sup>19</sup>F NMR, (3) the use of a peripheral *m,m'*-(CF<sub>3</sub>)<sub>2</sub>Ar group is a suitable instrument to control the steric bulk of ligand systems and (4) fluorine substituents are well suitable to control the electronic properties of ligand systems.

## Author contributions

Conceptualization: U. A., J. S. F., and G. C.; methodology: M. R. J. and A. H.; validation: G. C. and E. K.; formal analysis: G. C., E. K., A. H., and M. R. J.; investigation: G. C., E. K., and U. A.; resources: U. A.; writing – original draft preparation: U. A.; writing – review and editing: U. A., J. S. F., G. C., M. R. J., and E. K.; visualization: U. A. and G. C.; supervision: U. A., J. S. F., and G. C.; project administration: G. C. and U. A.; funding acquisition: U. A. and J. S. F. All authors have read and agreed to the published version of the manuscript.

## Conflicts of interest

There are no conflicts to declare.

## Acknowledgements

This research was funded by the DFG (Deutsche Forschungsgemeinschaft: Graduate School BIOQIC), the U.S. National Science Foundation (International Supplement to CHE-1802646), and the Alexander von Humboldt Foundation (fellowship to J. S. F.). We acknowledge the assistance of the Core Facility BioSupraMol supported by the DFG and of the High-Performance-Computing (HPC) Centre of the

Zentraleinrichtung für Datenverarbeitung (ZEDAT) of the Freie Universität Berlin for computational time and support.

## References

- 1 E. P. Gillis, K. J. Eastman, M. D. Hill, D. J. Donnelly and N. A. Meanwell, *J. Med. Chem.*, 2015, **58**, 8315.
- 2 F. Salsi, G. Bulhões Portapilla, S. Simon, M. Roca Jungfer, A. Hagenbach, S. de Albuquerque and U. Abram, *Inorg. Chem.*, 2019, **58**, 10129.
- 3 Y. Zhou, J. Wang, Z. Gu, S. Wang, W. Zhu, J. Luis Aceña, V. A. Soloshonok, K. Izawa and H. Liu, *Chem. Rev.*, 2016, **116**, 422.
- 4 O. Jacobsen, D. O. Kiesewetter and X. Chen, *Bioconjugate Chem.*, 2015, **26**, 1–18.
- 5 R. Halder and T. Ritter, *J. Org. Chem.*, 2021, **86**, 13873–13884.
- 6 U. Abram, Innovative PET and SPECT tracers, in *Quantification of Biophysical Parameters in Medical Imaging*, ed. I. Sack and T. Schaeffter, Springer International, 2017, pp. 255–279.
- 7 M. D. Bartholomä, A. S. Louie, J. F. Valliant and J. Zubieta, *Chem. Rev.*, 2010, **110**, 2903.
- 8 C. S. Cutler, H. M. Hennkens, N. Sisay, S. Huclier-Markai and S. S. Jurisson, *Chem. Rev.*, 2013, **113**, 858.
- 9 F. Salsi, M. Roca Jungfer, A. Hagenbach and U. Abram, *Eur. J. Inorg. Chem.*, 2020, **13**, 1222.
- 10 G. Claude, J. Genz, D. Weh, M. Roca Jungfer, A. Hagenbach, M. Gembicky, J. S. Figueroa and U. Abram, *Inorg. Chem.*, 2022, **61**, 16163.
- 11 G. Claude, D. Weh, A. Hagenbach, J. S. Figueroa and U. Abram, *Z. Anorg. Allg. Chem.*, 2022, e202200320.
- 12 M. C. Gil Valenzuela, J. Környei, M. Mikolajzak, K. Ozker, M. R. A. Pillai, M. Venkatesh, E. B. Araujo, M. Dondi, S. C. Gomes, R. Koga, E. Lavie, Z. F. Luo, J. Mustansar, D. V. S. Narasimhan, W. Paragulla, A. Robles and S. Verdera, *Technetium-99m Radiopharmaceuticals: Manufacture of Kits*, IAEA Technical Reports Series No. 466, International Atomic Energy Agency, Vienna, Austria, 2008, pp. 126–129.
- 13 L. W. Herman, V. Sharma, J. F. Kronauge, E. Barbaric, L. Herman and D. Piwnica-Worms, *J. Med. Chem.*, 1995, **38**, 2955–2963.
- 14 D. Piwnica-Worms, J. F. Kronauge, B. L. Holman, A. Davison and A. G. Jones, *Invest. Radiol.*, 1989, **24**, 25–29.
- 15 J. F. Kronauge and D. J. Mindiola, *Organometallics*, 2016, **35**, 3432–3435.
- 16 F. E. Hahn, L. Imhof and T. Lügger, *Inorg. Chim. Acta*, 1998, **269**, 347–349.
- 17 J. Bryan, R. E. Stenkamp, T. H. Tulip and J. M. Mayer, *Inorg. Chem.*, 1987, **26**, 2283–2288.
- 18 J. S. Figueroa and U. Abram, *Z. Anorg. Allg. Chem.*, 2020, **646**, 909–914.
- 19 G. Claude, F. Salsi, A. Hagenbach, M. Gembicky, M. Neville, C. Chan, J. S. Figueroa and U. Abram, *Organometallics*, 2020, **39**, 2287–2294.

- 20 G. Claude, L. Zeh, M. Roca Jungfer, A. Hagenbach, J. S. Figueroa and U. Abram, *Molecules*, 2022, **27**, 8546.
- 21 U. Abram, Rhenium, in *Comprehensive Coordination Chemistry II*, ed. J. A. McCleverty and T. J. Meyer, Elsevier, 2003, vol. 5, pp. 271–403.
- 22 G. K. Lahiri, S. Goswami, L. R. Falvello and A. Chakravorty, *Inorg. Chem.*, 1987, **26**, 3365–3370.
- 23 C. M. Archer, J. R. Dilworth, P. Jobanputra, M. E. Harman, M. B. Hursthouse and A. Karaulov, *Polyhedron*, 1991, **10**, 1539–1543.
- 24 M. Bakir, S. Paulson, P. Goodson and B. P. Sullivan, *Inorg. Chem.*, 1992, **31**, 1127–1129.
- 25 Yu.-P. Wang, C.-M. Che, K.-Y. Wong and S.-M. Peng, *Inorg. Chem.*, 1993, **32**, 5827–2832.
- 26 M. A. Masood and D. J. Hodgson, *Inorg. Chem.*, 1994, **33**, 2488–2490.
- 27 M. A. Masood, B. P. Sullivan and D. J. Hodgson, *Inorg. Chem.*, 1994, **33**, 5360–5362.
- 28 H. Luo, I. Setyawati, S. J. Rettig and C. Orvig, *Inorg. Chem.*, 1995, **34**, 2287–2299.
- 29 M. Bakir and B. P. Sullivan, *J. Chem. Soc., Dalton Trans.*, 1995, 1733–1738.
- 30 M. T. Ahmet, B. Coutinho, J. R. Dilworth, J. R. Miller, S. J. Parrott, Y. Zheng, M. Harman, M. B. Hursthouse and A. Malik, *J. Chem. Soc., Dalton Trans.*, 1995, 3041–3048.
- 31 M. Bakir, J. A. M. McKenzie and B. P. Sullivan, *Inorg. Chim. Acta*, 1997, **254**, 9–17.
- 32 F. Refosco, C. Bolzati, F. Tisato and G. Bandoli, *J. Chem. Soc., Dalton Trans.*, 1998, 923–930.
- 33 M. A. Masood, B. P. Sullivan and D. J. Hodgson, *Inorg. Chem.*, 1999, **38**, 5425–5430.
- 34 A. L. Suing, C. R. Dewan, P. S. White and H. H. Thorp, *Inorg. Chem.*, 2000, **39**, 6080–6085.
- 35 X. Couillens, M. Gressier, R. Turpin, M. Dartiguenave, Y. Coulais and A. L. Beauchamp, *J. Chem. Soc., Dalton Trans.*, 2002, 914–924.
- 36 M. Porchia, F. Tisato, F. Refosco, C. Bolzati, M. Cavazza-Ceccato, G. Bandoli and A. Dolmella, *Inorg. Chem.*, 2005, **44**, 4766–4776.
- 37 H. Braband, D. Przyrembel and U. Abram, *Z. Anorg. Allg. Chem.*, 2006, **632**, 779–785.
- 38 B. Kuhn and U. Abram, *Z. Anorg. Allg. Chem.*, 2008, **634**, 2982–2988.
- 39 B. Kuhn and U. Abram, *Z. Anorg. Allg. Chem.*, 2011, **637**, 242–245.
- 40 H. H. Nguyen, C. T. Pham and U. Abram, *Polyhedron*, 2015, **99**, 216–222.
- 41 S. Majumder, J. P. Naskar, A. Bhattacharya, R. Ganguly, P. Saha and S. Chowdhury, *J. Coord. Chem.*, 2015, **68**, 599–615.
- 42 P. Saha, J. P. Naskar, A. Bhattacharya, R. Ganguly, B. Saha and S. Chowdhury, *J. Coord. Chem.*, 2016, **69**, 303–317.
- 43 M. Roca Jungfer, A. Hagenbach, E. Schulz Lang and U. Abram, *Eur. J. Inorg. Chem.*, 2019, 4974–4984.
- 44 A. P. Borges, B. Possato, A. Hagenbach, A. E. H. Machado, V. M. Deflon, U. Abram and P. I. S. Maia, *Inorg. Chim. Acta*, 2021, **516**, 120110.
- 45 N. H. Huy and U. Abram, *Z. Anorg. Allg. Chem.*, 2008, **634**, 1560–1564.
- 46 X. Schoultz, T. I. A. Gerber, E. Hosten, R. Betz, L. Rhyman and P. Ramasami, *Polyhedron*, 2015, **96**, 6–15.
- 47 A. Barandov and U. Abram, *Polyhedron*, 2009, **28**, 1155–1159.
- 48 L. Wei, J. Zubieta and J. W. Babich, *Inorg. Chem.*, 2004, **43**, 6445–6454.
- 49 T. I. A. Gerber, D. Luzipo and P. Mayer, *Inorg. Chim. Acta*, 2004, **357**, 429–435.
- 50 J. B. Arterburn, K. V. Rao, D. M. Goreham, M. V. Valenzuela, M. S. Holguin, K. A. Hall, K. C. Ott and J. C. Bryan, *Organometallics*, 2000, **19**, 1789–1795.
- 51 C. Scholtysik, M. Roca Jungfer, A. Hagenbach and U. Abram, *Z. Anorg. Allg. Chem.*, 2018, **644**, 1451.
- 52 C. Scholtysik, C. Njiki Noufele, A. Hagenbach and U. Abram, *Inorg. Chem.*, 2019, **58**, 5241.
- 53 G. Bandoli, T. I. A. Gerber, J. Perilis and J. G. H. du Preez, *Inorg. Chim. Acta*, 1998, **278**, 96–100.
- 54 M. T. Ahmet, B. Coutinho, J. R. Dilworth, J. R. Miller, S. J. Parrott and Y. Zheng, *Polyhedron*, 1996, **15**, 2041–2050.
- 55 T. D. Lohrey, E. A. Cortes, J. I. Fostvedt, A. L. Oanta, A. Jain, R. G. Bergman and J. Arnold, *Inorg. Chem.*, 2020, **59**, 11096–11107.
- 56 P. Patil, M. Ahmadian-Moghaddam and A. Dömling, *Green Chem.*, 2020, **22**, 6902–6911.
- 57 L. A. Labios, M. D. Millard, A. L. Rheingold and J. S. Figueroa, *J. Am. Chem. Soc.*, 2009, **131**, 11318–11319.
- 58 T. B. Ditri, B. J. Fox, C. E. Moore, A. L. Rheingold and J. S. Figueroa, *Inorg. Chem.*, 2009, **48**, 8362–8375.
- 59 B. J. Fox, M. D. Millard, A. G. DiPasquale, A. L. Rheingold and J. S. Figueroa, *Angew. Chem., Int. Ed.*, 2009, **48**, 3473–3477.
- 60 B. J. Fox, Q. Y. Sun, A. G. DiPasquale, A. R. Fox, A. L. Rheingold and J. S. Figueroa, *Inorg. Chem.*, 2008, **47**, 9010–9020.
- 61 G. W. Margulieux, N. Weidemann, D. C. Lacy, C. E. Moore, A. L. Rheingold and J. S. Figueroa, *J. Am. Chem. Soc.*, 2010, **132**, 5033–5035.
- 62 M. A. Stewart, C. E. Moore, T. B. Ditri, L. A. Labios, A. L. Rheingold and J. S. Figueroa, *Chem. Commun.*, 2011, 47, 406–408.
- 63 D. W. Agnew, C. E. Moore, A. L. Rheingold and J. S. Figueroa, *Organometallics*, 2017, **36**, 363–371.
- 64 C. C. Mokhtarzadeh, C. E. Moore, A. L. Rheingold and J. S. Figueroa, *J. Am. Chem. Soc.*, 2018, **140**, 8100–8104.
- 65 D. W. Agnew, C. E. Moore, A. L. Rheingold and J. S. Figueroa, *Angew. Chem., Int. Ed.*, 2015, **54**, 12673–12677.
- 66 A. E. Carpenter, C. C. Mokhtarzadeh, D. S. Ripatti, I. Havrylyuk, R. Kamezawa, C. E. Moore, A. L. Rheingold and J. S. Figueroa, *Inorg. Chem.*, 2015, **54**, 2936.
- 67 D. W. Agnew, M. D. Sampson, C. E. Moore, A. L. Rheingold, C. P. Kubiak and J. S. Figueroa, *Inorg. Chem.*, 2016, **55**, 12400–12408.



- 68 D. W. Agnew, C. E. Moore, A. L. Rheingold and J. S. Figueroa, *Dalton Trans.*, 2017, **46**, 6700–6707.
- 69 M. J. Drance, J. D. Sears, A. M. Mrse, C. E. Moore, A. L. Rheingold, M. L. Neidig and J. S. Figueroa, *Science*, 2019, **363**, 1203–1205.
- 70 F. Salsi, M. Neville, M. Drance, A. Hagenbach, C. Chan, J. S. Figueroa and U. Abram, *Chem. Commun.*, 2020, **56**, 7009–7013.
- 71 F. Salsi, M. Neville, M. Drance, A. Hagenbach, J. S. Figueroa and U. Abram, *Organometallics*, 2021, **40**, 1336–1343.
- 72 N. Weidemann, G. W. Margulieux, C. E. Moore, A. L. Rheingold and J. S. Figueroa, *Inorg. Chim. Acta*, 2010, **364**, 238–245.
- 73 T. B. Ditri, A. E. Carpenter, D. S. Ripatti, E. Moore, A. L. Rheingold and J. S. Figueroa, *Inorg. Chem.*, 2013, **52**, 132216–113229.
- 74 F. Salsi, S. Wang, C. Teutloff, M. Busse, M. L. Neville, A. Hagenbach, R. Bittl, J. S. Figueroa and U. Abram, *Angew. Chem., Int. Ed.*, 2023, DOI: [10.1002/anie.202300254](https://doi.org/10.1002/anie.202300254).
- 75 G. M. Sheldrick, *SADABS*, University of Göttingen, Germany, 1996.
- 76 P. Coppens., *The Evaluation of Absorption and Extinction in Single-Crystal Structure Analysis. Crystallographic Computing*, Copenhagen, Muksgaard, 1979.
- 77 G. M. Sheldrick, A short history of SHELX, *Acta Crystallogr.*, 2008, **64**, 112.
- 78 G. M. Sheldrick, Crystal structure refinement with SHELXL, *Acta Crystallogr.*, 2015, **71**, 3.
- 79 O. V. Dolomanov, L. J. Bourhis, R. J. Gildea, J. A. K. Howard and H. Puschmann, *J. Appl. Crystallogr.*, 2009, **42**, 339–341.
- 80 H. Putz and K. Brandenburg, *DIAMOND, Crystal and Molecular Structure Visualization Crystal Impact, version 4.6.5*, GbR, Bonn, Germany, 2021.

Supporting information for the paper entitled:

**Phenylimido Complexes of Rhenium: Fluorine Substituents Provide Protection, Reactivity and Solubility**

*Guilhem Claude,<sup>a</sup> Erika Kulitzki,<sup>a</sup> Adelheid Hagenbach,<sup>a</sup> Maximilian Roca Jungfer,<sup>a</sup> Joshua R. Figueroa<sup>b\*</sup>, and Ulrich Abram<sup>a\*</sup>*

<sup>a</sup>Freie Universität Berlin, Institute of Chemistry and Biochemistry, Fabeckstr. 34–36,  
14195 Berlin, Germany

E-mail: [ulrich.abram@fu-berlin.de](mailto:ulrich.abram@fu-berlin.de)

<sup>b</sup>Department of Chemistry and Biochemistry, University of California, San Diego, La  
Jolla, California 92093, United States

E-mail: [jfig@ucsd.edu](mailto:jfig@ucsd.edu)

## Table of content

<b>Crystallographic data</b> .....	<b>6</b>
<b>Table S1:</b> Crystallographic data and data collection parameters .....	6
<b>Figure S1:</b> Ellipsoid representation of [Re(NPhF)Cl <sub>3</sub> (PPh <sub>3</sub> )(CN <sup>i</sup> Bu)] ( <b>2</b> ). The thermal ellipsoids are set at a 50% probability level. Hydrogen atoms are omitted for clarity. ....	10
<b>Table S2A:</b> Selected bond lengths (Å) and angles (°) in [Re(NPhF)Cl <sub>3</sub> (PPh <sub>3</sub> )(CN <sup>i</sup> Bu)] ( <b>2</b> ).....	10
<b>Figure S2:</b> Ellipsoid representation of [Re(NPhF)Cl <sub>3</sub> (PPh <sub>3</sub> )(CNPh)] ( <b>3</b> ). The thermal ellipsoids are set at a 50% probability level. Hydrogen atoms are omitted for clarity. ....	11
<b>Table S3:</b> Selected bond lengths (Å) and angles (°) in [Re(NPhF)Cl <sub>3</sub> (PPh <sub>3</sub> )(CNPh)] ( <b>3</b> ). .....	11
<b>Figure S3:</b> Ellipsoid representation of [Re(NPhF)Cl <sub>3</sub> (PPh <sub>3</sub> )(CNPh <sup>i-prop2</sup> )] ( <b>4</b> ). The thermal ellipsoids are set at a 50% probability level. Hydrogen atoms are omitted for clarity. ....	12
<b>Table S4:</b> Selected bond lengths (Å) and angles (°) in [Re(NPhF)Cl <sub>3</sub> (PPh <sub>3</sub> )(CNPh <sup>i-prop2</sup> )] ( <b>4</b> ).....	12
<b>Figure S4:</b> Ellipsoid representation of [Re(NPhF)Cl <sub>3</sub> (PPh <sub>3</sub> )(CNMes)] ( <b>5</b> ). The thermal ellipsoids are set at a 50% probability level. Hydrogen atoms are omitted for clarity. ....	13
<b>Table S5:</b> Selected bond lengths (Å) and angles (°) in [Re(NPhF)Cl <sub>3</sub> (PPh <sub>3</sub> )(CNMes)] ( <b>5</b> ). .....	13
<b>Figure S5:</b> Ellipsoid representation of [Re(NPhF)Cl <sub>3</sub> (PPh <sub>3</sub> )(CNPh <sup>pNO2</sup> )] ( <b>6</b> ). The thermal ellipsoids are set at a 50% probability level. Hydrogen atoms are omitted for clarity. ....	14
<b>Table S6:</b> Selected bond lengths (Å) and angles (°) in [Re(NPhF)Cl <sub>3</sub> (PPh <sub>3</sub> )(CNPh <sup>pNO2</sup> )] ( <b>6</b> ).....	14
<b>Figure S6:</b> Ellipsoid representation of [Re(NPhF)Cl <sub>3</sub> (CNAr <sup>Mes2</sup> ) <sub>2</sub> ] ( <b>7</b> ). The thermal ellipsoids are set at a 50% probability level. Hydrogen atoms are omitted for clarity. ....	15
<b>Table S7:</b> Selected bond lengths (Å) and angles (°) in [Re(NPhF)Cl <sub>3</sub> (CNAr <sup>Mes2</sup> ) <sub>2</sub> ] ( <b>7</b> )....	15
<b>Figure S7A:</b> Ellipsoid representation of [Re(NPhF)Cl <sub>3</sub> (CNAr <sup>Dipp2</sup> ) <sub>2</sub> ]·1.25 toluene·1/2 CH <sub>2</sub> Cl <sub>2</sub> ( <b>8</b> ), species 1. The thermal ellipsoids are set at a 50% probability level. Hydrogen atoms are omitted for clarity.....	16
<b>Table S8A:</b> Selected bond lengths (Å) and angles (°) in [Re(NPhF)Cl <sub>3</sub> (CNAr <sup>Dipp2</sup> ) <sub>2</sub> ]·1.25 toluene·1/2 CH <sub>2</sub> Cl <sub>2</sub> ( <b>8</b> ), species 1. ....	16
<b>Figure S7B:</b> Ellipsoid representation of [Re(NPhF)Cl <sub>3</sub> (CNAr <sup>Dipp2</sup> ) <sub>2</sub> ]·1.25 toluene·1/2 CH <sub>2</sub> Cl <sub>2</sub> ( <b>8</b> ), species 2. The thermal ellipsoids are set at a 50% probability level. Hydrogen atoms are omitted for clarity.....	17
<b>Table S8B:</b> Selected bond lengths (Å) and angles (°) in [Re(NPhF)Cl <sub>3</sub> (CNAr <sup>Dipp2</sup> ) <sub>2</sub> ]·1.25 toluene·1/2 CH <sub>2</sub> Cl <sub>2</sub> ( <b>8</b> ), species 2. ....	17
<b>Figure S8:</b> Ellipsoid representation of [Re(NPhF)Cl <sub>3</sub> (PPh <sub>3</sub> )(CNAr <sup>Tripp2</sup> )]·THF ( <b>9</b> ). The thermal ellipsoids are set at a 50% probability level. Hydrogen atoms are omitted for clarity. ....	18
<b>Table S9:</b> Selected bond lengths (Å) and angles (°) in [Re(NPhF)Cl <sub>3</sub> (PPh <sub>3</sub> )(CNAr <sup>Tripp2</sup> )]·THF ( <b>9</b> ).....	18

<b>Figure S9A:</b> Ellipsoid representation of [Re(NPhF)Cl <sub>3</sub> (CNAr <sup>Tripp2</sup> ) <sub>2</sub> ] ( <b>10</b> ), species 1. The thermal ellipsoids are set at a 50% probability level. Hydrogen atoms are omitted for clarity. ....	19
<b>Table S10A:</b> Selected bond lengths (Å) and angles (°) in [Re(NPhF)Cl <sub>3</sub> (CNAr <sup>Tripp2</sup> ) <sub>2</sub> ] ( <b>10</b> ), species 1. ....	19
<b>Figure S9B:</b> Ellipsoid representation of [Re(NPhF)Cl <sub>3</sub> (CNAr <sup>Tripp2</sup> ) <sub>2</sub> ] ( <b>10</b> ), species 2. The thermal ellipsoids are set at a 50% probability level. Hydrogen atoms are omitted for clarity. ....	20
<b>Table S10B:</b> Selected bond lengths (Å) and angles (°) in [Re(NPhF)Cl <sub>3</sub> (CNAr <sup>Tripp2</sup> ) <sub>2</sub> ] ( <b>10</b> ), species 2. ....	20
<b>Figure S10:</b> Ellipsoid representation of [Re(NPhF)Cl <sub>3</sub> (PPh <sub>3</sub> )(CNp-FAr <sup>DarF2</sup> )] ( <b>11</b> ). The thermal ellipsoids are set at a 50% probability level. Hydrogen atoms are omitted for clarity. ....	21
<b>Table S11:</b> Selected bond lengths (Å) and angles (°) in [Re(NPhF)Cl <sub>3</sub> (PPh <sub>3</sub> )(CNp-FAr <sup>DarF2</sup> )] ( <b>11</b> ).....	21
<b>Figure S11:</b> Ellipsoid representation of [Re(NPhF)Cl <sub>3</sub> (PPh <sub>3</sub> )(CNPh <sup>pF</sup> )] ( <b>12</b> ). The thermal ellipsoids are set at a 50% probability level. Hydrogen atoms are omitted for clarity. ....	22
<b>Table S12:</b> Selected bond lengths (Å) and angles (°) in [Re(NPhF)Cl <sub>3</sub> (PPh <sub>3</sub> )(CNPh <sup>pF</sup> )] ( <b>12</b> ).....	22
<b>Spectroscopic data and mass spectrometry</b> .....	<b>23</b>
<b>Figure S12:</b> IR (ATR) spectrum of [Re(NPhF)Cl <sub>3</sub> (PPh <sub>3</sub> )(CN <sup>i</sup> Bu)] ( <b>2</b> ).....	23
<b>Figure S13:</b> <sup>1</sup> H NMR spectrum of [Re(NPhF)Cl <sub>3</sub> (PPh <sub>3</sub> )(CN <sup>i</sup> Bu)] ( <b>2</b> ) in CD <sub>2</sub> Cl <sub>2</sub> . ....	23
<b>Figure S14:</b> <sup>19</sup> F NMR spectrum of [Re(NPhF)Cl <sub>3</sub> (PPh <sub>3</sub> )(CN <sup>i</sup> Bu)] ( <b>2</b> ) in CD <sub>2</sub> Cl <sub>2</sub> . ....	24
<b>Figure S15:</b> <sup>13</sup> C{ <sup>1</sup> H} NMR spectrum of [Re(NPhF)Cl <sub>3</sub> (PPh <sub>3</sub> )(CN <sup>i</sup> Bu)] ( <b>2</b> ) in CD <sub>2</sub> Cl <sub>2</sub> . ....	24
<b>Figure S16:</b> ESI+ mass spectrum of [Re(NPhF)Cl <sub>3</sub> (PPh <sub>3</sub> )(CN <sup>i</sup> Bu)] ( <b>2</b> ) in MeCN. ....	25
<b>Figure S17:</b> IR (ATR) spectrum of [Re(NPhF)Cl <sub>3</sub> (PPh <sub>3</sub> )(CNPh)] ( <b>3</b> ).....	25
<b>Figure S18:</b> ESI+ mass spectrum of [Re(NPhF)Cl <sub>3</sub> (PPh <sub>3</sub> )(CNPh)] ( <b>3</b> ) in MeCN. ....	26
<b>Figure S19:</b> IR (ATR) spectrum of [Re(NPhF)Cl <sub>3</sub> (PPh <sub>3</sub> )(CNPh <sup>i-prop2</sup> )] ( <b>3</b> ).....	26
<b>Figure S20:</b> <sup>1</sup> H NMR spectrum of [Re(NPhF)Cl <sub>3</sub> (PPh <sub>3</sub> )(CNPh <sup>i-prop2</sup> )] ( <b>4</b> ) in CD <sub>2</sub> Cl <sub>2</sub> . ....	27
<b>Figure S21:</b> <sup>19</sup> F NMR spectrum of [Re(NPhF)Cl <sub>3</sub> (PPh <sub>3</sub> )(CNPh <sup>i-prop2</sup> )] ( <b>4</b> ) in CD <sub>2</sub> Cl <sub>2</sub> . ....	27
<b>Figure S22:</b> <sup>13</sup> C{ <sup>1</sup> H} NMR of [Re(NPhF)Cl <sub>3</sub> (PPh <sub>3</sub> )(CNPh <sup>i-prop2</sup> )] ( <b>4</b> ) in CD <sub>2</sub> Cl <sub>2</sub> . ....	28
<b>Figure S23:</b> ESI+ mass spectrum of [Re(NPhF)Cl <sub>3</sub> (PPh <sub>3</sub> )(CNPh <sup>i-prop2</sup> )] ( <b>4</b> ) in MeCN. ....	28
<b>Figure S24:</b> IR (ATR) spectrum of [Re(NPhF)Cl <sub>3</sub> (PPh <sub>3</sub> )(CNMes)] ( <b>5</b> ).....	29
<b>Figure S25:</b> <sup>1</sup> H NMR spectrum of [Re(NPhF)Cl <sub>3</sub> (PPh <sub>3</sub> )(CNMes)] ( <b>5</b> ) in CD <sub>2</sub> Cl <sub>2</sub> shortly after dissolution.....	29
<b>Figure S26:</b> <sup>19</sup> F NMR spectrum of [Re(NPhF)Cl <sub>3</sub> (PPh <sub>3</sub> )(CNMes)] ( <b>5</b> ) in CD <sub>2</sub> Cl <sub>2</sub> shortly after dissolution.....	30
<b>Figure S27:</b> ESI+ mass spectrum of [Re(NPhF)Cl <sub>3</sub> (PPh <sub>3</sub> )(CNMes)] ( <b>5</b> ) in MeCN.....	30
<b>Figure S28:</b> IR (ATR) spectrum of [Re(NPhF)Cl <sub>3</sub> (PPh <sub>3</sub> )(CNPh <sup>pNO2</sup> )] ( <b>6</b> ).....	31

<b>Figure S29:</b> $^1\text{H}$ NMR spectrum of $[\text{Re}(\text{NPhF})\text{Cl}_3(\text{PPh}_3)(\text{CNPh}^{\text{pNO}_2})]$ ( <b>6</b> ) in $\text{CD}_2\text{Cl}_2$ shortly after dissolution.....	31
<b>Figure S30:</b> $^{19}\text{F}$ NMR spectrum of $[\text{Re}(\text{NPhF})\text{Cl}_3(\text{PPh}_3)(\text{CNPh}^{\text{pNO}_2})]$ ( <b>6</b> ) in $\text{CD}_2\text{Cl}_2$ shortly after dissolution.....	32
<b>Figure S31:</b> ESI+ mass spectrum of $[\text{Re}(\text{NPhF})\text{Cl}_3(\text{PPh}_3)(\text{CNPh}^{\text{pNO}_2})]$ ( <b>6</b> ) in MeCN.....	32
<b>Figure S32:</b> IR (ATR) spectrum of $[\text{Re}(\text{NPhF})\text{Cl}_3(\text{CNAr}^{\text{Mes}_2})_2]$ ( <b>7</b> ).....	33
<b>Figure S33:</b> $^1\text{H}$ NMR spectrum of $[\text{Re}(\text{NPhF})\text{Cl}_3(\text{CNAr}^{\text{Mes}_2})_2]$ ( <b>7</b> ) in $\text{CD}_2\text{Cl}_2$ .....	33
<b>Figure S34:</b> $^{19}\text{F}$ NMR spectrum of $[\text{Re}(\text{NPhF})\text{Cl}_3(\text{CNAr}^{\text{Mes}_2})_2]$ ( <b>7</b> ) in $\text{CD}_2\text{Cl}_2$ .....	34
<b>Figure S35:</b> $^{13}\text{C}\{^1\text{H}\}$ NMR spectrum of $[\text{Re}(\text{NPhF})\text{Cl}_3(\text{CNAr}^{\text{Mes}_2})_2]$ ( <b>7</b> ) in $\text{CD}_2\text{Cl}_2$ .....	34
<b>Figure S36:</b> ESI+ mass spectrum of $[\text{Re}(\text{NPhF})\text{Cl}_3(\text{CNAr}^{\text{Mes}_2})_2]$ ( <b>7</b> ) in MeCN.....	35
<b>Figure S37:</b> IR (ATR) spectrum of $[\text{Re}(\text{NPhF})\text{Cl}_3(\text{CNAr}^{\text{Dipp}_2})_2]$ ( <b>8</b> ).....	35
<b>Figure S38:</b> $^1\text{H}$ NMR spectrum of $[\text{Re}(\text{NPhF})\text{Cl}_3(\text{CNAr}^{\text{Dipp}_2})_2]$ ( <b>8</b> ) in $\text{CD}_2\text{Cl}_2$ .....	36
<b>Figure S39:</b> $^{19}\text{F}$ NMR spectrum of $[\text{Re}(\text{NPhF})\text{Cl}_3(\text{CNAr}^{\text{Dipp}_2})_2]$ ( <b>8</b> ) in $\text{CD}_2\text{Cl}_2$ .....	36
<b>Figure S40:</b> $^{13}\text{C}\{^1\text{H}\}$ NMR spectrum of $[\text{Re}(\text{NPhF})\text{Cl}_3(\text{CNAr}^{\text{Dipp}_2})_2]$ ( <b>8</b> ) in $\text{CD}_2\text{Cl}_2$ .....	37
<b>Figure S41:</b> ESI+ mass spectrum of $[\text{Re}(\text{NPhF})\text{Cl}_3(\text{CNAr}^{\text{Dipp}_2})_2]$ ( <b>8</b> ) in MeCN.....	37
<b>Figure S42:</b> IR (ATR) spectrum of $[\text{Re}(\text{NPhF})\text{Cl}_3(\text{CNAr}^{\text{Tripp}_2})_2]$ .....	38
<b>Figure S43:</b> $^1\text{H}$ NMR spectrum of $[\text{Re}(\text{NPhF})\text{Cl}_3(\text{CNAr}^{\text{Tripp}_2})_2]$ ( <b>10</b> ) in $\text{CD}_2\text{Cl}_2$ .....	38
<b>Figure S44:</b> $^{19}\text{F}$ NMR spectrum of $[\text{Re}(\text{NPhF})\text{Cl}_3(\text{CNAr}^{\text{Tripp}_2})_2]$ ( <b>10</b> ) in $\text{CD}_2\text{Cl}_2$ .....	39
<b>Figure S45:</b> $^{13}\text{C}\{^1\text{H}\}$ NMR spectrum of $[\text{Re}(\text{NPhF})\text{Cl}_3(\text{CNAr}^{\text{Tripp}_2})_2]$ ( <b>10</b> ) in $\text{CD}_2\text{Cl}_2$ .....	39
<b>Figure S46:</b> ESI+ mass spectrum of $[\text{Re}(\text{NPhF})\text{Cl}_3(\text{CNAr}^{\text{Tripp}_2})_2]$ ( <b>10</b> ) in MeCN.....	40
<b>Figure S47:</b> IR (ATR) spectrum of $[\text{Re}(\text{NPhF})\text{Cl}_3(\text{PPh}_3)(\text{CNp-FAr}^{\text{DarF}_2})]$ ( <b>11</b> ).....	40
<b>Figure S48:</b> $^1\text{H}$ NMR spectrum of $[\text{Re}(\text{NPhF})\text{Cl}_3(\text{PPh}_3)(\text{CNp-FAr}^{\text{DarF}_2})]$ ( <b>11</b> ) in acetone- $\text{d}_6$ .....	41
<b>Figure S49:</b> $^{19}\text{F}$ NMR spectrum of $[\text{Re}(\text{NPhF})\text{Cl}_3(\text{PPh}_3)(\text{CNp-FAr}^{\text{DarF}_2})]$ ( <b>11</b> ) in acetone- $\text{d}_6$ .....	41
<b>Figure S50:</b> $^{13}\text{C}\{^1\text{H}\}$ NMR spectrum of $[\text{Re}(\text{NPhF})\text{Cl}_3(\text{PPh}_3)(\text{CNp-FAr}^{\text{DarF}_2})]$ ( <b>11</b> ) in acetone- $\text{d}_6$ .....	42
<b>Figure S51:</b> ESI+ mass spectrum of $[\text{Re}(\text{NPhF})\text{Cl}_3(\text{PPh}_3)(\text{CNp-FAr}^{\text{DarF}_2})]$ in MeCN ( <b>11</b> ).....	42
<b>Figure S52:</b> IR (ATR) spectrum of $[\text{Re}(\text{NPhF})\text{Cl}_3(\text{PPh}_3)(\text{CNPh}^{\text{pF}})]$ ( <b>12</b> ).....	43
<b>Figure S53:</b> $^1\text{H}$ NMR of $[\text{Re}(\text{NPhF})\text{Cl}_3(\text{PPh}_3)(\text{CNPh}^{\text{pF}})]$ ( <b>12</b> ) in $\text{CD}_2\text{Cl}_2$ .....	43
<b>Figure S54:</b> $^{19}\text{F}$ NMR of $[\text{Re}(\text{NPhF})\text{Cl}_3(\text{PPh}_3)(\text{CNPh}^{\text{pF}})]$ ( <b>12</b> ) in $\text{CD}_2\text{Cl}_2$ .....	44
<b>Figure S55:</b> $^{13}\text{C}\{^1\text{H}\}$ NMR of $[\text{Re}(\text{NPhF})\text{Cl}_3(\text{PPh}_3)(\text{CNPh}^{\text{pF}})]$ ( <b>12</b> ) in $\text{CD}_2\text{Cl}_2$ .....	44
<b>Figure S56:</b> ESI+ mass spectrum of $[\text{Re}(\text{NPhF})\text{Cl}_3(\text{PPh}_3)(\text{CNPh}^{\text{pF}})]$ ( <b>12</b> ) in MeCN.....	45
<b>Figure S57:</b> $^{19}\text{F}$ NMR monitoring of reaction of $[\text{Re}(\text{NPhF})\text{Cl}_3(\text{PPh}_3)_2]$ with $\text{CNAr}^{\text{Tripp}_2}$ in a boiling toluene/acetonitrile mixture (5:1). <b>1</b> was recorded after 5 minutes, <b>2</b> after 1.5 h, <b>3</b> after 3.5 h, <b>4</b> after 5 h, <b>5</b> after 10h, <b>6</b> after 13h. As no significant different was observed between <b>5</b> and <b>6</b> , the heating was not continued. (a: $[\text{Re}(\text{NPhF})\text{Cl}_3(\text{PPh}_3)_2]$ ; b:	

[Re(NPhF)Cl <sub>3</sub> (PPh <sub>3</sub> )(CNA <sup>r</sup> <sub>Tripp2</sub> )]	c: minor intermediate compound, probably	
[Re(NPhF)Cl <sub>3</sub> (PPh <sub>3</sub> ) <sub>2</sub> (CNA <sup>r</sup> <sub>Tripp2</sub> )]	d: [Re(NPhF)Cl <sub>3</sub> (CNA <sup>r</sup> <sub>Tripp2</sub> ) <sub>2</sub> ]	46
<b>Computational chemistry</b>		<b>47</b>
<p><b>Table S13.</b> Calculated electrostatic potential surface properties of the isocyanide carbon atom at the Van der Waals (VdW) boundary for structures optimized at the B3LYP/6-311++G* level. Surface properties were evaluated at <math>\rho = 0.001</math> level using an electrostatic potential map basis with a grid-point spacing of 0.25. The last column contains the Surface-Averaged Donor Atom Potential SADAP = <math>(EP_{\min} + EP_{\max} + AP)/(ES_{\text{pos}} + ES_{\text{neg}})</math> as a combined descriptor of steric and electrostatic properties of the potential ligands, which allows an estimation of their reactivity.<sup>5</sup></p>		
<b>References</b>		<b>48</b>

## Crystallographic data

The intensities for the X-ray determinations were collected on STOE IPDS 2T with Mo K $\alpha$  radiation. The space groups were determined by the detection of systematic absences. Absorption corrections were carried out by integration methods.<sup>1</sup> Structure solution and refinement were performed with the SHELX program package.<sup>2,3</sup> Hydrogen atoms were derived from the final Fourier maps and refined or placed at calculated positions and treated with the 'riding model' option of SHELXL. The representation of molecular structures was done using the program DIAMOND 4.2.2.<sup>4</sup> Additional information on the structure determinations has been deposited with the Cambridge Crystallographic Data Centre.

**Table S1:** Crystallographic data and data collection parameters

	[Re(NPhF)Cl <sub>3</sub> (PPh <sub>3</sub> )(CN <sup>t</sup> Bu)] (2)	[Re(NPhF)Cl <sub>3</sub> (PPh <sub>3</sub> )(CNPh)] (3)	[Re(NPhF)Cl <sub>3</sub> (PPh <sub>3</sub> )(CNPh <sup>i-propyl</sup> )] (4)
Empirical formula	C <sub>29</sub> H <sub>26</sub> Cl <sub>3</sub> FN <sub>2</sub> PRe	C <sub>31</sub> H <sub>24</sub> Cl <sub>3</sub> FN <sub>2</sub> PRe	C <sub>37</sub> H <sub>36</sub> Cl <sub>3</sub> FN <sub>2</sub> PRe
Formula weight	747.05	767.04	851.20
Temperature/K	200.0	100.0	200
Crystal system	triclinic	monoclinic	monoclinic
Space group	P $\bar{1}$	P2 <sub>1</sub> /c	P2 <sub>1</sub> /c
a/Å	10.2945(6)	12.4219(9)	18.349(4)
b/Å	14.5070(8)	11.5944(8)	10.552(2)
c/Å	21.6560(1)	20.6804(2)	19.299(4)
$\alpha$ /°	70.369(4)	90	90
$\beta$ /°	83.840(5)	106.880(3)	99.46(3)
$\gamma$ /°	89.494(5)	90	90
Volume/Å <sup>3</sup>	3027.3(3)	2850.2(4)	3686.1(1)
Z	4	4	4
$\rho_{\text{calc}}$ / cm <sup>3</sup>	1.639	1.788	1.534
$\mu$ / mm <sup>-1</sup>	4.358	4.632	3.590
F(000)	1464.0	1496.0	1688.0
Crystal size / mm <sup>3</sup>	0.28 × 0.17 × 0.08	0.21 × 0.18 × 0.04	0.58 × 0.35 × 0.13
Radiation	MoK $\alpha$ ( $\lambda$ = 0.71073)	MoK $\alpha$ ( $\lambda$ = 0.71073)	Mo K $\alpha$ ( $\lambda$ = 0.71073)
2 $\theta$ range for data collection/°	6.69 to 52.154	4.528 to 54.274	6.702 to 51.998
Index ranges	-12 ≤ h ≤ 12, -17 ≤ k ≤ 16, -26 ≤ l ≤ 26	-15 ≤ h ≤ 15, -14 ≤ k ≤ 14, -26 ≤ l ≤ 26	-22 ≤ h ≤ 22, -12 ≤ k ≤ 12, - 23 ≤ l ≤ 23
Reflections collected	25804	49900	26788
Independent reflections	11870 [R <sub>int</sub> = 0.0368, R <sub>sigma</sub> = 0.0481]	6252 [R <sub>int</sub> = 0.0354, R <sub>sigma</sub> = 0.0196]	7171 [R <sub>int</sub> = 0.0401, R <sub>sigma</sub> = 0.0309]
Data/restraints/parameters	11870/0/667	6252/0/352	7171/500/410
Goodness-of-fit on F <sup>2</sup>	0.888	1.141	0.979
Final R indexes [ $\geq 2\sigma$ (I)]	R <sub>1</sub> = 0.0235, wR <sub>2</sub> = 0.0411	R <sub>1</sub> = 0.0268, wR <sub>2</sub> = 0.0564	R <sub>1</sub> = 0.0252, wR <sub>2</sub> = 0.0541
Final R indexes [all data]	R <sub>1</sub> = 0.0413, wR <sub>2</sub> = 0.0439	R <sub>1</sub> = 0.0288, wR <sub>2</sub> = 0.0571	R <sub>1</sub> = 0.0358, wR <sub>2</sub> = 0.0565
Largest diff. peak/hole / e Å <sup>-3</sup>	0.53/-0.78	2.53/-1.21	0.57/-0.97
Flack	–	–	–
Diffractometer	IPDS 2T	D8 Venture	IPDS 2T
CCDC access code	2236802	2236803	2236804

**Table S1 (continued):** Crystallographic data and data collection parameters.

	[Re(NPhF)Cl <sub>3</sub> (PPh <sub>3</sub> )(CNMes)] (5)	[Re(NPhF)Cl <sub>3</sub> (PPh <sub>3</sub> )(CNPh <sup>pNO<sub>2</sub></sup> )] (6)	[Re(NPhF)Cl <sub>3</sub> (CNAr <sup>Mes<sub>2</sub></sup> ) <sub>2</sub> ] x 1.5 toluene (7)
Empirical formula	C <sub>34</sub> H <sub>30</sub> Cl <sub>3</sub> FN <sub>2</sub> PRe	C <sub>31</sub> H <sub>23</sub> Cl <sub>3</sub> FN <sub>3</sub> O <sub>2</sub> PRe	C <sub>66.5</sub> H <sub>66</sub> Cl <sub>3</sub> FN <sub>3</sub> Re
Formula weight	809.12	812.04	1218.77
Temperature/K	200	200	200.0
Crystal system	monoclinic	monoclinic	triclinic
Space group	P2 <sub>1</sub> /n	P2 <sub>1</sub> /c	P $\bar{1}$
a/Å	9.6268(7)	9.0634(2)	12.5541(7)
b/Å	20.7312(1)	25.461(5)	13.5237(7)
c/Å	16.4187(1)	13.352(3)	20.8711(1)
$\alpha$ /°	90	90	77.386(4)
$\beta$ /°	100.002(5)	99.20(3)	86.283(4)
$\gamma$ /°	90	90	64.117(4)
Volume / Å <sup>3</sup>	3227.0(3)	3041.4(11)	3109.2(3)
Z	4	4	2
$\rho_{\text{calc}}$ g/cm <sup>3</sup>	1.665	1.773	1.302
$\mu$ / mm <sup>-1</sup>	4.096	4.352	2.118
F(000)	1592.0	1584.0	1242
Crystal size / mm <sup>3</sup>	0.31 × 0.143 × 0.02	0.33 × 0.157 × 0.03	0.3 × 0.2 × 0.2
Radiation	Mo K $\alpha$ ( $\lambda$ = 0.71073)	Mo K $\alpha$ ( $\lambda$ = 0.71073)	MoK $\alpha$ ( $\lambda$ = 0.71073)
2 $\theta$ range for data collection/°	6.636 to 51.996	6.618 to 52	6.672 to 51.998
Index ranges	-10 ≤ h ≤ 11, -25 ≤ k ≤ 25, -20 ≤ l ≤ 20	-11 ≤ h ≤ 11, -31 ≤ k ≤ 31, -16 ≤ l ≤ 15	-14 ≤ h ≤ 15, -15 ≤ k ≤ 16, -25 ≤ l ≤ 25
Reflections collected	18114	17337	25031
Independent reflections	6313 [R <sub>int</sub> = 0.0394, R <sub>sigma</sub> = 0.0452]	5953 [R <sub>int</sub> = 0.0637, R <sub>sigma</sub> = 0.0749]	12158 [R <sub>int</sub> = 0.0674, R <sub>sigma</sub> = 0.0614]
Data/restraints/parameters	6313/0/382	5953/0/379	12158/0/578
Goodness-of-fit on F <sup>2</sup>	0.919	0.822	0.961
Final R indexes [ $I \geq 2\sigma(I)$ ]	R <sub>1</sub> = 0.0271, wR <sub>2</sub> = 0.0470	R <sub>1</sub> = 0.0281, wR <sub>2</sub> = 0.0423	R <sub>1</sub> = 0.0368, wR <sub>2</sub> = 0.0873
Final R indexes [all data]	R <sub>1</sub> = 0.0458, wR <sub>2</sub> = 0.0501	R <sub>1</sub> = 0.0568, wR <sub>2</sub> = 0.0459	R <sub>1</sub> = 0.0459, wR <sub>2</sub> = 0.0901
Largest diff. peak/hole / e Å <sup>-3</sup>	0.54/-1.07	0.56/-0.70	1.19/-1.15
Flack	—	—	—
Diffractometer	IPDS 2T	IPDS 2T	IPDS 2T
CCDC access code	2236805	2236806	2236807



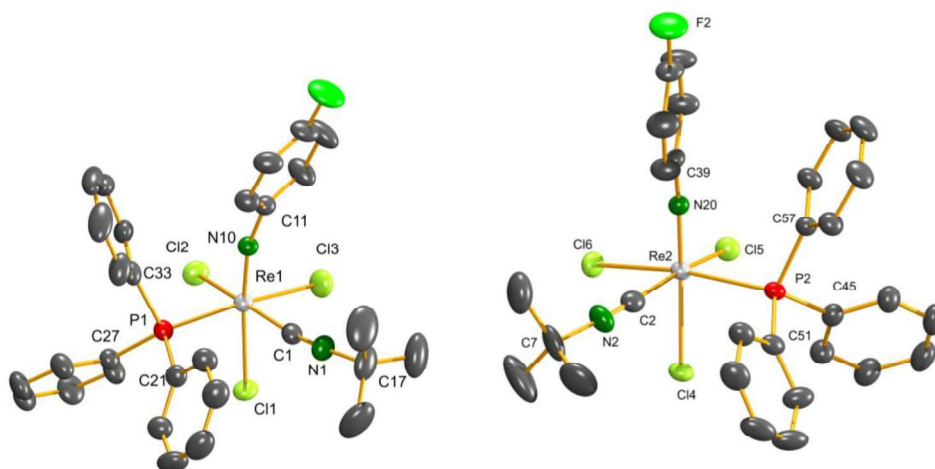
**Table S1 (continued):** Crystallographic data and data collection parameters.

	[Re(NPhF)Cl <sub>3</sub> (CNAr <sup>Dipp2</sup> ) <sub>2</sub> ] (8) + 0.5 CH <sub>2</sub> Cl <sub>2</sub> + 1.25 toluene*	[Re(NPhF)Cl <sub>3</sub> (PPh <sub>3</sub> )(CNAr <sup>Tripp2</sup> )] (9) + THF	[Re(NPhF)Cl <sub>3</sub> (CNAr <sup>Tripp2</sup> ) <sub>2</sub> ] (10)
Empirical formula	C <sub>154.5</sub> H <sub>178</sub> Cl <sub>3</sub> F <sub>2</sub> N <sub>6</sub> Re <sub>2</sub>	C <sub>65</sub> H <sub>76</sub> Cl <sub>3</sub> FN <sub>2</sub> OPRe	C <sub>80</sub> H <sub>102</sub> Cl <sub>3</sub> FN <sub>3</sub> Re
Formula weight	2813.02	1243.79	1417.19
Temperature/K	100	200	200
Crystal system	triclinic	triclinic	monoclinic
Space group	P1	P $\bar{1}$	P2 <sub>1</sub> /n
a/Å	14.706(3)	10.858(2)	24.4087(9)
b/Å	16.346(3)	14.422(3)	25.0277(7)
c/Å	17.419(5)	20.631(4)	28.2885(1)
$\alpha^\circ$	84.392(8)	77.64(3)	90
$\beta^\circ$	82.455(9)	75.03(3)	108.962(3)
$\gamma^\circ$	63.855(5)	81.35(3)	90
Volume / Å <sup>3</sup>	3722.5(2)	3033.2(1)	16343.5(1)
Z	1	2	8
$\rho_{\text{calc}}$ g/cm <sup>3</sup>	1.255	1.362	1.152
$\mu$ / mm <sup>-1</sup>	1.820	2.206	1.626
F(000)	1451.0	1276.0	5904.0
Crystal size / mm <sup>3</sup>	0.24 × 0.21 × 0.18	0.32 × 0.143 × 0.05	0.9 × 0.5 × 0.5
Radiation	MoK $\alpha$ ( $\lambda$ = 0.71073)	Mo K $\alpha$ ( $\lambda$ = 0.71073)	Mo K $\alpha$ ( $\lambda$ = 0.71073)
2 $\theta$ range for data collection/ $^\circ$	4.722 to 55.978	6.73 to 52	6.618 to 52
Index ranges	-19 ≤ h ≤ 19, -21 ≤ k ≤ 21, - 22 ≤ l ≤ 22	-13 ≤ h ≤ 13, -17 ≤ k ≤ 17, -25 ≤ l ≤ 25	-30 ≤ h ≤ 30, -30 ≤ k ≤ 30, -34 ≤ l ≤ 34
Reflections collected	167349	25108	107340
Independent reflections	35322 [R <sub>int</sub> = 0.0455, R <sub>sigma</sub> = 0.0472]	11861 [R <sub>int</sub> = 0.0721, R <sub>sigma</sub> = 0.1409]	32003 [R <sub>int</sub> = 0.0901, R <sub>sigma</sub> = 0.1020]
Data/restraints/parameters	35322/1904/1479	11861/0/679	32003/2108/1595
Goodness-of-fit on F <sup>2</sup>	1.045	0.755	0.881
Final R indexes [ $l \geq 2\sigma$ (I)]	R <sub>1</sub> = 0.0396, wR <sub>2</sub> = 0.0993	R <sub>1</sub> = 0.0417, wR <sub>2</sub> = 0.0551	R <sub>1</sub> = 0.0524, wR <sub>2</sub> = 0.1164
Final R indexes [all data]	R <sub>1</sub> = 0.0460, wR <sub>2</sub> = 0.1039	R <sub>1</sub> = 0.0810, wR <sub>2</sub> = 0.0618	R <sub>1</sub> = 0.1130, wR <sub>2</sub> = 0.1346
Largest diff. peak/hole / e Å <sup>-3</sup>	1.74/-1.49	0.69/-0.65	1.17/-1.51
Flack	0.009(2)	—	—
Diffractometer	D8 Venture	IPDS 2T	IPDS 2T
CCDC access code	2236808	2236809	2236810

\*The unusual space group P1 has been checked for higher symmetry by several methods, but no inversion center has been found.

**Table S1 (continued):** Crystallographic data and data collection parameters.

	[Re(NPhF)Cl <sub>3</sub> (PPh <sub>3</sub> )(CNp-FAr <sup>DarF<sub>2</sub></sup> )] x 0.5 CH <sub>2</sub> Cl <sub>2</sub> ( <b>11</b> )	[Re(NPhF)Cl <sub>3</sub> (PPh <sub>3</sub> )(CNPh <sup>PF</sup> )] ( <b>12</b> )
Empirical formula	C <sub>47</sub> H <sub>27</sub> Cl <sub>3</sub> F <sub>14</sub> N <sub>2</sub> PRE	C <sub>31</sub> H <sub>23</sub> Cl <sub>3</sub> F <sub>2</sub> N <sub>2</sub> PRE
Formula weight	1209.22	785.03
Temperature/K	105.0	200
Crystal system	tetragonal	monoclinic
Space group	I4 <sub>1</sub> /a	P2 <sub>1</sub> /n
a/Å	46.9293(1)	11.170(2)
b/Å	46.9293(1)	21.178(4)
c/Å	8.3649(2)	12.895(3)
α/°	90	90
β/°	90	103.82(3)
γ/°	90	90
Volume / Å <sup>3</sup>	18422.5(9)	2962.1(1)
Z	16	4
ρ <sub>calc</sub> g/cm <sup>3</sup>	1.744	1.760
μ / mm <sup>-1</sup>	7.935	4.464
F(000)	9440.0	1528.0
Crystal size / mm <sup>3</sup>	0.15 × 0.1 × 0.08	0.21 × 0.07 × 0.027
Radiation	CuKα (λ = 1.54178)	MoKα (λ = 0.71073)
2θ range for data collection/°	5.326 to 133.24	6.626 to 52.016
Index ranges	-55 ≤ h ≤ 55, -55 ≤ k ≤ 55, -9 ≤ l ≤ 9	-13 ≤ h ≤ 13, -26 ≤ k ≤ 26, -14 ≤ l ≤ 15
Reflections collected	173200	17347
Independent reflections	8121 [R <sub>int</sub> = 0.0672, R <sub>sigma</sub> = 0.0185]	5800 [R <sub>int</sub> = 0.0596, R <sub>sigma</sub> = 0.0714]
Data/restraints/parameters	8121/6/633	5800/0/362
Goodness-of-fit on F <sup>2</sup>	1.030	0.886
Final R indexes [I ≥ 2σ (I)]	R <sub>1</sub> = 0.0287, wR <sub>2</sub> = 0.0703	R <sub>1</sub> = 0.0358, wR <sub>2</sub> = 0.0597
Final R indexes [all data]	R <sub>1</sub> = 0.0332, wR <sub>2</sub> = 0.0734	R <sub>1</sub> = 0.0663, wR <sub>2</sub> = 0.0652
Largest diff. peak/hole / e Å <sup>-3</sup>	1.48/-0.96	1.44/-1.26
Flack	—	—
Diffractometer	D8 Venture	IPDS 2T
CCDC access code	2236811	2236812



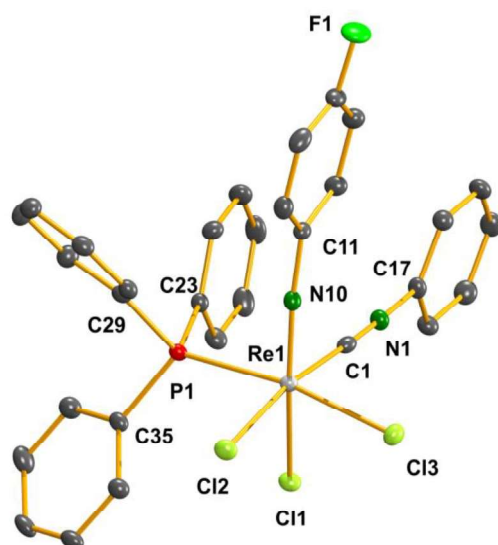
**Figure S1:** Ellipsoid representation of  $[\text{Re}(\text{NPhF})\text{Cl}_3(\text{PPh}_3)(\text{CN}^t\text{Bu})]$  (**2**). The thermal ellipsoids are set at a 50% probability level. Hydrogen atoms are omitted for clarity.

**Table S2A:** Selected bond lengths (Å) and angles (°) in  $[\text{Re}(\text{NPhF})\text{Cl}_3(\text{PPh}_3)(\text{CN}^t\text{Bu})]$  (**2**).

Re1-Cl2	2.4252(10)	P1-C21	1.812(4)	Re1-Cl3	2.4252(10)
Re1-Cl1	2.3994(9)	P1-C27	1.829(3)	Re1-N10	1.715(3)
Re1-P1	2.4593(9)	P1-C33	1.830(3)	Re1-C1	2.020(4)
N10-C11	1.391(4)	C1-N1	1.151(5)	N1-C17	1.458(5)
Cl2-Re1-Cl1	91.91(3)	Cl1-Re1-P1	84.47(3)	C11-N10-Re1	164.4(3)
Cl2-Re1-P1	92.38(3)	Cl1-Re1-Cl3	89.43(4)	C1-Re1-P1	94.61(11)
Cl2-Re1-Cl3	86.06(4)	Cl3-Re1-P1	173.65(3)	N1-C1-Re1	172.9(3)
C1-Re1-Cl2	169.35(10)	C1-Re1-Cl1	80.79(9)	C1-N1-C17	175.7(4)

**Table S2B:** Selected bond lengths (Å) and angles (°) in  $[\text{Re}(\text{NPhF})\text{Cl}_3(\text{PPh}_3)(\text{CN}^t\text{Bu})]$  (**2**).

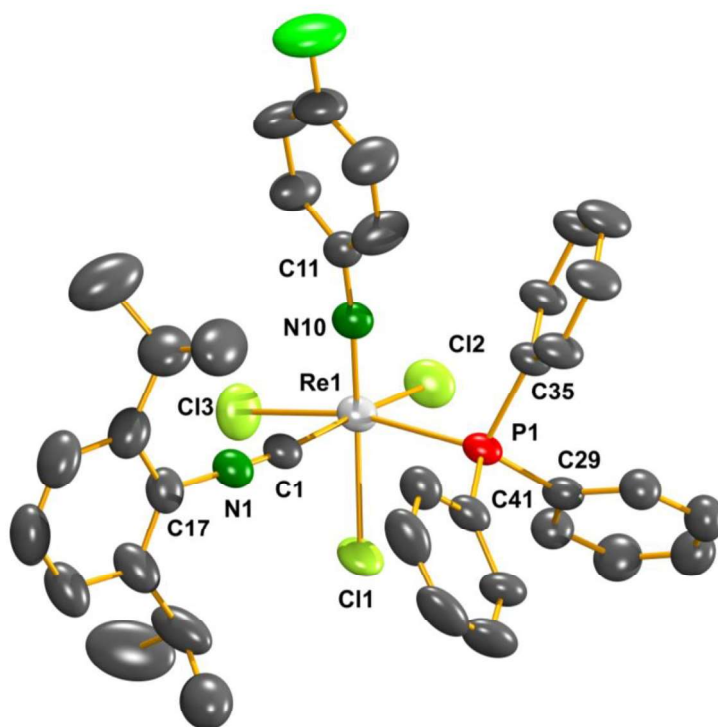
Re2-Cl5	2.3887(9)	P2-C45	1.841(4)	Re2-Cl6	2.4144(9)
Re2-Cl4	2.4276(8)	P2-C51	1.816(3)	Re2-N20	1.715(3)
Re2-P2	2.4473(9)	P2-C57	1.818(3)	Re2-C2	2.045(4)
N20-C39	1.382(4)	C2-N2	1.146(5)	N2-C7	1.463(5)
Cl4-Re2-Cl5	92.15(3)	Cl4-Re2-P2	82.98(3)	C39-N20-Re2	166.7(2)
Cl5-Re2-P2	88.41(3)	Cl4-Re2-Cl6	87.77(3)	C2-Re2-P2	97.1(1)
Cl5-Re2-Cl6	85.87(3)	Cl6-Re2-P2	168.93(3)	N2-C2-Re2	173.8(3)
C2-Re2-Cl5	167.96(1)	C2-Re2-Cl4	78.03(1)	C2-N2-C7	167.6(4)



**Figure S2:** Ellipsoid representation of  $[\text{Re}(\text{NPhF})\text{Cl}_3(\text{PPH}_3)(\text{CNPh})]$  (**3**). The thermal ellipsoids are set at a 50% probability level. Hydrogen atoms are omitted for clarity.

**Table S3:** Selected bond lengths (Å) and angles (°) in  $[\text{Re}(\text{NPhF})\text{Cl}_3(\text{PPH}_3)(\text{CNPh})]$  (**3**).

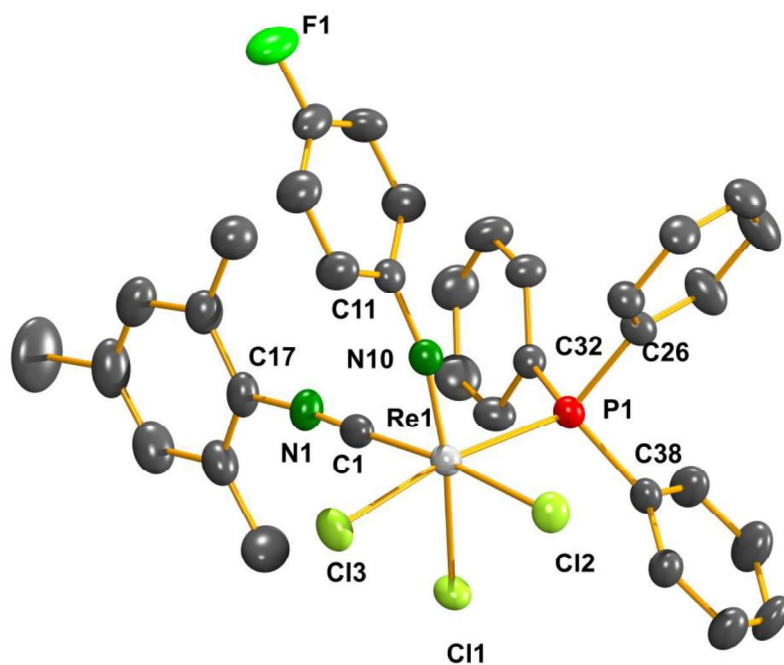
Re1-Cl2	2.3921(9)	P1-C23	1.819(4)	Re1-Cl3	2.4254(9)
Re1-Cl1	2.4097(9)	P1-C29	1.828(4)	Re1-N10	1.730(3)
Re1-P1	2.4539(9)	P1-C35	1.830(4)	Re1-C1	2.029(4)
N10-C11	1.378(4)	C1-N1	1.165(5)	N1-C17	1.397(5)
Cl2-Re1-Cl1	92.29(3)	Cl1-Re1-P1	84.40(3)	C11-N10-Re1	168.7(3)
Cl2-Re1-P1	90.63(3)	Cl1-Re1-Cl3	87.00(3)	C1-Re1-P1	91.74(1)
Cl2-Re1-Cl3	85.46(3)	Cl3-Re1-P1	170.41(3)	N1-C1-Re1	177.7(3)
C1-Re1-Cl2	169.85(10)	C1-Re1-Cl1	91.74(10)	C1-N1-C17	177.7(4)



**Figure S3:** Ellipsoid representation of  $[\text{Re}(\text{NPhF})\text{Cl}_3(\text{PPh}_3)(\text{CNPh}^{i\text{-prop}2})]$  (**4**). The thermal ellipsoids are set at a 50% probability level. Hydrogen atoms are omitted for clarity.

**Table S4:** Selected bond lengths (Å) and angles (°) in  $[\text{Re}(\text{NPhF})\text{Cl}_3(\text{PPh}_3)(\text{CNPh}^{i\text{-prop}2})]$  (**4**).

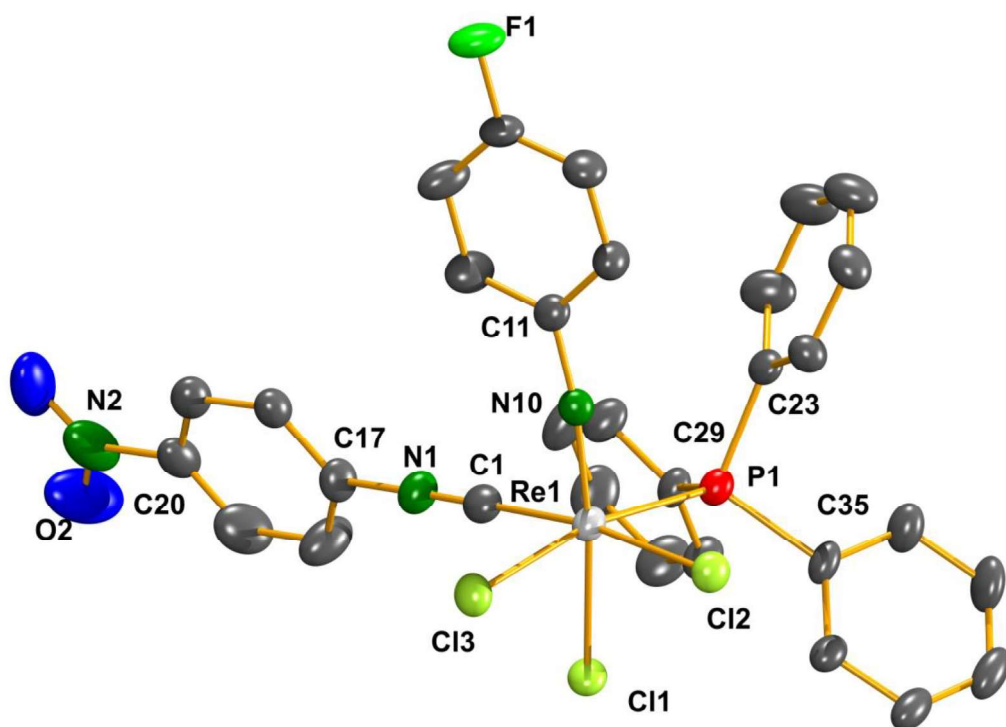
Re1-Cl2	2.3946(1)	P1-C29	1.832(3)	Re1-Cl3	2.4144(10)
Re1-Cl1	2.4294(9)	P1-C35	1.821(3)	Re1-N10	1.722(3)
Re1-P1	2.4476(9)	P1-C41	1.823(3)	Re1-C1	2.023(3)
N10-C11	1.385(4)	C1-N1	1.147(4)	N1-C17	1.404(4)
Cl2-Re1-Cl1	93.93(4)	Cl1-Re1-P1	79.36(3)	C11-N10-Re1	172.1(2)
Cl2-Re1-P1	89.44(4)	Cl1-Re1-Cl3	86.88(4)	C1-Re1-P1	97.52(10)
Cl2-Re1-Cl3	86.71(4)	Cl3-Re1-P1	165.42(3)	N1-C1-Re1	170.6(3)
C1-Re1-Cl2	169.54(9)	C1-Re1-Cl1	79.78(9)	C1-N1-C17	172.6(3)



**Figure S4:** Ellipsoid representation of  $[\text{Re}(\text{NPhF})\text{Cl}_3(\text{PPh}_3)(\text{CNMes})]$  (**5**). The thermal ellipsoids are set at a 50% probability level. Hydrogen atoms are omitted for clarity.

**Table S5:** Selected bond lengths (Å) and angles (°) in  $[\text{Re}(\text{NPhF})\text{Cl}_3(\text{PPh}_3)(\text{CNMes})]$  (**5**).

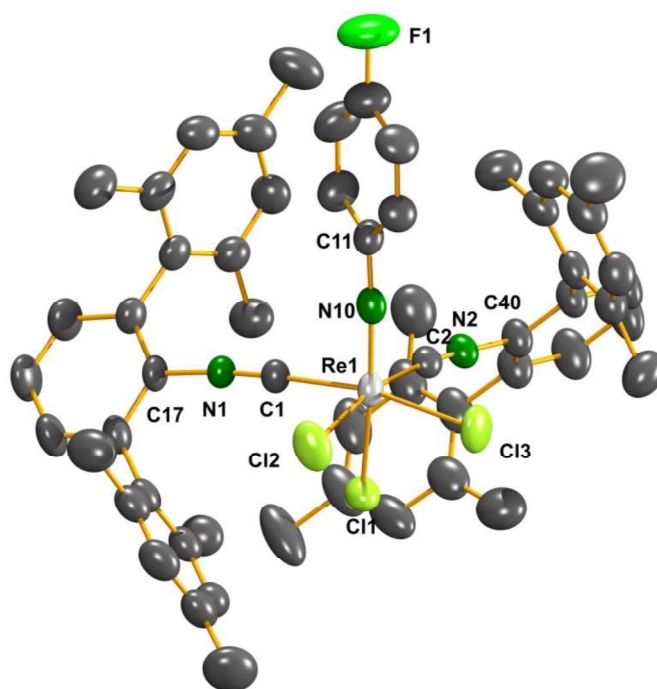
Re1-Cl2	2.4034(1)	P1-C26	1.828(4)	Re1-Cl3	2.4345(9)
Re1-Cl1	2.3957(1)	P1-C32	1.815(4)	Re1-N10	1.712(3)
Re1-P1	2.4631(1)	P1-C38	1.828(4)	Re1-C1	2.030(4)
N10-C11	1.399(5)	C1-N1	1.151(5)	N1-C17	1.404(5)
Cl2-Re1-Cl1	92.88(4)	Cl1-Re1-P1	85.04(3)	C11-N10-Re1	166.0(3)
Cl2-Re1-P1	88.75(3)	Cl1-Re1-Cl3	88.05(4)	C1-Re1-P1	92.00(11)
Cl2-Re1-Cl3	86.53(4)	Cl3-Re1-P1	171.42(3)	N1-C1-Re1	176.9(3)
C1-Re1-Cl2	173.33(1)	C1-Re1-Cl1	80.58(11)	C1-N1-C17	174.1(4)



**Figure S5:** Ellipsoid representation of  $[\text{Re}(\text{NPhF})\text{Cl}_3(\text{PPh}_3)(\text{CNPh}^{\text{pNO}_2})]$  (**6**). The thermal ellipsoids are set at a 50% probability level. Hydrogen atoms are omitted for clarity.

**Table S6:** Selected bond lengths (Å) and angles (°) in  $[\text{Re}(\text{NPhF})\text{Cl}_3(\text{PPh}_3)(\text{CNPh}^{\text{pNO}_2})]$  (**6**).

Re1-Cl2	2.3967(1)	P1-C23	1.827(4)	Re1-Cl3	2.4203(13)
Re1-Cl1	2.4282(1)	P1-C29	1.801(4)	Re1-N10	1.712(3)
Re1-P1	2.4537(1)	P1-C35	1.834(4)	Re1-C1	2.021(5)
N10-C11	1.390(5)	C1-N1	1.162(6)	N1-C17	1.397(6)
Cl2-Re1-Cl1	94.32(4)	Cl1-Re1-P1	82.76(4)	C11-N10-Re1	171.1(3)
Cl2-Re1-P1	88.88(4)	Cl1-Re1-Cl3	86.30(4)	C1-Re1-P1	93.47(14)
Cl2-Re1-Cl3	86.92(4)	Cl3-Re1-P1	167.95(3)	N1-C1-Re1	176.6(4)
C1-Re1-Cl2	171.69(1)	C1-Re1-Cl1	78.09(13)	C1-N1-C17	178.2(5)

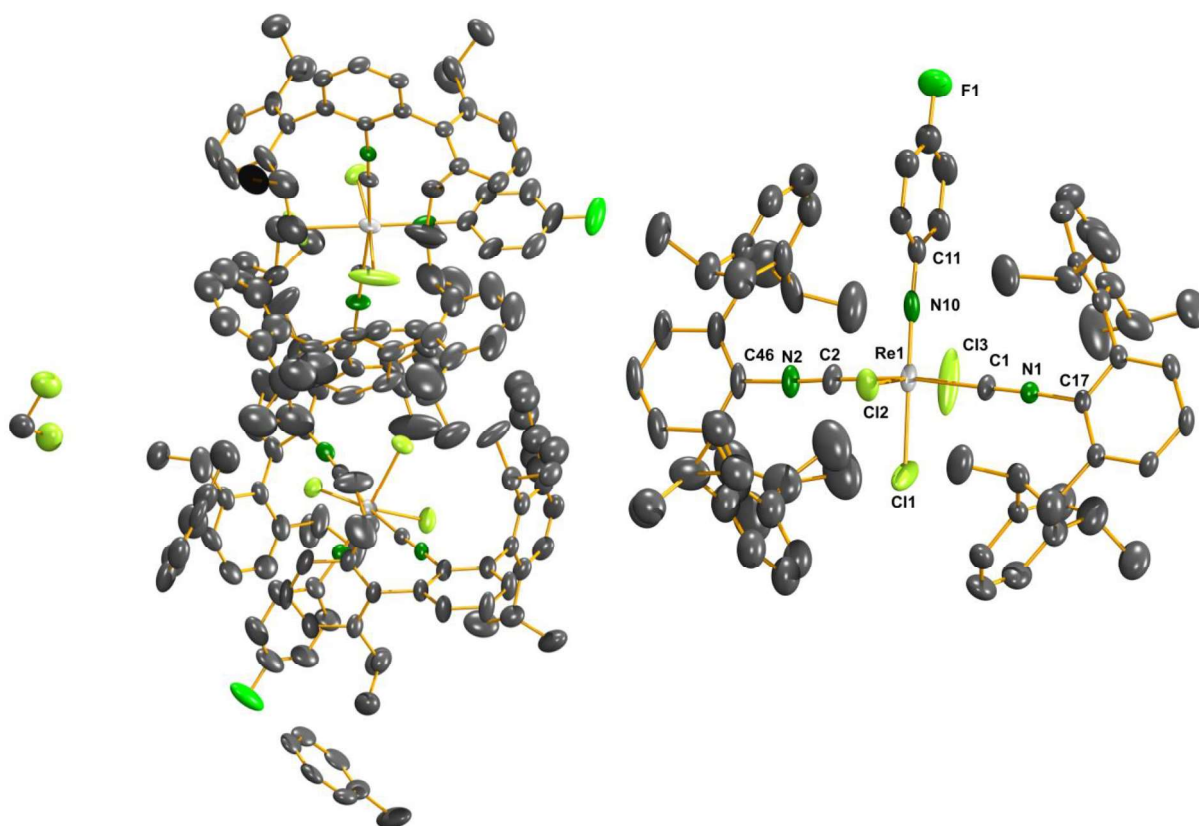


**Figure S6:** Ellipsoid representation of  $[\text{Re}(\text{NPhF})\text{Cl}_3(\text{CNAr}^{\text{Mes}2})_2]$  (**7**). The thermal ellipsoids are set at a 50% probability level. Hydrogen atoms are omitted for clarity.

**Table S7:** Selected bond lengths (Å) and angles (°) in  $[\text{Re}(\text{NPhF})\text{Cl}_3(\text{CNAr}^{\text{Mes}2})_2]$  (**7**).

Re1-Cl2	2.3855(1)	N1-C1	1.140(5)	Re1-Cl3	2.3783(1)
Re1-Cl1	2.4001(1)	N2-C40	1.399(5)	Re1-N10	1.724(3)
C2-N2	1.149(5)	Re1-C2	2.034(4)	Re1-C1	2.043(4)
N10-C11	1.363(5)	N1-C17	1.395(5)	N2-C2	1.149(5)
Cl2-Re1-Cl1	89.12(5)	Cl1-Re1-C2	80.13(1)	C11-N10-Re1	173.0(3)
Cl2-Re1-C2	167.75(1)	Cl2-Re1-Cl3	87.59(5)	C1-Re1-C2	96.89(2)
Cl1-Re1-Cl3	90.24(5)	N2-C2-Re1	174.2(4)	N1-C1-Re1	176.6(3)
C1-Re1-Cl2	86.88(1)	C1-Re1-Cl1	79.77(1)	C1-N1-C17	174.7(4)

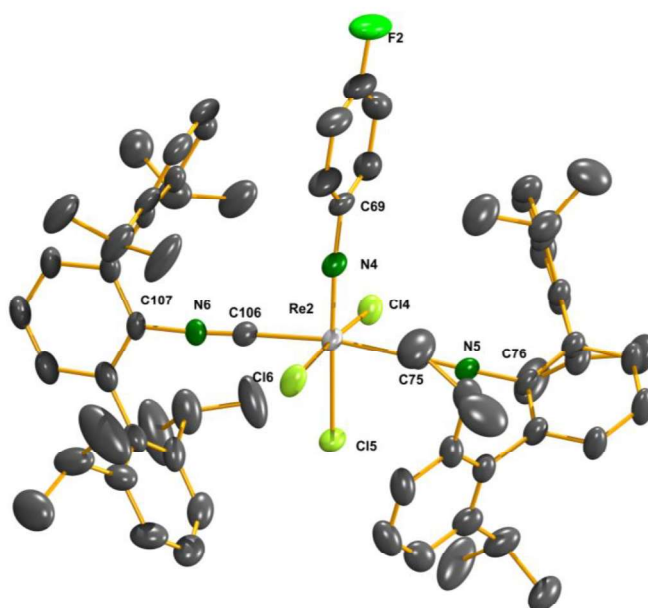




**Figure S7A:** Ellipsoid representation of  $[\text{Re}(\text{NPhF})\text{Cl}_3(\text{CNAr}^{\text{Dipp}2})_2] \cdot 1.25 \text{ toluene} \cdot 1/2 \text{ CH}_2\text{Cl}_2$  (**8**), species 1. The thermal ellipsoids are set at a 50% probability level. Hydrogen atoms are omitted for clarity. One of the crystallographically independent species (see labelled compound) shows unusually large ellipsoids for Cl1 and Cl3. This is mainly due to packing effects and have not been constrained by EADP instructions.

**Table S8A:** Selected bond lengths (Å) and angles (°) in  $[\text{Re}(\text{NPhF})\text{Cl}_3(\text{CNAr}^{\text{Dipp}2})_2] \cdot 1.25 \text{ toluene} \cdot 1/2 \text{ CH}_2\text{Cl}_2$  (**8**), species 1.

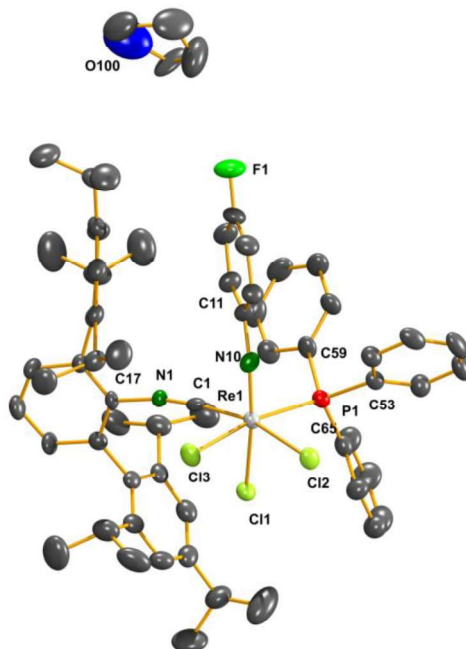
Re1-Cl2	2.392(2)	N1-C1	1.142(8)	Re1-Cl3	2.383(2)
Re1-Cl1	2.367(3)	N2-C46	1.412(8)	Re1-N10	1.728(7)
C2-N2	1.155(9)	Re1-C2	2.056(7)	Re1-C1	2.075(6)
N10-C11	1.373(1)	N1-C17	1.394(7)	N2-C2	1.155(9)
Cl2-Re1-Cl1	86.01(12)	Cl1-Re1-C2	86.5(2)	C11-N10-Re1	177.3(5)
Cl2-Re1-C2	91.2(2)	Cl2-Re1-Cl3	173.66(2)	C1-Re1-C2	172.3(3)
Cl1-Re1-Cl3	87.68(2)	N2-C2-Re1	176.5(7)	N1-C1-Re1	179.0(7)
C1-Re1-Cl2	90.29(19)	C1-Re1-Cl1	86.0(2)	C1-N1-C17	176.8(6)



**Figure S7B:** Ellipsoid representation of  $[\text{Re}(\text{NPhF})\text{Cl}_3(\text{CNAr}^{\text{Dipp}2})_2] \cdot 1.25 \text{ toluene} \cdot 1/2 \text{ CH}_2\text{Cl}_2$  (**8**), species 2. The thermal ellipsoids are set at a 50% probability level. Hydrogen atoms are omitted for clarity.

**Table S8B:** Selected bond lengths (Å) and angles (°) in  $[\text{Re}(\text{NPhF})\text{Cl}_3(\text{CNAr}^{\text{Dipp}2})_2] \cdot 1.25 \text{ toluene} \cdot 1/2 \text{ CH}_2\text{Cl}_2$  (**8**), species 2.

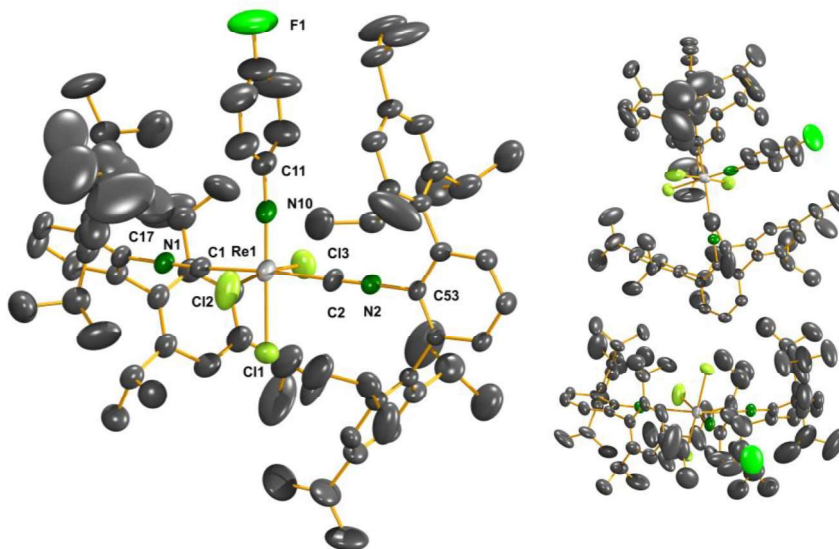
Re2-Cl4	2.4267(2)	N5-C76	1.145(8)	Re2-Cl6	2.3975(2)
Re2-Cl5	2.3801(2)	N6-C106	1.415(8)	Re2-N4	1.722(6)
C106-N6	1.160(9)	Re2-C106	2.055(7)	Re2-C75	2.066(6)
N6-C107	1.409(9)	N4-C69	1.370(9)	N5-C75	1.151(8)
C75-Re2-Cl5	85.66(2)	Cl4-Re2-C106	94.1(3)	C69-N4-Re2	171.5(6)
Cl5-Re2-C106	86.0(2)	Cl5-Re2-Cl6	87.54(7)	C106-Re2-C75	171.6(3)
Cl4-Re2-Cl6	172.88(7)	N6-C106-Re2	178.3(6)	N5-C75-Re2	178.2(6)
C75-Re2-Cl5	85.66(2)	C106-Re2-Cl4	89.63(2)	C75-N5-C76	177.5(&)



**Figure S8:** Ellipsoid representation of  $[\text{Re}(\text{NPhF})\text{Cl}_3(\text{PPh}_3)(\text{CNAr}^{\text{Tripp2}})]\cdot\text{THF}$  (**9**). The thermal ellipsoids are set at a 50% probability level. Hydrogen atoms are omitted for clarity.

**Table S9:** Selected bond lengths (Å) and angles (°) in  $[\text{Re}(\text{NPhF})\text{Cl}_3(\text{PPh}_3)(\text{CNAr}^{\text{Tripp2}})]\cdot\text{THF}$  (**9**).

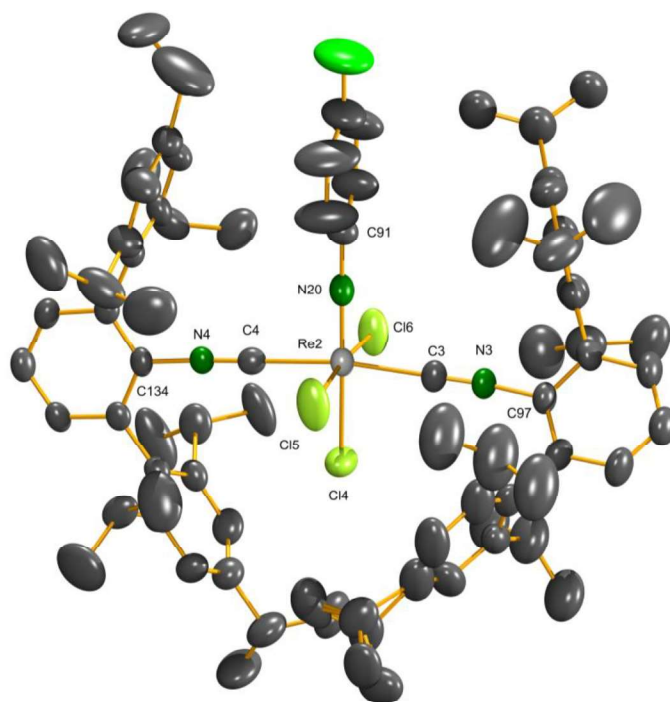
Re1-Cl2	2.3958(1)	P1-C53	1.824(5)	Re1-Cl3	2.4173(2)
Re1-Cl1	2.3771(2)	P1-C59	1.823(5)	Re1-N10	1.711(4)
Re1-P1	2.4602(2)	P1-C65	1.805(5)	Re1-C1	2.027(5)
N10-C11	1.409(6)	C1-N1	1.167(5)	N1-C17	1.405(5)
Cl2-Re1-Cl1	86.17(5)	Cl1-Re1-P1	86.23(5)	C11-N10-Re1	168.7(3)
Cl2-Re1-P1	86.17(5)	Cl1-Re1-Cl3	87.59(5)	C1-Re1-P1	100.96(14)
Cl2-Re1-Cl3	86.56(5)	Cl3-Re1-P1	170.35(5)	N1-C1-Re1	170.4(4)
C1-Re1-Cl2	166.31(14)	C1-Re1-Cl1	77.82(14)	C1-N1-C17	164.9(5)



**Figure S9A:** Ellipsoid representation of  $[\text{Re}(\text{NPhF})\text{Cl}_3(\text{CNAr}^{\text{Tripp2}})_2]$  (**10**), species 1. The thermal ellipsoids are set at a 50% probability level. Hydrogen atoms are omitted for clarity.

**Table S10A:** Selected bond lengths (Å) and angles (°) in  $[\text{Re}(\text{NPhF})\text{Cl}_3(\text{CNAr}^{\text{Tripp2}})_2]$  (**10**), species 1.

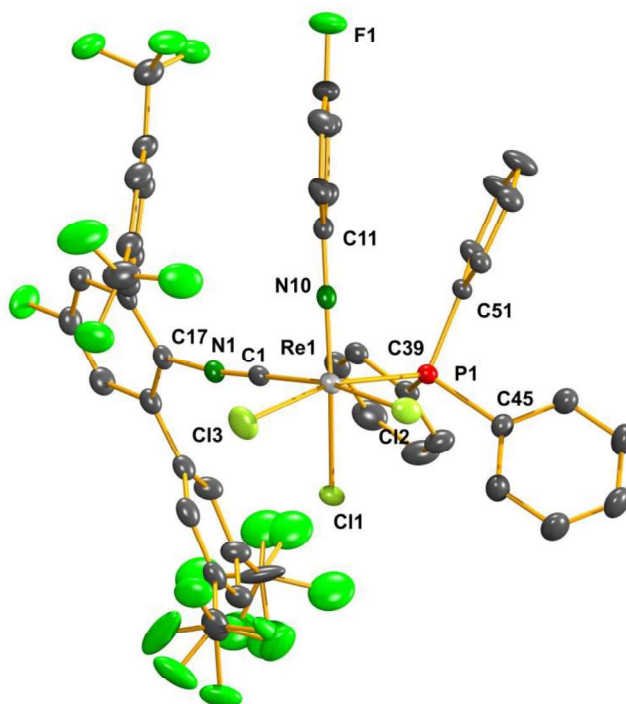
Re1-Cl2	2.417(2)	N1-C1	1.135(7)	Re1-Cl3	2.3972(2)
Re1-Cl1	2.3627(2)	N2-C53	1.412(6)	Re1-N10	1.698(6)
C2-N2	1.139(7)	Re1-C2	2.084(6)	Re1-C1	2.093(6)
N10-C11	1.397(8)	N1-C17	1.408(7)		
Cl2-Re1-Cl1	85.81(8)	Cl1-Re1-C2	86.25(2)	C11-N10-Re1	177.1(5)
Cl2-Re1-C2	93.07(2)	Cl2-Re1-Cl3	171.09(9)	C1-Re1-C2	173.9(2)
Cl1-Re1-Cl3	85.32(7)	N2-C2-Re1	177.3(6)	N1-C1-Re1	177.3(6)
C1-Re1-Cl2	89.32(19)	C1-Re1-Cl1	88.38(2)	C1-N1-C17	178.4(7)



**Figure S9B:** Ellipsoid representation of  $[\text{Re}(\text{NPhF})\text{Cl}_3(\text{CNAr}^{\text{Tripp}2})_2]$  (**10**), species 2. The thermal ellipsoids are set at a 50% probability level. Hydrogen atoms are omitted for clarity.

**Table S10B:** Selected bond lengths (Å) and angles (°) in  $[\text{Re}(\text{NPhF})\text{Cl}_3(\text{CNAr}^{\text{Tripp}2})_2]$  (**10**), species 2.

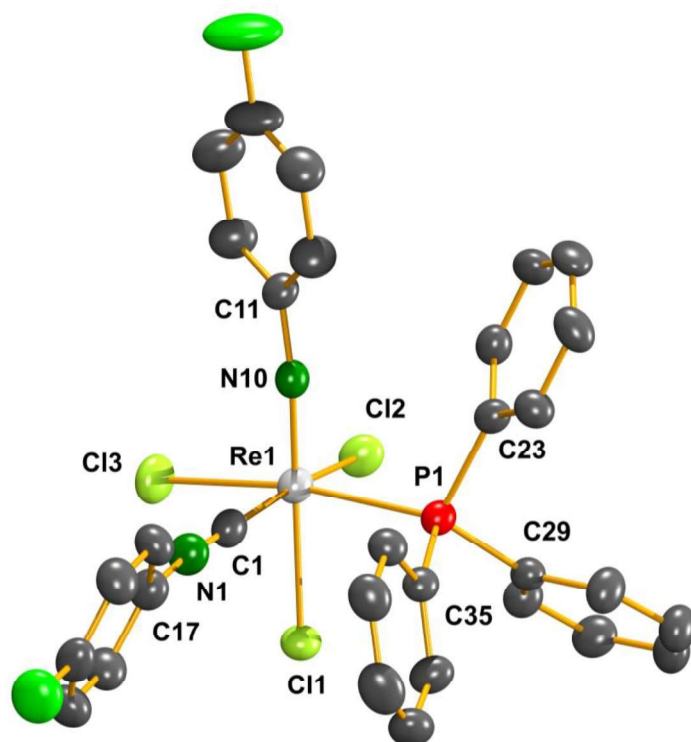
Re2-Cl5	2.4016(2)	N3-C3	1.135(7)	Re2-Cl6	2.4016(2)
Re2-Cl4	2.3609(2)	N3-C97	1.397(7)	Re2-N20	1.711(5)
C4-N4	1.148(7)	Re2-C4	2.076(6)	Re2-C3	2.090(6)
N20-C91	1.376(8)	N3-C97	1.397(7)		
C4-Re2-Cl4	84.67(2)	Cl4-Re2-C4	84.67(2)	C91-N20-Re2	178.7(5)
Cl5-Re2-C4	88.52(2)	Cl5-Re2-Cl6	173.17(9)	C3-Re2-C4	170.8(2)
Cl4-Re2-Cl6	86.17(9)	N4-C4-Re2	179.5(7)	N3-C3-Re2	175.4(5)
C3-Re2-Cl5	92.44(2)	C3-Re2-Cl4	86.23(2)	C4-N4-C134	177.2(6)



**Figure S10:** Ellipsoid representation of  $[\text{Re}(\text{NPhF})\text{Cl}_3(\text{PPh}_3)(\text{CNp-FAr}^{\text{DarF}_2})]$  (**11**). The thermal ellipsoids are set at a 50% probability level. Hydrogen atoms are omitted for clarity.

**Table S11:** Selected bond lengths (Å) and angles ( $^\circ$ ) in  $[\text{Re}(\text{NPhF})\text{Cl}_3(\text{PPh}_3)(\text{CNp-FAr}^{\text{DarF}_2})]$  (**11**).

Re1-Cl2	2.4013(8)	P1-C39	1.816(3)	Re1-Cl3	2.3879(8)
Re1-Cl1	2.4253(7)	P1-C45	1.835(3)	Re1-N10	1.721(3)
Re1-P1	2.4494(8)	P1-C51	1.822(3)	Re1-C1	2.022(3)
N10-C11	1.380(4)	C1-N1	1.151(4)	N1-C17	1.393(4)
Cl2-Re1-Cl1	94.67(3)	Cl1-Re1-P1	79.30(3)	C11-N10-Re1	170.4(2)
Cl2-Re1-P1	89.00(3)	Cl1-Re1-Cl3	86.86(3)	C1-Re1-P1	96.37(8)
Cl2-Re1-Cl3	86.10(3)	Cl3-Re1-P1	164.88(3)	N1-C1-Re1	174.6(3)
C1-Re1-Cl2	169.98(9)	C1-Re1-Cl1	78.10(8)	C1-N1-C17	172.2(3)



**Figure S11:** Ellipsoid representation of  $[\text{Re}(\text{NPhF})\text{Cl}_3(\text{PPh}_3)(\text{CNPh}^{\text{PF}})]$  (**12**). The thermal ellipsoids are set at a 50% probability level. Hydrogen atoms are omitted for clarity.

**Table S12:** Selected bond lengths (Å) and angles (°) in  $[\text{Re}(\text{NPhF})\text{Cl}_3(\text{PPh}_3)(\text{CNPh}^{\text{PF}})]$  (**12**).

Re1-Cl2	2.407(2)	P1-C23	1.832(5)	Re1-Cl3	2.4129(2)
Re1-Cl1	2.437(2)	P1-C35	1.822(5)	Re1-N10	1.705(4)
Re1-P1	2.470(2)	P1-C29	1.833(5)	Re1-C1	2.024(6)
N10-C11	1.395(7)	C1-N1	1.156(7)	N1-C17	1.396(7)
Cl2-Re1-Cl1	89.91(5)	Cl1-Re1-P1	81.81(5)	C11-N10-Re1	172.9(4)
Cl2-Re1-P1	93.14(5)	Cl1-Re1-Cl3	88.81(6)	C1-Re1-P1	91.33(16)
Cl2-Re1-Cl3	86.95(6)	Cl3-Re1-P1	170.62(5)	N1-C1-Re1	176.9(5)
C1-Re1-Cl2	169.89(16)	C1-Re1-Cl1	81.75(16)	C1-N1-C17	173.0(6)

## Spectroscopic data and mass spectrometry

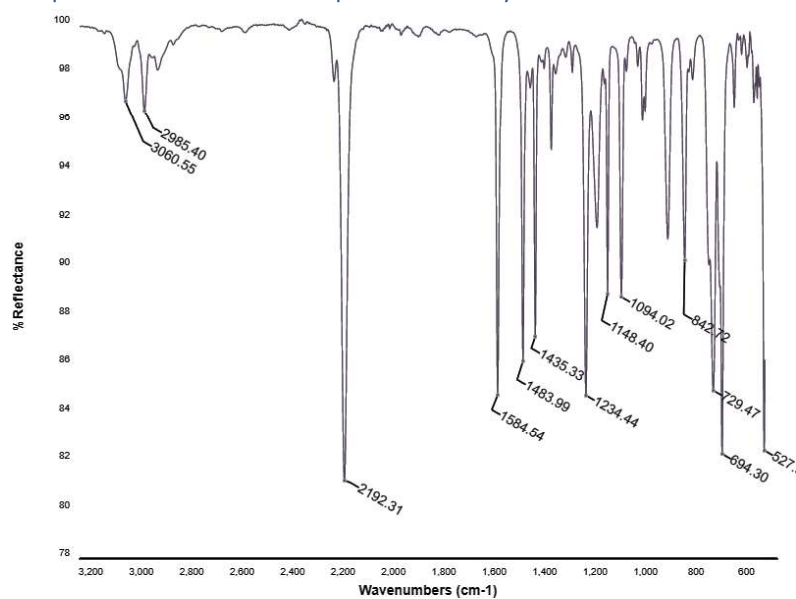


Figure S12: IR (ATR) spectrum of  $[\text{Re}(\text{NPhF})\text{Cl}_3(\text{PPh}_3)(\text{CN}^t\text{Bu})]$  (**2**).

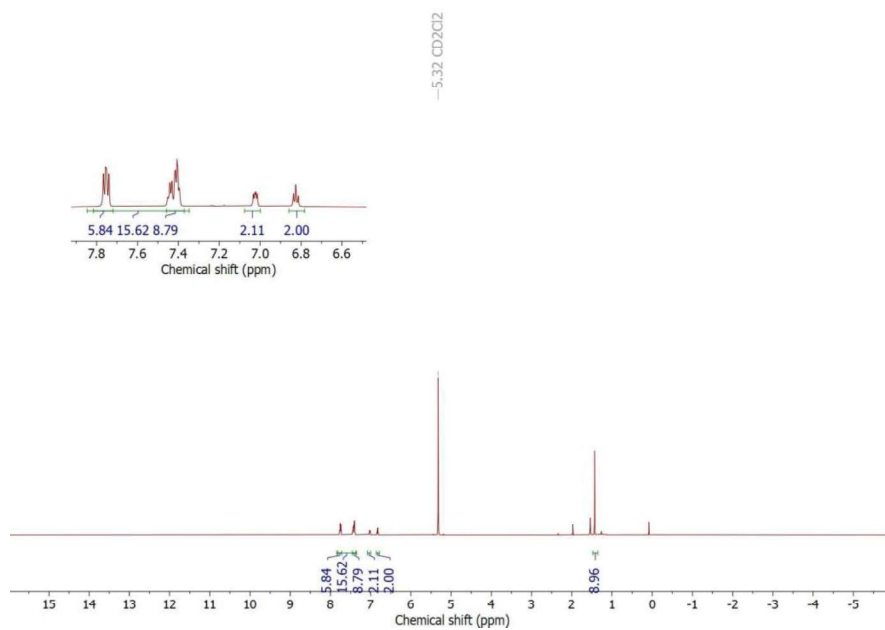
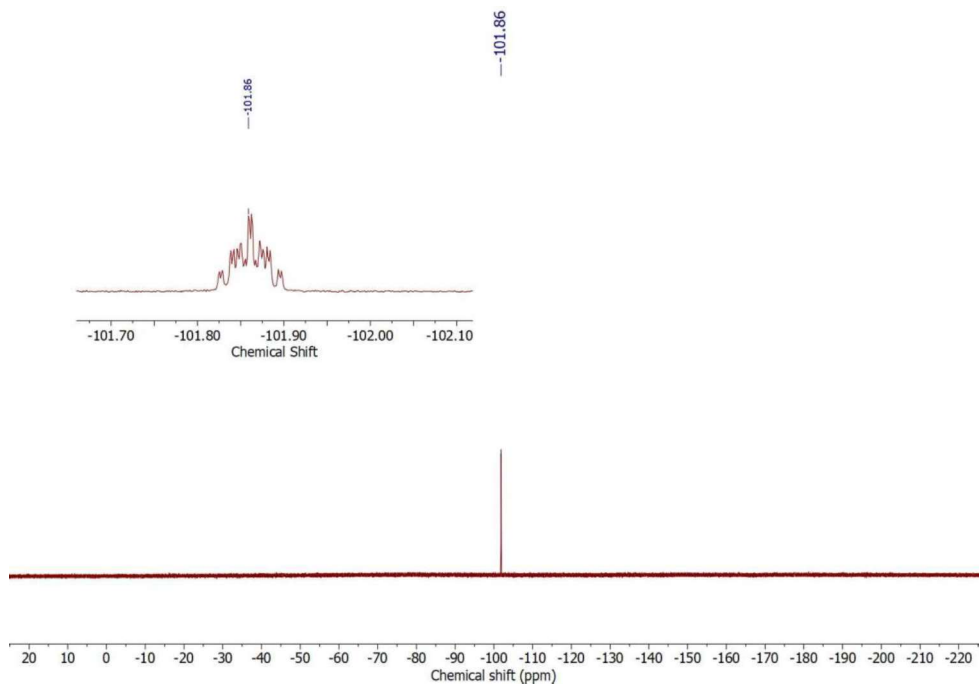
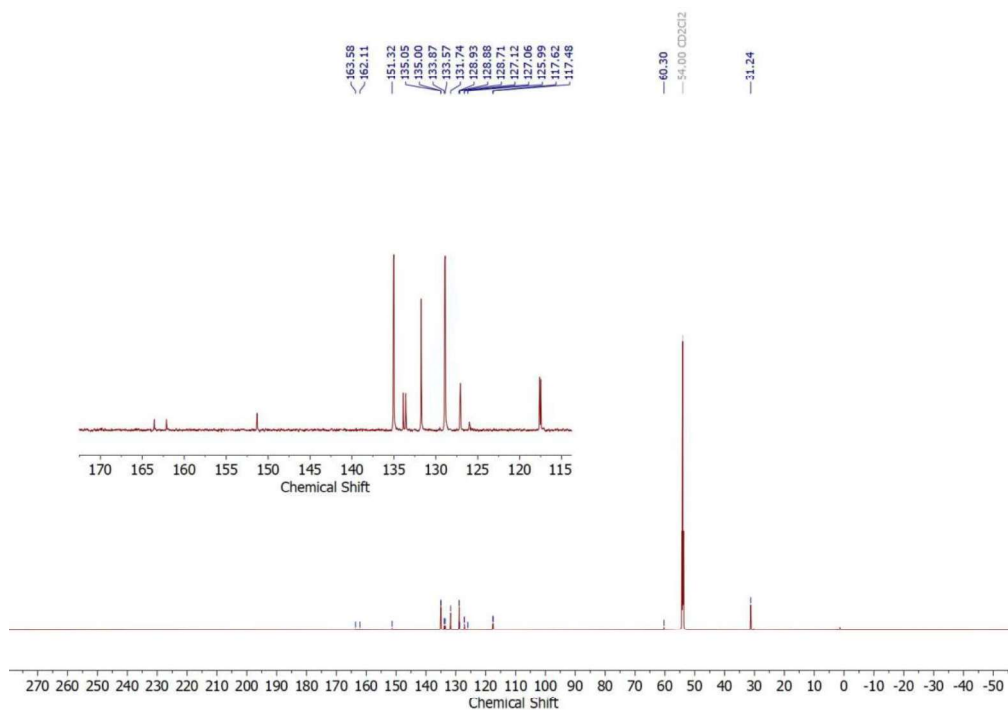


Figure S13:  $^1\text{H}$  NMR spectrum of  $[\text{Re}(\text{NPhF})\text{Cl}_3(\text{PPh}_3)(\text{CN}^t\text{Bu})]$  (**2**) in  $\text{CD}_2\text{Cl}_2$ .

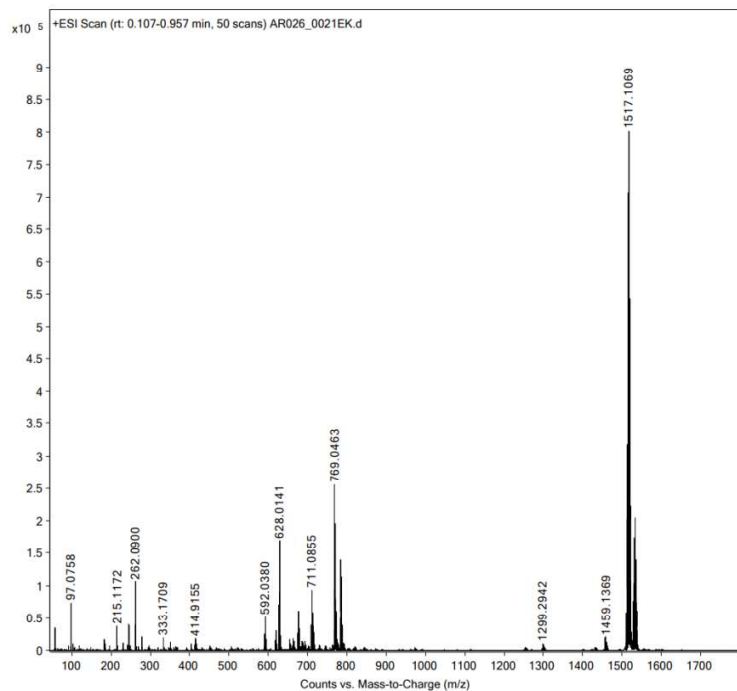




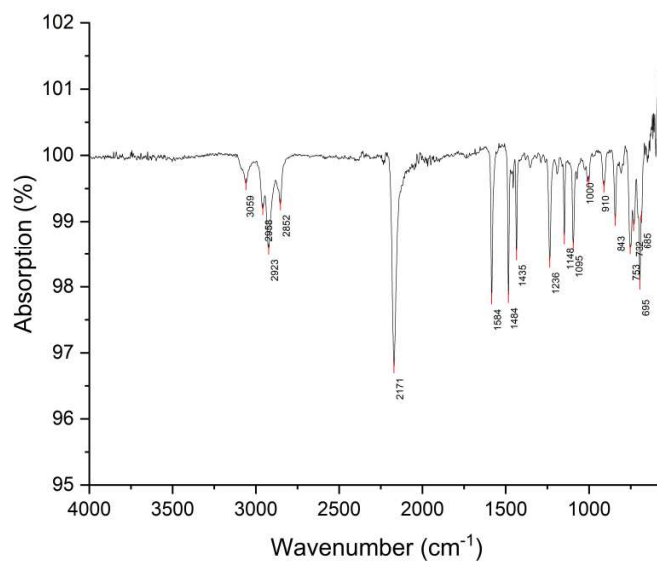
**Figure S14:**  $^{19}\text{F}$  NMR spectrum of  $[\text{Re}(\text{NPhF})\text{Cl}_3(\text{PPh}_3)(\text{CN}^t\text{Bu})]$  (**2**) in  $\text{CD}_2\text{Cl}_2$ .



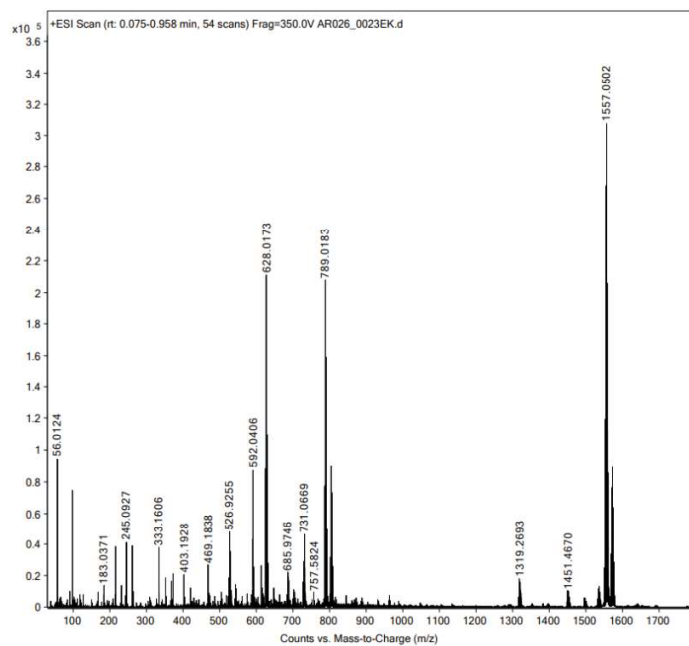
**Figure S15:**  $^{13}\text{C}\{^1\text{H}\}$  NMR spectrum of  $[\text{Re}(\text{NPhF})\text{Cl}_3(\text{PPh}_3)(\text{CN}^t\text{Bu})]$  (**2**) in  $\text{CD}_2\text{Cl}_2$ .



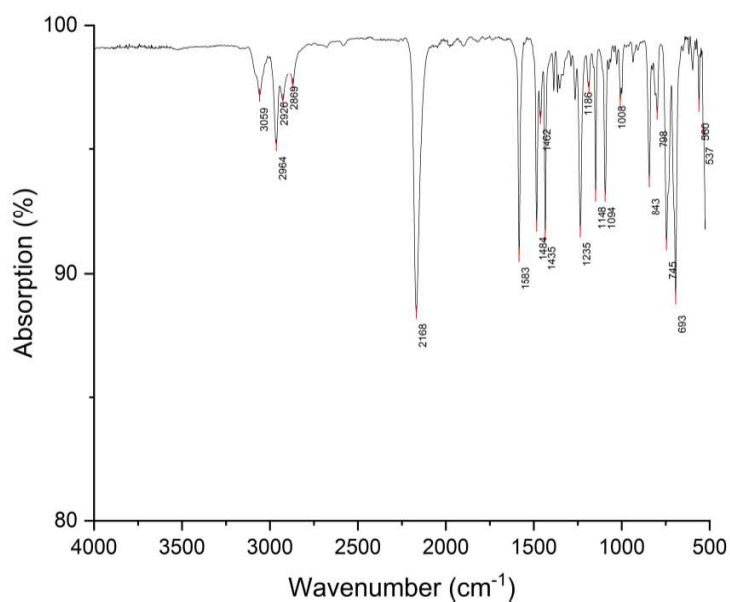
**Figure S16:** ESI+ mass spectrum of  $[\text{Re}(\text{NPhF})\text{Cl}_3(\text{PPh}_3)(\text{CN}^t\text{Bu})]$  (**2**) in MeCN.



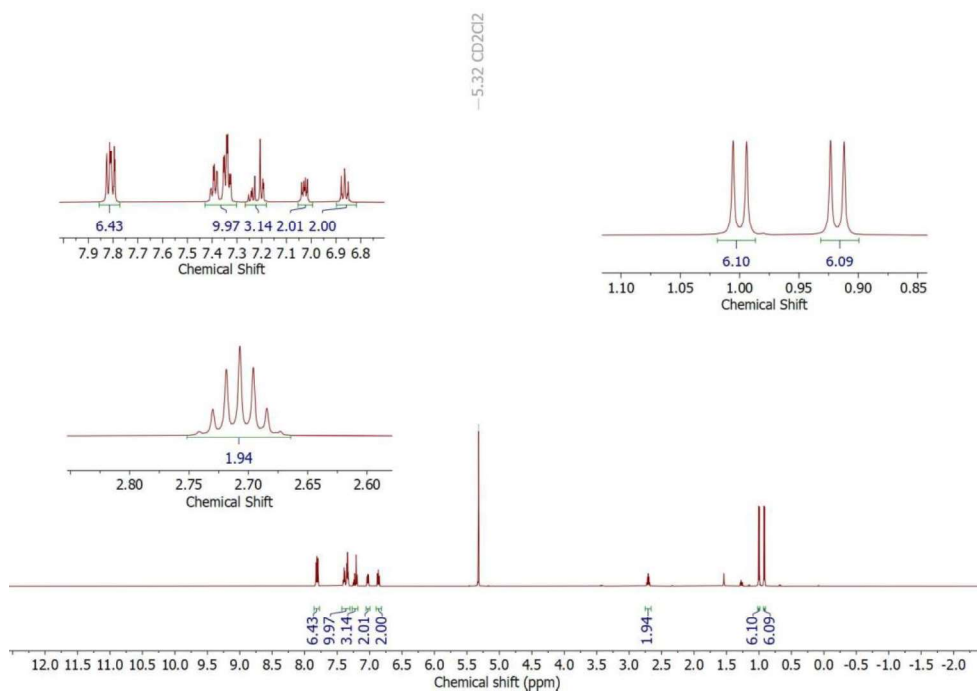
**Figure S17:** IR (ATR) spectrum of  $[\text{Re}(\text{NPhF})\text{Cl}_3(\text{PPh}_3)(\text{CNPh})]$  (**3**).



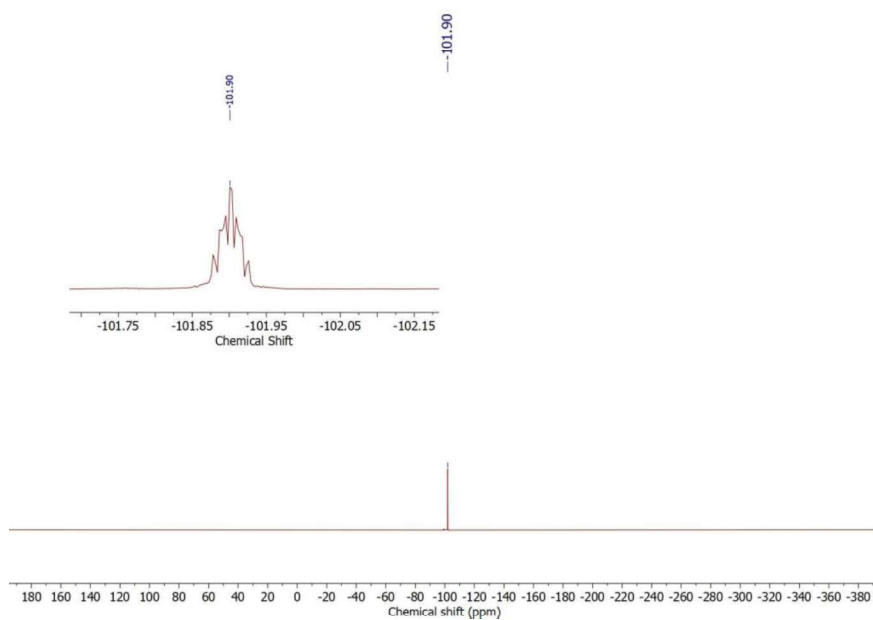
**Figure S18:** ESI+ mass spectrum of  $[\text{Re}(\text{NPhF})\text{Cl}_3(\text{PPh}_3)(\text{CNPh})]$  (**3**) in MeCN.



**Figure S19:** IR (ATR) spectrum of  $[\text{Re}(\text{NPhF})\text{Cl}_3(\text{PPh}_3)(\text{CNPh}^{\text{i-prop2}})]$  (**3**).



**Figure S20:** <sup>1</sup>H NMR spectrum of [Re(NPhF)Cl<sub>3</sub>(PPh<sub>3</sub>)(CNPh<sup>i-prop2</sup>)] (**4**) in CD<sub>2</sub>Cl<sub>2</sub>.



**Figure S21:** <sup>19</sup>F NMR spectrum of [Re(NPhF)Cl<sub>3</sub>(PPh<sub>3</sub>)(CNPh<sup>i-prop2</sup>)] (**4**) in CD<sub>2</sub>Cl<sub>2</sub>.

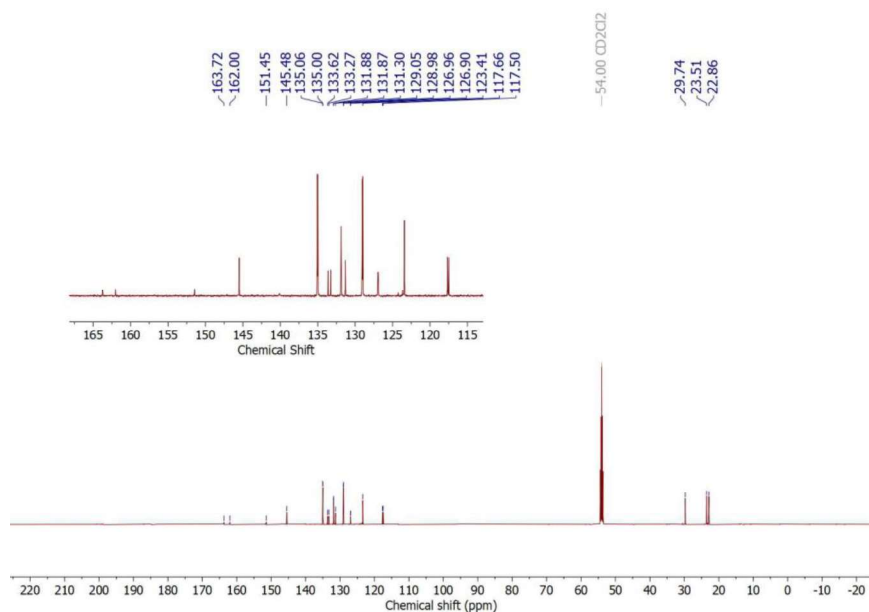


Figure S22:  $^{13}\text{C}\{^1\text{H}\}$  NMR of  $[\text{Re}(\text{NPhF})\text{Cl}_3(\text{PPh}_3)(\text{CNPh}^i\text{-prop}^2)]$  (**4**) in  $\text{CD}_2\text{Cl}_2$ .

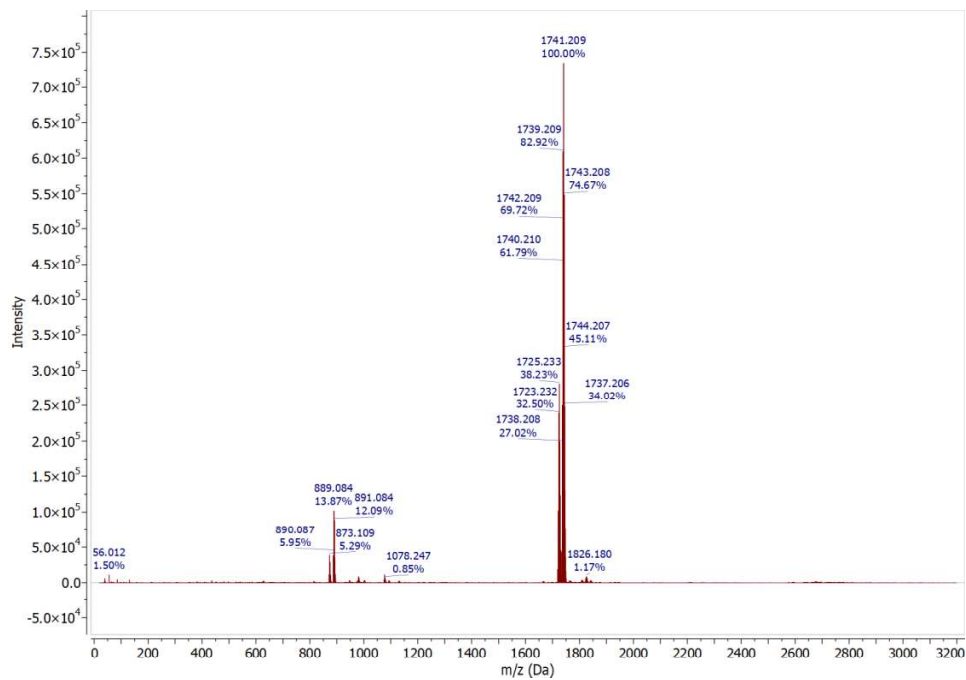
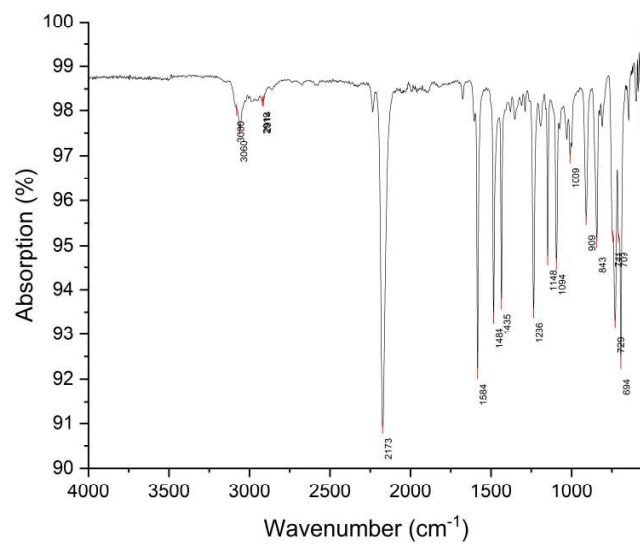
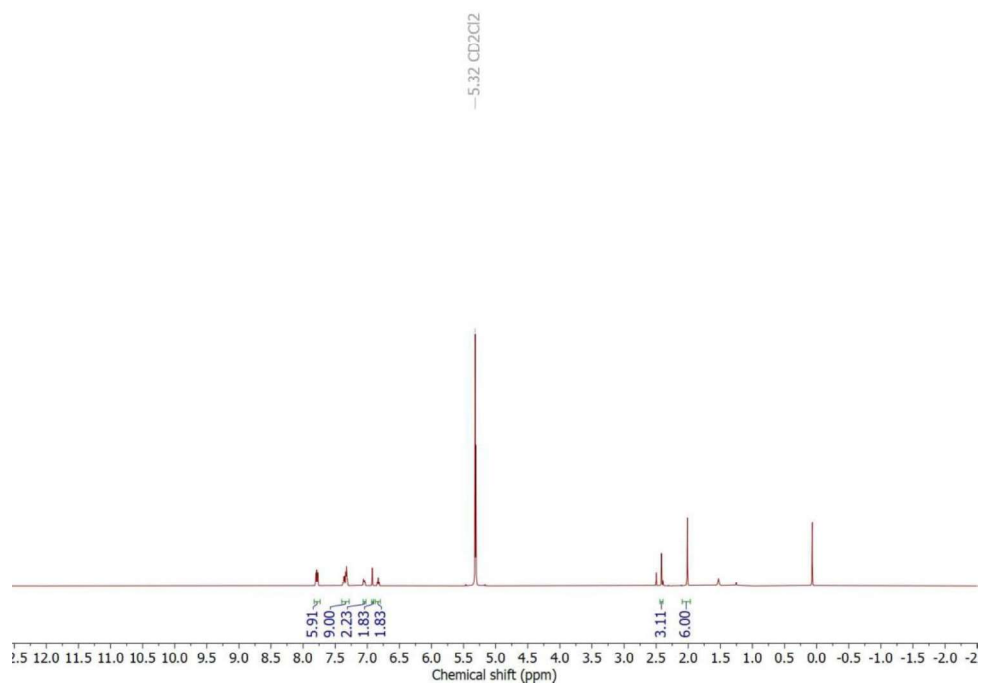


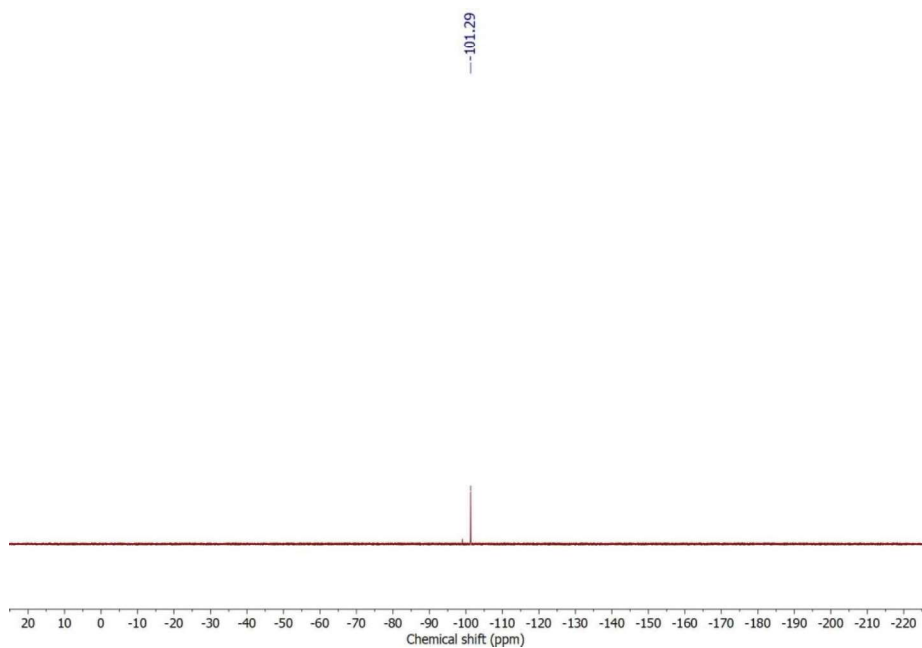
Figure S23: ESI+ mass spectrum of  $[\text{Re}(\text{NPhF})\text{Cl}_3(\text{PPh}_3)(\text{CNPh}^i\text{-prop}^2)]$  (**4**) in MeCN.



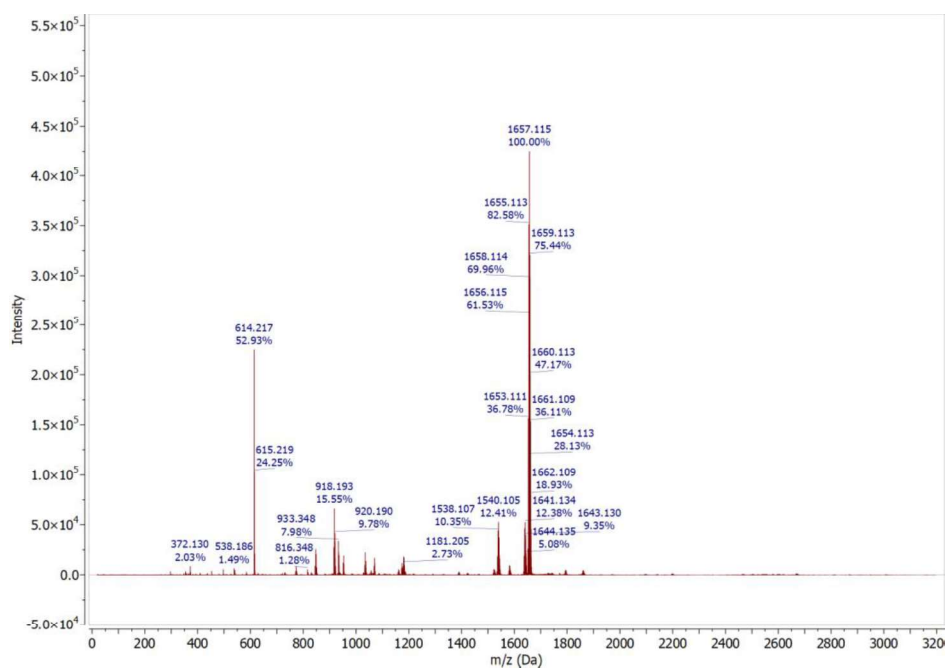
**Figure S24:** IR (ATR) spectrum of  $[\text{Re}(\text{NPhF})\text{Cl}_3(\text{PPh}_3)(\text{CNMe})]$  (**5**).



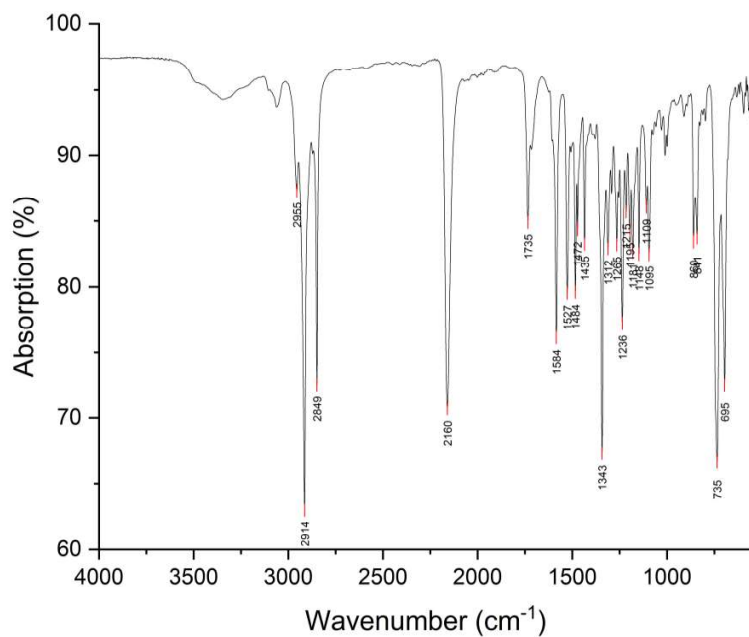
**Figure S25:**  $^1\text{H}$  NMR spectrum of  $[\text{Re}(\text{NPhF})\text{Cl}_3(\text{PPh}_3)(\text{CNMe})]$  (**5**) in  $\text{CD}_2\text{Cl}_2$  shortly after dissolution.



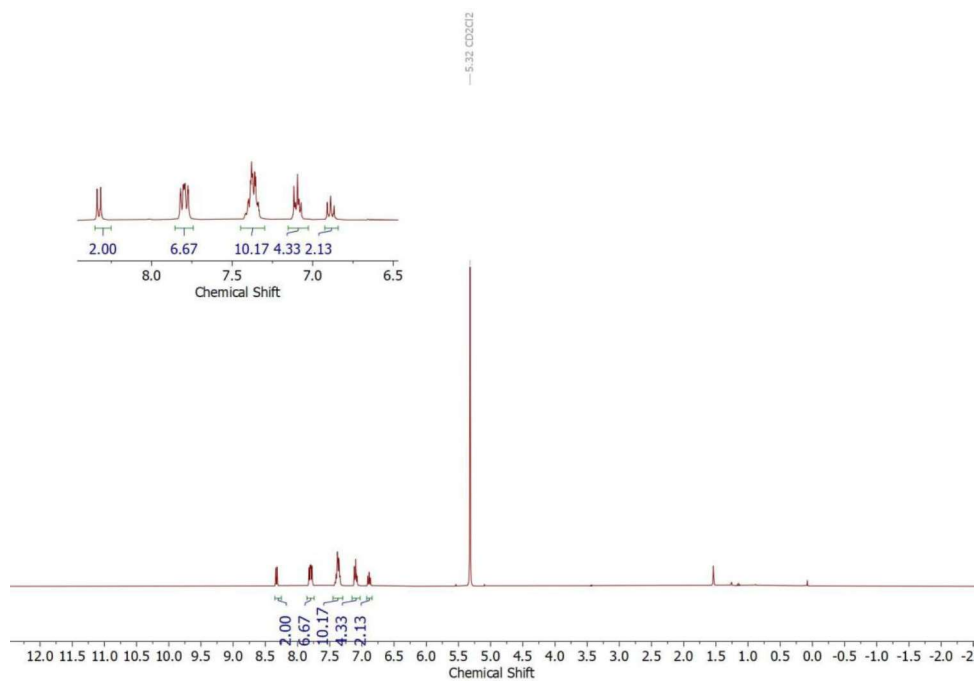
**Figure S26:**  $^{19}\text{F}$  NMR spectrum of  $[\text{Re}(\text{NPhF})\text{Cl}_3(\text{PPh}_3)(\text{CNMe}_s)]$  (**5**) in  $\text{CD}_2\text{Cl}_2$  shortly after dissolution.



**Figure S27:** ESI+ mass spectrum of  $[\text{Re}(\text{NPhF})\text{Cl}_3(\text{PPh}_3)(\text{CNMe}_s)]$  (**5**) in MeCN.

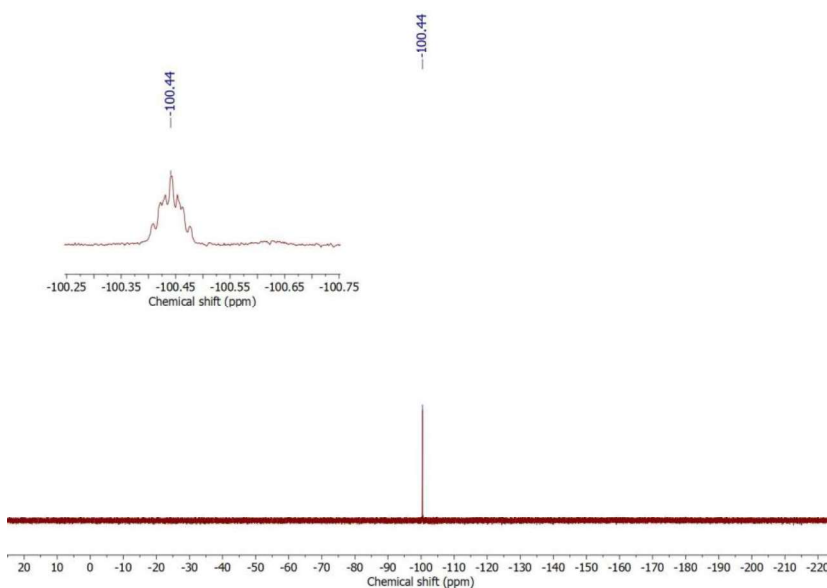


**Figure S28:** IR (ATR) spectrum of  $[\text{Re}(\text{NPhF})\text{Cl}_3(\text{PPh}_3)(\text{CNPh}^{\text{pNO}_2})]$  (**6**).

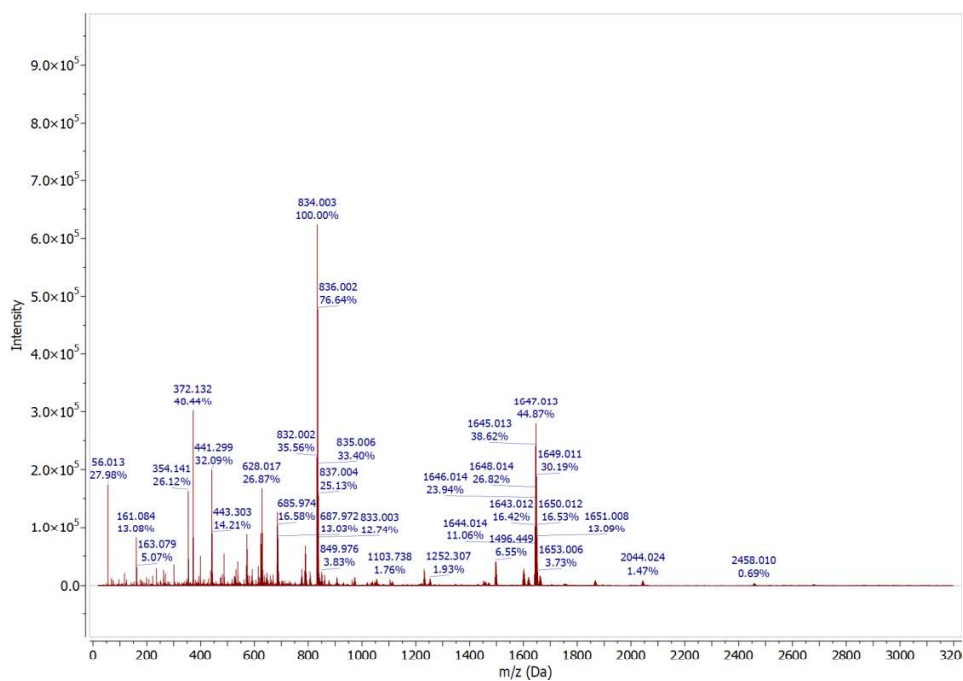


**Figure S29:**  $^1\text{H}$  NMR spectrum of  $[\text{Re}(\text{NPhF})\text{Cl}_3(\text{PPh}_3)(\text{CNPh}^{\text{pNO}_2})]$  (**6**) in  $\text{CD}_2\text{Cl}_2$  shortly after dissolution.

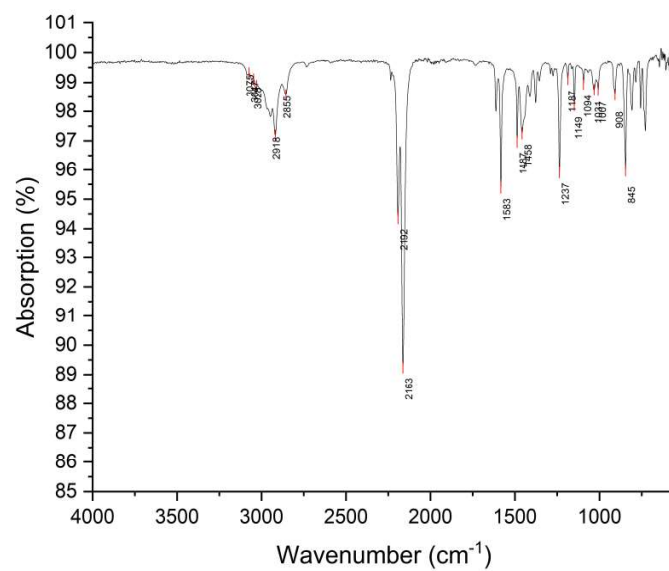




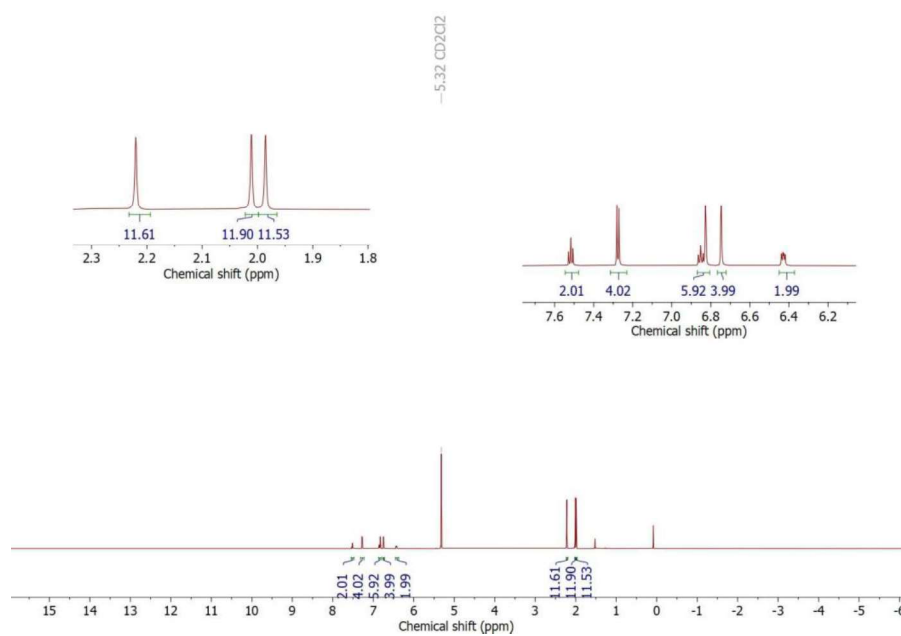
**Figure S30:**  $^{19}\text{F}$  NMR spectrum of  $[\text{Re}(\text{NPhF})\text{Cl}_3(\text{PPh}_3)(\text{CNPh}^{\text{pNO}_2})]$  (**6**) in  $\text{CD}_2\text{Cl}_2$  shortly after dissolution.



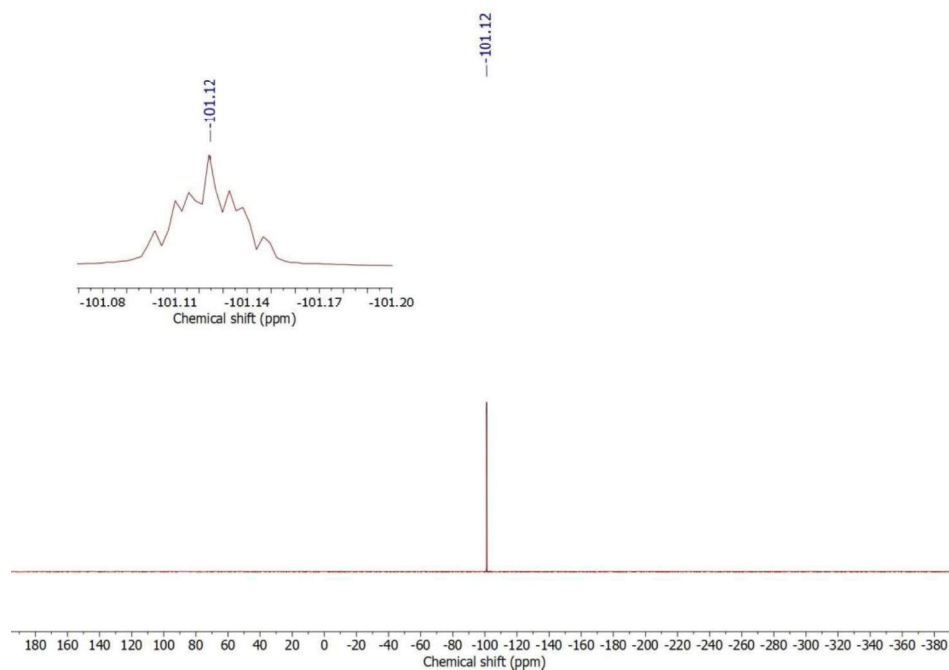
**Figure S31:** ESI+ mass spectrum of  $[\text{Re}(\text{NPhF})\text{Cl}_3(\text{PPh}_3)(\text{CNPh}^{\text{pNO}_2})]$  (**6**) in MeCN.



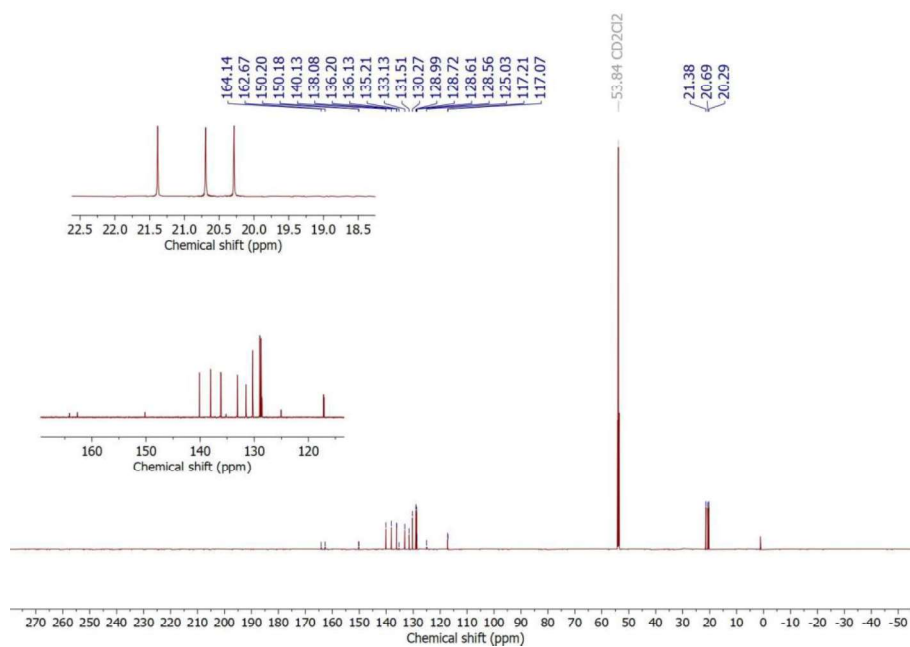
**Figure S32:** IR (ATR) spectrum of  $[\text{Re}(\text{NPhF})\text{Cl}_3(\text{CNAr}^{\text{Mes}_2})_2]$  (**7**).



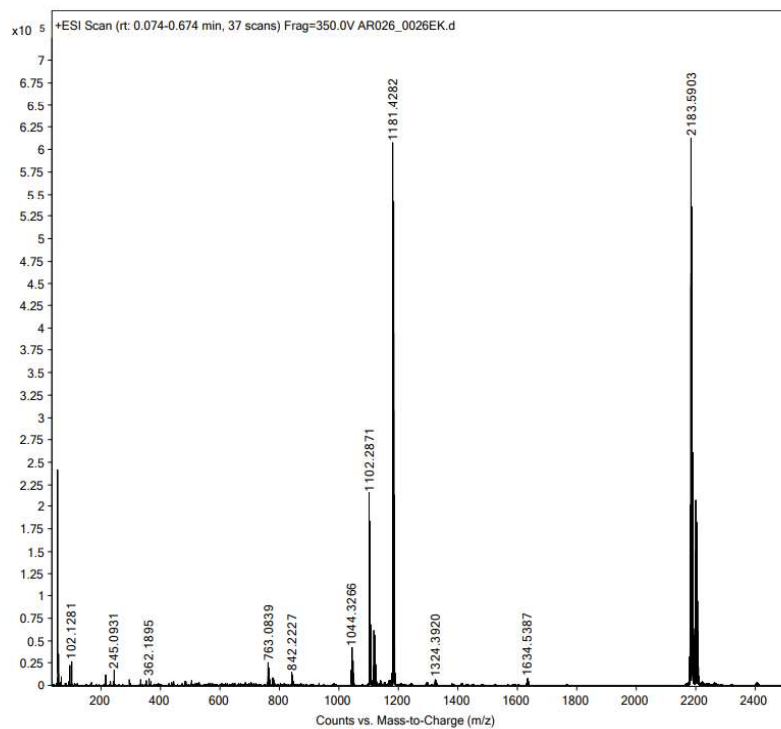
**Figure S33:**  $^1\text{H}$  NMR spectrum of  $[\text{Re}(\text{NPhF})\text{Cl}_3(\text{CNAr}^{\text{Mes}_2})_2]$  (**7**) in  $\text{CD}_2\text{Cl}_2$ .



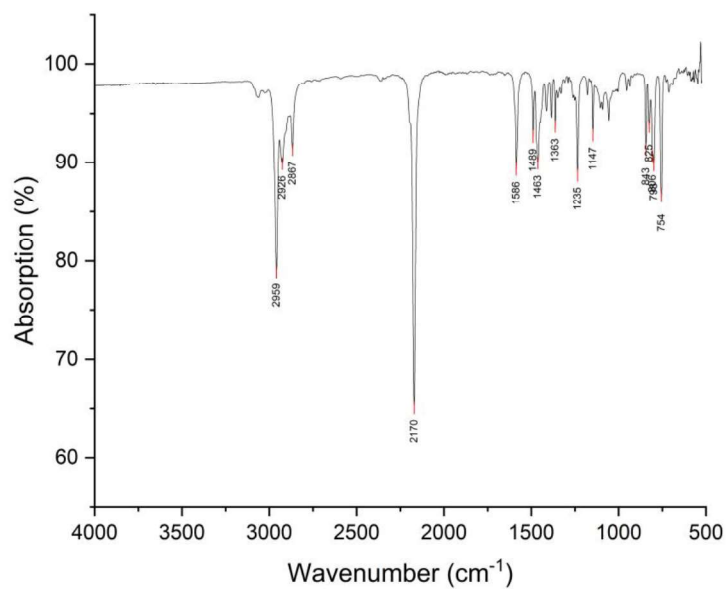
**Figure S34:**  $^{19}\text{F}$  NMR spectrum of  $[\text{Re}(\text{NPhF})\text{Cl}_3(\text{CNAr}^{\text{Mes}2})_2]$  (**7**) in  $\text{CD}_2\text{Cl}_2$ .



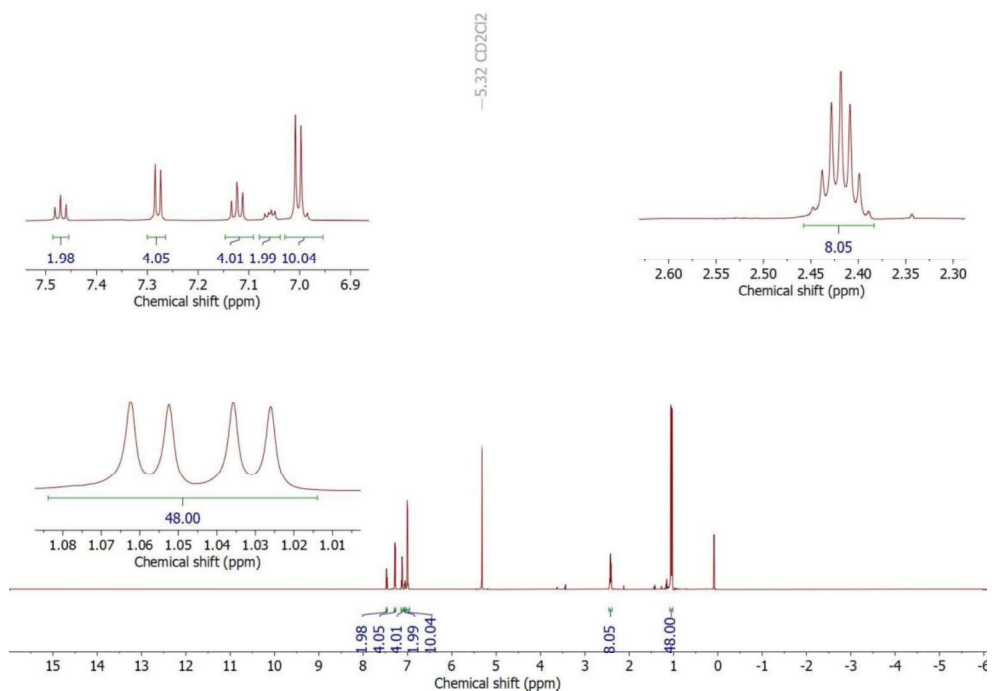
**Figure S35:**  $^{13}\text{C}\{^1\text{H}\}$  NMR spectrum of  $[\text{Re}(\text{NPhF})\text{Cl}_3(\text{CNAr}^{\text{Mes}2})_2]$  (**7**) in  $\text{CD}_2\text{Cl}_2$ .



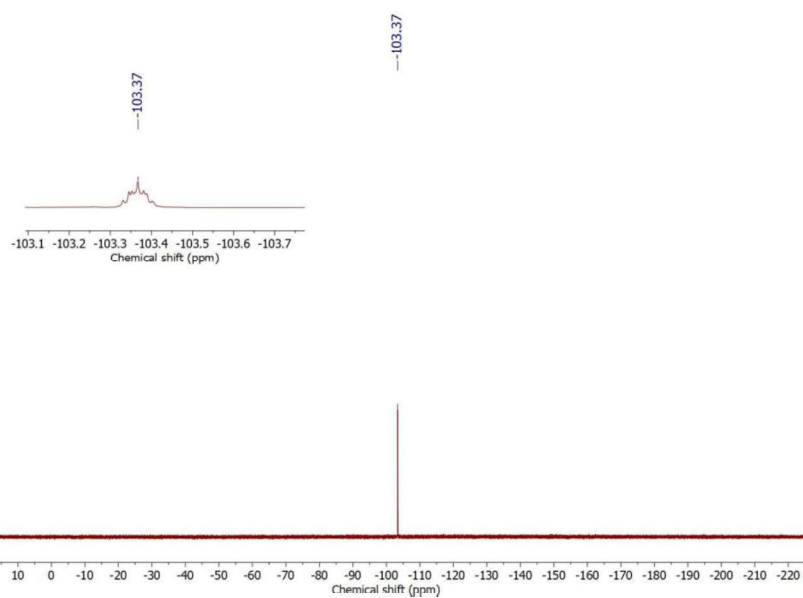
**Figure S36:** ESI+ mass spectrum of [Re(NPhF)Cl<sub>3</sub>(CNAr<sup>Mes2</sup>)<sub>2</sub>] (**7**) in MeCN.



**Figure S37:** IR (ATR) spectrum of [Re(NPhF)Cl<sub>3</sub>(CNAr<sup>Dipp2</sup>)<sub>2</sub>] (**8**).



**Figure S38:**  $^1\text{H}$  NMR spectrum of  $[\text{Re}(\text{NPhF})\text{Cl}_3(\text{CNAr}^{\text{Dipp}2})_2]$  (**8**) in  $\text{CD}_2\text{Cl}_2$ .



**Figure S39:**  $^{19}\text{F}$  NMR spectrum of  $[\text{Re}(\text{NPhF})\text{Cl}_3(\text{CNAr}^{\text{Dipp}2})_2]$  (**8**) in  $\text{CD}_2\text{Cl}_2$ .

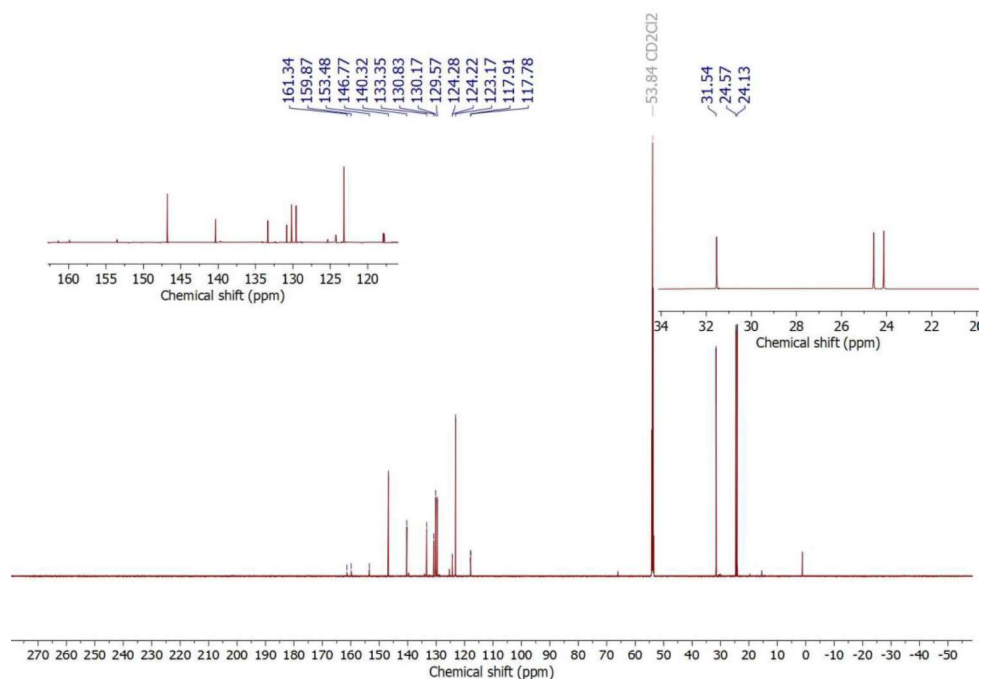


Figure S40:  $^{13}\text{C}\{^1\text{H}\}$  NMR spectrum of  $[\text{Re}(\text{NPhF})\text{Cl}_3(\text{CNAr}^{\text{Dipp}2})_2]$  (**8**) in  $\text{CD}_2\text{Cl}_2$ .

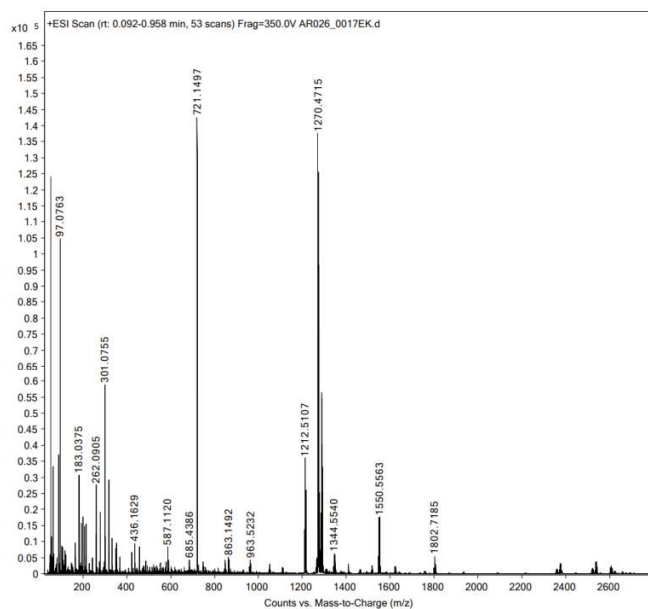
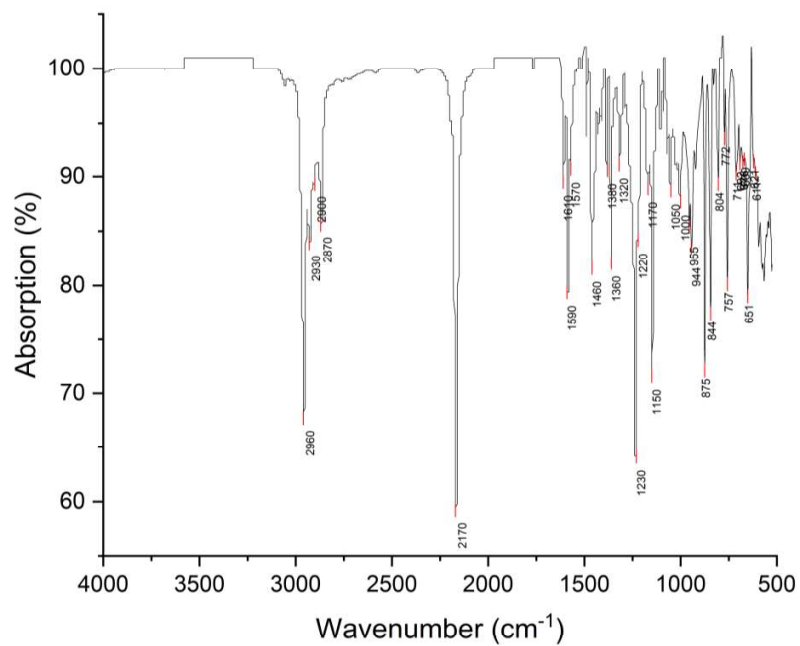
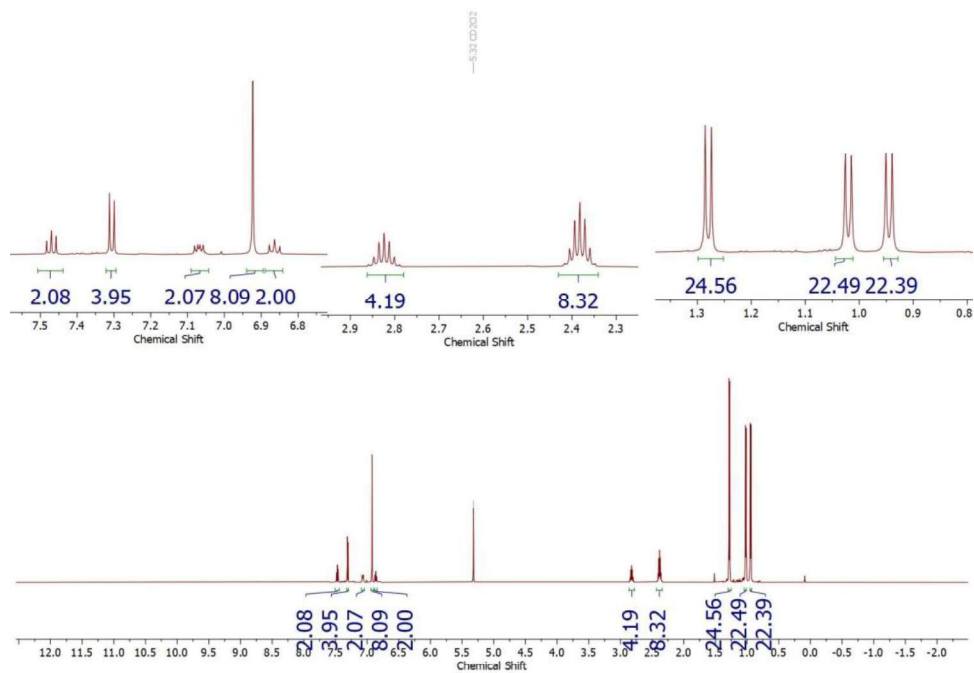


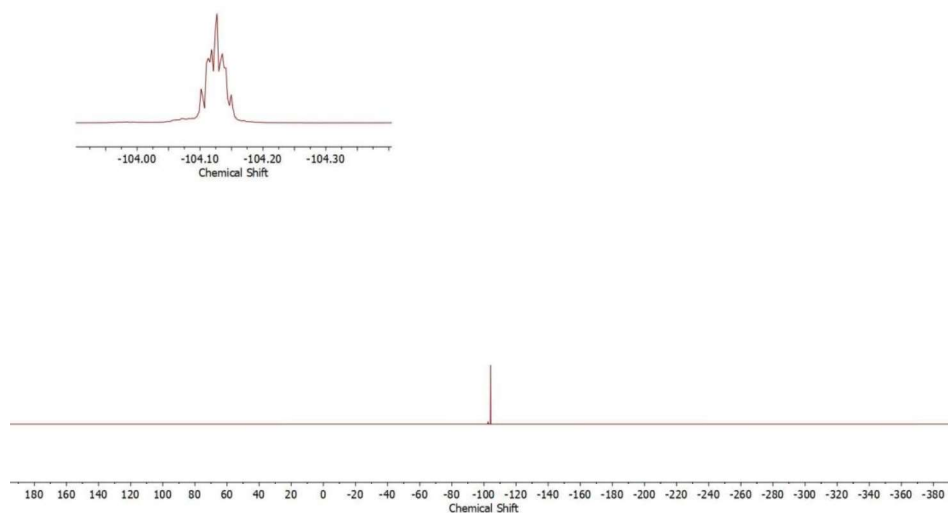
Figure S41: ESI+ mass spectrum of  $[\text{Re}(\text{NPhF})\text{Cl}_3(\text{CNAr}^{\text{Dipp}2})_2]$  (**8**) in MeCN.



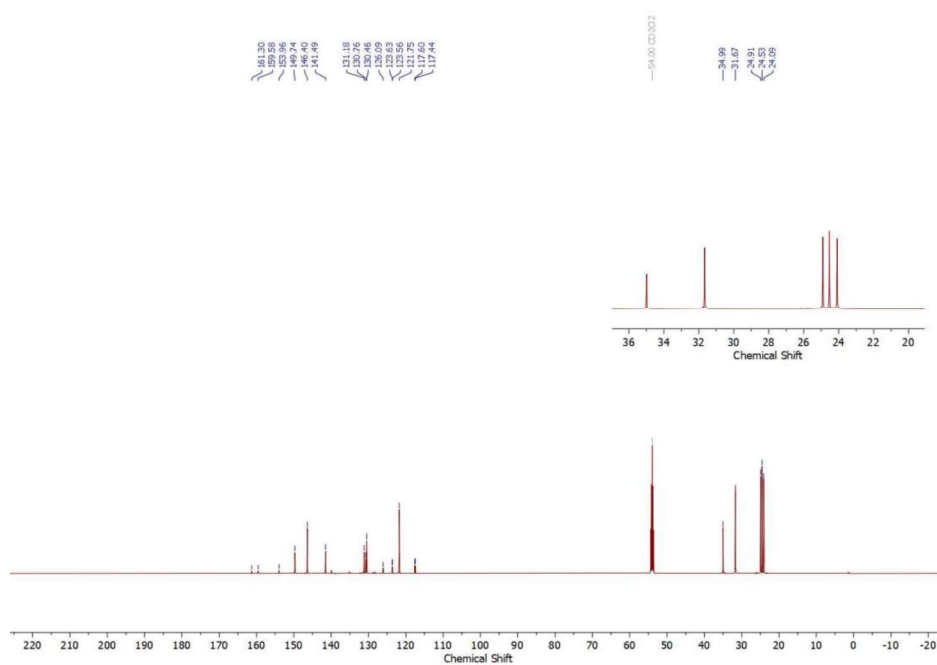
**Figure S42:** IR (ATR) spectrum of  $[\text{Re}(\text{NPhF})\text{Cl}_3(\text{CNAr}^{\text{Tripp}2})_2]$



**Figure S43:**  $^1\text{H}$  NMR spectrum of  $[\text{Re}(\text{NPhF})\text{Cl}_3(\text{CNAr}^{\text{Tripp}2})_2]$  (**10**) in  $\text{CD}_2\text{Cl}_2$ .



**Figure S44:**  $^{19}\text{F}$  NMR spectrum of  $[\text{Re}(\text{NPhF})\text{Cl}_3(\text{CNAr}^{\text{Tripp}2})_2]$  (**10**) in  $\text{CD}_2\text{Cl}_2$ .



**Figure S45:**  $^{13}\text{C}\{^1\text{H}\}$  NMR spectrum of  $[\text{Re}(\text{NPhF})\text{Cl}_3(\text{CNAr}^{\text{Tripp}2})_2]$  (**10**) in  $\text{CD}_2\text{Cl}_2$ .



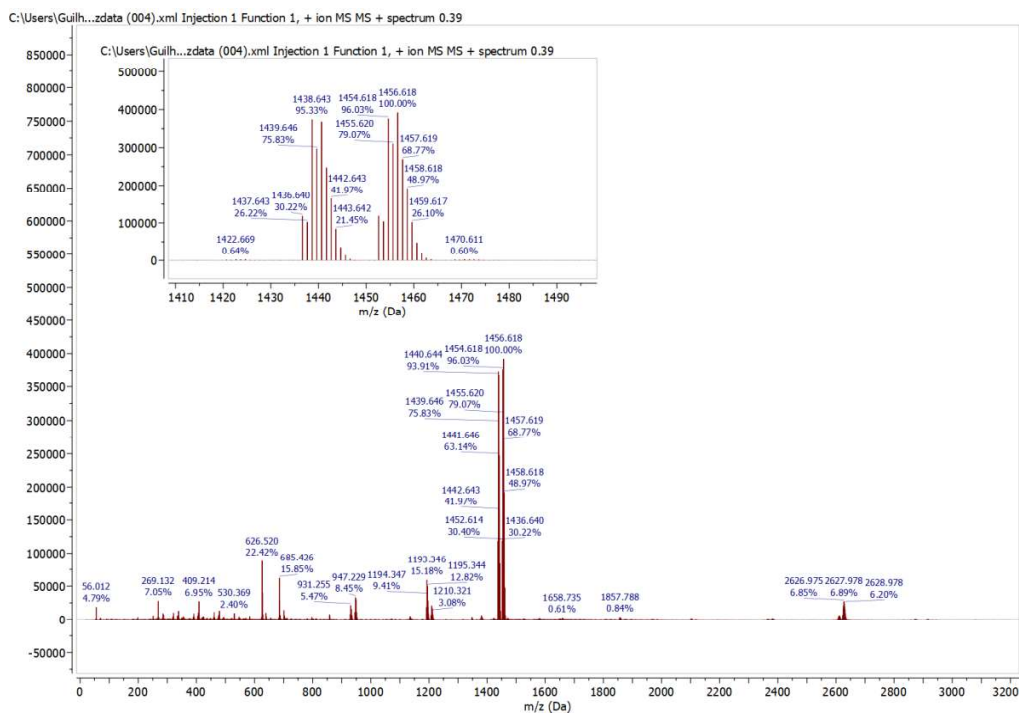


Figure S46: ESI+ mass spectrum of  $[\text{Re}(\text{NPhF})\text{Cl}_3(\text{CNAr}^{\text{Tripp2}})_2]$  (**10**) in MeCN.

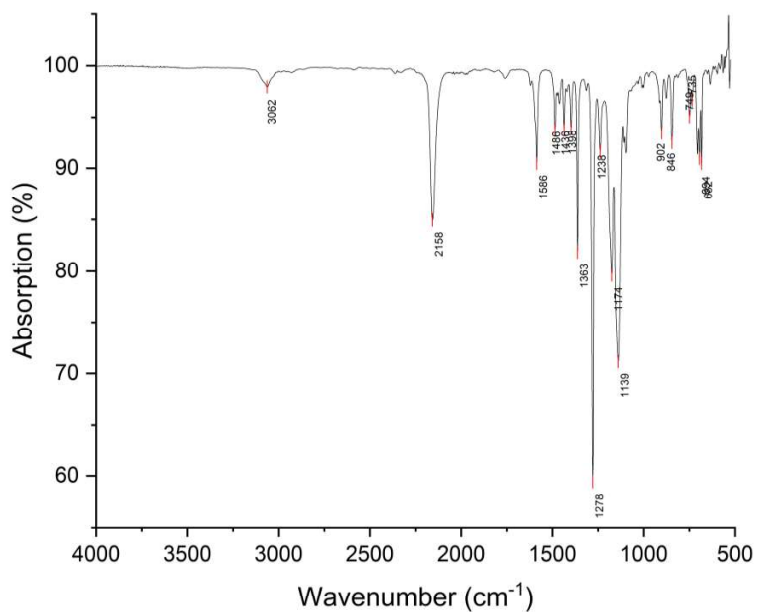
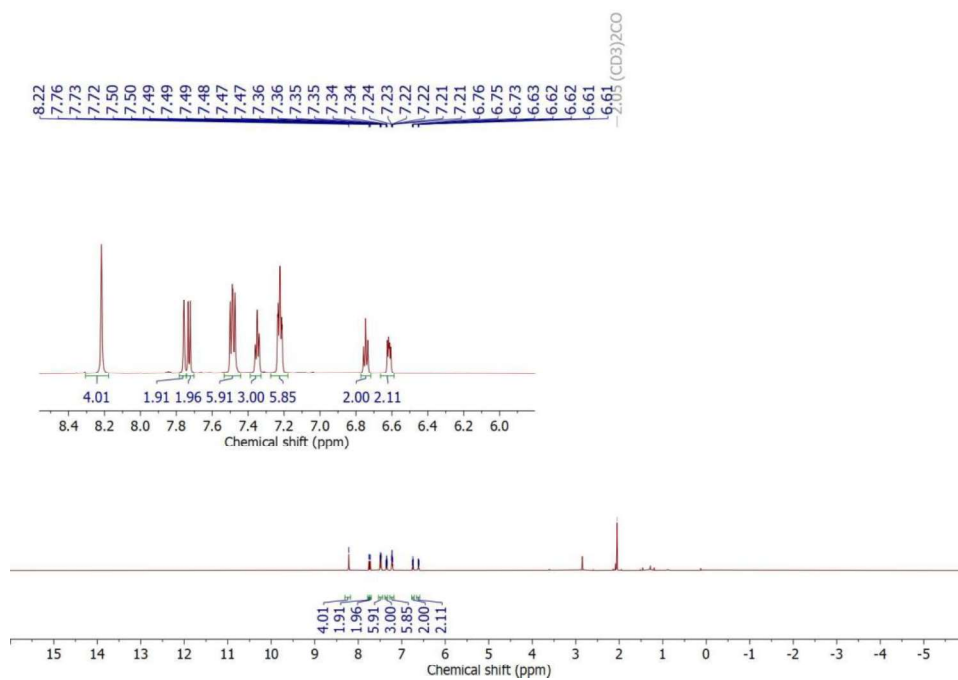
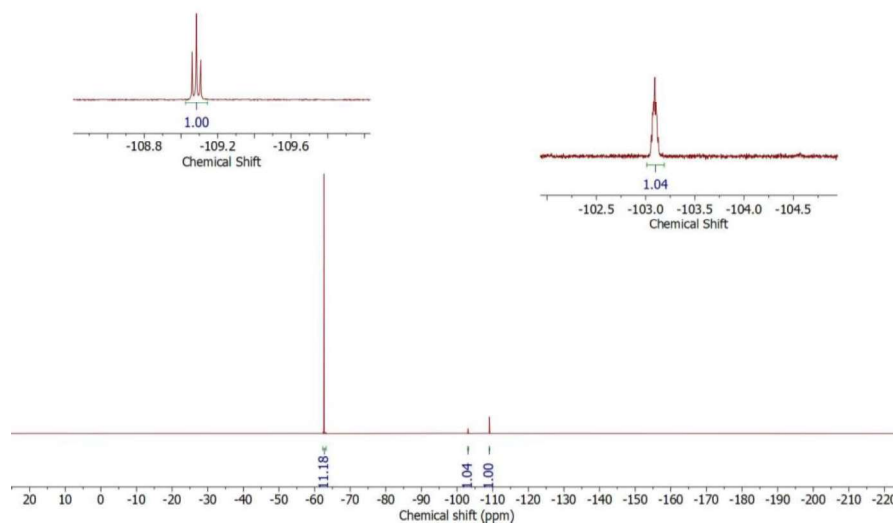


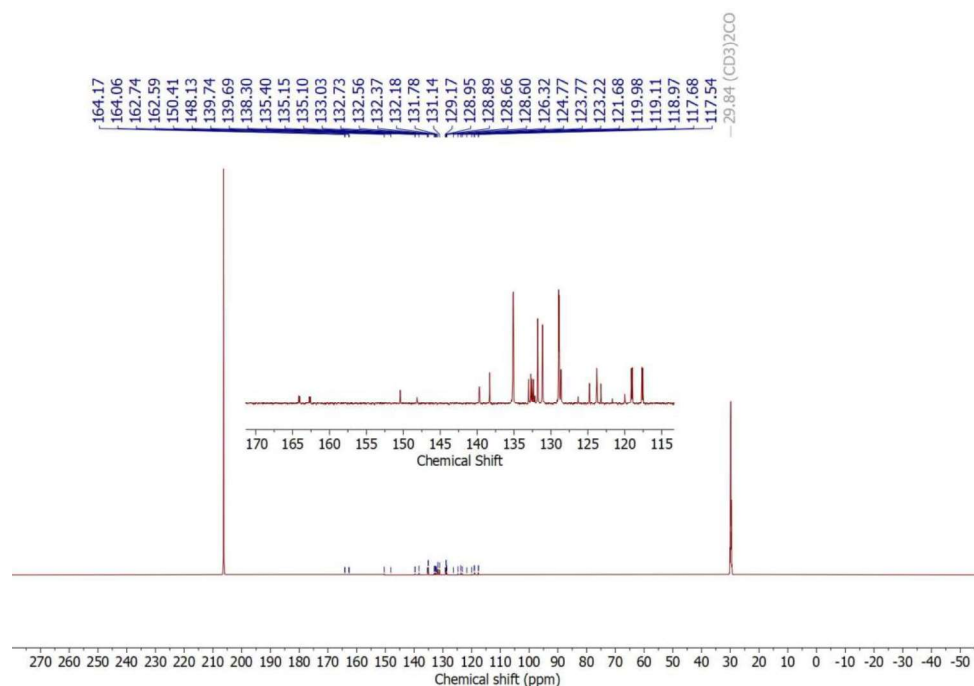
Figure S47: IR (ATR) spectrum of  $[\text{Re}(\text{NPhF})\text{Cl}_3(\text{PPh}_3)(\text{CNp-FAR}^{\text{DarF2}})]$  (**11**).



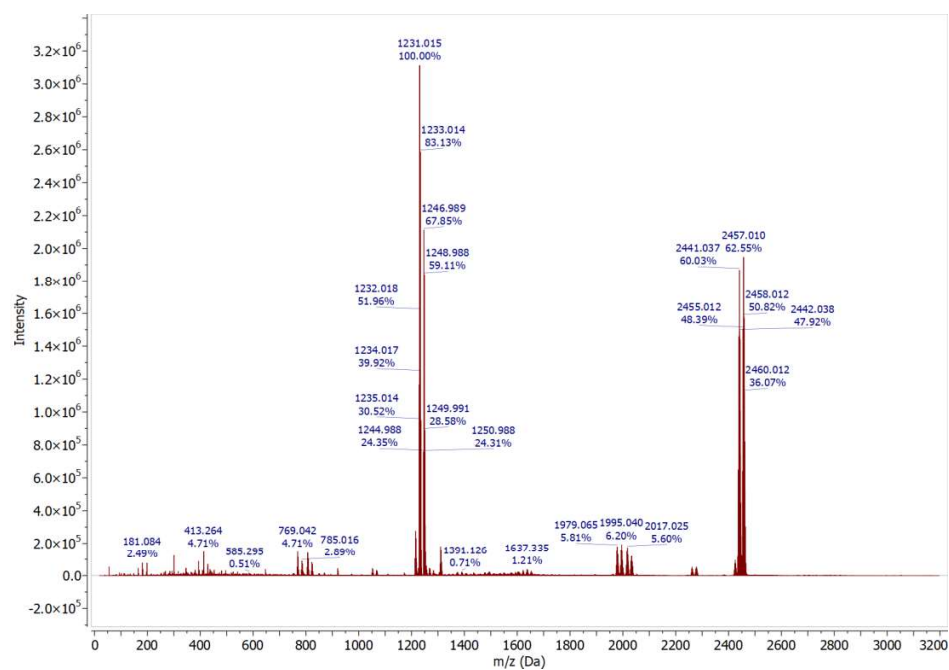
**Figure S48:** <sup>1</sup>H NMR spectrum of [Re(NPhF)Cl<sub>3</sub>(PPh<sub>3</sub>)(CNp-Far<sup>DarF2</sup>)] (11) in acetone-d<sub>6</sub>.



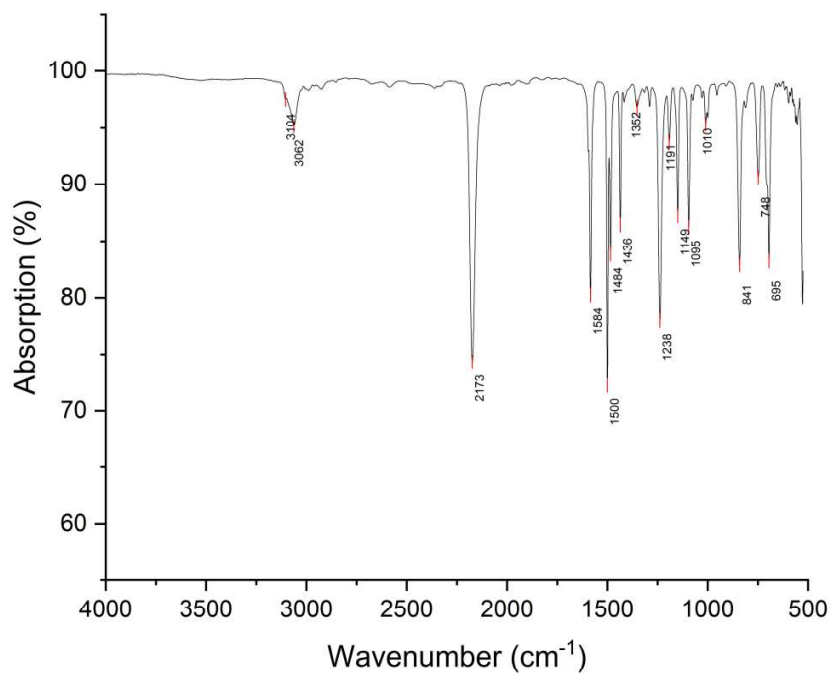
**Figure S49:** <sup>19</sup>F NMR spectrum of [Re(NPhF)Cl<sub>3</sub>(PPh<sub>3</sub>)(CNp-Far<sup>DarF2</sup>)] (11) in acetone-d<sub>6</sub>.



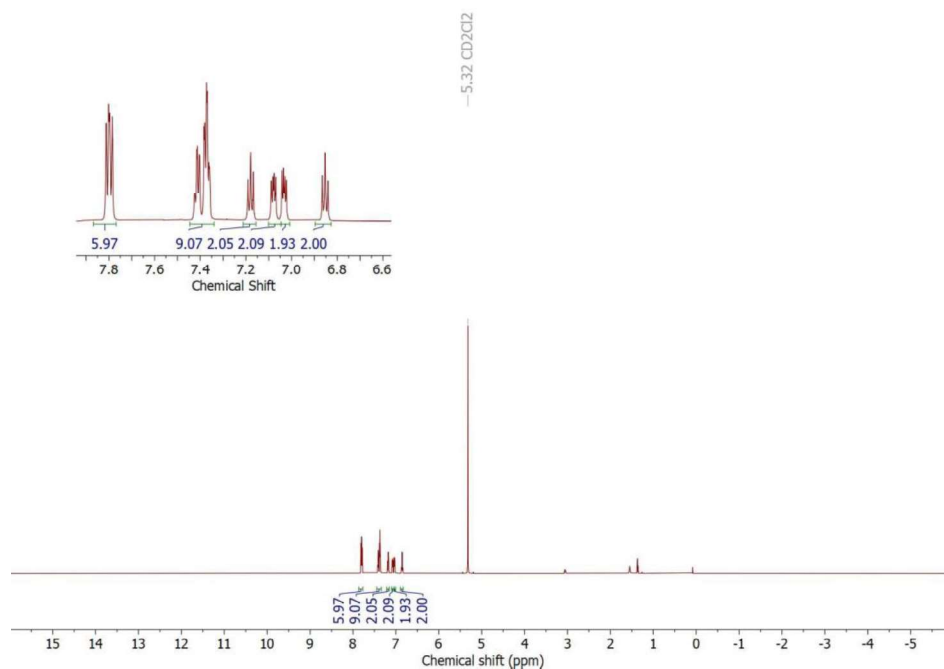
**Figure S50:**  $^{13}\text{C}\{^1\text{H}\}$  NMR spectrum of  $[\text{Re}(\text{NPhF})\text{Cl}_3(\text{PPh}_3)(\text{CNp-FAr}^{\text{DarF}_2})]$  (**11**) in acetone- $d_6$ .



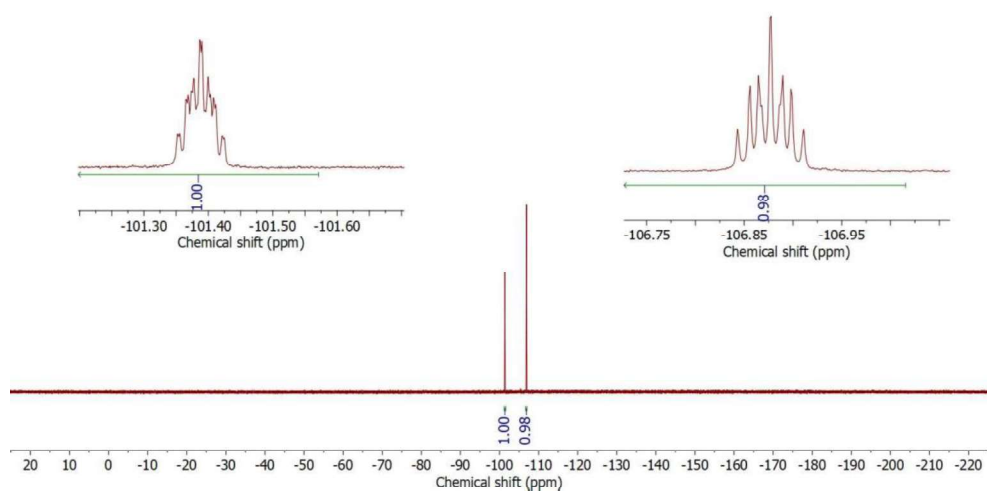
**Figure S51:** ESI+ mass spectrum of  $[\text{Re}(\text{NPhF})\text{Cl}_3(\text{PPh}_3)(\text{CNp-FAr}^{\text{DarF}_2})]$  in MeCN (**11**).



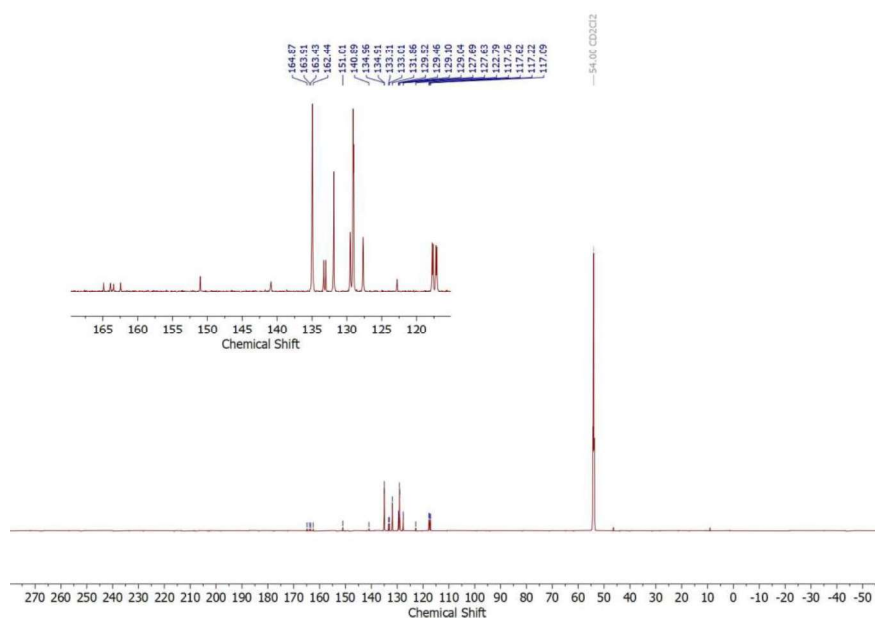
**Figure S52:** IR (ATR) spectrum of  $[\text{Re}(\text{NPhF})\text{Cl}_3(\text{PPh}_3)(\text{CNPh}^{\text{PF}})]$  (**12**).



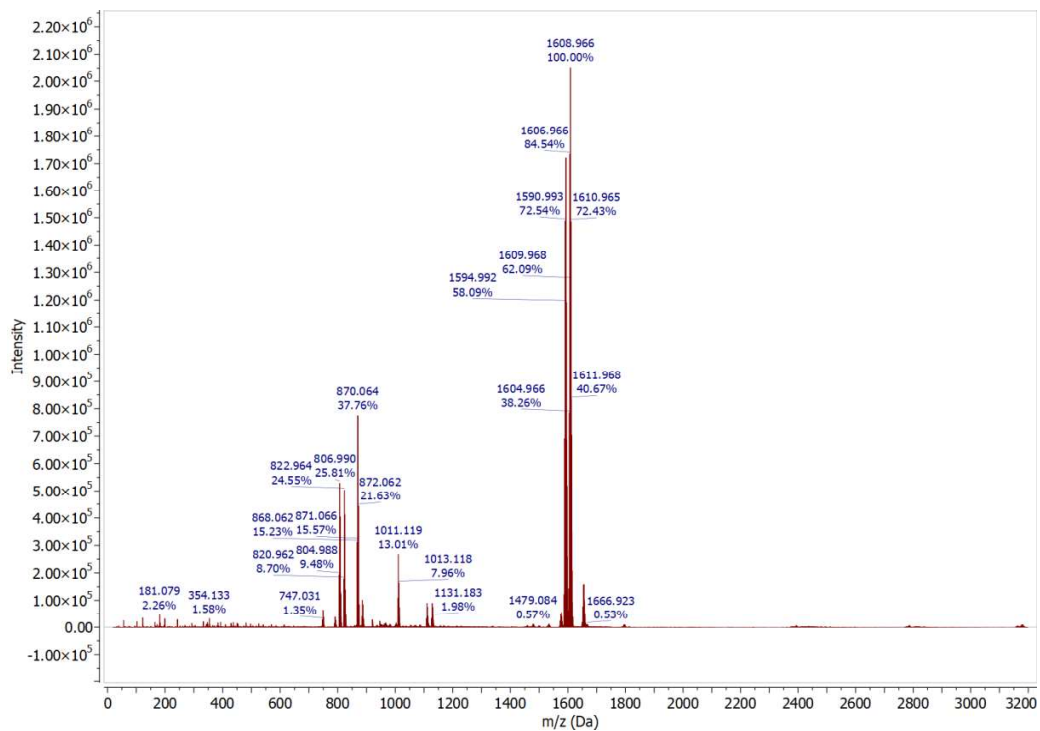
**Figure S53:**  $^1\text{H}$  NMR of  $[\text{Re}(\text{NPhF})\text{Cl}_3(\text{PPh}_3)(\text{CNPh}^{\text{PF}})]$  (**12**) in  $\text{CD}_2\text{Cl}_2$ .



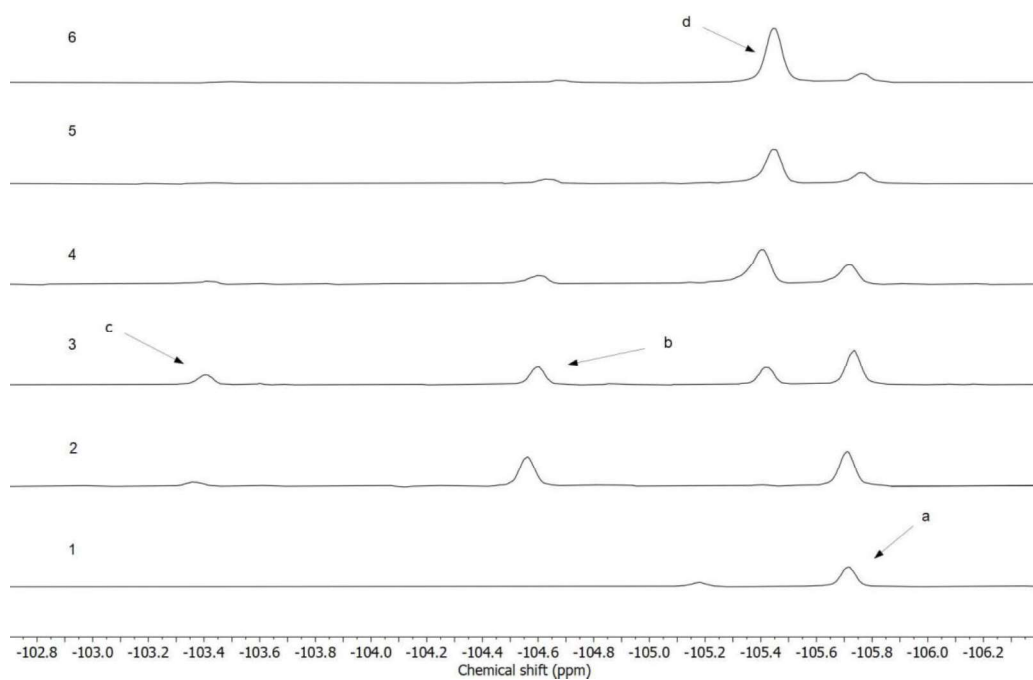
**Figure S54:**  $^{19}\text{F}$  NMR of  $[\text{Re}(\text{NPhF})\text{Cl}_3(\text{PPh}_3)(\text{CNPh}^{\text{PF}})]$  (12) in  $\text{CD}_2\text{Cl}_2$ .



**Figure S55:**  $^{13}\text{C}\{^1\text{H}\}$  NMR of  $[\text{Re}(\text{NPhF})\text{Cl}_3(\text{PPh}_3)(\text{CNPh}^{\text{PF}})]$  (12) in  $\text{CD}_2\text{Cl}_2$ .



**Figure S56:** ESI+ mass spectrum of  $[\text{Re}(\text{NPhF})\text{Cl}_3(\text{PPh}_3)(\text{CNPh}^{\text{PF}})]$  (**12**) in MeCN.



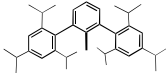
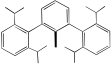
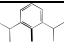
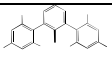
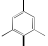
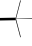
**Figure S57:**  $^{19}\text{F}$  NMR monitoring of reaction of  $[\text{Re}(\text{NPhF})\text{Cl}_3(\text{PPh}_3)_2]$  with  $\text{CNAr}^{\text{Tripp}2}$  in a boiling toluene/acetonitrile mixture (5:1). **1** was recorded after 5 minutes, **2** after 1.5 h, **3** after 3.5 h, **4** after 5 h, **5** after 10h, **6** after 13h. As no significant different was observed between **5** and **6**, the heating was not continued. (a:  $[\text{Re}(\text{NPhF})\text{Cl}_3(\text{PPh}_3)_2]$ ; b:  $[\text{Re}(\text{NPhF})\text{Cl}_3(\text{PPh}_3)(\text{CNAr}^{\text{Tripp}2})]$ ; c: minor intermediate compound, probably  $[\text{Re}(\text{NPhF})\text{Cl}_3(\text{PPh}_3)_2(\text{CNAr}^{\text{Tripp}2})]$ ; d:  $[\text{Re}(\text{NPhF})\text{Cl}_3(\text{CNAr}^{\text{Tripp}2})_2]$ ).

## Computational chemistry

As a simple descriptor for the overall donor/acceptor properties of the isocyanides, we determined the quotient from a sum parameter containing the calculated potential energy extrema and the averaged potential energy on the Van der Waals surface of the carbon donor atoms (kcal/mol), and the exposed VdW surface area ( $\text{\AA}^2$ ): the **Surface-Averaged Donor Atom Potential (SADAP)** (Equ. 1). The results for the isocyanides discussed in the present study are summarized in Table 2. The derived sum parameter corresponds to the average interaction energy of the isocyanide carbon atom with positively and negatively charged moieties over its entire accessible surface.<sup>5</sup>

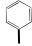

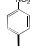
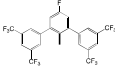
$$SADAP = \frac{EP_{min} + EP_{max} + AP}{ES_{pos} + ES_{neg}} \quad (\text{Equ. 1})$$

**Table S13.** Calculated electrostatic potential surface properties of the isocyanide carbon atom at the Van der Waals (VdW) boundary for structures optimized at the B3LYP/6-311++G\*\* level. Surface properties were evaluated at  $\rho = 0.001$  level using an electrostatic potential map basis with a grid-point spacing of 0.25. The last column contains the Surface-Averaged Donor Atom Potential  $SADAP = (EP_{min} + EP_{max} + AP)/(ES_{pos} + ES_{neg})$  as a combined descriptor of steric and electrostatic properties of the potential ligands, which allows an estimation of their reactivity.<sup>5</sup>

CN-R	Exposed VdW surface, ES ( $\text{\AA}^2$ )		Extrema for potential energies at VdW surface, EP (kcal/mol)		Average potential energies at VdW surface, AP (kcal/mol)	Surface-averaged donor atom potential SADAP, (kcal/mol $\text{\AA}^2$ )
	ES <sub>pos</sub>	ES <sub>neg</sub>	EP <sub>min</sub>	EP <sub>max</sub>	$\varnothing_{\text{overall}}$	SADAP
 CNAr <sup>TRIPP2</sup>	0.00	22.23	-38.01	-9.31	-26.65	-3.33
 CNAr <sup>Dipp2</sup>	0.00	22.13	-37.64	-8.87	-26.04	-3.28
 CNPh <sup>i-prop2</sup>	0.00	25.99	-35.47	-5.16	-21.20	-2.38
 CNAr <sup>Mes2</sup>	0.00	30.10	-39.20	-7.01	-25.11	-2.37
 CNMes	0.00	28.89	-36.79	-6.83	-21.68	-2.26
 CN <sup>t</sup> Bu	0.00	31.43	-39.63	-5.86	-22.00	-2.15

S47

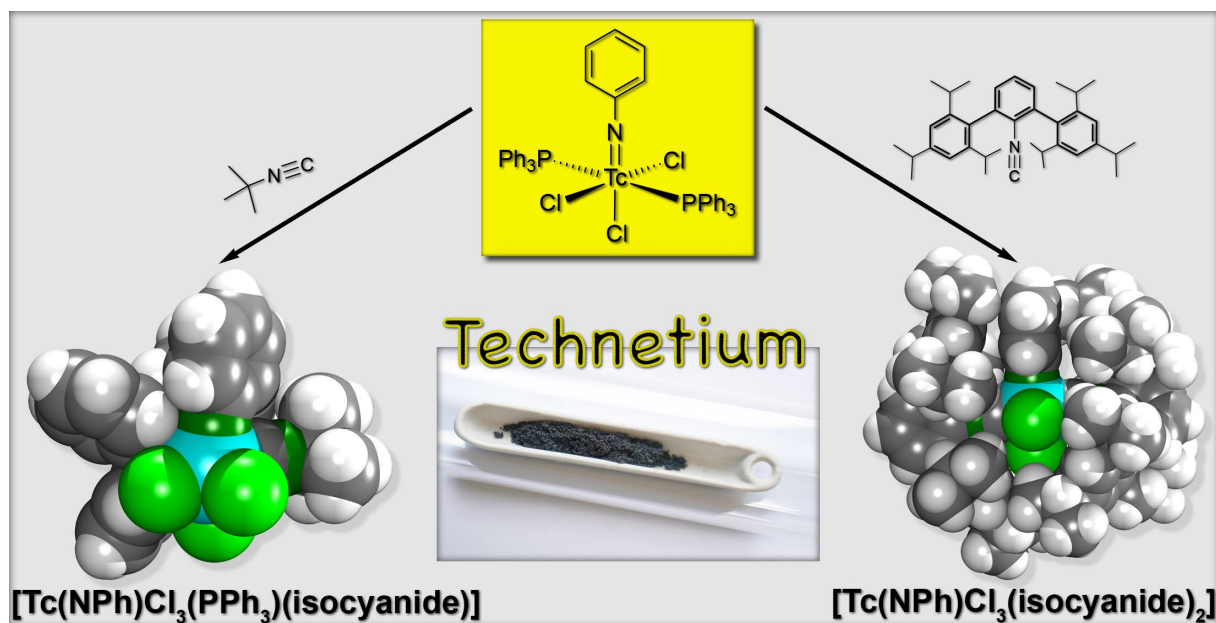


 CNPh	0.05	31.28	-35.20	1.72	-18.01	-1.64
 CNPh <sup>F</sup>	1.67	29.53	-32.02	7.05	-14.10	-1.25
 CNPh <sup>NO2</sup>	6.15	24.86	-28.59	9.44	-10.27	-0.95
 CNp-FAI <sup>DArF2</sup>	20.50	6.74	-11.49	69.07	16.88	2.73

## References

1. P. Coppens, *The Evaluation of Absorption and Extinction in Single-Crystal Structure Analysis. Crystallographic Computing*; Copenhagen, Muksgaard, **1979**.
2. G. M. Sheldrick, A short history of SHELX. *Acta Crystallogr.* 2008, **64**, 112–122.
3. G. M. Sheldrick, Crystal structure refinement with SHELXL. *Acta Crystallogr.* 2015, **71**, 3–8.
4. H. Putz, K. Brandenburg, *DIAMOND, Crystal and Molecular Structure Visualization*, Crystal Impact; Version 4.6.5; GbR: Bonn, Germany, **2021**.
5. G. Claude, J. Genz, D. Weh, M. Roca Jungfer, A. Hagenbach, M. Gembicky, J. S. Figueroa and U. Abram, *Inorg. Chem.* 2022, **61**, 16163-16176.

## 5.4. The Chemistry of Phenylimidotechnetium(V) Complexes with Isocyanides: Steric and Electronic Factors



Reproduced from Claude, G.; Zeh, L.; Roca Jungfer, M.; Hagenbach, A.; Figueroa, J. S.; Abram, U. The Chemistry of Phenylimidotechnetium(V) Complexes with Isocyanides: Steric and Electronic Factors. *Molecules* **2022**, *27*, 8546.

DOI: 10.3390/molecules27238546

© 2022 by the authors. Licensee MDPI, Basel, Switzerland.

### Author Contributions:

Guilhem Claude, Ulrich Abram and Joshua Figueroa designed the project. Guilhem Claude performed the synthesis and characterization of the compounds. Maximilian Roca Jungfer performed DFT calculations. Guilhem Claude and Adelheid Hagenbach calculated the X-ray structures. Laura Zeh performed some of the experiments during her bachelor thesis under the supervision of Guilhem Claude and Ulrich Abram. Ulrich Abram and Joshua Figueroa supervised the project, provided scientific guidance and suggestions, and wrote a draft of the manuscript.

Article

# The Chemistry of Phenylimidotechnetium(V) Complexes with Isocyanides: Steric and Electronic Factors

 Guilhem Claude <sup>1</sup>, Laura Zeh <sup>1</sup>, Maximilian Roca Jungfer <sup>1</sup>, Adelheid Hagenbach <sup>1</sup> , Joshua S. Figueroa <sup>2,\*</sup> and Ulrich Abram <sup>1,\*</sup>
<sup>1</sup> Institute of Chemistry and Biochemistry, Freie Universität Berlin, Fabeckstr. 34/36, 14195 Berlin, Germany

<sup>2</sup> Department of Chemistry and Biochemistry, University of California San Diego, La Jolla, CA 92093, USA

\* Correspondence: jsfig@ucsd.edu (J.S.F.); ulrich.abram@fu-berlin.de (U.A.)

**Abstract:** Organometallic approaches are of ongoing interest for the development of novel functional <sup>99m</sup>Tc radiopharmaceuticals, while the basic organotechnetium chemistry seems frequently to be little explored. Thus, structural and reactivity studies with the long-lived isotope <sup>99</sup>Tc are of permanent interest as the foundation for further progress in the related radiopharmaceutical research with this artificial element. Particularly the knowledge about the organometallic chemistry of high-valent technetium compounds is scarcely developed. Here, phenylimido complexes of technetium(V) with different isocyanides are introduced. They have been synthesized by ligand-exchange procedures starting from [Tc(NPh)Cl<sub>3</sub>(PPh<sub>3</sub>)<sub>2</sub>]. Different reactivity patterns and products have been obtained depending on the steric and electronic properties of the individual ligands. This involves the formation of 1:1 and 1:2 exchange products of Tc(V) with the general formulae [Tc(NPh)Cl<sub>3</sub>(PPh<sub>3</sub>)(isocyanide)], *cis*- or *trans*-[Tc(NPh)Cl<sub>3</sub>(isocyanide)<sub>2</sub>], but also the reduction in the metal and the formation of cationic technetium(I) complex of the formula [Tc(isocyanide)<sub>6</sub>]<sup>+</sup> when *p*-fluorophenyl isocyanide is used. The products have been studied by single-crystal X-ray diffraction and spectroscopic methods, including IR and multinuclear NMR spectroscopy. DFT calculations on the different isocyanides allow the prediction of their reactivity towards electron-rich and electron-deficient metal centers by means of the empirical SADAP parameter, which has been derived from the potential energy surface of the electron density on their potentially coordinating carbon atoms.

**Keywords:** technetium; phenylimides; isocyanides; ligand exchange; reactivity; DFT



**Citation:** Claude, G.; Zeh, L.; Roca Jungfer, M.; Hagenbach, A.; Figueroa, J.S.; Abram, U. The Chemistry of Phenylimidotechnetium(V) Complexes with Isocyanides: Steric and Electronic Factors. *Molecules* **2022**, *27*, 8546. <https://doi.org/10.3390/molecules27238546>

Academic Editors: Cristina Bolzati, Debora Carpanese and Laura Melendez-Alafort

Received: 28 October 2022  
Accepted: 29 November 2022  
Published: 4 December 2022

**Publisher's Note:** MDPI stays neutral with regard to jurisdictional claims in published maps and institutional affiliations.



**Copyright:** © 2022 by the authors. Licensee MDPI, Basel, Switzerland. This article is an open access article distributed under the terms and conditions of the Creative Commons Attribution (CC BY) license (<https://creativecommons.org/licenses/by/4.0/>).

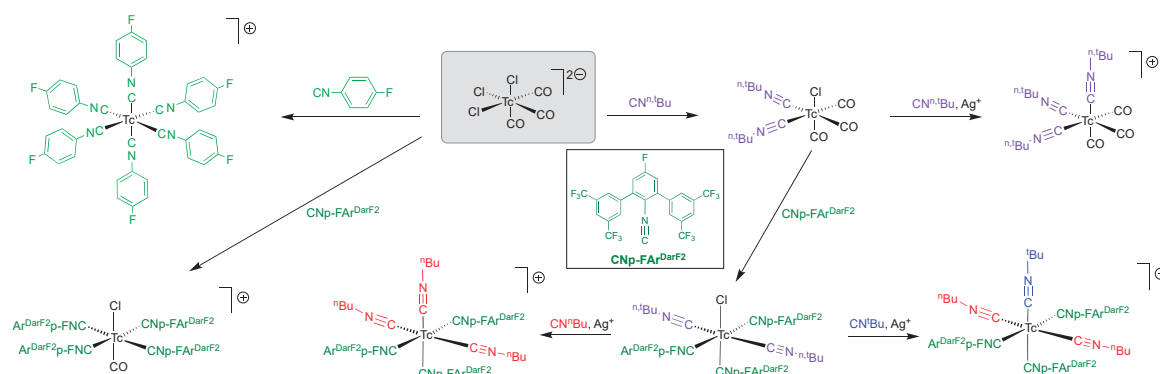
## 1. Introduction

The impressive success story of the <sup>99m</sup>Tc-Sestamibi (Cardiolite), a cationic hexakis(isocyanide) complex of technetium(I) with the ether-substituted MIBI ligand shown in Figure 1, dominates the chemistry of isocyanide complexes of technetium [1–4]. Thus, many such [Tc(CNR)<sub>6</sub>]<sup>+</sup> complexes have been isolated and tested for their biological behavior [5–7]. <sup>99m</sup>Tc is a metastable nuclear isomer, which practically emits the exclusively  $\gamma$  radiation of E <sub>$\gamma$</sub>  = 141 keV. Its short half-life of 6 h and the ready availability via a <sup>99</sup>Mo/<sup>99m</sup>Tc isotope generator make this nuclide the workhorse in diagnostic nuclear medicine, with some 40 million procedures per year. This accounts for approximately 80% of all nuclear medical procedures and 85% of diagnostic scans in nuclear medicine worldwide [8].

The concentration of the <sup>99m</sup>TcO<sub>4</sub><sup>−</sup> solutions, which are eluted from commercial <sup>99</sup>Mo/<sup>99m</sup>Tc generators, is approximately on a nanomolar level. This is a clear advantage for the medicinal use of the prepared drugs since classical toxicity problems normally play no role in such dilute solutions. On the other hand, structural and spectroscopic investigations, which are important for the development and improvement of drugs, are largely prohibited by dilution. They are commonly performed using a second isotope of technetium: the long-lived <sup>99</sup>Tc. <sup>99</sup>Tc is a weak  $\beta^-$  emitter with a low  $\beta$  energy (E <sub>$\beta$ max</sub> = 0.292 MeV) and a half-life of 2.1 × 10<sup>5</sup> years. It is available in macroscopic amounts as one of the major

products of nuclear fission and is isolated from spent nuclear fuel solutions. Its weak  $\beta$  radiation allows the handling of  $^{99}\text{Tc}$  compounds in milligram amounts in normal glassware, provided that general radiation protection protocols are applied.

Alkyl and aryl isocyanides are frequently regarded as structural and electronic surrogates for carbonyl ligands, even when a tendency is observed to act as stronger  $\sigma$ -donors and as weaker  $\pi$ -acceptors. Such a general description, however, is merely a rough approximation, and particularly the  $\pi$ -acceptor properties may be strongly influenced by the organic substituents of the ligands. Steric effects and the formal oxidation state of the metal ion will also influence the strength of the resulting metal–carbon bonds. Systematic studies about this point are rare, which is related to the fact that in many papers about the coordination chemistry of isocyanides, commercially available and stable ligands such as *tert*-butyl or cyclohexyl isocyanides are favorably used [9]. A more detailed assessment of the influence of electronic factors on the coordination behavior of highly substituted aryl isocyanides is available for a number of chromium(0) compounds, where a special role for aryl isocyanides with electron-withdrawing substituents was found [10]. Similar results were derived very recently for carbonyltechnetium(I) compounds, which react with differently substituted isocyanides in very different manners (Scheme 1) [11]. It became evident that simple alkyl isocyanides were not able to replace carbonyl ligands, while this was readily possible with aryl isocyanides which have a fluorine substituent in 4-position. Steric factors give control over the degree of the achieved ligand exchange. The influence of the substituents at the isocyanide ligands in such reactions has been reasoned with the DFT-derived electrostatic potential at the accessible surface of the corresponding isocyanide carbon atoms. The corresponding Surface-Averaged Donor Atom Potential (SADAP) parameter allowed predictions concerning the reactivity of the individual isocyanides with the regarded  $d^6$  systems in a synthetic and operationally convenient way [11]. It would now be interesting to see if the derived SADAP parameter is also suitable for electron-poor metal centers such as technetium(V) complexes, where no or almost no back-bonding to ligand orbitals should be expected.



**Scheme 1.** Reactions of carbonyltechnetium(I) complexes with differently substituted isocyanides [11].

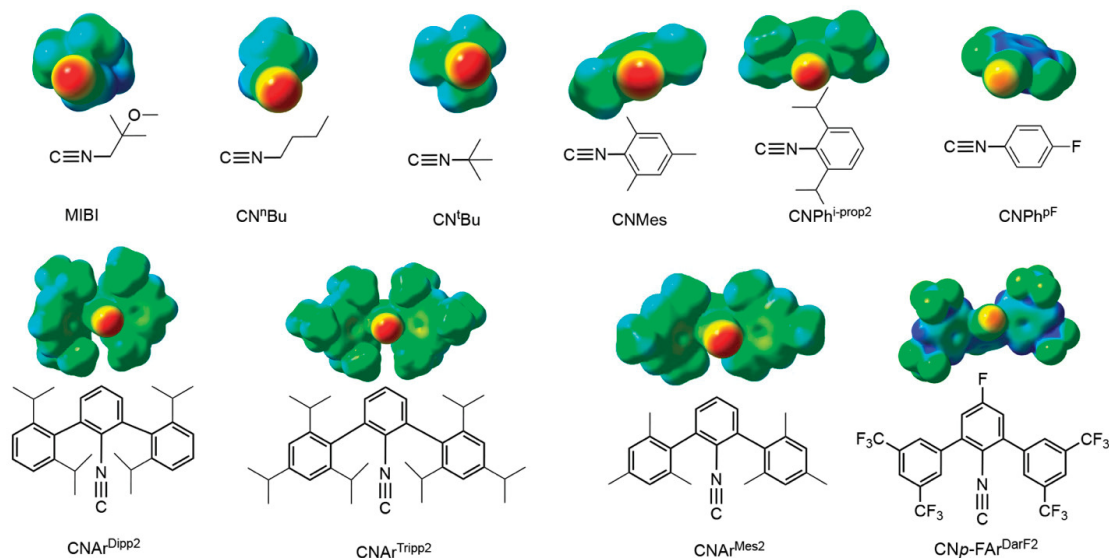
There are only a very few examples of Tc(V) isocyanide complexes. Unlike the related rhenium compounds [12–14], oxotechnetium(V) complexes are readily reduced by isocyanides, and corresponding complexes could not (yet) be isolated. Thus, there exist only two nitridotechnetium(V) and phenylimidotechnetium(V) complexes with sterically encumbered terphenyl isocyanides [15]. Particularly the phenylimido compounds are interesting for a comparative study since the “NPh<sup>2-</sup>” ligand is isoelectronic to “O<sup>2-</sup>” but not prone to reduction. This may allow a comparison of the reaction behavior of different isocyanides with the  $[\text{Tc}(\text{NPh})]^{2-}$  core, but also between technetium and rhenium, given that comparable rhenium complexes can also be synthesized. For both metals, there exist

corresponding  $[M(NPh)Cl_3(PPh_3)_2]$  complexes as potential starting materials [16,17], and ligand-exchange procedures starting from  $[Tc(NPh)Cl_3(PPh_3)_2]$  have been used to prepare novel technetium(V) complexes with phosphines, dithiolenes, acetylacetonates, or other ligands [18–22].

## 2. Results and Discussion

### 2.1. The Ligands

The results obtained during reactions of tricarbonyltechnetium(I) complexes and other metal centers with isocyanides strongly indicate that this class of ligands should not be regarded in the same undifferentiated way as carbonyl surrogates, although a few correlations between the properties of some isocyanides and their highest occupied molecular orbitals (HOMO) and lowest unoccupied molecular orbitals (LUMO) have been discussed in the past [23–26]. It has been found that electronic as well as steric effects strongly influence their coordination capabilities [10–15,27–35]. The electronic effects can best be described by a consideration of the electrostatic potentials located at the donor carbon atoms. Such parameters are generally accepted as tools for an evaluation of the nucleophilicity (electron-richness) or electrophilicity (electron-deficiency) of atoms or fragments of molecules [36–38]. With the intention to apply such measures also for the estimation of  $\sigma$ -donor/ $\pi$ -acceptor properties of isocyanides, we modeled several isocyanides by DFT calculations at the B3LYP/6-311++G\* level. Details of the calculations are outlined in Ref. [11]. The final self-consistent field densities were used for the construction of mappings of the electrostatic potentials onto the density isosurfaces ( $MO = 0.02$ ;  $\rho = 0.004$ ). They revealed stunning substitution-dependent differences when normalized to the potential boundaries [ $e/\text{\AA}^3$ ] of the intermediate donor CNMe. The corresponding electrostatic potential maps for the isocyanides discussed in this paper are shown in Figure 1, while corresponding maps for a large number of other isocyanides are published elsewhere [11].



**Figure 1.** Isocyanides discussed in the present paper together with their electrostatic potential mapping ( $MO = 0.02$ ;  $\rho_{iso} = 0.004$ ) normalized to the potential boundaries of CNMe ( $7.478 \times 10^{-2} [e/\text{\AA}^3]$ ; blue = positive, red = negative) [11].

Electron-deficient regions on the surface of the  $C \equiv N$  carbon atom could enable improved  $\pi$ -back donation (at least when bonded to electron-rich metal ions), while electron-rich regions on the surface of the same carbon atom would be responsible for a better  $\sigma$ -donation. Steric restraints on the donor carbon atom can be partially included in such

an approach by averaging the obtained potential energies over the *accessible* surface of the potential donor atoms, which means the surface on the VdW boundary of a specific atom but not in the VdW boundary of another atom. Thus, we calculated the electrostatic and steric surface properties of the carbon atoms potentially involved in isocyanide-metal binding [38]. The sterically demanding isocyanides expectedly showed a less overall accessible surface area, while the less encumbered isocyanides had a larger overall accessible carbon surface. In a similar way, the rather electron-accepting isocyanides (partial  $\pi$ -acceptors) showed an increased positive surface area at the potential donor carbon atom compared to the rather  $\sigma$ -donor ligands, which had no positive surface exposure on their isocyanide carbon atom.

The charge distribution on the surface also plays a crucial role in the interplay between  $\pi$ -acceptance and  $\sigma$ -donation. We introduced a simple descriptor for the overall donor/acceptor properties of isocyanides using the calculated potential energies (extrema and averaged values) on the vdW surface of the  $C \equiv N$  carbon atom and the exposed VdW surface area [11]. The resulting **Surface-Averaged Donor Atom Potential (SADAP)** sum parameter ( $SADAP = \frac{EP_{min} + EP_{max} + AP}{ES_{pos} + ES_{neg}}$ ) corresponds to the averaged interaction energy of the  $C \equiv N$  carbon atom with positively and negatively charged moieties over the entire accessible surface. Table 1 contains the SADAP measures for the isocyanides discussed in the present paper, together with their components. The corresponding values of many more isocyanides are given as Supplementary Materials.

**Table 1.** Calculated electrostatic potential surface properties of the isocyanide carbon atom at the VdW boundary for structures optimized at the B3LYP/6-311++G\*\* level. Surface properties were evaluated at  $\rho = 0.001$  level using an electrostatic potential map basis with a grid-point spacing of 0.25. The last column contains the **surface-averaged donor atom potential SADAP** =  $(EP_{min} + EP_{max} + AP)/(ES_{pos} + ES_{neg})$  as a combined descriptor of steric and electrostatic properties of the potential ligands, which allows an estimation of their reactivity (ES: exposed VdW surface, EP: minimum and maximum potential energy at the VdW surface, AP: averaged potential energy at the VdW surface).

Isocyanide	Exposed VdW Surface, ES ( $\text{\AA}^2$ )		Extrema for Potential Energies at VdW Surface, EP (kcal/mol)		Average Potential Energies at VdW Surface, AP (kcal/mol)	SADAP
	ES <sub>pos</sub>	ES <sub>neg</sub>	EP <sub>min</sub>	EP <sub>max</sub>	AP <sub>overall</sub>	
CNA <sub>r</sub> <sup>Tripp2</sup>	0.00	22.23	−38.01	−9.31	−26.65	−3.33
CNA <sub>r</sub> <sup>Diipp2</sup>	0.00	22.13	−37.64	−8.87	−26.04	−3.28 <sup>1</sup>
CNPh <sup>i-prop2</sup>	0.00	25.99	−35.47	−5.16	−21.20	−2.38
CNA <sub>r</sub> <sup>Mes2</sup>	0.00	30.10	−39.20	−7.01	−25.11	−2.37
CNMes	0.00	28.89	−36.79	−6.83	−21.68	−2.26
CN <sup>i</sup> Bu	0.00	31.43	−39.63	−5.86	−22.00	−2.15 <sup>1</sup>
CN <sup>n</sup> Bu	0.00	31.58	−38.51	−5.52	−21.36	−2.07 <sup>1</sup>
MIBI	0.02	29.07	−35.96	2.30	−18.65	−1.80
CNH	0.00	31.12	−31.48	−4.62	−16.42	−1.69 <sup>1</sup>
CNPh <sup>p-F</sup>	1.67	29.53	−32.02	7.05	−14.10	−1.25 <sup>1</sup>
CNp-FAr <sup>DArF2</sup>	20.50	6.74	−11.49	69.07	16.88	2.73 <sup>1</sup>

<sup>1</sup> Value taken from Ref. [11].

For the electron-rich ( $d^6$ ) carbonyltechnetium(I) complexes shown in Scheme 1, the calculated SADAP parameters nicely correlate with the observed reactivity of the compounds (e.g., the ability of certain isocyanides to replace carbonyl ligands) [11]. Isocyanides with progressively positive overall sum parameters replace CO ligands on the low-valent metal complexes, while those with negative sum parameters are  $\sigma$ -donors with predominantly negligible back-bonding properties. Consequently, no, or only a slow exchange of carbonyl ligands is observed with the latter group of isocyanides. It should, however, be noted that particularly the  $\pi$ -acceptor behavior of the isocyanides in such complexes (expressed by the  $\nu_{C \equiv N}$  IR frequencies in the different complexes) is also significantly influenced by the nature and number of co-ligands [11,39].

In comparison, we found that the HOMO and LUMO energies (or those of the respective lone-pair at carbon and the  $\pi^*_{CN}$  orbitals), as well as the magnitude of the  $LP_C-\pi^*_{CN}$

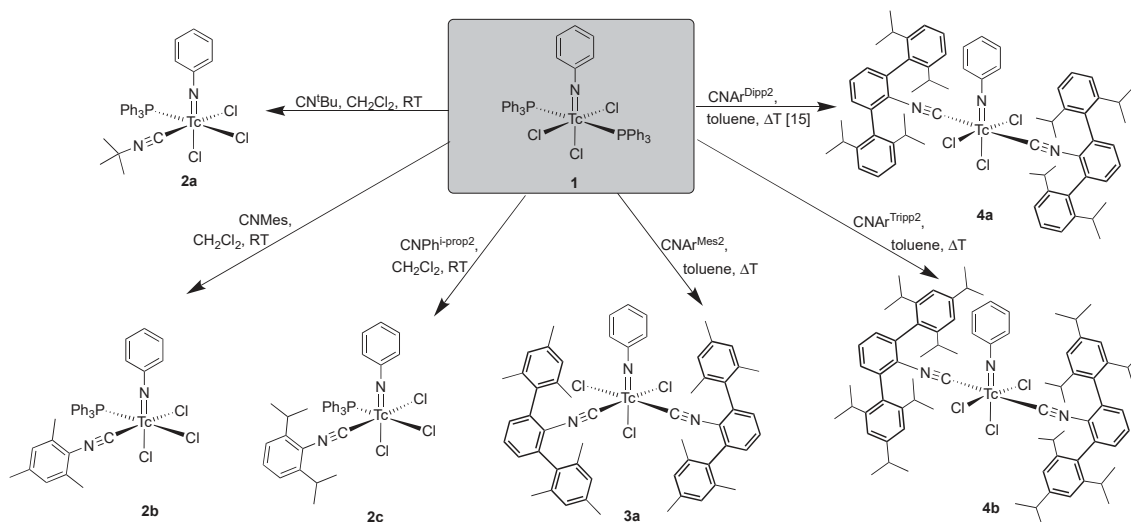
gaps in the free ligands, do not reflect the reactivity well and, therefore, suggest the molecular-orbital-derived electrostatic surface potential parameter SADAP as a better descriptor for the reactivity compared to direct molecular orbital approaches. Since the above-mentioned considerations are exclusively 'ligand-based', we also calculated the electronic properties of some model complexes of the theoretical high-valent composition  $[\text{Tc}^{\text{VII}}\text{O}_3(\text{CO}/\text{CNR})]^+$  and the low-valent composition  $[\text{Tc}^{\text{I}}(\text{CO})_5(\text{CO}/\text{CNR})]^+$  ( $\text{R} = \text{Ph}^{\text{F5}}$ ,  $\text{Ph}^{\text{p-F}}$ ,  $\text{Ph}$ ,  $^t\text{Bu}$ ,  $\text{Ar}^{\text{DArF2}}$ ) with some representative isocyanides of considerably different SADAP parameters. Expectedly, for the fully oxidized technetium(VII) compounds, only  $\sigma$ -bonds were found; however, the number of electrons shared in the bond decreased in the non-intuitive order  $\text{CO} < \text{CNPh}^{\text{F5}} < \text{CN Ph}^{\text{p-F}} < \text{CNPh} < \text{CN}^t\text{Bu} < \text{CNAr}^{\text{DArF2}}$ . In contrast, the technetium atoms in the  $[\text{Tc}^{\text{I}}(\text{CO})_5(\text{CO}/\text{CNR})]^+$  cations show pronounced  $\pi$ -back donating behavior from two Tc lone-pairs to the two  $\pi^*_{\text{CN}}$  orbitals with second-order perturbation energies between 8 and 14 kJ/mol in the order of  $\text{CO} > \text{CNPh}^{\text{F5}} > \text{CNAr}^{\text{DArF2}} > \text{CN Ph}^{\text{p-F}} > \text{CNPh} > \text{CN}^t\text{Bu}$ , while the ordering of the number of shared electrons in the  $\sigma$ -bonds is  $\text{CO} > \text{CNPh}^{\text{F5}} > \text{CN Ph}^{\text{p-F}} > \text{CNPh} > \text{CNAr}^{\text{DArF2}} > \text{CN}^t\text{Bu}$ . It should be noted that only the second-order perturbation energies somewhat reflect the reactivity predictions made by SADAP, albeit at much higher computational costs, and common convergence problems arise—especially for large ligands. The corresponding parameters for the model compounds and the HOMO/LUMO information of some representative complexes are given in the Supplementary Materials.

Having in mind the nice correlation between the SADAP measures of Table 1 and the reactivity of the corresponding isocyanides with carbonyltechnetium(I) compounds [11], it should be interesting to compare the influence of steric and electronic parameters of the isocyanide ligands on the coordination to electron-poor metal ions such as the phenylimido-technetium(V) core of the present study.

## 2.2. Reactions of $[\text{Tc}(\text{NPh})\text{Cl}_3(\text{PPh}_3)_2]$ with Alkyl and (Alkyl-Substituted) Aryl Isocyanides

$[\text{Tc}(\text{NPh})\text{Cl}_3(\text{PPh}_3)_2]$  (1) has been proven to be a suitable precursor material for the synthesis of other phenylimido complexes of technetium [18–22]. The compound is sufficiently soluble in solvents such as  $\text{CHCl}_3$  or  $\text{CH}_2\text{Cl}_2$  and is stable enough to resist prolonged heating in organic solvents. This is unlike the behavior of the rhenium analog  $[\text{Re}(\text{NPh})\text{Cl}_3(\text{PPh}_3)_2]$ , which is practically insoluble in all common organic solvents and is, thus, only partially suitable as a starting material for ligand exchange reactions [40]. The solubility of such compounds can be increased by the introduction of a fluorine atom at the imido ligand, as has been demonstrated by the synthesis of  $[\text{Re}(\text{NC}_6\text{H}_4(p\text{-F}))\text{Cl}_3(\text{PPh}_3)_2]$ , and its use as a precursor for the synthesis of corresponding complexes with  $\beta$ -diketonates [40,41]. Such an approach is not suitable for related technetium compounds since the corresponding complexes with the  $p$ -substituted  $\{=\text{NC}_6\text{H}_4(p\text{-F})\}^{2-}$  or  $\{=\text{NC}_6\text{H}_4(p\text{-CF}_3)\}^{2-}$  ligands undergo rapid hydrolysis, which is followed by a reduction in the metal and the formation of the technetium(IV) complex  $[\text{TcCl}_4(\text{PPh}_3)_2]$  [41].

Fortunately, such decompositions are not common for the unsubstituted phenylimido complex, and  $[\text{Tc}(\text{NPh})\text{Cl}_3(\text{PPh}_3)_2]$  (1) reacts readily with alkyl isocyanides (e.g.,  $\text{CN}^t\text{Bu}$ ) and small alkyl-substituted phenyl isocyanides such as  $\text{CNMe}$  or  $\text{CNPh}^{\text{i-Pr}^{\text{top2}}}$  under replacement of one triphenylphosphine ligand and the formation of complexes of type 2. The reactions proceed already at room temperature in solvents such as  $\text{CH}_2\text{Cl}_2$  or  $\text{CHCl}_3$  (Scheme 2). The use of an excess of the isocyanides or heating does not result in the formation of products with two or more of such CNR ligands but causes problems during the isolation of the products in crystalline form by the presence of excess ligand and/or its decomposition products.



**Scheme 2.** Reactions of  $[\text{Tc}(\text{NPh})\text{Cl}_3(\text{PPh}_3)_2]$  with alkyl and (alkyl-substituted) aryl isocyanides.

Interestingly, another course of the reaction is observed when  $[\text{Tc}(\text{NPh})\text{Cl}_3(\text{PPh}_3)_2]$  is treated with an excess of the sterically encumbered *m*-terphenylisocyanides  $\text{CNAr}^{\text{Mes}2}$ ,  $\text{CNAr}^{\text{Dipp}2}$ , or  $\text{CNAr}^{\text{Tripp}2}$ . In such cases, bis-complexes are formed under the replacement of both  $\text{PPh}_3$  ligands. These reactions require elevated temperatures, but we found no evidence for the formation of 1:1 ligand-exchange products under milder conditions or with the addition of only one equivalent of the terphenylisocyanides.

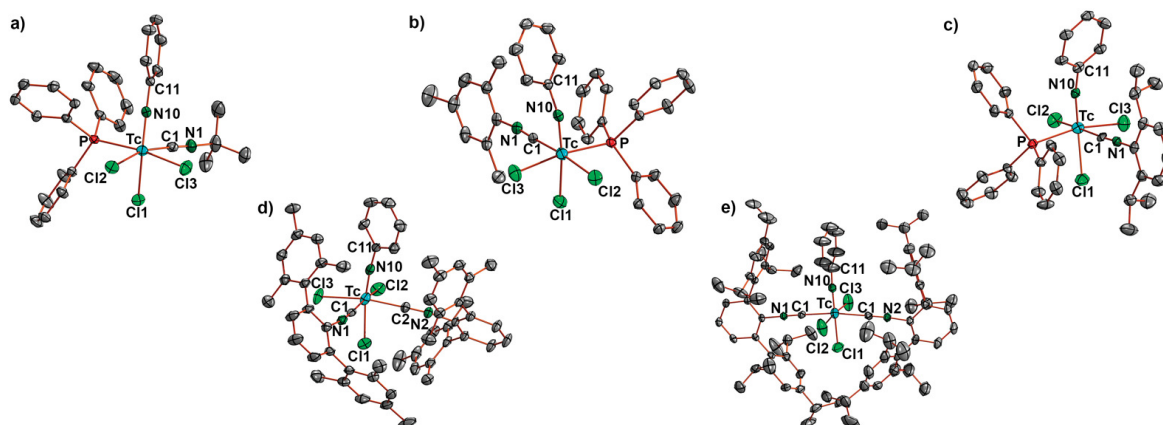
The observed difference in the reactivity goes along with the electrostatic potentials located at the carbon donor atoms of the isocyanides (Figure 1) and the clear differences found for the derived SADAP values calculated for the individual ligands ( $-3.38$  and  $-3.28$  for  $\text{CNAr}^{\text{Tripp}2}$  and  $\text{CNAr}^{\text{Dipp}2}$  and values between  $-2.28$  and  $-2.15$  for  $\text{CN}^t\text{Bu}$ ,  $\text{CNMe}$ , and  $\text{CNPh}^1\text{-prop}$ , Table 1). This means that the electron-rich isocyanides with a pronounced  $\sigma$ -donor and diminished  $\pi$ -acceptor behavior (such as  $\text{CNAr}^{\text{Tripp}2}$  and  $\text{CNAr}^{\text{Dipp}2}$ ) show a higher tendency for ligand exchange reactions at the electron-poor  $d^2$  metal centers of the technetium(V) complexes of the present study. The domination of the ' $\sigma$ -donation' comes not completely unexpected and reflects a reversed behavior compared to the carbonyltechnetium(I) complexes of Scheme 1, where the  $\pi$ -back donation from the electron-rich  $d^6$  system and the competition with the good  $\pi$ -acceptor CO plays a major role [11]. Thus, ligands with a progressively positive overall sum parameter easily and rapidly replace CO ligands, while those with negative sum parameters have predominantly  $\sigma$ -donating properties, which rule the ligand-exchange behavior with electron-deficient metal centers as in phenylimidotechnetium(V) complexes. The absence of  $\pi$ -back donation is also reflected by the  $\nu_{\text{CN}}$  IR frequencies. They appear in the Tc(V) complexes generally at higher wavenumbers than in the spectra of the uncoordinated ligands.

The  $[\text{Tc}(\text{NPh})\text{Cl}_3(\text{PPh}_3)(\text{isocyanide})]$  complexes **2** are green crystalline solids, while the bis-complexes **3a** and **4** are yellow-green. Both types of complexes are fairly soluble in  $\text{CH}_2\text{Cl}_2$  or  $\text{CHCl}_3$  and insoluble in hydrocarbons. As solids, they are indefinitely stable at ambient temperatures in the air. As  $d^2$  systems with a multiply bonded phenylimido ligand, the novel compounds are diamagnetic and give well-resolved  $^1\text{H}$  spectra (see Experimental and Supplementary Materials). Their limited solubility, however, prevents the measurement of the  $^{13}\text{C}$  NMR spectra with sufficient quality.

Single crystals of the complexes suitable for X-ray diffraction were obtained from  $\text{CH}_2\text{Cl}_2$ /hydrocarbon mixtures. Ellipsoid plots of the molecular structures are shown in Figure 2. Table 2 contains some selected bond lengths and angles. The Tc–N10 bond lengths are between  $1.692(5)$  and  $1.725(6)$  Å, which is clearly in the range of technetium–nitrogen



double bonds and agreement with the values of other phenylimido complexes of technetium [15–22,41]. The Tc-N10-C11 bonds of the mono-substituted complexes **2** are slightly bent away from the bulky PPh<sub>3</sub> ligand. A similar effect is observed for the bis-substituted *cis*-[Tc(NPh)Cl<sub>3</sub>(CNAr<sup>Mes2</sup>)<sub>2</sub>] (**3a**), in which the two bulky isocyanide ligands are coordinated in *cis* positions to each other, and a slightly bent arrangement of the {NPh}<sup>2-</sup> ligand lowers the steric stress at the central part of the molecule.



**Figure 2.** Ellipsoid representations of the molecular structures of (a) [Tc(NPh)Cl<sub>3</sub>(PPh<sub>3</sub>)(CN<sup>t</sup>Bu)] (**2a**), (b) [Tc(NPh)Cl<sub>3</sub>(PPh<sub>3</sub>)(CNMes)] (**2b**), (c) [Tc(NPh)Cl<sub>3</sub>(PPh<sub>3</sub>)(CNPh<sup>i-prop2</sup>)] (**2c**), (d) *cis*-[Tc(NPh)Cl<sub>3</sub>(CNAr<sup>Mes2</sup>)<sub>2</sub>] (**3a**) and (e) *trans*-[Tc(NPh)Cl<sub>3</sub>(CNAr<sup>Tripp2</sup>)<sub>2</sub>] (**4b**).

**Table 2.** Selected bond lengths (Å) and angles (°) for [Tc(NPh)Cl<sub>3</sub>(PPh<sub>3</sub>)(CN<sup>t</sup>Bu)] (**2a**), [Tc(NPh)Cl<sub>3</sub>(PPh<sub>3</sub>)(CNMes)] (**2b**), [Tc(NPh)Cl<sub>3</sub>(PPh<sub>3</sub>)(CNPh<sup>i-prop2</sup>)] (**2c**), *cis*-[Tc(NPh)Cl<sub>3</sub>(CNAr<sup>Mes2</sup>)<sub>2</sub>] (**3a**) and *trans*-[Tc(NPh)Cl<sub>3</sub>(CNAr<sup>Tripp2</sup>)<sub>2</sub>] (**4b**).

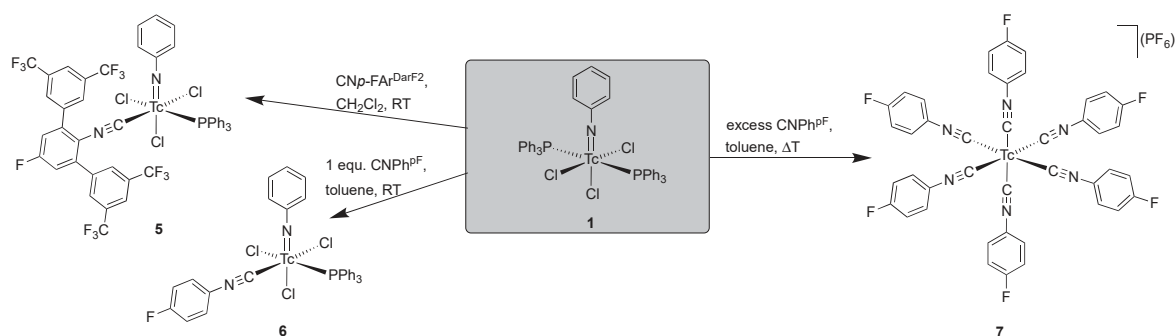
	Tc-N10	Tc-Cl1	Tc-Cl2	Tc-Cl3	Tc-C1	Tc-C2	C1-N1	C2-N2	Tc-N10-C11	N10-Tc-C11
<b>2a</b>	1.711(2)	2.4131(6)	2.3909(6)	2.4154(6)	2.057(2)		1.133(3)		163.5(2)	160.78(6)
<b>2b</b>	1.705(2)	2.3972(7)	2.4033(6)	2.4388(6)	2.037(3)		1.152(3)		164.5(2)	165.24(7)
<b>2c</b>	1.725(6)	2.413(2)	2.421(2)	2.409(2)	2.030(8)		1.18(1)		167.4(6)	165.2(2)
<b>3a</b>	1.699(3)	2.400(1)	2.391(1)	2.3877(8)	2.056(4)	2.034(3)	1.147(4)	1.160(4)	171.7(3)	166.0(1)
<b>4b</b> *	1.714(5)	2.347(2)	2.393(2)	2.395(2)	2.076(5)	2.095(5)	1.150(6)	1.139(6)	177.7(2)	176.9(6)
	1.692(5)	2.361(2)	2.399(2)	2.417(2)	2.095(5)	2.095(5)	1.138(6)	1.135(6)	178.9(2)	178.9(2)

\* Values for two independent species.

It is interesting to note that the lower steric bulk of the CNAr<sup>Mes2</sup> ligand allows the electronically favored *cis* coordination, while the CNAr<sup>Diipp2</sup> and CNAr<sup>Tripp2</sup> ligands are directed into the *trans*-conformation in compounds **4a** and **4b**. Similar findings are reported for nitridotechnetium(V) and oxidorhenium(V) complexes [14,15]. Notably, for the latter group of compounds, even the mixed-isocyanide complex [ReOCl<sub>3</sub>(CNAr<sup>Mes2</sup>)(CNAr<sup>Diipp2</sup>)]<sup>-</sup> allows *cis*-coordination for the two isocyanides. The lower steric bulk of CNAr<sup>Mes2</sup> might also allow for the more dynamic behavior of this ligand. Although we only isolated compound **3a** in its *cis* conformation, the NMR spectra of the corresponding reaction mixtures and solutions of **3** indicate a kind of fluxional behavior of this complex in solution with the formation of additional species. This can be regarded as a hint for a potential isomerization but also for the formation of mono- or tris-isocyanide complexes that cannot completely be excluded. Sterically, the latter option might also be possible since a corresponding dicarbonylmanganese(I) complex, [Mn(CO)<sub>2</sub>Br(CNAr<sup>Mes2</sup>)<sub>3</sub>] hosts three CNAr<sup>Mes2</sup> ligands in meridional positions [32].

### 2.3. Reactions of $[\text{Tc}(\text{NPh})\text{Cl}_3(\text{PPh}_3)_2]$ with Fluorine-Substituted Aryl Isocyanides

A ligand with particularly interesting properties is  $\text{CN}p\text{-FAR}^{\text{DarF2}}$ . It combines a fluorine-substituted central phenyl ring with two bulky bis(trifluoromethyl)phenyl substituents. It is extremely electron-deficient at the isocyanide carbon atom, which makes it a good  $\pi$ -acceptor, and even allows for the exchange of carbonyl ligands [11,35]. Unlike the reactions with the  $d^6$  systems in Scheme 1, these properties should be without relevance for reactions with the electron-deficient technetium(V) complexes. Additionally, during a ligand exchange reaction with  $[\text{Tc}(\text{NPh})\text{Cl}_3(\text{PPh}_3)_2]$ , only one  $\text{CN}p\text{-FAR}^{\text{DarF2}}$  ligand enters the coordination sphere of the metal, and pale green crystals of  $[\text{Tc}(\text{NPh})\text{Cl}_3(\text{PPh}_3)(\text{CN}p\text{-FAR}^{\text{DarF2}})]$  (**5**) are formed (Scheme 3).



**Scheme 3.** Reactions of  $[\text{Tc}(\text{NPh})\text{Cl}_3(\text{PPh}_3)_2]$  with  $\text{CN}p\text{-FAR}^{\text{DarF2}}$  and  $\text{CNPh}^{\text{pF}}$ .

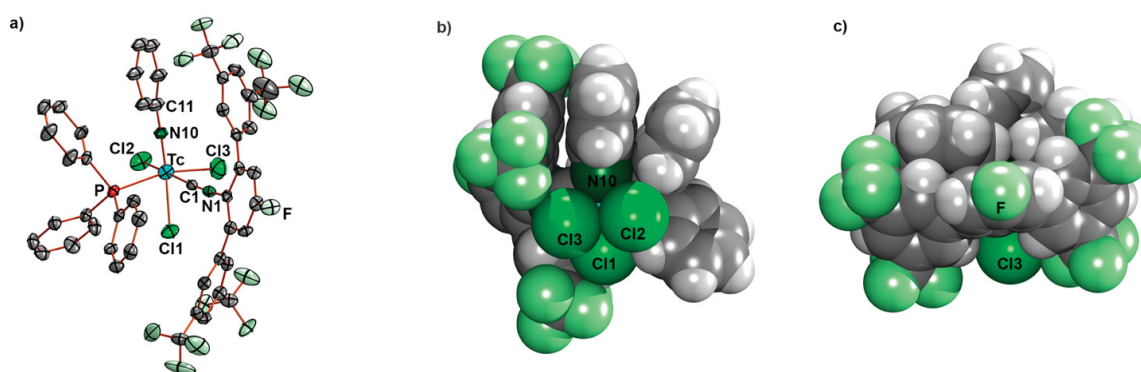
Attempted reactions with an excess of the ligand did not result in the formation of technetium complexes with more  $\text{CN}p\text{-FAR}^{\text{DarF2}}$  ligands. Since steric reasons seem to be irrelevant for this result and technetium complexes with up to four  $\text{CN}p\text{-FAR}^{\text{DarF2}}$  ligands in their coordination sphere are known [11,35], we attribute the observed reaction behavior to electronic reasons. Such an assumption is supported by the SADAP parameter of  $\text{CN}p\text{-FAR}^{\text{DarF2}}$ , which is the most positive in Table 1 and suggests a predominantly poor  $\sigma$ -donor behavior. Nevertheless, the  $\nu_{\text{CN}}$  frequency in complex **5** also appears at a higher wavenumber ( $2176\text{ cm}^{-1}$ ) than in the uncoordinated isocyanide.

Single crystals of  $[\text{Tc}(\text{NPh})\text{Cl}_3(\text{PPh}_3)(\text{CN}p\text{-FAR}^{\text{DarF2}})]$  (**5**) suitable for X-ray diffraction were obtained by slow diffusion of *n*-hexane into a solution of the complex in  $\text{CH}_2\text{Cl}_2$ . An ellipsoid representation of the molecular structure of **5** is depicted in Figure 3a, while Figure 3b,c illustrates the steric bulk caused by the *cis*-coordinated isocyanide and  $\text{PPh}_3$  ligands. The bonding situation around the technetium atom of complex **5** is expectedly very similar to those found for complexes **2a**, **2b**, and **2c** with a Tc-N10 double bond of  $1.710(4)\text{ \AA}$  and a slightly bent N10-Tc-Cl1 axis.

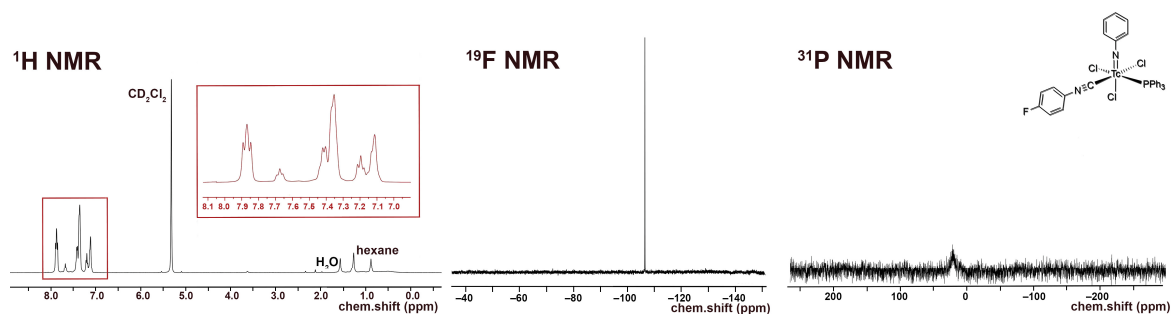
In contrast to the compounds of type **2**, solutions of  $[\text{Tc}(\text{NPh})\text{Cl}_3(\text{PPh}_3)(\text{CN}p\text{-FAR}^{\text{DarF2}})]$  (**5**) are not infinitely stable. A gradual decomposition of **5** becomes evident when solutions of the compound are heated. This can be concluded from the appearance of novel  $^{19}\text{F}$  NMR signals in such solutions (see Supplementary Materials).

Even more unstable is the ligand exchange product of  $[\text{Tc}(\text{NPh})\text{Cl}_3(\text{PPh}_3)_2]$  with  $\text{CNPh}^{\text{pF}}$ :  $[\text{Tc}(\text{NPh})\text{Cl}_3(\text{PPh}_3)(\text{CNPh}^{\text{pF}})]$  (**6**). This ligand has been chosen as a sterically unencumbered mimic for  $\text{CN}p\text{-FAR}^{\text{DarF2}}$ . The isocyanide carbon atom of  $\text{CNPh}^{\text{pF}}$  is also extremely electron deficient with only a small negative SADAP parameter of  $-1.25$  (Table 1), for which a reactivity similar to  $\text{CN}p\text{-FAR}^{\text{DarF2}}$  or alkyl or simple aryl isocyanides should be expected. Indeed, the 1:1 ligand exchange product **6** could be isolated, but the synthesis had to be performed under mild conditions, and quick precipitation of the product was required to obtain a pure compound.  $[\text{Tc}(\text{NPh})\text{Cl}_3(\text{PPh}_3)(\text{CNPh}^{\text{pF}})]$  is a pale green, microcrystalline complex that is readily soluble in  $\text{CH}_2\text{Cl}_2$ . The  $^1\text{H}$  and  $^{19}\text{F}$  NMR spectra of reasonable quality can be recorded for the pure compound from fresh solutions of the complex in this solvent (Figure 4). A well-resolved  $^{31}\text{P}$  NMR spectrum could not be obtained. Such

a behavior is not unusual for (low-symmetric) phosphine complexes of technetium and is commonly explained by scalar couplings with the large quadrupole moment of  $^{99}\text{Tc}$  ( $Q = -0.19 \text{ \AA} \times 10^{-28} \text{ m}^2$ ) [42,43]. Such couplings can cause extreme line-broadenings, which make the resolution of  $^{31}\text{P}$  signals frequently impossible [44–47], which is also observed for the complexes of type 2. An ongoing decomposition of the compound in the solution becomes evident by the detection of an increasing number of  $^{19}\text{F}$  NMR signals within one day in the solution. The infrared spectrum of complex 6 shows the  $\nu_{\text{CN}}$  band at  $2186 \text{ cm}^{-1}$ , which is at a higher wavenumber than that of the uncoordinated ligand ( $2129 \text{ cm}^{-1}$ ) and confirms the assumption that a potential  $\pi$ -acceptor behavior of  $\text{CNPh}^{\text{PF}}$  is not significant for the phenylimido complexes of technetium(V).



**Figure 3.** (a) Ellipsoid representation of the molecular structure of  $[\text{Tc}(\text{NPh})\text{Cl}_3(\text{PPh}_3)(\text{CNp}\text{-FAr}^{\text{Dar}}\text{F}_2)]$  (5) and illustration of the steric bulk caused by the isocyanide and  $\text{PPh}_3$  ligands by (b) A view along the phenylimido plane and (c) A view along the isocyanide bond. Selected bond lengths and angles: Tc-N10 1.710(4) Å, Tc-Cl1 2.434(2) Å, Tc-Cl2 2.398(2) Å, Tc-Cl3 2.389(2) Å, Tc-C1 2.009(5) Å, C1-N1 1.176(6) Å, N10-Tc-Cl1 165.5(2)°.



**Figure 4.**  $^1\text{H}$ ,  $^{19}\text{F}$  and  $^{31}\text{P}$  NMR spectra of  $[\text{Tc}(\text{NPh})\text{Cl}_3(\text{PPh}_3)(\text{CNPh}^{\text{PF}})]$  (6) in  $\text{CD}_2\text{Cl}_2$ .

A completely unexpected product was found for the reaction of  $[\text{Tc}(\text{NPh})\text{Cl}_3(\text{PPh}_3)_2]$  with an excess of  $\text{CNPh}^{\text{PF}}$  in boiling toluene. The reaction of compound 1 with  $\text{CNPh}^{\text{PF}}$  under such conditions gives the Tc(I) cation  $[\text{Tc}(\text{CNPh}^{\text{PF}})_6]^+$ . Such behavior of  $\text{CNPh}^{\text{PF}}$  has been observed before during reactions with  $(\text{NBu}_4)[\text{Tc}^{\text{I}}_2(\text{CO})_6\text{Cl}_3]$  or  $[\text{Tc}^{\text{I}}(\text{CO})_3(\text{CN}^t\text{Bu})_2\text{Cl}]$  [11]. However, in the latter cases, it could readily be explained by the activity of the fluorine-substituted ligand as a strong  $\pi$ -acceptor. In the case of the technetium(V) complexes of the present study, this does not apply. However, having in mind the inherent instability of the 1:1 exchange product  $[\text{Tc}(\text{NPh})\text{Cl}_3(\text{PPh}_3)(\text{CNPh}^{\text{PF}})]$ , we regard it as highly probable that in the course of the reaction, the technetium–nitrogen bond is cleaved, which should result in a rapid reduction in the metal to low oxidation states. Consequently, the strong  $\pi$ -acceptor  $\text{CNPh}^{\text{PF}}$  will gradually

dominate the chemistry in the system, and the formation of the stable  $[\text{Tc}(\text{CNPh}^{\text{PF}})_6]^+$  cation becomes unavoidable.

The hexakis complex can be isolated as  $\text{PF}_6^-$  salt in the form of colorless microcrystals.  $[\text{Tc}(\text{CNPh}^{\text{PF}})_6](\text{PF}_6)$  (**7**) is infinitely stable in the air. It shows a narrow ( $\nu_{1/2} = 42$  Hz)  $^{99}\text{Tc}$  NMR signal at  $-1886$  ppm, which comes close to the value of  $[\text{Tc}(\text{CNPh})_6]^+$  in  $\text{CDCl}_3$  ( $-1889$  ppm), but is appreciably de-shielded relative to the values found for hexakistechnetium(I) cations with alkyl isocyanides ( $-1914$  to  $-1964$  ppm) [45]. The infrared spectrum of **7** displays the  $\nu_{\text{CN}}$  band at  $2087\text{ cm}^{-1}$ , which corresponds to a bathochromic shift of ca.  $30\text{ cm}^{-1}$  relative to the value in uncoordinated  $\text{CNPh}^{\text{PF}}$  and indicates a marked  $\pi$ -back-donation to the isocyanide ligand in this technetium(I) complex.

### 3. Materials and Methods

Unless otherwise stated, reagent-grade starting materials were purchased from commercial sources and either used as received or purified by standard procedures. The solvents were dried and deoxygenated according to standard procedures.  $[\text{Tc}(\text{NPh})\text{Cl}_3(\text{PPh}_3)_2]$  (**1**),  $\text{CNAr}^{\text{TriPP}^2}$  and  $[\text{Tc}(\text{NPh})\text{Cl}_3(\text{CNAr}^{\text{DiPP}^2})_2]$  (**4a**) were prepared by procedures in the literature [10,15,16]. The syntheses of  $\text{CN}^p\text{-FAr}^{\text{DarF}^2}$ ,  $\text{CNPh}^{\text{PF}}$ ,  $\text{CNMe}$ s, and  $\text{CNPh}^i\text{-prop}^2$  were performed by modified procedures from the literature [9,11]. The NMR spectra were recorded with JEOL 400 MHz ECS or ECZ multinuclear spectrometers. The values given for the  $^{99}\text{Tc}$  chemical shifts are referenced to potassium pertechnetate in water. IR spectra were recorded with a Shimadzu FTIR 8300 spectrometer as KBr pellets. Intensities are classified as vs. = very strong, s = strong, m = medium, w = weak, vw = very weak, and sh = shoulder.

#### 3.1. Radiation Precautions

$^{99}\text{Tc}$  is a long-lived, weak  $\beta^-$  emitter ( $E_{\text{max}} = 0.292$  MeV). Normal glassware provides adequate protection against weak beta radiation when milligram amounts are used. Secondary X-rays (bremsstrahlung) play a significant role only when larger amounts of  $^{99}\text{Tc}$  are handled. All manipulations were performed in a laboratory approved for the handling of radioactive materials.

#### 3.2. Syntheses

The general procedure for the  $[\text{Tc}(\text{NPh})\text{Cl}_3(\text{PPh}_3)(\text{CNR})]$  Complexes **2**:  $[\text{Tc}(\text{NPh})\text{Cl}_3(\text{PPh}_3)_2]$  (**1**) (41 mg, 0.05 mmol) was dissolved in  $\text{CH}_2\text{Cl}_2$  (5 mL). The corresponding isocyanide (0.055 mmol) was added, and the solution was stirred for 10 min at room temperature. Volatiles were removed under reduced pressure, and the residue was resuspended in  $\text{Et}_2\text{O}$  (5 mL) and filtered. The obtained solid was washed with  $\text{Et}_2\text{O}$  ( $3 \times 5$  mL) and then dried under reduced pressure. Single crystals suitable for X-ray diffraction were obtained by the slow diffusion of n-hexane into solutions of the complexes in  $\text{CH}_2\text{Cl}_2$ . The obtained crystals were filtered, washed with a small amount of  $\text{Et}_2\text{O}$ , and dried under reduced pressure.

$[\text{Tc}(\text{NPh})\text{Cl}_3(\text{PPh}_3)(\text{CN}^t\text{Bu})]$  (**2a**): Green needles. Yield: 15 mg, 47%. IR ( $\text{cm}^{-1}$ ): 3057 (w), 2984 (w), 2918 (w), 2207 (s,  $\nu_{\text{C}\equiv\text{N}}$ ), 1437 (s), 1191 (m), 1092 (m), 749 (m), 695 (s), 525 (s).  $^1\text{H}$  NMR ( $\text{CD}_2\text{Cl}_2$ , ppm):  $\delta = 7.82$  (m<sub>c</sub>, 6H, *o*-H (PPh<sub>3</sub>)), 7.65 (t,  $J = 7.46$  Hz, 1H, *p*-H (arom. NPh)), 7.46 (m<sub>c</sub>, 3H, *p*-H (PPh<sub>3</sub>)), 7.39 (m<sub>c</sub>, 6H, *m*-H (PPh<sub>3</sub>)), 7.30 (d,  $J = 7.84$  Hz, 2H, *o*-H (arom. NPh)), 7.17 (t,  $J = 7.75$  Hz, 2H, *m*-H (arom. NPh)), 1.38 (s, 9H, (CH<sub>3</sub>)<sub>3</sub>).

$[\text{Tc}(\text{NPh})\text{Cl}_3(\text{PPh}_3)(\text{CNMe})]$  (**2b**): Green needles. Yield: 10 mg, 28%. IR ( $\text{cm}^{-1}$ ): 3057 (w), 2920 (w), 2187 (s,  $\nu_{\text{C}\equiv\text{N}}$ ), 1480 (w), 1435 (m), 1310 (w), 1092 (m), 747 (m), 693 (s), 523 (s).  $^1\text{H}$  NMR ( $\text{CD}_2\text{Cl}_2$ , ppm): 7.87 (m<sub>c</sub>, 6H, *o*-H (PPh<sub>3</sub>)), 7.66 (t,  $J = 7.47$  Hz, 1H, *p*-H (arom. NPh)), 7.41–7.31 (m, 11H, *m*-/*p*-H (PPh<sub>3</sub>), *o*-H (arom. NPh)), 7.18 (t,  $J = 7.77$  Hz, 2H, *m*-H (arom. NPh)), 6.87 (s, 2H, *m*-H (arom. CNMes)), 2.32 (s, 3H, *p*-CH<sub>3</sub> (CNMes)), 1.94 (s, 6H, *o*-CH<sub>3</sub> (CNMes)).

$[\text{Tc}(\text{NPh})\text{Cl}_3(\text{PPh}_3)(\text{CNPh}^i\text{-prop}^2)]$  (**2c**): Green-yellow, dichroic needles. Yield: 26 mg, 70%. IR ( $\text{cm}^{-1}$ ): 3055 (w), 2695 (m), 2922 (w), 2183 (s,  $\nu_{\text{C}\equiv\text{N}}$ ), 1572 (m), 1477 (m), 1433 (s), 980 (w),

804 (w), 746 (m), 692 (m), 525 (m).  $^1\text{H NMR}$  ( $\text{CD}_2\text{Cl}_2$ , ppm): 7.89 (m, 6H, o-H( $\text{PPh}_3$ )), 7.69 (t,  $J = 8.0$  Hz, 1H,  $p$ -H (arom. NPh)), 7.43–7.29 (m, 12H,  $m$ -/ $p$ -H ( $\text{PPh}_3$ ), H( $\text{CNPh}^{\text{i-prop}2}$ )), 7.20 (t,  $J = 8.0$  Hz, 2H,  $m$ -H (arom. NPh)), 7.14 (d,  $J = 7.7$  Hz, 2H, o-H (arom. NPh)), 2.68 (h,  $J = 6.8$  Hz, i-prop CH), 0.97 (d,  $J = 7.0$  Hz, i-prop  $\text{CH}_3$ ), 0.89 (d,  $J = 7.0$  Hz, i-prop  $\text{CH}_3$ ).

Subsequently, *cis*-[Tc(NPh)Cl<sub>3</sub>(CNAr<sup>Mes2</sup>)<sub>2</sub>] (**3a**): [Tc(NPh)Cl<sub>3</sub>(PPh<sub>3</sub>)] (**1**) (82 mg, 0.1 mmol) was suspended in toluene (5 mL). CNAr<sup>Mes2</sup> (68 mg, 0.2 mmol) was added, and the reaction mixture was heated under reflux for one hour. It became dark green and homogenous upon heating. The resultant solution was slowly evaporated at 5 °C. After one day, the first crop of a few yellow-green needles (compound **3a**) suitable for X-ray diffraction were obtained and analyzed by IR spectroscopy. Upon further evaporation of the solvent, more of the aforementioned needles was obtained along with other green crystals of different shapes, which were not suitable for X-ray diffraction. They were filtered off and washed with small amounts of n-pentane and studied by  $^1\text{H NMR}$  spectroscopy. Three sets of resonances were observed in the methyl region, suggesting the presence of at least three isomers which could be *cis*/*trans*-[Tc(NPh)Cl<sub>3</sub>(CNAr<sup>Mes2</sup>)<sub>2</sub>] or *cis*/*trans*-[Tc(NPh)Cl<sub>3</sub>(PPh<sub>3</sub>)(CNAr<sup>Mes2</sup>)]. **3a**: Yellow-green needles. IR ( $\text{cm}^{-1}$ ): 3058 (w), 2919 (m), 2851 (w), 2178 (s,  $\nu_{\text{C}\equiv\text{N}}$ ), 1572 (m), 1433 (m), 1308 (w), 1094 (w), 845 (w), 749 (w), 695 (m), 521 (m). The isomeric mixture was of [Tc(NPh)Cl<sub>3</sub>(CNAr<sup>Mes2</sup>)<sub>2</sub>] and [Tc(NPh)Cl<sub>3</sub>(PPh<sub>3</sub>)(CNAr<sup>Mes2</sup>)]: IR ( $\text{cm}^{-1}$ ): 3058 (w), 2919 (m), 2851 (w), 2178 (s,  $\nu_{\text{C}\equiv\text{N}}$ ), 1572 (m), 1433 (m), 1308 (w), 1094 (w), 845 (w), 749 (w), 695 (m), 521 (m).  $^1\text{H NMR}$  ( $\text{CD}_2\text{Cl}_2$ , ppm): 7.78–6.58 (m, aryl), 2.20 (s,  $\text{CH}_3$ ), 2.11 (s,  $\text{CH}_3$ ), 2.05 (s,  $\text{CH}_3$ ), 2.02 (s,  $\text{CH}_3$ ), 1.96 (s,  $\text{CH}_3$ ), 1.94 (s,  $\text{CH}_3$ ).

*trans*-[Tc(NPh)Cl<sub>3</sub>(CNAr<sup>Tripp2</sup>)<sub>2</sub>] (**4b**): [Tc(NPh)Cl<sub>3</sub>(PPh<sub>3</sub>)] (**1**) (41 mg, 0.05 mmol) was suspended in toluene (5 mL). CNAr<sup>Tripp2</sup> (51 mg, 0.1 mmol) was added, and the reaction mixture was heated under reflux for one hour. It became slightly red and homogenous upon heating. The resultant solution was slowly evaporated at 5 °C. After five days, green-yellow crystals suitable for X-ray diffraction were obtained. They were filtered off and washed with small amounts of cold MeOH and n-pentane, and then dried under a reduced pressure. Yield: 39 mg, 72%. IR ( $\text{cm}^{-1}$ ): 3057 (w), 2957 (s), 2866 (s), 2184 (s,  $\nu_{\text{C}\equiv\text{N}}$ ), 1607 (m), 1576 (m), 1570 (m), 1461 (s), 1439 (s), 1362 (s), 1316 (m), 1191 (m), 1121 (m), 1071 (w), 943 (w), 874 (s), 807 (m), 722 (m), 697 (s), 543 (s).  $^1\text{H NMR}$  ( $\text{CD}_2\text{Cl}_2$ , ppm): 7.73 (t,  $J = 7.33$  Hz, 1H,  $p$ -H (arom. NPh)), 7.50 (t,  $J = 6.8$  Hz, 2H, CNAr<sup>Tripp2</sup>), 7.41 (d,  $J = 7.46$  Hz, 2H, o-H (arom. NPh)), 7.26 (d,  $J = 7.46$  Hz, 4H, CNAr<sup>Tripp2</sup>), 7.14 (t,  $J = 6.68$  Hz, 2H,  $m$ -H (arom. NPh)), 6.92 (s, 8H, CNAr<sup>Tripp2</sup>), 2.83 (h,  $J = 6.1$  Hz, 4H, (i-prop CH)), 2.38 (h,  $J = 6.3$  Hz, 8H, (i-prop CH)), 1.32 (d,  $J = 6.52$  Hz, 24H, (i-prop  $\text{CH}_3$ )), 1.01 (d,  $J = 6.0$  Hz, 24H, (i-prop  $\text{CH}_3$ )), 0.96 (d,  $J = 6.0$  Hz, 24H, (i-prop  $\text{CH}_3$ )).

[Tc(NPh)Cl<sub>3</sub>(PPh<sub>3</sub>)(CNp-FAr<sup>DarF2</sup>)] (**5**): [Tc(NPh)Cl<sub>3</sub>(PPh<sub>3</sub>)<sub>2</sub>] (**1**) (41 mg, 0.05 mmol) was dissolved in  $\text{CH}_2\text{Cl}_2$  (5 mL). CNp-FAr<sup>DarF2</sup> (30 mg, 0.055 mmol) was added, and the dark green solution was stirred for 20 min at room temperature. A pale green solid was precipitated by the addition of an excess of n-hexane (approximately 30 mL). The immediately formed precipitate was washed with pentane and a small amount of diethyl ether, redissolved in  $\text{CH}_2\text{Cl}_2$  (1 mL), and overlaid with n-hexane. Pale green columns were formed together with brown oil. The crystals were separated and washed with pentane alongside a small amount of diethyl ether, and the crystallization procedure was repeated in the described way. The resultant single crystals were suitable for X-ray diffraction. Pale green needles. Yield: 22 mg, 40%. IR ( $\text{cm}^{-1}$ ): 3057 (w), 2176 (vs,  $\nu_{\text{C}\equiv\text{N}}$ ), 1482 (w), 1435 (m), 1364 (m), 1279 (s), 1179 (s), 1135 (s), 1092 (m), 905 (w), 743 (m), 701 (m), 693 (m) 520 (m).  $^1\text{H NMR}$  ( $\text{CD}_2\text{Cl}_2$ , ppm): 7.90 (s, 4H, CNp-FAr<sup>DarF2</sup>), 7.61 (s, 2H, CNp-FAr<sup>DarF2</sup>), 7.55 (t,  $J = 7.1$  Hz, 1H,  $p$ -H (arom. NPh)), 7.46 (t,  $J = 8.4$  Hz, 6H, o-H ( $\text{PPh}_3$ )), 7.31 (t,  $J = 6.9$  Hz, 3H,  $p$ -H ( $\text{PPh}_3$ )), 7.25 (d,  $J = 7.7$  Hz, 2H,  $m$ -H (CNp-FAr<sup>DarF2</sup>)), 7.16 (t,  $J = 6.0$  Hz, 6H,  $m$ -H ( $\text{PPh}_3$ )), 6.89 (t,  $J = 7.2$  Hz, 2H,  $m$ -H (arom. NPh)), 6.71 (d,  $J = 6.9$  Hz, 2H, o-H (arom. NPh)).  $^{19}\text{F NMR}$  ( $\text{CD}_2\text{Cl}_2$ , ppm): -65.0 (s, 12F,  $m,m'$ -CF<sub>3</sub> (CNp-FAr<sup>DarF2</sup>)), -107.9 (s, 1F,  $p$ -F (CNp-FAr<sup>DarF2</sup>)).

$[Tc(NPh)Cl_3(PPh_3)(CNPh^F)]$  (6): 100  $\mu$ L of a solution prepared from  $CNPh^F$  (160  $\mu$ L) and toluene (940  $\mu$ L) was added to a suspension of  $[Tc(NPh)Cl_3(PPh_3)_2]$  (1) (41 mg, 0.05 mmol) in  $CH_2Cl_2$  (5 mL). The mixture was gently heated and held at a temperature of 30 °C until the reaction mixture became homogenous (approximately 2 min). Then, *n*-hexane (20 mL) was immediately added, which resulted in the formation of a pale green precipitate. The obtained solid (pure compound 6 with some incorporated *n*-hexane) was filtered off, washed with diethyl ether alongside *n*-hexane, and then dried under reduced pressure. Complex 6 is stable as a solid but decomposes at room temperature in solvents such as dichloromethane or acetone. Yield: 20 mg, 57%. IR ( $cm^{-1}$ ): 3422 (br), 3058 (w), 2923 (w), 2186 (vs,  $\nu_{C\equiv N}$ ), 1570 (w), 1499 (s), 1435 (m), 1239 (w), 1092 (m), 990 (w), 841 (m), 749 (m), 697 (s), 521 (s).  $^1H$  NMR ( $CD_2Cl_2$ , ppm): 7.80 (m, 6H, o-H( $PPh_3$ )), 7.68 (t,  $J = 8.0$  Hz, 1H, *p*-H (arom. NPh)), 7.46–7.31 (m, 11H), 7.20 (t,  $J = 8.0$  Hz, 2H, *m*-H (arom.)), 7.17–7.07 (m, 4H), 1.27 ( $CH_2$ , 0.2 *n*-hexane), 0.88 ( $CH_3$ , 0.2 *n*-hexane).  $^{19}F$  NMR ( $CD_2Cl_2$ , ppm):  $-106.5$ .

$[Tc(CNPh^F)_6](PF_6)$  (7):  $[Tc(NPh)Cl_3(PPh_3)_2]$  (1) (41 mg, 0.05 mmol) was suspended in toluene (5 mL).  $CNPh^F$  (45.9  $\mu$ L, 0.5 mmol) was added, and the solution was heated under reflux for one hour. The reaction mixture became homogeneous upon heating and changed its color to pale yellow within the first ten minutes. Then, a solid started to precipitate. The reaction mixture was cooled to room temperature and filtered. The obtained solid was washed with a small amount of toluene and redissolved in MeOH.  $NH_4(PF_6)$  (0.5 g) was dissolved in a water/MeOH mixture (5 mL, 1:1) which was added. A colorless solid precipitated, which was filtered off and washed sequentially with water, MeOH, and  $Et_2O$ . Yield: 12 mg, 26%. IR ( $cm^{-1}$ ): 2918 (w), 2087 (s,  $\nu_{C\equiv N}$ ), 1501 (m), 1235 (m), 1154 (m), 836 (m), 558 (w).  $^1H$  NMR ( $CD_2Cl_2$ , ppm): 7.46 (m, 12H, o-H ( $CNPh^F$ )), 7.16 (t,  $J = 8.5$  Hz, 12H, *m*-H ( $CNPh^F$ )).  $^{19}F$  NMR ( $CD_2Cl_2$ , ppm):  $-73.4$  (d,  $^1J(^{19}F-^{31}P) = 670$  Hz, 6F,  $PF_6$ ),  $-109.2$  (s, 6F, ( $CNPh^F$ )).  $^{99}Tc$  NMR ( $CD_2Cl_2$ , ppm):  $-1886$  (s,  $\nu_{1/2} = 42$  Hz).

### 3.3. X-ray Crystallography

The intensities for the X-ray determinations were collected on the STOE IPDS II instrument with Mo  $K\alpha$  radiation. The space groups were determined by the detection of systematic absences. Absorption corrections were carried out by multi-scan or integration methods [48]. The structure solution and refinement were performed with the SHELX program package [49,50]. Hydrogen atoms were derived from the final Fourier maps and were refined or placed at calculated positions and treated with the ‘riding model’ option of SHELXL.

Compound 2c crystallizes in the non-centrosymmetric space group  $Pca2_1$ . The absolute structure has been determined with a Flack parameter of 0.06(6). Compound 3 co-crystallizes with  $CH_2Cl_2$  molecules in the large voids between the complex molecules. One molecule of dichloromethane could be located and refined. A sum of 102 e, which corresponds to another 2.5 molecules of  $CH_2Cl_2$ , has been ‘removed’ from the final Fourier map by means of a solvent mask of OLEX2 [51]. The positional disorder of isopropyl or  $CF_3$  groups has been addressed during the refinement of the crystal structures of compounds 4b and 5. Details can be inspected in the Supplementary Materials and/or the corresponding cif files.

The representation of molecular structures was conducted using the program DIAMOND 4.2.2 [52].

### 3.4. Computational Details

DFT calculations were performed on the high-performance computing systems of the Freie Universität Berlin ZEDAT (Curta) using the program package GAUSSIAN 16 [53,54]. The gas phase geometry optimizations were performed using initial coordinates generated using GAUSSVIEW and Avogadro [55,56]. The calculations were performed with the hybrid density functional B3LYP [57–59]. The Stuttgart relativistic small core basis set with its associated pseudo potential has been used for Tc [60,61]. The 6-311++G\*\* basis set was used to model all other elements [62–66]. All basis functions, as well as the

ECPs, were obtained from the EMSL database [67]. The surface properties module of the multifunctional wave-function analyzer MultiWFN was used for the calculation of the surface properties [38,68].

#### 4. Conclusions

Using the Tc-phenylimido core, high-oxidation state isocyanide complexes of technetium(V) can be prepared and isolated as stable molecular species.  $[\text{Tc}(\text{NPh})\text{Cl}_3(\text{PPh}_3)_2]$  has been proven to be a suitable starting material for such reactions. One or both of the  $\text{PPh}_3$  ligands can be replaced by isocyanides depending on the electronic properties and the steric bulk of the incoming ligands. A DFT-based sum parameter (SADAP) describing the electrostatic potential at the isocyanide carbon atom is a good measure to predict the reactivity of isocyanides with metal ions. In contrast to low-valent technetium complexes, where electron-deficient isocyanides (less negative or positive SADAP parameters) show the highest exchange rates, reactions with electron-rich isocyanides such as  $\text{CNAr}^{\text{Mes}_2}$  or  $\text{CNAr}^{\text{Tripp}_2}$  (ligands with very negative SADAP parameters) form bis-complexes with the  $d^2$  systems under study. On the contrary, ligands with a lower electron density located at the isocyanide carbon atoms prefer the formation of 1:1 complexes. Such a behavior correlates with the  $\sigma$ -donor and  $\pi$ -acceptor properties of the ligands in the formed complexes in a way that for the complex formation with the electron-poor  $\{\text{Tc}^{\text{V}}(\text{NPh})\}^{3-}$  core, the  $\sigma$ -donor abilities of the ligands clearly dominate. This is also reflected by the positions of the  $\nu_{\text{CN}}$  bands in the IR spectra of the complexes (Table 3). They are all found at higher wavenumbers relative to the spectra of the uncoordinated ligands.

**Table 3.**  $\nu_{\text{CN}}$  Frequencies in the complexes under study compared with the values in the uncoordinated ligands.

	2a ( $\text{CN}^t\text{Bu}$ )	2b ( $\text{CNMes}$ )	2c ( $\text{CNPh}^i\text{-prop}^2$ )	3a ( $\text{CNAr}^{\text{Mes}_2}$ )	4a* ( $\text{CNAr}^{\text{Dipp}_2}$ )	4b ( $\text{CNAr}^{\text{Tripp}_2}$ )	5 ( $\text{CN}^p\text{-FAr}^{\text{DarF}_2}$ )	6 ( $\text{CNPh}^{\text{PF}}$ )	7 ( $\text{CNPh}^{\text{PF}}$ )
	2207	2187	2183	2177	2187	2184	2176	2186	2087
Ligand	2135	2114	2113	2120	2124	2114	2119	2129	2129

\* Values taken from Ref. [15].

A considerable  $\pi$ -acceptor behavior (also reflected by a bathochromic shift of the corresponding  $\nu_{\text{CN}}$  band) is only observed when the metal ion is reduced as a consequence of the cleavage of the technetium–nitrogen double bond. Such a reaction pathway has been observed for  $\text{CNPh}^{\text{PF}}$ .

**Supplementary Materials:** The following supporting information can be downloaded at: <https://www.mdpi.com/article/10.3390/molecules27238546/s1>, Table S1: Crystallographic data and data collection parameter; Figure S1: Ellipsoid representation of  $[\text{Tc}(\text{NPh})\text{Cl}_3(\text{PPh}_3)(\text{CN}^t\text{Bu})] \cdot \text{CH}_2\text{Cl}_2$  (**2a**). The thermal ellipsoids are set at a 50% probability level. Hydrogen atoms are omitted for clarity. A number of 42 reflections below  $\theta_{\text{min}}$  is missing due to the large unit cell and the data collection with the IPDS T2 measuring routine; Table S2: Selected bond lengths ( $\text{\AA}$ ) and angles ( $^\circ$ ) in  $[\text{Tc}(\text{NPh})\text{Cl}_3(\text{PPh}_3)(\text{CN}^t\text{Bu})] \cdot \text{CH}_2\text{Cl}_2$  (**2a**); Figure S2: Ellipsoid representation of  $[\text{Tc}(\text{NPh})\text{Cl}_3(\text{PPh}_3)(\text{CNMes})]$  (**2b**). The thermal ellipsoids are set at a 50% probability level. Hydrogen atoms are omitted for clarity. A number of 16 reflections below  $\theta_{\text{min}}$  is missing due to the large unit cell and the data collection with the IPDS T2 measuring routine; Table S3: Selected bond lengths ( $\text{\AA}$ ) and angles ( $^\circ$ ) in  $[\text{Tc}(\text{NPh})\text{Cl}_3(\text{PPh}_3)(\text{CNMes})]$  (**2b**); Figure S3: Ellipsoid representation of  $[\text{Tc}(\text{NPh})\text{Cl}_3(\text{PPh}_3)(\text{CNPh}^i\text{-prop}^2)] \cdot \text{C}_7\text{H}_8$  (**2c**). The thermal ellipsoids are set at a 50% probability level. Hydrogen atoms are omitted for clarity. A number of 11 reflections below  $\theta_{\text{min}}$  is missing due to the large unit cell and the data collection with the IPDS T2 measuring routine. Flack parameter of the non-centrosymmetric structure: 0.06(6); Table S4: Selected bond lengths ( $\text{\AA}$ ) and angles ( $^\circ$ ) in  $[\text{Tc}(\text{NPh})\text{Cl}_3(\text{PPh}_3)(\text{CNPh}^i\text{-prop}^2)]$  (**2c**); Figure S4: Ellipsoid representation of *cis*- $[\text{Tc}(\text{NPh})\text{Cl}_3(\text{CNAr}^{\text{Mes}_2})_2] \cdot \text{CH}_2\text{Cl}_2$  (**3**). The thermal ellipsoids are set at a 50% probability level. Hydrogen atoms are omitted for clarity. A number of 70 reflections below  $\theta_{\text{min}}$  is missing due to the large unit cell and the data collection with the IPDS T2 measuring

routine. Only one molecule of solvent  $\text{CH}_2\text{Cl}_2$  could be located. An overall number of 102 e- has been 'removed' from the large voids, which are contained in the structure, by a solvent mask using OLEX2 (Dolomanov, O.V., Bourhis, L.J., Gildea, R.J., Howard, J.A.K. & Puschmann, H. (2009), *J. Appl. Cryst.* 42, 339–341). This corresponds to approximately 2.5 more molecules of  $\text{CH}_2\text{Cl}_2$ ; Table S5: Selected bond lengths (Å) and angles (°) in *cis*-[Tc(NPh)Cl<sub>3</sub>(CNAr<sup>Mes2</sup>)<sub>2</sub>] ·  $\text{CH}_2\text{Cl}_2$  (**3**); Figure S5: Ellipsoid representation of *trans*-[Tc(NPh)Cl<sub>3</sub>(CNAr<sup>Tripp2</sup>)<sub>2</sub>] (**4b**). The thermal ellipsoids are set at a 50% probability level. Hydrogen atoms are omitted for clarity. A number of 70 reflections below  $\theta_{\text{min}}$  is missing due to the large unit cell and the data collection with the IPDS T2 measuring routine. One carbon of an isopropyl group has an unusually large ellipsoid due to an elongation of the distal isopropyl moieties. A solvent-accessible void is caused by the molecular packing and does not contain any substantial residual electron density. (b) Visualization of the disorder found for one of the isopropyl groups in the two crystallographically independent species of these large molecules; Table S6: Selected bond lengths (Å) and angles (°) in *trans*-[Tc(NPh)Cl<sub>3</sub>(CNAr<sup>Tripp2</sup>)<sub>2</sub>] (**4b**); Figure S6: Ellipsoid representation of [Tc(NPh)Cl<sub>3</sub>(PPh<sub>3</sub>)(CNp-FAR<sup>DarF2</sup>)] (**5**). The thermal ellipsoids are set at a 50% probability level. Hydrogen atoms are omitted for clarity. The ratio of unique to observed reflections is too low leading to a B alert. This is due to the measurement routine of the IPDS 2T; Table S7: Selected bond lengths (Å) and angles (°) in *trans*-[Tc(NPh)Cl<sub>3</sub>(PPh<sub>3</sub>)(CNp-FAR<sup>DarF2</sup>)] (**5**); Figure S7: <sup>1</sup>H NMR spectrum of [Tc(NPh)Cl<sub>3</sub>(PPh<sub>3</sub>)(CN<sup>t</sup>Bu)] (**2a**) in  $\text{CD}_2\text{Cl}_2$ ; Figure S8: IR (KBr) spectrum of p[Tc(NPh)Cl<sub>3</sub>(PPh<sub>3</sub>)(CN<sup>t</sup>Bu)] (**2a**); Figure S9: <sup>1</sup>H NMR spectrum of [Tc(NPh)(PPh<sub>3</sub>)(CNMes)Cl<sub>3</sub>] (**2b**) in  $\text{CD}_2\text{Cl}_2$ ; Figure S10: <sup>1</sup>H,<sup>1</sup>H COSY NMR spectrum of *cis*-[Tc(NPh)(PPh<sub>3</sub>)(CNMes)Cl<sub>3</sub>] (**2b**) in  $\text{CD}_2\text{Cl}_2$ ; Figure S11: IR (KBr) spectrum of [Tc(NPh)(PPh<sub>3</sub>)(CNMes)Cl<sub>3</sub>] (**2b**); Figure S12: <sup>1</sup>H NMR spectrum of [Tc(NPh)Cl<sub>3</sub>(PPh<sub>3</sub>)(CNPh<sup>i-Prop2</sup>)] (**2c**) in  $\text{CD}_2\text{Cl}_2$ ; Figure S13: IR (KBr) spectrum of [Tc(NPh)Cl<sub>3</sub>(PPh<sub>3</sub>)(CNPh<sup>i-Prop2</sup>)] (**2c**); Figure S14: <sup>1</sup>H NMR spectrum of isomers of [Tc(NPh)Cl<sub>3</sub>(PPh<sub>3</sub>)(CNAr<sup>Mes2</sup>)] (**3a**) in  $\text{CD}_2\text{Cl}_2$ ; Figure S15: <sup>1</sup>H NMR spectrum of *trans*-[Tc(NPh)Cl<sub>3</sub>(CNAr<sup>Tripp2</sup>)<sub>2</sub>] (**4b**) in  $\text{CD}_2\text{Cl}_2$ ; Figure S16: IR (KBr) spectrum of *trans*-[Tc(NPh)(CNAr<sup>Tripp2</sup>)Cl<sub>3</sub>] (**4b**); Figure S17: <sup>1</sup>H NMR spectrum of [Tc(NPh)Cl<sub>3</sub>(PPh<sub>3</sub>)(CNp-FAR<sup>DarF2</sup>)] (**5**) in  $\text{CD}_2\text{Cl}_2$ ; Figure S18: <sup>19</sup>F NMR spectrum of [Tc(NPh)Cl<sub>3</sub>(PPh<sub>3</sub>)(CNp-FAR<sup>DarF2</sup>)] (**5**) in  $\text{CD}_2\text{Cl}_2$ ; Figure S19: <sup>19</sup>F NMR spectra recorded during the reaction of [Tc(NPh)Cl<sub>3</sub>(PPh<sub>3</sub>)(CNp-FAR<sup>DarF2</sup>)] (**5**) with CNp-FAR<sup>DarF2</sup> in THF. Spectrum 1 was recorded after the addition of one equivalent of CNp-FAR<sup>DarF2</sup> to **5**. Spectrum 2 was recorded after heating the previously obtained solution for 10 min in boiling THF. Spectrum 3 was recorded after heating a solution of complex **5** for 10 min in boiling THF; Figure S20: IR (KBr) spectrum of [Tc(NPh)Cl<sub>3</sub>(PPh<sub>3</sub>)(CNp-FAR<sup>DarF2</sup>)] (**5**); Figure S21: <sup>1</sup>H NMR spectrum of [Tc(NPh)Cl<sub>3</sub>(PPh<sub>3</sub>)(CNPh<sup>F</sup>)] (**6**) in  $\text{CD}_2\text{Cl}_2$ ; Figure S22: <sup>19</sup>F NMR spectrum of [Tc(NPh)Cl<sub>3</sub>(PPh<sub>3</sub>)(CNPh<sup>F</sup>)] (**6**) in  $\text{CD}_2\text{Cl}_2$ ; Figure S23: <sup>31</sup>P{<sup>1</sup>H} NMR spectrum of [Tc(NPh)Cl<sub>3</sub>(PPh<sub>3</sub>)(CNPh<sup>F</sup>)] (**6**) in  $\text{CD}_2\text{Cl}_2$ ; Figure S24: IR (KBr) spectrum of [Tc(NPh)Cl<sub>3</sub>(PPh<sub>3</sub>)(CNPh<sup>F</sup>)] (**6**); Figure S25: <sup>1</sup>H NMR spectrum of [Tc(CNPh<sup>p-F</sup>)<sub>6</sub>][PF<sub>6</sub>] (**7**) in  $\text{CD}_2\text{Cl}_2$ ; Figure S26: <sup>19</sup>F NMR spectrum of [Tc(CNPh<sup>p-F</sup>)<sub>6</sub>][PF<sub>6</sub>] (**7**) in  $\text{CD}_2\text{Cl}_2$ ; Figure S27: <sup>99</sup>Tc NMR spectrum of [Tc(CNPh<sup>p-F</sup>)<sub>6</sub>][PF<sub>6</sub>] (**7**) in  $\text{CD}_2\text{Cl}_2$ ; Figure S28: IR (KBr) spectrum of [Tc(CNPh<sup>p-F</sup>)<sub>6</sub>][PF<sub>6</sub>] (**7**); Table S8: Calculated electrostatic potential surface properties of the isocyanide carbon atom at the Van der Waals (VdW) boundary for structures optimized at the B3LYP/6-311++G\*\* level. Surface properties were evaluated at  $\rho = 0.001$  level using an electrostatic potential map basis with a grid-point spacing of 0.25. The last column contains the Surface-Averaged Donor Atom Potential SADAP =  $(\text{EP}_{\text{min}} + \text{EP}_{\text{max}} + \text{AP}) / (\text{ES}_{\text{pos}} + \text{ES}_{\text{neg}})$  as a combined descriptor of steric and electrostatic properties of the potential ligands, which allows an estimation of their reactivity; Table S9:  $\text{LP}_{\text{C}} / \pi^*_{\text{CN}}$  properties of some representative, free isocyanides, number of donated  $\sigma_{\text{Tc}}$  electrons ( $\#e^-$ ;  $\text{LP}_{\text{C}} \rightarrow \text{LP}^*_{\text{Tc}}$ ), and second order perturbation parameters (interaction energy  $E$ ; energy difference between the two orbitals  $E_i - E_j$ ; overlap parameter  $A$ ) for  $\text{LP}_{\text{Tc}} \rightarrow \pi^*_{\text{CN}}$  in the model complexes  $[\text{TCO}_3(\text{CO}/\text{CNR})]^+$  and  $[\text{TC}(\text{CO})_5(\text{CO}/\text{CNR})]^+$  ( $R = \text{Ph}^{\text{F5}}, \text{Ph}^{\text{p-F}}, \text{Ph}, \text{tBu}, \text{Ar}^{\text{DarF2}}$ ).



**Author Contributions:** Conceptualization, U.A., J.S.F. and G.C.; methodology, G.C. and L.Z.; software, A.H. and M.R.J.; validation, G.C., U.A. and M.R.J.; formal analysis, G.C., L.Z., A.H. and M.R.J.; investigation, G.C., L.Z. and U.A.; resources, U.A.; data curation, G.C. and U.A.; writing—original draft preparation, U.A.; writing—review and editing, U.A., G.C., M.R.J., J.S.F. and L.Z.; visualization, U.A., G.C. and M.R.J.; supervision, U.A. and J.S.F.; project administration, G.C. and U.A.; funding acquisition, U.A. and J.S.F. All authors have read and agreed to the published version of the manuscript.

**Funding:** This research was funded by the DFG (Deutsche Forschungsgemeinschaft: Graduate School BIOQIC), the U.S. National Science Foundation (International Supplement to CHE-1802646), and the Alexander von Humboldt Foundation (Fellowship to J.S.F.). We acknowledge the assistance of the Core Facility BioSupraMol supported by the DFG and thank the High-Performance Computing Centre of the Zentraleinrichtung für Datenverarbeitung of the Freie Universität Berlin for computational time.

**Institutional Review Board Statement:** Not applicable.

**Informed Consent Statement:** Not applicable.

**Data Availability Statement:** Not applicable.

**Conflicts of Interest:** The authors declare no conflict of interest.

## References

- Kronauge, J.F.K.; Mendiola, D.J. The value of Stable Metal-Carbon Bonds in Nuclear Medicine and the Cardiolute Story. *Organometallics* **2016**, *35*, 3432–3435. [CrossRef]
- Abrams, M.J.; Davison, A.; Jones, A.G.; Costello, C.; Pang, H. Synthesis and Characterization of Hexakis(alkyl isocyanide) and Hexakis(aryl isocyanide) Complexes of Technetium(I). *Inorg. Chem.* **1983**, *22*, 2798–2800. [CrossRef]
- Abrams, M.J.; Davison, A.; Faggiani, R.; Jones, A.G.; Lock, C.J.L. Chemistry and Structure of Hexakis(thiourea-S)technetium(III) Trichloride Tetrahydrate,  $[\text{Tc}(\text{SC}(\text{NH}_2)_2)_6]\text{Cl}_3 \cdot 4\text{H}_2\text{O}$ . *Inorg. Chem.* **1984**, *23*, 3284–3288. [CrossRef]
- Technetium-99m Radiopharmaceuticals: Manufacture of Kits*; IAEA Technical Reports Series No. 466; International Atomic Energy Agency: Vienna, Austria, 2008; pp. 126–129.
- Herman, L.W.; Sharma, V.; Kronauge, J.F.; Barbaric, E.; Herman, L.; Piwnica-Worms, D. Novel Hexakis(areneisonitrile)technetium(I) Complexes as Radioligands Targeted to the Multidrug Resistance P-Glycoprotein. *J. Med. Chem.* **1995**, *38*, 2955–2963. [CrossRef] [PubMed]
- Piwnica-Worms, D.; Kronauge, J.F.; Holman, B.L.; Davison, A.; Jones, A.G. Comparative Myocardial Uptake Characteristics of Hexakis (Alkylisonitrile) Technetium(I) Complexes. *Investig. Radiol.* **1989**, *24*, 25–29. [CrossRef]
- Kronauge, J.F.; Davison, A.; Roseberrry, A.M.; Costello, C.E.; Maleknia, S.; Jones, A.G. Synthesis, and Identification of the Monocation  $\text{Tc}(\text{CPI})_6^+$  in  $\text{Tc}(\text{CNC}(\text{CH}_3)_2\text{COOCH}_3)_6\text{Cl}$  and Its Hydrolysis Products. *Inorg. Chem.* **1991**, *30*, 4265–4271. [CrossRef]
- World Nuclear Association. Radioisotopes in Medicine. Available online: <https://www.world-nuclear.org/information-library/non-power-nuclear-applications/radioisotopes-research/radioisotopes-in-medicine.aspx> (accessed on 21 August 2022).
- Patil, P.; Ahmadian-Moghaddam, M.; Dömling, A. Isocyanide 2.0. *Green Chem.* **2020**, *22*, 6902–6911. [CrossRef]
- Carpenter, A.E.; Mokhtarzadeh, C.C.; Ripatti, D.S.; Havrylyuk, I.; Kamezawa, R.; Moore, C.E.; Rheingold, A.L.; Figueroa, J.S. Comparative Measure of the Electronic Influence of Highly Substituted Aryl Isocyanides. *Inorg. Chem.* **2015**, *54*, 2936–2944. [CrossRef]
- Claude, G.; Genz, J.; Weh, D.; Roca Jungfer, M.; Hagenbach, A.; Gembicky, M.; Figueroa, J.S.; Abram, U. Mixed-isocyanide Complexes of Technetium under Steric and Electronic Control. *Inorg. Chem.* **2022**, *61*, 16163–16176. [CrossRef]
- Hahn, F.E.; Imhof, L.; Lügger, T. Synthesis of trichlorooxo-bis(2,6-dimethylphenylisocyanide) rhenium(V) and crystal structure of  $\mu$ -oxo-bis[dichlorooxo-bis(2,6-dimethylphenylisocyanide) dirhenium(V)]. *Inorg. Chim. Acta* **1998**, *269*, 347–349. [CrossRef]
- Bryan, J.; Stenkamp, R.E.; Tulip, T.H.; Mayer, J.M. Oxygen atom transfer among rhenium, sulfur, and phosphorus. Characterization and reactivity of  $\text{Re}(\text{O})\text{Cl}_3(\text{Me}_2\text{S})(\text{OPPh}_3)$  and  $\text{Re}(\text{O})\text{Cl}_3(\text{CNCMe}_3)_2$ . *Inorg. Chem.* **1987**, *26*, 2283–2288. [CrossRef]
- Figueroa, J.S.; Abram, U. Oxidorhenium(V) and Rhenium(III) Complexes with m-Terphenyl Isocyanides. *Z. Anorg. Allg. Chem.* **2020**, *646*, 909–914. [CrossRef]
- Claude, G.; Salsi, F.; Hagenbach, A.; Gembicky, M.; Neville, M.; Chan, C.; Figueroa, J.S.; Abram, U. Structural and Redox Variations in Technetium Complexes Supported by m-Terphenyl Isocyanides. *Organometallics* **2020**, *39*, 2287–2294. [CrossRef]
- Nicholson, T.; Davison, A.; Jones, A.G. The synthesis of a technetium(V) phenylimido complex from pertechnetate. The single crystal X-ray structure of  $[\text{TcCl}_3(\text{NPh})(\text{PPh}_3)_2]\text{-CH}_2\text{Cl}_2$ . *Inorg. Chim. Acta* **1991**, *187*, 51–57. [CrossRef]
- Chatt, J.; Garforth, J.D.; Johnson, N.P.; Rowe, G.A. Nitrido- and Arylimido-complexes of Rhenium. *J. Chem. Soc.* **1964**, 1012–1020. [CrossRef]
- Nicholson, T.; Storm, S.L.; Davis, W.M.; Davison, A.; Jones, A.G. The synthesis and characterization of  $[\text{TcCl}_3(\text{NPh})(\text{Ph}_2\text{PCH}_2\text{CH}_2\text{PPh}_2)]$  and  $[\text{TcCl}_3(\text{NPh})(\text{PPh}_3)_2]$ . The single crystal X-ray structure of  $[\text{TcCl}_3(\text{NPh})(\text{Ph}_2\text{PCH}_2\text{CH}_2\text{PPh}_2)]$ . *Inorg. Chim. Acta* **1992**, *196*, 27–34. [CrossRef]

19. Rochon, F.F.; Melanson, R.; Kong, P.-C. Synthesis and Crystal Structures of (Phosphine)technetium(V) Complexes with Phenylimido and Phenylidiazenido Ligands Using the Precursor PhNHNHCOCH<sub>3</sub>. *Inorg. Chem.* **1995**, *34*, 2273–2277. [[CrossRef](#)]
20. Nicholson, T.; Davison, A.; Zubieta, J.A.; Chen, C.; Jones, A.G. The synthesis and characterization of a cationic technetium(V) phenylimido complex. The X-ray crystal structure of [TcCl<sub>2</sub>(NPh)(PMe<sub>2</sub>Ph)<sub>3</sub>](BPh<sub>4</sub>). *Inorg. Chim. Acta* **1995**, *230*, 205–208. [[CrossRef](#)]
21. Kuhn, B.; Abram, U. Phenylimido Complexes of Technetium and Rhenium with Maleonitriledithiolate. *Z. Anorg. Allg. Chem.* **2011**, *637*, 242–245. [[CrossRef](#)]
22. Porchia, M.; Tisato, F.; Refosco, F.; Bolzati, C.; Cavazza-Ceccato, M.; Dolmella, A. New Approach to the Chemistry of Technetium(V) and Rhenium(V) Phenylimido Complexes: Novel [M(NPh)PNP]<sup>3+</sup> Metal Fragments (M = Tc, Re; PNP = Aminodiphosphine) Suitable for the Synthesis of Stable Mixed-Ligand Compounds. *Inorg. Chem.* **2005**, *44*, 4766–4776. [[CrossRef](#)]
23. Kuznetsov, M.L. Theoretical studies of transition metal complexes with nitriles and isocyanides. *Russ. Chem. Rev.* **2002**, *71*, 265–282. [[CrossRef](#)]
24. Csonka, I.P.; Szepes, L.; Modelli, A. Donor–acceptor properties of isonitriles studied by photoelectron spectroscopy and electron transmission spectroscopy. *J. Mass Spectrom.* **2004**, *39*, 1456–1466. [[CrossRef](#)] [[PubMed](#)]
25. Saillard, J.Y.; Le Beuze, A.; Simonneaux, G.; Le Maux, P.; Jaouen, G. Variation of R in the isocyanide series RNC: As an example of the concept of controlled modifications of the properties of ligands for organometallic synthesis. *J. Mol. Struct. (Theochem)* **1981**, *86*, 149–154. [[CrossRef](#)]
26. Guy, M.P.; Guy, J.T., Jr.; Bennett, D.W. A theoretical comparison of the electronic structures of alkyl and aryl isocyanide ligands. *J. Mol. Struct. (Theochem)* **1985**, *122*, 95–99. [[CrossRef](#)]
27. Hieber, W.; Lux, F.; Herget, C. Über Kohlenoxidverbindungen des Technetiums. *Z. Naturforsch.* **1965**, *20b*, 1159–1165. [[CrossRef](#)]
28. Lorenz, B.; Findeisen, M.; Olk, B.; Schmidt, K. Technetium(I) Complexes Tc(CO)<sub>3</sub>BrL<sub>2</sub> (L = Phosphine, Pyridine, Isocyanide). *Z. Anorg. Allg. Chem.* **1988**, *566*, 160–168. [[CrossRef](#)]
29. Alberto, R.; Schibli, R.; Egli, A.; Hermann, W.A.; Artus, G.; Abram, U.; Kaden, T.A. Metal carbonyl syntheses. XXII. Low-pressure carbonylation of [MOCl<sub>4</sub>]<sup>−</sup> and [MO<sub>4</sub>]<sup>−</sup>. The technetium(I) and rhenium(I) complexes [NEt<sub>4</sub>]<sub>2</sub>[MCl<sub>3</sub>(CO)<sub>3</sub>]. *J. Organomet. Chem.* **1995**, *492*, 217–224. [[CrossRef](#)]
30. Alberto, R.; Schibli, R.; Angst, D.; Schubiger, P.A.; Abram, U.; Abram, S.; Kaden, T.A. Application of technetium and rhenium carbonyl chemistry to nuclear medicine. Preparation of [NEt<sub>4</sub>]<sub>2</sub>[TcCl<sub>3</sub>(CO)<sub>3</sub>] from [NBu<sub>4</sub>][TcO<sub>4</sub>] and structure of [NEt<sub>4</sub>][Tc<sub>2</sub>(μ-Cl)<sub>3</sub>(CO)<sub>6</sub>]; structures of the model complexes [NEt<sub>4</sub>][Re<sub>2</sub>(μ-OEt)<sub>2</sub>(μ-OAc)(CO)<sub>6</sub>] and [ReBr(−CH<sub>2</sub>S(CH<sub>2</sub>)<sub>2</sub>Cl)<sub>2</sub>(CO)<sub>3</sub>]. *Transit. Met. Chem.* **1997**, *22*, 597–601.
31. Ditri, T.; Fox, B.; Moore, C.; Rheingold, A.; Figueroa, J. Effective Control of Ligation and Geometric Isomerism: Direct Comparison of Steric Properties Associated with Bis-mesityl and Bis-diisopropylphenyl m-Terphenyl Isocyanides. *Inorg. Chem.* **2009**, *48*, 8362–8375. [[CrossRef](#)]
32. Stewart, M.A.; Moore, C.E.; Ditri, T.B.; Labios, L.A.; Rheingold, A.L.; Figueroa, J.S. Electrophilic functionalization of well-behaved manganese monoanions supported by m-terphenyl isocyanides. *Chem. Commun.* **2011**, *47*, 406–408. [[CrossRef](#)]
33. Ditri, T.B.; Carpenter, A.E.; Ripatti, D.S.; Moore, C.E.; Rheingold, A.L.; Figueroa, J.S. Chloro- and Trifluoromethyl-Substituted Flanking-Ring m-Terphenyl Isocyanides: η<sup>6</sup>-Arene Binding to Zero-Valent Molybdenum Centers and Comparison to Alkyl-Substituted Derivatives. *Inorg. Chem.* **2013**, *52*, 13216–13229. [[CrossRef](#)] [[PubMed](#)]
34. Salsi, S.; Neville, M.; Drance, M.; Hagenbach, A.; Chan, C.C.; Figueroa, J.S.; Abram, U. A closed-shell monomeric rhenium(1-) anion provided my m-terphenyl isocyanide ligation. *Chem. Commun.* **2020**, *56*, 7009–7012. [[CrossRef](#)] [[PubMed](#)]
35. Salsi, F.; Neville, M.; Drance, M.; Hagenbach, A.; Figueroa, J.S.; Abram, U. {M<sup>I</sup>(CO)X(CNp-FAr<sup>DArF</sup>)<sub>4</sub>} (DArF = 3,5-(CF<sub>3</sub>)<sub>2</sub>C<sub>6</sub>H<sub>3</sub>; M = Re, Tc; X = Br, Cl) Complexes: Convenient Platforms for the Synthesis of Low-valent Rhenium and Technetium Compounds. *Organometallics* **2021**, *40*, 1336–1343. [[CrossRef](#)]
36. Tasi, G.; Pálinkó, I. Using Molecular Electrostatic Potential Maps for Similarity Studies. *Top. Curr. Chem.* **1995**, *174*, 46–71.
37. Kikuchi, O.; Yamaguchi, K.; Morihashi, K.; Yokoyama, Y.; Nakayama, M. Molecular Electrostatic Potential Map Analysis of Metal Cation Interaction with Nucleophilic Molecules. *Bull. Chem. Soc. Jpn.* **1993**, *66*, 2412–2414. [[CrossRef](#)]
38. Lu, T.; Chen, F. Quantitative analysis of molecular surface based on improved Marching Tetrahedra algorithm. *J. Mol. Graph. Model.* **2012**, *38*, 314–323. [[CrossRef](#)]
39. Carpenter, A.E.; Chan, C.; Rheingold, A.L.; Figueroa, J.S. A Well-Defined Isocyano Analogue of HCo(CO)<sub>4</sub>. 1: Synthesis, Decomposition, and Catalytic 1,1-Hydrogenation of Isocyanodes. *Organometallics* **2016**, *35*, 2319–2326. [[CrossRef](#)]
40. Scholtysik, C.; Roca Jungfer, M.; Hagenbach, A.; Abram, U. Reactions of [ReOCl<sub>3</sub>(PPh<sub>3</sub>)<sub>2</sub>] with 4-Fluoroaniline. *Z. Anorg. Allg. Chem.* **2018**, *644*, 1451–1455. [[CrossRef](#)]
41. Scholtysik, C.; Njiki Noufele, C.; Hagenbach, A.; Abram, U. Complexes of Technetium(V) and Rhenium(V) with β-Diketonates. *Inorg. Chem.* **2019**, *58*, 5241–5252. [[CrossRef](#)]
42. Wendlandt, D.; Bauche, J.; Luc, P. Hyperfine structure in Tc I: Experiment and theory. *J. Phys. B At. Mol. Phys.* **1977**, *10*, 1989–2002. [[CrossRef](#)]
43. Mikhalev, V.A. <sup>99m</sup>Tc NMR Spectroscopy. *Radiochemistry* **2005**, *47*, 319–333. [[CrossRef](#)]
44. Abram, U.; Lorenz, L.; Kaden, L.; Scheller, D. Nitrido Complexes of Technetium with Tertiary Phosphines and Arsines. *Polyhedron* **1988**, *7*, 285–289. [[CrossRef](#)]

45. O'Connell, L.A.; Pearlstein, R.M.; Davison, A.; Thornback, J.R.; Kronauge, J.F.; Jones, A.G. Technetium-99 NMR spectroscopy: Chemical shift trends and long range coupling effects. *Inorg. Chim. Acta* **1989**, *161*, 39–43. [[CrossRef](#)]
46. Ackermann, J.; Abdulkader, A.; Scholtysik, C.; Roca Jungfer, M.; Hagenbach, A.; Abram, U.  $[\text{Tc}^{\text{I}}(\text{NO})\text{X}(\text{Cp})(\text{PPh}_3)]$  Complexes ( $\text{X}^- = \text{I}^-, \text{I}_3^-, \text{SCN}^-, \text{CF}_3\text{SO}_3^-, \text{ or } \text{CF}_3\text{COO}^-$ ) and Their Reactions. *Organometallics* **2019**, *38*, 4471–4478. [[CrossRef](#)]
47. Roca Jungfer, M.; Elsholz, L.; Abram, U. Technetium Hydrides Revisited: Syntheses, Structures, and Reactions of  $[\text{TcH}_3(\text{PPh}_3)_4]$  and  $[\text{TcH}(\text{CO})_3(\text{PPh}_3)_2]$ . *Organometallics* **2021**, *40*, 3095–3112. [[CrossRef](#)]
48. Coppens, P. *The Evaluation of Absorption and Extinction in Single-Crystal Structure Analysis*. *Crystallographic Computing*; Muksgaard: Copenhagen, Denmark, 1979.
49. Sheldrick, G.M. A short history of SHELX. *Acta Crystallogr.* **2008**, *64*, 112–122. [[CrossRef](#)]
50. Sheldrick, G.M. Crystal structure refinement with SHELXL. *Acta Crystallogr.* **2015**, *71*, 3–8.
51. Dolomanov, O.V.; Bourhis, L.J.; Gildea, R.J.; Howard, J.A.K.; Puschmann, H. OLEX2: A complete structure solution, refinement and analysis program. *J. Appl. Cryst.* **2009**, *42*, 339–341. [[CrossRef](#)]
52. Putz, H.; Brandenburg, K. (Eds.) *DIAMOND, Crystal and Molecular Structure Visualization Crystal Impact*; Version 4.6.5; GbR: Bonn, Germany, 2021.
53. Bennett, L.; Melchers, B.; Proppe, B. Curta: A General-Purpose High-Performance Computer at ZEDAT, Freie Universität Berlin. Internal Report. Available online: <https://refubium.fu-berlin.de/handle/fub188/26993> (accessed on 21 August 2022). [[CrossRef](#)]
54. Frisch, M.J.; Trucks, G.W.; Schlegel, H.B.; Scuseria, G.E.; Robb, M.A.; Cheeseman, J.R.; Scalmani, G.; Barone, V.; Petersson, G.A.; Nakatsuji, H.; et al. *Gaussian 16, Revision B.01*; Gaussian, Inc.: Wallingford, CT, USA, 2016.
55. Dennington, R.; Keith, T.A.; Millam, J.M. *GaussView, Version 6*; Semichem Inc.: Shawnee Mission, KS, USA, 2016.
56. Hanwell, M.D.; Curtis, D.E.; Lonie, D.C.; Vandermeersch, C.; Zurek, E.; Hutchison, G.R. Avogadro: An advanced semantic chemical editor, visualization, and analysis platform. *J. Cheminf.* **2012**, *4*, 17. [[CrossRef](#)]
57. Vosko, S.H.; Wilk, L.; Nusair, M. Accurate spin-dependent electron liquid correlation energies for local spin density calculations: A critical analysis. *Can. J. Phys.* **1980**, *58*, 1200–1211. [[CrossRef](#)]
58. Becke, A.D. Density-functional thermochemistry. III. The role of exact exchange. *J. Chem. Phys.* **1993**, *98*, 5648–5652. [[CrossRef](#)]
59. Lee, C.; Yang, W.; Parr, R.G. Development of the Colle-Salvetti correlation-energy formula into a functional of the electron density. *Phys. Rev.* **1988**, *37*, 785–789. [[CrossRef](#)] [[PubMed](#)]
60. Andrae, D.; Häußermann, U.; Dolg, M.; Stoll, H.; Preuß, H. Energy-adjusted ab initio pseudopotentials for the second and third row transition elements. *Theor. Chim. Acta* **1990**, *77*, 123–141. [[CrossRef](#)]
61. Martin, J.M.L.; Sundermann, A. Correlation consistent valence basis sets for use with the Stuttgart-Dresden-Bonn relativistic effective core potentials: The atoms Ga-Kr and In-Xe. *J. Chem. Phys.* **2001**, *114*, 3408–3420. [[CrossRef](#)]
62. Clark, T.; Chandrasekhar, J.; Spitznagel, G.W.; Schleyer, P.V.R. Efficient diffuse function-augmented basis sets for anion calculations. III. The 3-21+G basis set for first-row elements, Li-F. *J. Comput. Chem.* **1983**, *4*, 294–301. [[CrossRef](#)]
63. Francl, M.M.; Pietro, W.J.; Hehre, W.J.; Binkley, J.S.; Gordon, M.S.; DeFrees, D.J.; Pople, J.A. Self-consistent molecular orbital methods. XXIII. A polarization-type basis set for second-row elements. *J. Chem. Phys.* **1982**, *77*, 3654–3665. [[CrossRef](#)]
64. Krishnan, R.; Binkley, J.S.; Seeger, R.; Pople, J.A. Self-consistent molecular orbital methods. XX. A basis set for correlated wave functions. *J. Chem. Phys.* **1980**, *72*, 650–654. [[CrossRef](#)]
65. McLean, A.D.; Chandler, G.S. Contracted Gaussian basis sets for molecular calculations. I. Second row atoms,  $Z = 11-18$ . *J. Chem. Phys.* **1980**, *72*, 5639–5648. [[CrossRef](#)]
66. Spitznagel, G.W.; Clark, T.; von Rague Schleyer, P.; Hehre, W.J. An evaluation of the performance of diffuse function-augmented basis sets for second row elements, Na-Cl. *J. Comput. Chem.* **1987**, *8*, 1109–1116. [[CrossRef](#)]
67. Schuchardt, K.L.; Didier, B.T.; Elsethagen, T.; Sun, L.; Gurumoorthi, V.; Chase, J.; Li, J.; Windus, T.L. Basis Set Exchange: A Community Database for Computational Sciences. *J. Chem. Inf. Model.* **2007**, *47*, 1045–1052. [[CrossRef](#)]
68. Lu, T.; Chen, F. Multiwfn: A multifunctional wavefunction analyzer. *J. Comput. Chem.* **2012**, *33*, 580–592. [[CrossRef](#)] [[PubMed](#)]

Supporting information for the paper entitled:

**The Chemistry of Phenylimidotechneium(V) Complexes with Isocyanides: Steric and Electronic Factors**

*Guilhem Claude,<sup>1</sup> Laura Zeh,<sup>1</sup> Maximilian Roca Jungfer,<sup>1</sup> Adelheid Hagenbach,<sup>1</sup> Joshua R. Figueroa<sup>2\*</sup>, and Ulrich Abram<sup>1\*</sup>*

<sup>1</sup>Freie Universität Berlin, Institute of Chemistry and Biochemistry, Fabeckstr. 34–36, 14195 Berlin, Germany

E-mail: ulrich.abram@fu-berlin.de

<sup>2</sup> Department of Chemistry and Biochemistry, University of California, San Diego, La Jolla, California 92093, United States

E-mail: jsfig@ucsd.edu

## Table content

Crystallographic data .....	5
<b>Table S1:</b> Crystallographic data and data collection parameters .....	5
<b>Figure S1:</b> Ellipsoid representation of <i>fac</i> -[Tc(NPh)Cl <sub>3</sub> (PPh <sub>3</sub> )(CN <sup>i</sup> Bu)] · CH <sub>2</sub> Cl <sub>2</sub> ( <b>2a</b> ). The thermal ellipsoids are set at a 50% probability level. Hydrogen atoms are omitted for clarity. A number of 42 reflections below theta <sub>min</sub> is missing due to the large unit cell and the data collection with the IPDS T2 measuring routine. ....	7
<b>Table S2:</b> Selected bond lengths (Å) and angles (°) in <i>fac</i> - [Tc(NPh)Cl <sub>3</sub> (PPh <sub>3</sub> )(CN <sup>i</sup> Bu)] · CH <sub>2</sub> Cl <sub>2</sub> ( <b>2a</b> ). ....	7
<b>Figure S2:</b> Ellipsoid representation of <i>fac</i> -[Tc(NPh)Cl <sub>3</sub> (PPh <sub>3</sub> )(CNMes)] ( <b>2b</b> ). The thermal ellipsoids are set at a 50% probability level. Hydrogen atoms are omitted for clarity. A number of 16 reflections below theta <sub>min</sub> is missing due to the large unit cell and the data collection with the IPDS T2 measuring routine. ....	8
<b>Table S3:</b> Selected bond lengths (Å) and angles (°) in <i>fac</i> - [Tc(NPh)Cl <sub>3</sub> (PPh <sub>3</sub> )(CNMes)] ( <b>2b</b> ). ....	8
<b>Figure S3:</b> Ellipsoid representation of <i>fac</i> -[Tc(NPh)Cl <sub>3</sub> (PPh <sub>3</sub> )(CNPh <sup>i-prop2</sup> )] · C <sub>7</sub> H <sub>8</sub> ( <b>2c</b> ). The thermal ellipsoids are set at a 50% probability level. Hydrogen atoms are omitted for clarity. A number of 11 reflections below theta <sub>min</sub> is missing due to the large unit cell and the data collection with the IPDS T2 measuring routine. Flack parameter of the non-centrosymmetric structure: 0.06(6). ....	9
<b>Table S4:</b> Selected bond lengths (Å) and angles (°) in <i>fac</i> -[Tc(NPh)Cl <sub>3</sub> (PPh <sub>3</sub> )(CNPh <sup>i-prop2</sup> )] ( <b>2c</b> ). ....	9
<b>Figure S4:</b> Ellipsoid representation of <i>cis, fac</i> -[Tc(NPh)Cl <sub>3</sub> (CNAr <sup>Mes2</sup> ) <sub>2</sub> ]-CH <sub>2</sub> Cl <sub>2</sub> ( <b>3</b> ). The thermal ellipsoids are set at a 50% probability level. Hydrogen atoms are omitted for clarity. A number of 70 reflections below theta <sub>min</sub> is missing due to the large unit cell and the data collection with the IPDS T2 measuring routine. Only one molecule of solvent CH <sub>2</sub> Cl <sub>2</sub> could be located. An overall number of 102 e <sup>-</sup> has been 'removed' from the large. Voids, which are contained in the structure, by a solvent mask using OLEX2 (Dolomanov, O.V., Bourhis, L.J., Gildea, R.J, Howard, J.A.K. & Puschmann, H. (2009), J. Appl. Cryst. 42, 339-341). This corresponds to approximately 2.5 more molecules of CH <sub>2</sub> Cl <sub>2</sub> . ....	10
<b>Table S5:</b> Selected bond lengths (Å) and angles (°) in <i>cis, fac</i> -[Tc(NPh)Cl <sub>3</sub> CNAr <sup>Mes2</sup> ] <sub>2</sub> · CH <sub>2</sub> Cl <sub>2</sub> ( <b>3</b> ). ....	10
<b>Figure S5:</b> a) Ellipsoid representation of <i>trans, mer</i> -[Tc(NPh)Cl <sub>3</sub> (CNAr <sup>Tripp2</sup> ) <sub>2</sub> ] ( <b>4b</b> ). The thermal ellipsoids are set at a 50% probability level. Hydrogen atoms are omitted for clarity. A number of 70 reflections below theta <sub>min</sub> is missing due to the large unit cell and the data collection with the IPDS T2 measuring routine. One carbon of an isopropyl group has an unusually large ellipsoid due to an elongation of the distal isopropyl moieties. A solvent accessible void is caused by the molecular packing and does not contain any substantial residual electron density. b) Visualization of the disorder found for one of the isopropyl groups in the two crystallographically independent species of these large molecules. ....	11
<b>Table S6:</b> Selected bond lengths (Å) and angles (°) in <i>trans, mer</i> -[Tc(NPh)Cl <sub>3</sub> CNAr <sup>Tripp2</sup> ] <sub>2</sub> ] ( <b>4b</b> ). ....	11

<b>Figure S6:</b> Ellipsoid representation of <i>fac</i> -[Tc(NPh)Cl <sub>3</sub> (PPh <sub>3</sub> )(CN <i>p</i> -FAR <sup>DarF2</sup> )] ( <b>5</b> ). The thermal ellipsoids are set at a 50% probability level. Hydrogen atoms are omitted for clarity. The ratio of unique to observed reflections is too low leading to a B alert. This is due to the measurement routine of the IPDS 2T.....	12
<b>Table S7:</b> Selected bond lengths (Å) and angles (°) in <i>fac</i> -[Tc(NPh)Cl <sub>3</sub> (PPh <sub>3</sub> )(CN <i>p</i> -FAR <sup>DarF2</sup> )] ( <b>5</b> ).....	12
Spectroscopic data.....	13
<b>Figure S7:</b> <sup>1</sup> H NMR spectrum of <i>fac</i> -[Tc(NPh)Cl <sub>3</sub> (PPh <sub>3</sub> )(CN <sup>t</sup> Bu)] ( <b>2a</b> ) in CD <sub>2</sub> Cl <sub>2</sub> .....	13
<b>Figure S8:</b> IR (KBr) spectrum of <i>fac</i> -[Tc(NPh)Cl <sub>3</sub> (PPh <sub>3</sub> )(CN <sup>t</sup> Bu)] ( <b>2a</b> ).....	13
<b>Figure S9:</b> <sup>1</sup> H NMR spectrum of.....	14
<b>Figure S10:</b> <sup>1</sup> H, <sup>1</sup> H COSY NMR spectrum of <i>fac</i> -[Tc(NPh)(PPh <sub>3</sub> )(CNMes)Cl <sub>3</sub> ] ( <b>2b</b> ) in CD <sub>2</sub> Cl <sub>2</sub> .....	14
<b>Figure S11:</b> IR (KBr) spectrum of <i>fac</i> -[Tc(NPh)(PPh <sub>3</sub> )(CNMes)Cl <sub>3</sub> ] ( <b>2b</b> ). ....	15
<b>Figure S12:</b> <sup>1</sup> H NMR spectrum of <i>fac</i> -[Tc(NPh)Cl <sub>3</sub> (PPh <sub>3</sub> )(CNPh <sup>i-prop2</sup> )] ( <b>2c</b> ) in CD <sub>2</sub> Cl <sub>2</sub> ....	15
<b>Figure S13:</b> IR (KBr) spectrum of <i>fac</i> -[Tc(NPh)Cl <sub>3</sub> (PPh <sub>3</sub> )(CNPh <sup>i-prop2</sup> )] ( <b>2c</b> ). ....	16
<b>Figure S14:</b> <sup>1</sup> H NMR spectrum of isomers of <i>fac</i> -[Tc(NPh)Cl <sub>3</sub> (PPh <sub>3</sub> )(CNAr <sup>Mes2</sup> )] ( <b>3a</b> ) in CD <sub>2</sub> Cl <sub>2</sub> . ....	16
<b>Figure S15:</b> <sup>1</sup> H NMR spectrum of <i>trans,mer</i> -[Tc(NPh)Cl <sub>3</sub> (CNAr <sup>Tripp2</sup> ) <sub>2</sub> ] ( <b>4b</b> ) in CD <sub>2</sub> Cl <sub>2</sub> . ...	17
<b>Figure S16:</b> IR (KBr) spectrum of <i>trans,mer</i> -[Tc(NPh)(CNAr <sup>Tripp2</sup> )Cl <sub>3</sub> ] ( <b>4b</b> ).....	17
<b>Figure S17:</b> <sup>1</sup> H NMR spectrum of <i>fac</i> -[Tc(NPh)Cl <sub>3</sub> (PPh <sub>3</sub> )(CN <i>p</i> -FAR <sup>DarF2</sup> )] ( <b>5</b> ) in CD <sub>2</sub> Cl <sub>2</sub> . ...	18
<b>Figure S18:</b> <sup>19</sup> F NMR spectrum of <i>fac</i> - [Tc(NPh)Cl <sub>3</sub> (PPh <sub>3</sub> )(CN <i>p</i> -FAR <sup>DarF2</sup> )] ( <b>5</b> ) in CD <sub>2</sub> Cl <sub>2</sub> . ....	18
<b>Figure S19:</b> <sup>19</sup> F NMR spectra recorded during the reaction of <i>fac</i> -[Tc(NPh)Cl <sub>3</sub> (PPh <sub>3</sub> )(CN <i>p</i> -FAR <sup>DarF2</sup> )] ( <b>5</b> ) with CN <i>p</i> -FAR <sup>DarF2</sup> in THF. Spectrum 1 was recorded after the addition of one equivalent of CN <i>p</i> -FAR <sup>DarF2</sup> to <b>5</b> . Spectrum 2 was recorded after heating the previously obtained solution for 10 min in boiling THF. Spectrum 3 was recorded after heating a solution of complex <b>5</b> for 10 min in boiling THF. ....	19
<b>Figure S20:</b> IR (KBr) spectrum of <i>fac</i> -[Tc(NPh)Cl <sub>3</sub> (PPh <sub>3</sub> )(CN <i>p</i> -FAR <sup>DarF2</sup> )] ( <b>5</b> ). ....	19
<b>Figure S21:</b> <sup>1</sup> H NMR spectrum of <i>fac</i> -[Tc(NPh)Cl <sub>3</sub> (PPh <sub>3</sub> )(CNPh <sup>pF</sup> )] ( <b>6</b> ) in CD <sub>2</sub> Cl <sub>2</sub> . ....	20
<b>Figure S22:</b> <sup>19</sup> F NMR spectrum of <i>fac</i> -[Tc(NPh)Cl <sub>3</sub> (PPh <sub>3</sub> )(CNPh <sup>pF</sup> )] ( <b>6</b> ) in CD <sub>2</sub> Cl <sub>2</sub> . ....	20
<b>Figure S23:</b> <sup>31</sup> P{ <sup>1</sup> H} NMR spectrum of <i>fac</i> -[Tc(NPh)Cl <sub>3</sub> (PPh <sub>3</sub> )(CNPh <sup>pF</sup> )] ( <b>6</b> ) in CD <sub>2</sub> Cl <sub>2</sub> ... ..	21
<b>Figure S24:</b> IR (KBr) spectrum of <i>fac</i> -[Tc(NPh)Cl <sub>3</sub> (PPh <sub>3</sub> )(CNPh <sup>pF</sup> )] ( <b>6</b> ). ....	21
<b>Figure S25:</b> <sup>1</sup> H NMR spectrum of <i>fac</i> -[Tc(CNPh <sup>pF</sup> ) <sub>6</sub> ][PF <sub>6</sub> ] ( <b>7</b> ) in CD <sub>2</sub> Cl <sub>2</sub> .....	22
<b>Figure S26:</b> <sup>19</sup> F NMR spectrum of [Tc(CNPh <sup>pF</sup> ) <sub>6</sub> ][PF <sub>6</sub> ] ( <b>7</b> ) in CD <sub>2</sub> Cl <sub>2</sub> .....	22
<b>Figure S27:</b> <sup>99</sup> Tc NMR spectrum of [Tc(CNPh <sup>pF</sup> ) <sub>6</sub> ][PF <sub>6</sub> ] ( <b>7</b> ) in CD <sub>2</sub> Cl <sub>2</sub> . ....	23
<b>Figure S28:</b> IR (KBr) spectrum of [Tc(CNPh <sup>pF</sup> ) <sub>6</sub> ][PF <sub>6</sub> ] ( <b>7</b> ). ....	23
<b>DFT Calculations</b> .....	24
<b>Table S8.</b> Calculated electrostatic potential surface properties of the isocyanide carbon atom at the Van der Waals (VdW) boundary for structures optimized at the B3LYP/6-311++G** level. Surface properties were evaluated at ρ = 0.001 level using an	

electrostatic potential map basis with a grid-point spacing of 0.25. The last column contains the Surface-Averaged Donor Atom Potential SADAP =  $(EP_{\min} + EP_{\max} + AP)/(ES_{\text{pos}} + ES_{\text{neg}})$  as a combined descriptor of steric and electrostatic properties of the potential ligands, which allows an estimation of their reactivity. ....24

**Table S9.** LP/ $\pi^*_{\text{CN}}$  properties of some representative, free isocyanides, number of donated  $\sigma_{\text{CTc}}$  electrons ( $\#e^-$ ;  $LP_{\text{c}} \rightarrow LP^*_{\text{Tc}}$ ) and second order perturbation parameters (interaction energy  $E$ ; energy difference between the two orbitals  $E_i - E_j$ ; overlap parameter  $A$ ) for  $LP_{\text{Tc}} \rightarrow \pi^*_{\text{CN}}$  in the model complexes  $[\text{TcO}_3(\text{CO/CNR})]^+$  and  $[\text{Tc}(\text{CO})_5(\text{CO/CNR})]^+$  ( $R = \text{Ph}^{\text{F5}}, \text{Ph}^{\text{p-F}}, \text{Ph}, \text{tBu}, \text{Ar}^{\text{DArF2}}$ ).....28

## Crystallographic data

The intensities for the X-ray determinations were collected on STOE IPDS 2T with Mo K $\alpha$  radiation. The space groups were determined by the detection of systematic absences. Absorption corrections were carried out by integration methods (Coppens, P. The Evaluation of Absorption and Extinction in Single-Crystal Structure Analysis. Crystallographic Computing; Copenhagen, Muksgaard, **1979**). Structure solution and refinement were performed with the SHELX program package. Hydrogen atoms were derived from the final Fourier maps and refined or placed at calculated positions and treated with the 'riding model' option of SHELXL. The representation of molecular structures was done using the program DIAMOND 4.2.2. Additional information on the structure determinations has been deposited with the Cambridge Crystallographic Data Centre.

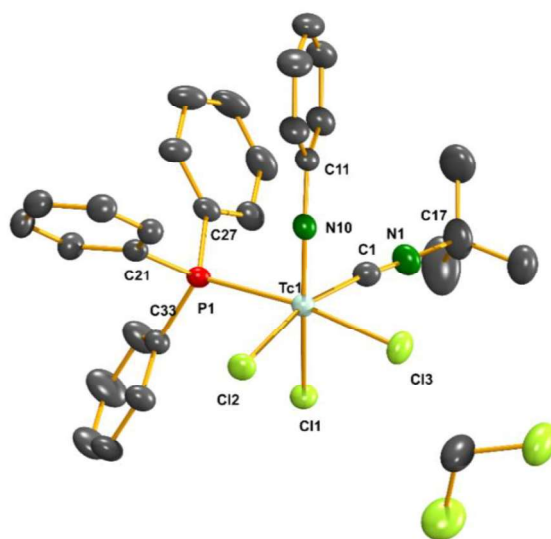
**Table S1:** Crystallographic data and data collection parameters

	<i>fac</i> -[Tc(NPh)Cl <sub>3</sub> (PPh <sub>3</sub> )(CN <sup>t</sup> Bu)] · CH <sub>2</sub> Cl <sub>2</sub> ( <b>2a</b> )	<i>fac</i> -[Tc(NPh)Cl <sub>3</sub> (PPh <sub>3</sub> )(CNMes)] ( <b>2b</b> )	<i>fac</i> -[Tc(NPh)Cl <sub>3</sub> (PPh <sub>3</sub> )(CNPh <sup>+</sup> prop <sup>2</sup> )] · C <sub>7</sub> H <sub>8</sub> ( <b>2c</b> )
Empirical formula	C <sub>30</sub> H <sub>31</sub> Cl <sub>3</sub> N <sub>2</sub> PTc	C <sub>34</sub> H <sub>31</sub> Cl <sub>3</sub> N <sub>2</sub> PTc	C <sub>44</sub> H <sub>45</sub> Cl <sub>3</sub> N <sub>2</sub> PTc
Formula weight	725.79	702.93	837.14
Temperature/K	200.0	200.0	293(2)
Crystal system	triclinic	monoclinic	orthorhombic
Space group	P-1	P2 <sub>1</sub> /n	Pca2 <sub>1</sub>
a/Å	9.8713(7)	9.5714(7)	21.988(4)
b/Å	12.5882(9)	20.816(1)	10.556(2)
c/Å	14.1290(1)	16.296(1)	17.683(4)
$\alpha$ /°	80.628(6)	90	90
$\beta$ /°	74.909(6)	99.504(5)	90
$\gamma$ /°	73.409(6)	90	90
Volume/Å <sup>3</sup>	1617.1(2)	3202.2(3)	4104.1(14)
Z	2	4	4
$\rho_{\text{calc}}$ / cm <sup>3</sup>	1.491	1.458	1.355
$\mu$ / mm <sup>-1</sup>	0.930	0.776	0.618
F(000)	736.0	1432.0	1728.0
Crystal size / mm <sup>3</sup>	0.66 × 0.56 × 0.38	0.3 × 0.24 × 0.2	0.35 × 0.2 × 0.2
Radiation	MoK $\alpha$ ( $\lambda$ = 0.71073)	MoK $\alpha$ ( $\lambda$ = 0.71073)	MoK $\alpha$ ( $\lambda$ = 0.71073)
2 $\theta$ range for data collection/°	9.484 to 51.992	7.242 to 58.496	6.768 to 58.482
Index ranges	-10 ≤ h ≤ 12, -15 ≤ k ≤ 15, -17 ≤ l ≤ 15	-10 ≤ h ≤ 13, -28 ≤ k ≤ 28, -22 ≤ l ≤ 22	-19 ≤ h ≤ 30, -11 ≤ k ≤ 14, -23 ≤ l ≤ 24
Reflections collected	13325	25489	16632
Independent reflections	6302 [R <sub>int</sub> = 0.0473, R <sub>sigma</sub> = 0.0355]	8612 [R <sub>int</sub> = 0.0927, R <sub>sigma</sub> = 0.0795]	9691 [R <sub>int</sub> = 0.1047, R <sub>sigma</sub> = 0.1771]
Data/restraints/parameters	6302/0/355	8612/0/373	9691/521/465
Goodness-of-fit on F <sup>2</sup>	1.045	0.887	0.802
Final R indexes [ $I \geq 2\sigma(I)$ ]	R <sub>1</sub> = 0.0303, wR <sub>2</sub> = 0.0769	R <sub>1</sub> = 0.0377, wR <sub>2</sub> = 0.0846	R <sub>1</sub> = 0.0552, wR <sub>2</sub> = 0.0903
Final R indexes [all data]	R <sub>1</sub> = 0.0346, wR <sub>2</sub> = 0.0785	R <sub>1</sub> = 0.0599, wR <sub>2</sub> = 0.0903	R <sub>1</sub> = 0.1262, wR <sub>2</sub> = 0.1065
Largest diff. peak/hole / e Å <sup>-3</sup>	0.50/-0.94	0.75/-1.34	0.48/-0.50
Flack parameter	-	-	-0.06(6)
CCDC access code	2208603	2208604	2208605



**Table S1 (continued):** Crystallographic data and data collection parameters.

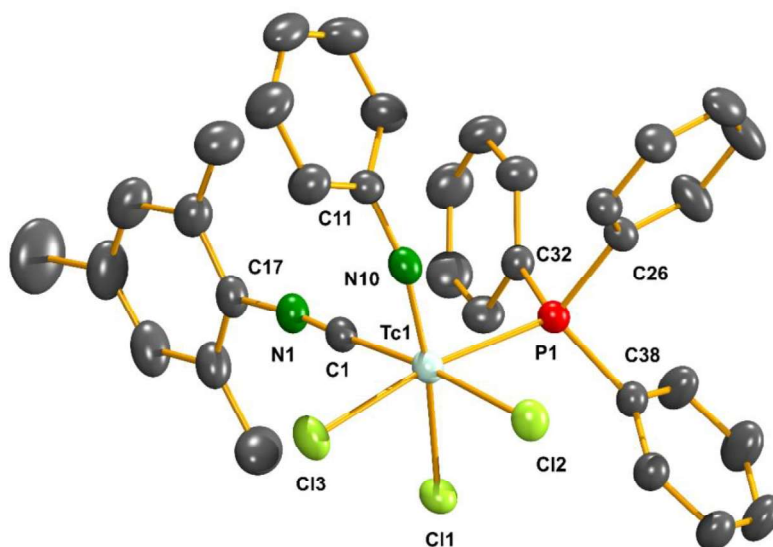
	<i>cis</i> -[Tc(NPh)Cl <sub>3</sub> (CNAr <sup>Mes2</sup> ) <sub>2</sub> ] · CH <sub>2</sub> Cl <sub>2</sub> ( <b>3</b> )	<i>trans</i> -[Tc(NPh)Cl <sub>3</sub> (CNAr <sup>Tripp2</sup> ) <sub>2</sub> ] ( <b>4b</b> )	<i>fac</i> -[Tc(NPh)Cl <sub>3</sub> (PPh <sub>3</sub> )(CNP-FAr <sup>DarF2</sup> )] ( <b>5</b> )
Empirical formula	C <sub>57</sub> H <sub>57</sub> Cl <sub>5</sub> N <sub>3</sub> Tc	C <sub>80</sub> H <sub>103</sub> Cl <sub>3</sub> N <sub>3</sub> Tc	C <sub>47</sub> H <sub>28</sub> Cl <sub>3</sub> F <sub>13</sub> N <sub>2</sub> PTc
Formula weight	1059.30	1311.00	1103.03
Temperature/K	200.0	200.0	200.0
Crystal system	triclinic	monoclinic	monoclinic
Space group	P-1	P2 <sub>1</sub> /n	P2 <sub>1</sub> /n
<i>a</i> /Å	12.4573(9)	24.4011(9)	8.5399(8)
<i>b</i> /Å	13.3922(11)	24.9304(7)	22.855(2)
<i>c</i> /Å	19.8431(16)	28.0596(13)	23.501(2)
$\alpha$ /°	96.377(7)	90	90
$\beta$ /°	92.599(6)	108.814(3)	98.416(7)
$\gamma$ /°	114.514(6)	90	90
Volume / Å <sup>3</sup>	2978.1(4)	16157.5(11)	4537.4(7)
Z	2	8	4
$\rho_{\text{calc}}$ g/cm <sup>3</sup>	1.181	1.078	1.615
$\mu$ / mm <sup>-1</sup>	0.501	0.317	0.620
F(000)	1096.0	5584.0	2200.0
Crystal size / mm <sup>3</sup>	0.6 × 0.36 × 0.2	0.9 × 0.72 × 0.46	0.2 × 0.133 × 0.1
Radiation	MoK $\alpha$ ( $\lambda$ = 0.71073)	MoK $\alpha$ ( $\lambda$ = 0.71073)	MoK $\alpha$ ( $\lambda$ = 0.71073)
2 $\theta$ range for data collection/°	6.698 to 51.996	6.646 to 49.998	3.932 to 51
Index ranges	-15 ≤ <i>h</i> ≤ 15, -13 ≤ <i>k</i> ≤ 16, -24 ≤ <i>l</i> ≤ 24	-29 ≤ <i>h</i> ≤ 29, -29 ≤ <i>k</i> ≤ 29, -33 ≤ <i>l</i> ≤ 24	-10 ≤ <i>h</i> ≤ 10, -27 ≤ <i>k</i> ≤ 27, -27 ≤ <i>l</i> ≤ 28
Reflections collected	25752	82662	27078
Independent reflections	11656 [R <sub>int</sub> = 0.0749, R <sub>sigma</sub> = 0.1151]	28300 [R <sub>int</sub> = 0.1080, R <sub>sigma</sub> = 0.0972]	8443 [R <sub>int</sub> = 0.1506, R <sub>sigma</sub> = 0.2363]
Data/restraints/parameters	11656/0/607	28300/1886/1498	8443/854/621
Goodness-of-fit on F <sup>2</sup>	0.833	0.999	0.669
Final R indexes [ <i>I</i> ≥ 2 $\sigma$ ( <i>I</i> )]	R <sub>1</sub> = 0.0471, wR <sub>2</sub> = 0.0832	R <sub>1</sub> = 0.0817, wR <sub>2</sub> = 0.2151	R <sub>1</sub> = 0.0477, wR <sub>2</sub> = 0.0657
Final R indexes [all data]	R <sub>1</sub> = 0.0915, wR <sub>2</sub> = 0.0929	R <sub>1</sub> = 0.1273, wR <sub>2</sub> = 0.2422	R <sub>1</sub> = 0.1479, wR <sub>2</sub> = 0.0819
Largest diff. peak/hole / e Å <sup>-3</sup>	0.41/-0.58	1.59/-1.00	0.70/-0.70
CCDC access code	2208606	2208607	2208608



**Figure S1:** Ellipsoid representation of *fac*-[Tc(NPh)Cl<sub>3</sub>(PPh<sub>3</sub>)(CN<sup>*i*</sup>Bu)] · CH<sub>2</sub>Cl<sub>2</sub> (**2a**). The thermal ellipsoids are set at a 50% probability level. Hydrogen atoms are omitted for clarity. A number of 42 reflections below  $\theta_{\min}$  is missing due to the large unit cell and the data collection with the IPDS T2 measuring routine.

**Table S2:** Selected bond lengths (Å) and angles (°) in *fac*- [Tc(NPh)Cl<sub>3</sub>(PPh<sub>3</sub>)(CN<sup>*i*</sup>Bu)] · CH<sub>2</sub>Cl<sub>2</sub> (**2a**).

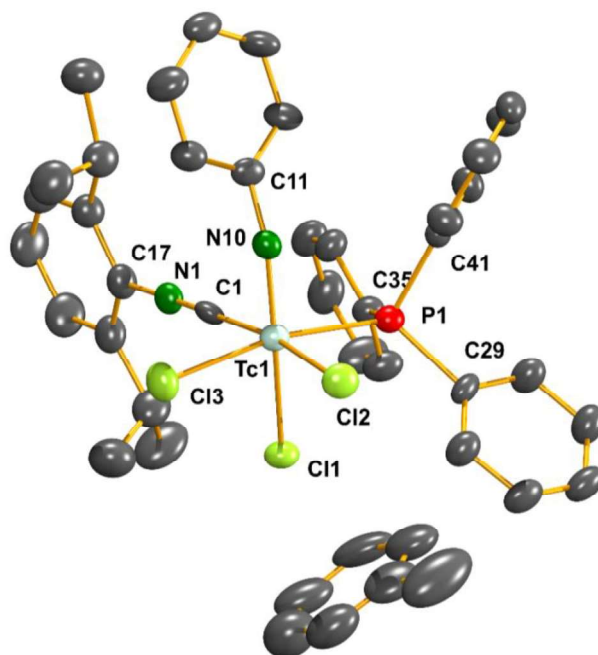
Tc1-Cl2	2.3909(6)	P1-C27	1.824(2)	Tc1-Cl3	2.4154(6)
Tc1-Cl1	2.4131(6)	P1-C33	1.819(2)	Tc1-N10	1.7114(18)
Tc1-P1	2.4602(6)	P1-C21	1.828(2)	Tc1-C1	2.057(2)
N10-C11	1.388(3)	C1-N1	1.133(3)	N1-C17	1.470(3)
Cl2-Tc1-Cl1	91.06(22)	Cl1-Tc1-P1	84.90(2)	C11-N10-Tc1	163.55(2)
Cl2-Tc1-P1	87.21(2)	Cl1-Tc1-Cl3	89.85(2)	C1-Tc1-P1	99.94(7)
Cl2-Tc1-Cl3	86.79(2)	Cl3-Tc1-P1	171.95(2)	N1-C1-Tc1	173.1(2)
C1-Tc1-Cl2	165.95(7)	C1-Tc1-Cl1	77.68(6)	C1-N1-C17	178.0(3)



**Figure S2.** Ellipsoid representation of *fac*-[Tc(NPh)Cl<sub>3</sub>(PPh<sub>3</sub>)(CNMes)] (**2b**). The thermal ellipsoids are set at a 50% probability level. Hydrogen atoms are omitted for clarity. A number of 16 reflections below  $\theta_{\min}$  is missing due to the large unit cell and the data collection with the IPDS T2 measuring routine.

**Table S3:** Selected bond lengths (Å) and angles (°) in *fac*- [Tc(NPh)Cl<sub>3</sub>(PPh<sub>3</sub>)(CNMes)] (**2b**).

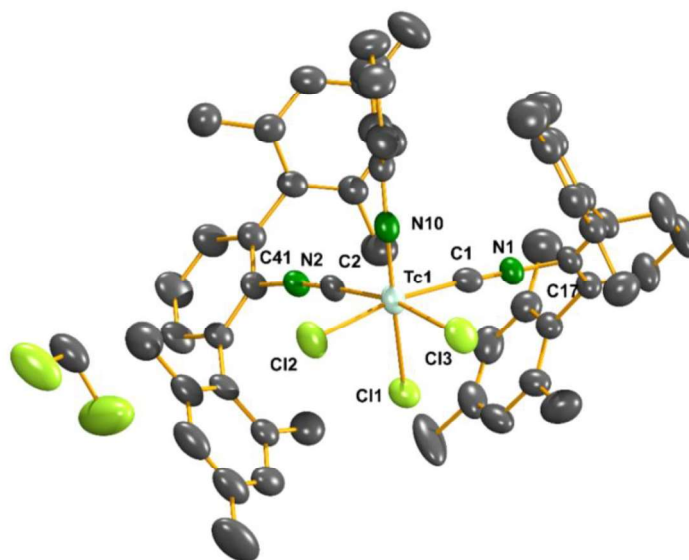
Tc1-Cl2	2.4033(6)	P1-C26	1.827(3)	Tc1-Cl3	2.4388(6)
Tc1-Cl1	2.3972(7)	P1-C32	1.820(2)	Tc1-N10	1.705(22)
Tc1-P1	2.4654(6)	P1-C26	1.827(3)	Tc1-C1	2.037(3)
N10-C11	1.382(3)	C1-N1	1.152(3)	N1-C17	1.403(3)
Cl2-Tc1-Cl1	93.88(3)	Cl1-Tc1-P1	84.00(2)	C11-N10-Tc1	164.51(2)
Cl2-Tc1-P1	88.00(2)	Cl2-Tc1-Cl3	88.31(2)	C1-Tc1-P1	92.33(7)
Cl1-Tc1-Cl3	88.78(2)	Cl3-Tc1-P1	171.65(2)	N1-C1-Tc1	177.3(2)
C1-Tc1-Cl2	174.06(7)	C1-Tc1-Cl1	80.26(7)	C1-N1-C17	173.7(3)



**Figure S3:** Ellipsoid representation of *fac*-[Tc(NPh)Cl<sub>3</sub>(PPh<sub>3</sub>)(CNPh<sup>*i*-prop<sup>2</sup></sup>)] · C<sub>7</sub>H<sub>8</sub> (**2c**). The thermal ellipsoids are set at a 50% probability level. Hydrogen atoms are omitted for clarity. A number of 11 reflections below  $\theta_{\min}$  is missing due to the large unit cell and the data collection with the IPDS T2 measuring routine. Flack parameter of the non-centrosymmetric structure: 0.06(6).

**Table S4:** Selected bond lengths (Å) and angles (°) in *fac*-[Tc(NPh)Cl<sub>3</sub>(PPh<sub>3</sub>)(CNPh<sup>*i*-prop<sup>2</sup></sup>)] (**2c**).

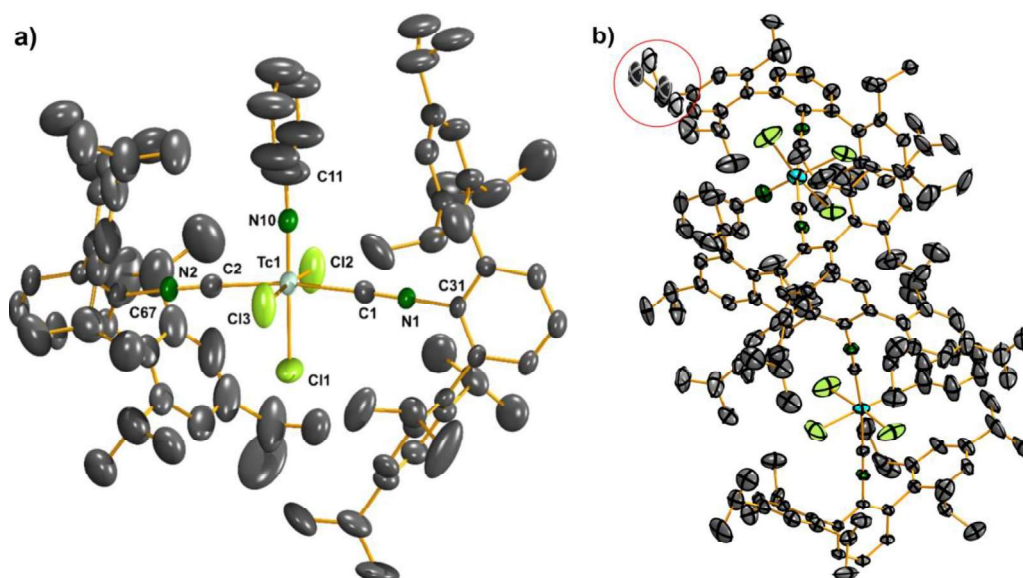
Tc1-Cl2	2.421(2)	P1-C41	1.834(9)	Tc1-Cl3	2.409(2)
Tc1-Cl1	2.413(2)	P1-C35	1.808(1)	Tc1-N10	1.725(6)
Tc1-P1	2.452(2)	P1-C29	1.854(9)	Tc1-C1	2.030(8)
N10-C11	1.374(1)	C1-N1	1.1834(1)	N1-C17	1.390(1)
Cl2-Tc1-Cl1	94.62(8)	Cl1-Tc1-P1	79.67(8)	C11-N10-Tc1	167.4(6)
Cl2-Tc1-P1	92.96(1)	Cl2-Tc1-Cl3	87.35(1)	C1-Tc1-P1	92.7(3)
Cl1-Tc1-Cl3	87.35(1)	Cl3-Tc1-P1	87.75(9)	N1-C1-Tc1	176.7(9)
C1-Tc1-Cl2	172.0(3)	C1-Tc1-Cl1	80.9(2)	C1-N1-C17	178.8(9)



**Figure S4:** Ellipsoid representation of *cis, fac*-[Tc(NPh)Cl<sub>3</sub>(CNAr<sup>Mes2</sup>)<sub>2</sub>] $\cdot$ CH<sub>2</sub>Cl<sub>2</sub> (**3**). The thermal ellipsoids are set at a 50% probability level. Hydrogen atoms are omitted for clarity. A number of 70 reflections below  $\theta_{\min}$  is missing due to the large unit cell and the data collection with the IPDS T2 measuring routine. Only one molecule of solvent CH<sub>2</sub>Cl<sub>2</sub> could be located. An overall number of 102 e<sup>-</sup> has been ‘removed’ from the large. Voids, which are contained in the structure, by a solvent mask using OLEX2 (Dolomanov, O.V., Bourhis, L.J., Gildea, R.J., Howard, J.A.K. & Puschmann, H. (2009), *J. Appl. Cryst.* 42, 339-341). This corresponds to approximately 2.5 more molecules of CH<sub>2</sub>Cl<sub>2</sub>.

**Table S5:** Selected bond lengths (Å) and angles (°) in *cis, fac*-[Tc(NPh)Cl<sub>3</sub>-CNAr<sup>Mes2</sup>]<sub>2</sub>  $\cdot$  CH<sub>2</sub>Cl<sub>2</sub> (**3**).

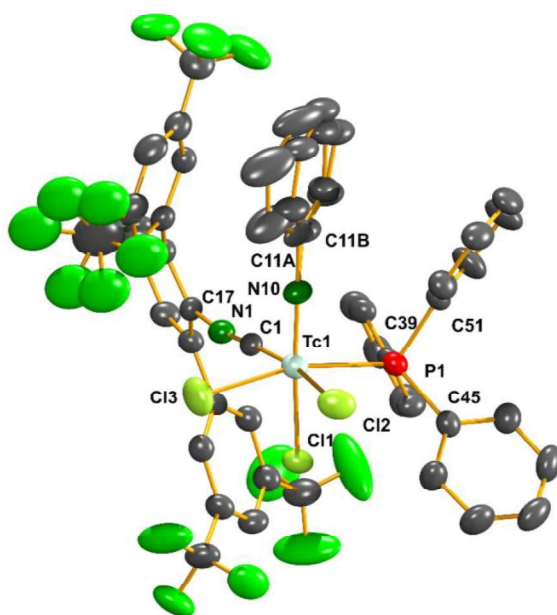
Tc1-Cl2	2.3909(1)	N1-C17	1.392(5)	Tc1-Cl3	2.3877(9)
Tc1-Cl1	2.4004(1)	N2-C41	1.1411(4)	Tc1-N10	1.699(3)
C2-N2	1.160(4)	Tc1-C2	2.034(3)	Tc1-C1	2.056(4)
N10-C11	1.380(4)	C1-N1	1.147(4)		
Cl2-Tc1-Cl1	87.70(9)	Cl1-Tc1-C2	86.41(2)	C11-N10-Tc1	176.9(6)
Cl2-Tc1-C2	92.21(1)	Cl2-Tc1-Cl3	174.04(9)	C1-Tc1-C2	171.7(2)
Cl1-Tc1-Cl3	86.40(9)	N2-C2-Tc1	175.4(4)	N1-C1-Tc1	177.9(5)
C1-Tc1-Cl2	88.65(1)	C1-Tc1-Cl1	85.38(2)	C1-N1-C31	179.3(6)



**Figure S5:** a) Ellipsoid representation of *trans,mer*-[Tc(NPh)Cl<sub>3</sub>(CNAr<sup>Tripp2</sup>)<sub>2</sub>] (**4b**). The thermal ellipsoids are set at a 50% probability level. Hydrogen atoms are omitted for clarity. A number of 70 reflections below  $\theta_{\min}$  is missing due to the large unit cell and the data collection with the IPDS T2 measuring routine. One carbon of an isopropyl group has an unusually large ellipsoid due to an elongation of the distal isopropyl moieties. A solvent accessible void is caused by the molecular packing and does not contain any substantial residual electron density. b) Visualization of the disorder found for one of the isopropyl groups in the two crystallographically independent species of these large molecules.

**Table S6:** Selected bond lengths (Å) and angles (°) in *trans,mer*-[Tc(NPh)Cl<sub>3</sub>-CNAr<sup>Tripp2</sup>]<sub>2</sub>] (**4b**).

Tc1-Cl2	2.3933(2)	N1-C1	1.150(6)	Tc1-Cl3	2.3946(2)
Tc1-Cl1	2.3470(2)	N2-C67	1.1416(6)	Tc1-N10	1.714(5)
C2-N2	1.139(6)	Tc1-C2	2.097(5)	Tc1-C1	2.076(5)
N10-C11	1.361(1)	N1-C31	1.409(6)		
Cl2-Tc1-Cl1	87.70(9)	Cl1-Tc1-C2	86.41(2)	C11-N10-Tc1	176.9(6)
Cl2-Tc1-C2	92.21(1)	Cl2-Tc1-Cl3	174.04(9)	C1-Tc1-C2	171.7(2)
Cl1-Tc1-Cl3	86.40(9)	N2-C2-Tc1	175.4(4)	N1-C1-Tc1	177.9(5)
C1-Tc1-Cl2	91.69(1)	C1-Tc1-Cl1	85.38(2)	C1-N1-C31	179.3(6)

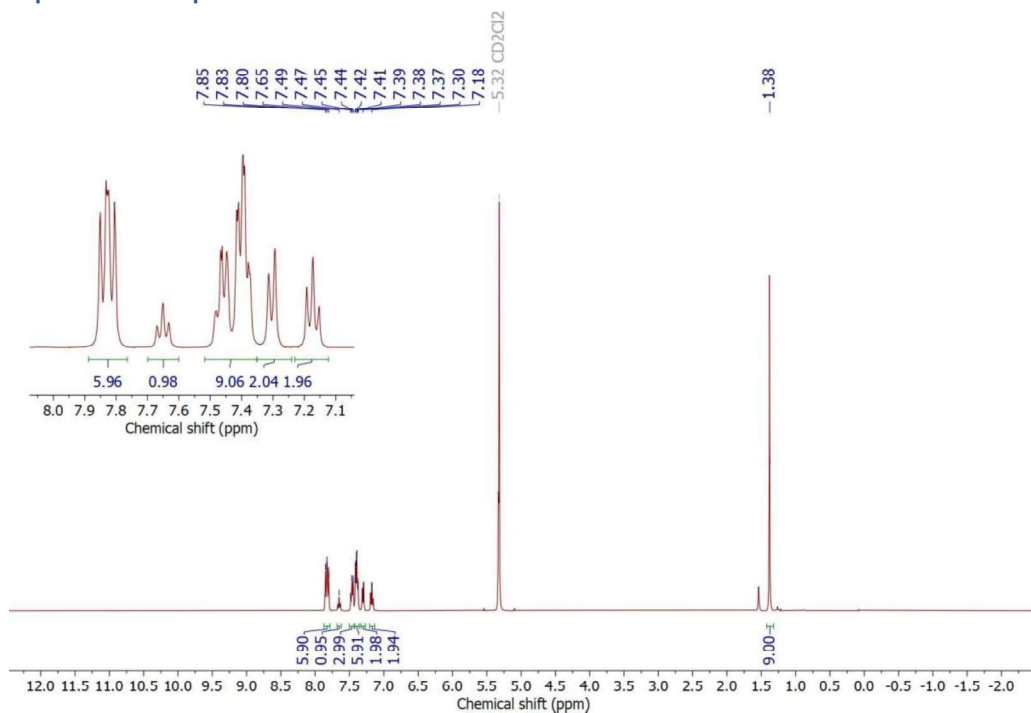


**Figure S6:** Ellipsoid representation of *fac*-[Tc(NPh)Cl<sub>3</sub>(PPh<sub>3</sub>)(CN*p*-FAr<sup>DarF2</sup>)] (**5**). The thermal ellipsoids are set at a 50% probability level. Hydrogen atoms are omitted for clarity. The ratio of unique to observed reflections is too low leading to a B alert. This is due to the measurement routine of the IPDS 2T.

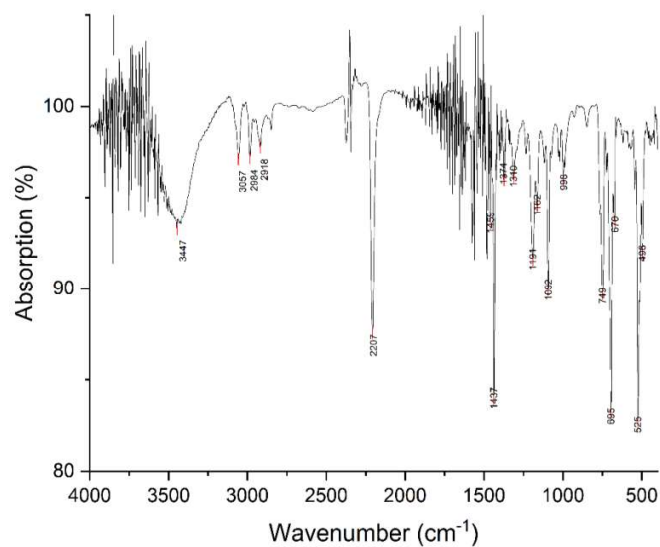
**Table S7:** Selected bond lengths (Å) and angles (°) in *fac*-[Tc(NPh)Cl<sub>3</sub>(PPh<sub>3</sub>)(CN*p*-FAr<sup>DarF2</sup>)] (**5**).

Tc1-Cl2	2.4338(2)	P1-C45	1.821(5)	Tc1-Cl3	2.3890(2)
Tc1-Cl1	2.3977(2)	P1-C39	1.793(5)	Tc1-N10	1.710(4)
Tc1-P1	2.4423(2)	P1-C51	1.812(5)	Tc1-C1	2.009(5)
N10-C11A	1.395(1)	C1-N1	1.176(6)	N1-C17	1.401(6)
Cl2-Tc1-Cl1	96.17(5)	Cl1-Tc1-P1	90.42(5)	C11A-N10-Tc1	168.3(1)
Cl2-Tc1-P1	77.65(5)	Cl2-Tc1-Cl3	86.94(6)	C1-Tc1-P1	94.83(2)
Cl1-Tc1-Cl3	87.80(6)	Cl3-Tc1-P1	164.21(6)	N1-C1-Tc1	174.9(5)
C1-Tc1-Cl2	78.68(2)	C1-Tc1-Cl1	171.66(2)	C1-N1-C17	172.0(5)

## Spectroscopic data

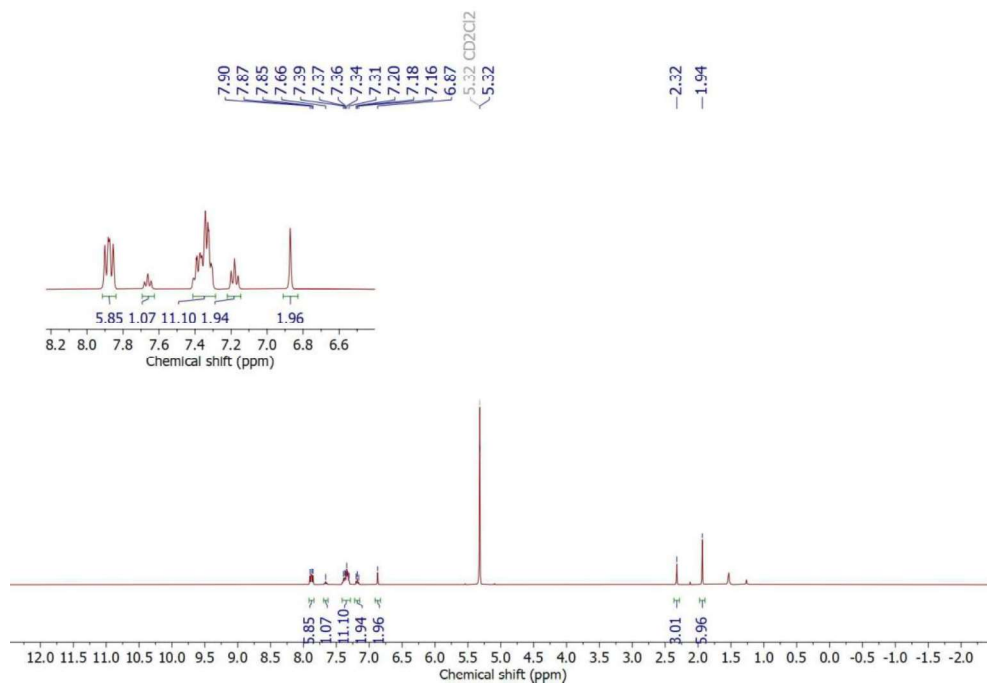


**Figure S7:**  $^1\text{H}$  NMR spectrum of *fac*-[Tc(NPh)Cl<sub>3</sub>(PPh<sub>3</sub>)(CN<sup>t</sup>Bu)] (**2a**) in CD<sub>2</sub>Cl<sub>2</sub>.

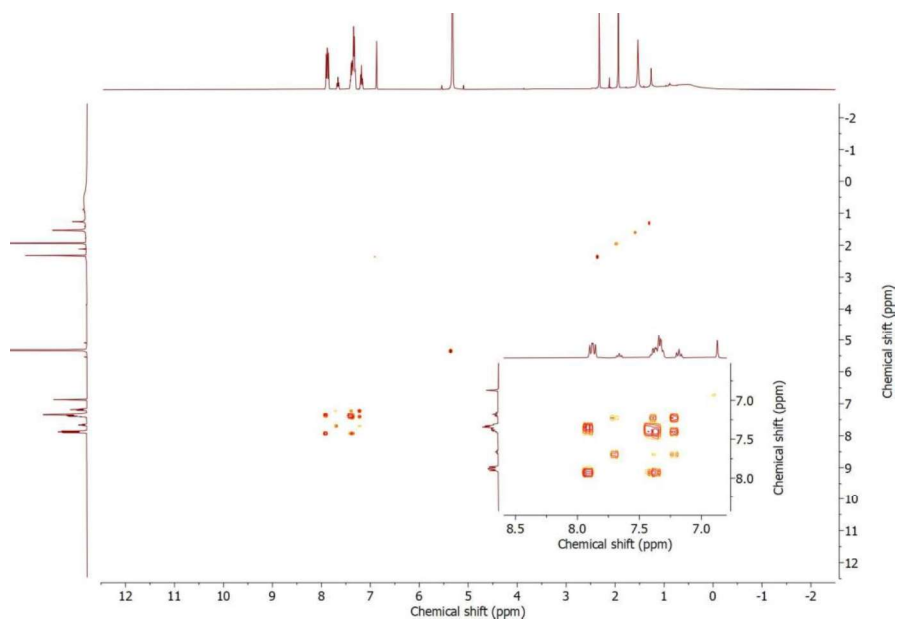


**Figure S8:** IR (KBr) spectrum of *fac*-[Tc(NPh)Cl<sub>3</sub>(PPh<sub>3</sub>)(CN<sup>t</sup>Bu)] (**2a**).

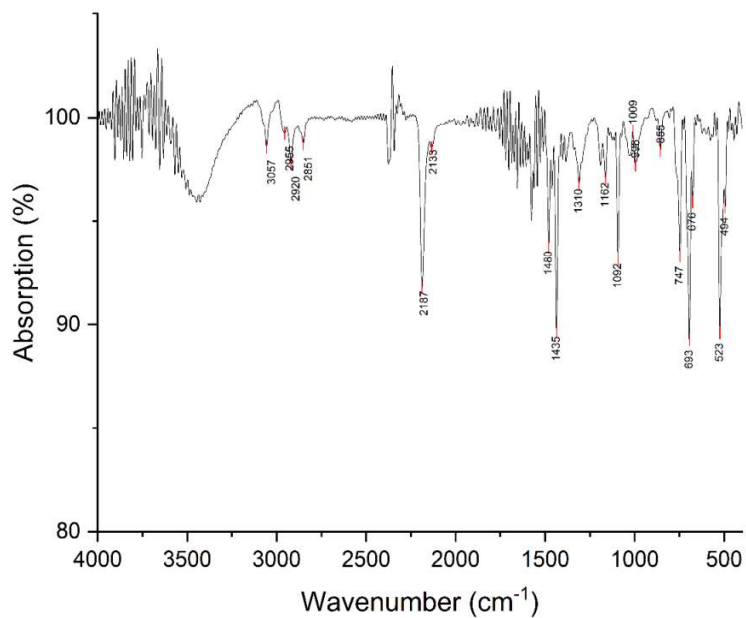




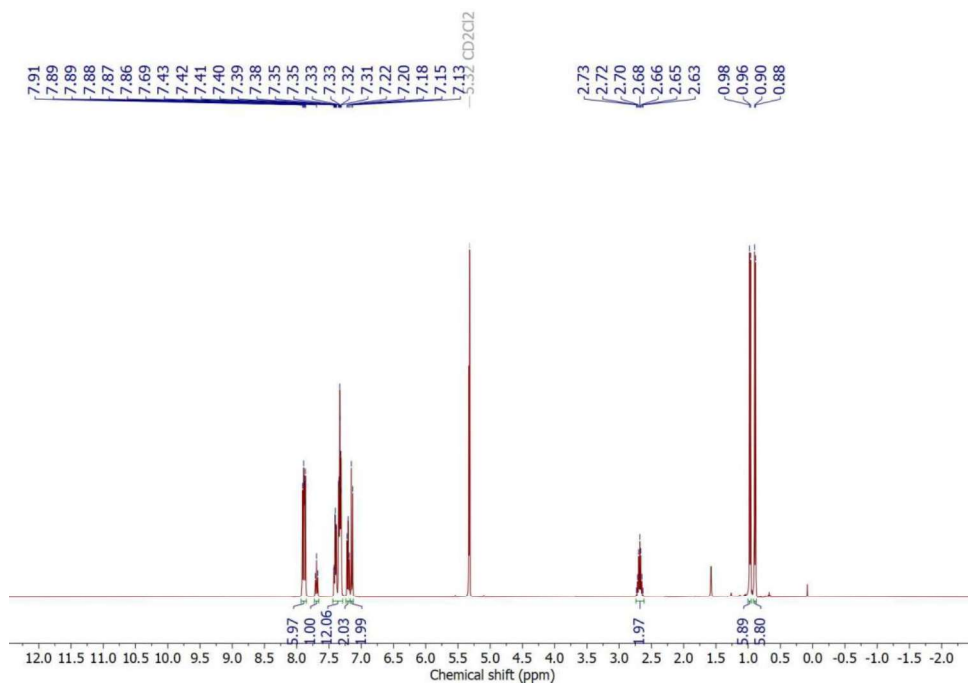
**Figure S9:**  $^1\text{H}$  NMR spectrum of *fac*-[Tc(NPh)(PPh<sub>3</sub>)(CNMes)Cl<sub>3</sub>] (**2b**) in CD<sub>2</sub>Cl<sub>2</sub>.



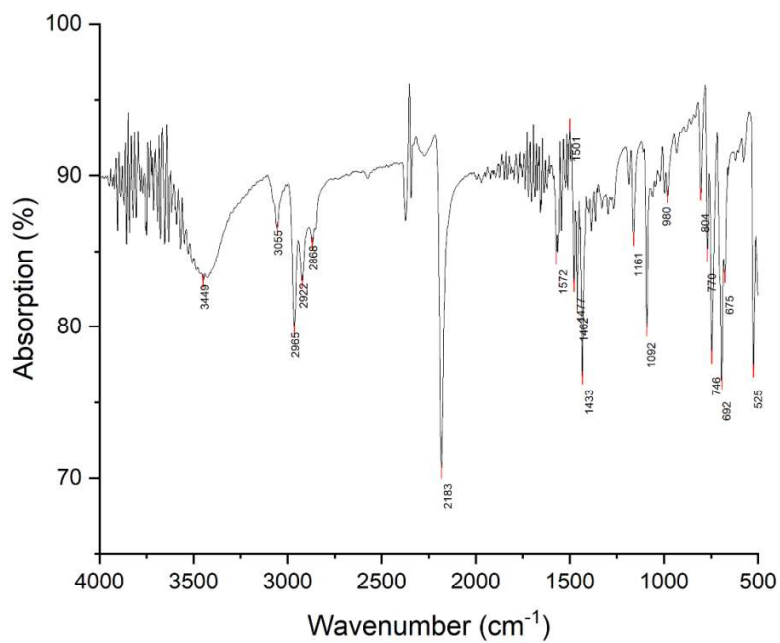
**Figure S10:**  $^1\text{H}, ^1\text{H}$  COSY NMR spectrum of *fac*-[Tc(NPh)(PPh<sub>3</sub>)(CNMes)Cl<sub>3</sub>] (**2b**) in CD<sub>2</sub>Cl<sub>2</sub>.



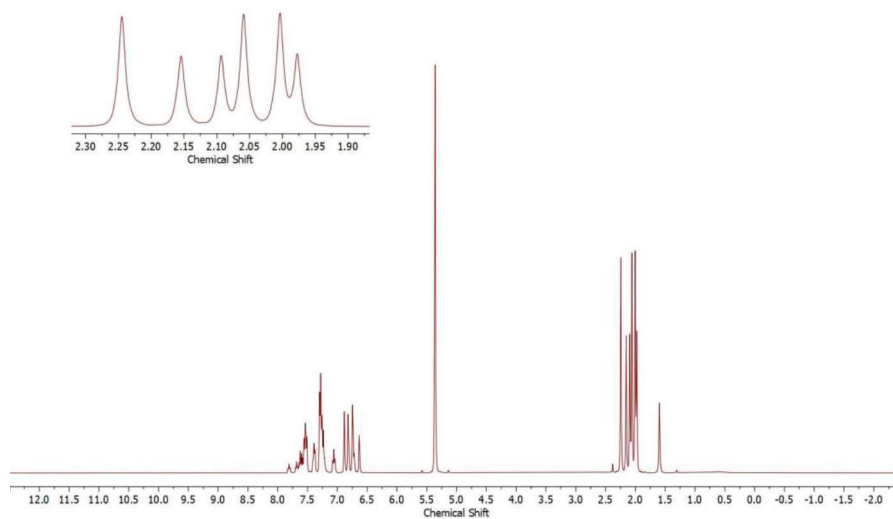
**Figure S11:** IR (KBr) spectrum of *fac*-[Tc(NPh)(PPh<sub>3</sub>)(CNMes)Cl<sub>3</sub>] (**2b**).



**Figure S12:** <sup>1</sup>H NMR spectrum of *fac*-[Tc(NPh)Cl<sub>3</sub>(PPh<sub>3</sub>)(CNPh<sup>i-prop2</sup>)] (**2c**) in CD<sub>2</sub>Cl<sub>2</sub>.



**Figure S13:** IR (KBr) spectrum of *fac*-[Tc(NPh)Cl<sub>3</sub>(PPh<sub>3</sub>)(CNPh<sup>*i-prop*</sup>2)] (**2c**).



**Figure S14:** <sup>1</sup>H NMR spectrum of isomers of *fac*-[Tc(NPh)Cl<sub>3</sub>(PPh<sub>3</sub>)(CNAr<sup>Mes</sup>2)] (**3a**) in CD<sub>2</sub>Cl<sub>2</sub>.

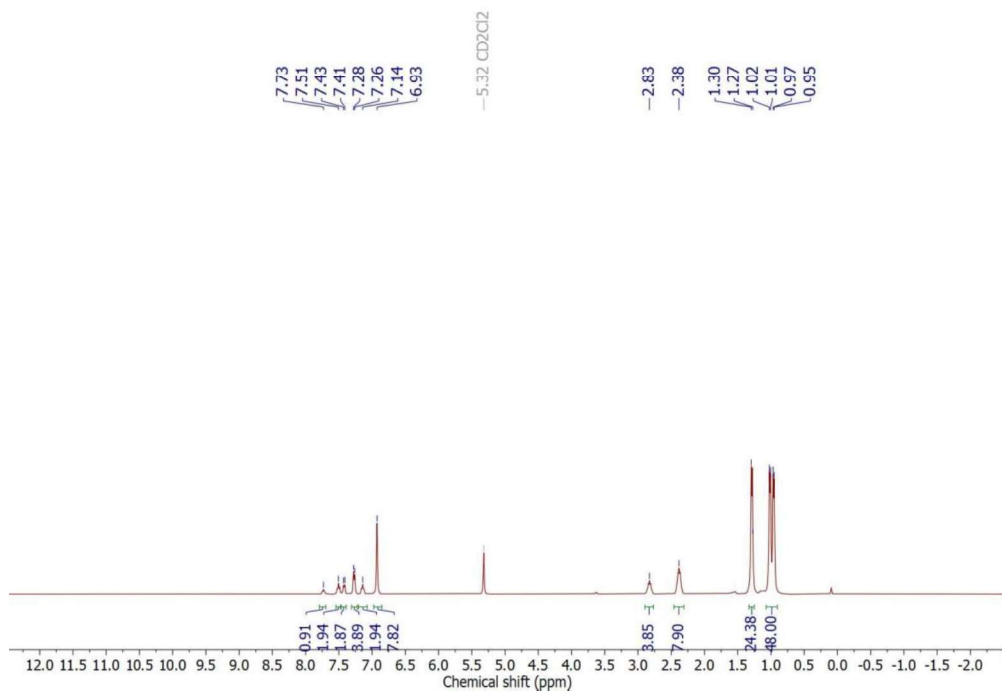


Figure S15:  $^1\text{H}$  NMR spectrum of *trans,mer*-[Tc(NPh)Cl<sub>3</sub>(CNAr<sup>Tripp2</sup>)<sub>2</sub>] (**4b**) in CD<sub>2</sub>Cl<sub>2</sub>.

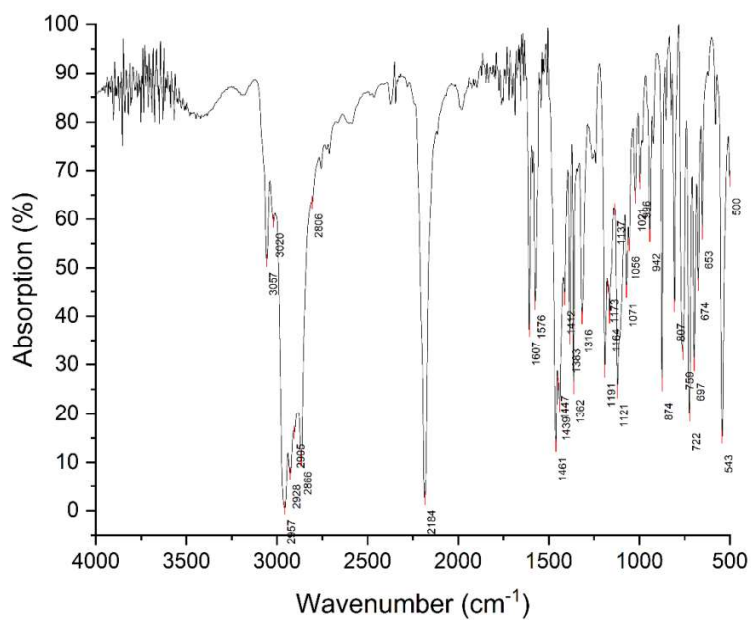
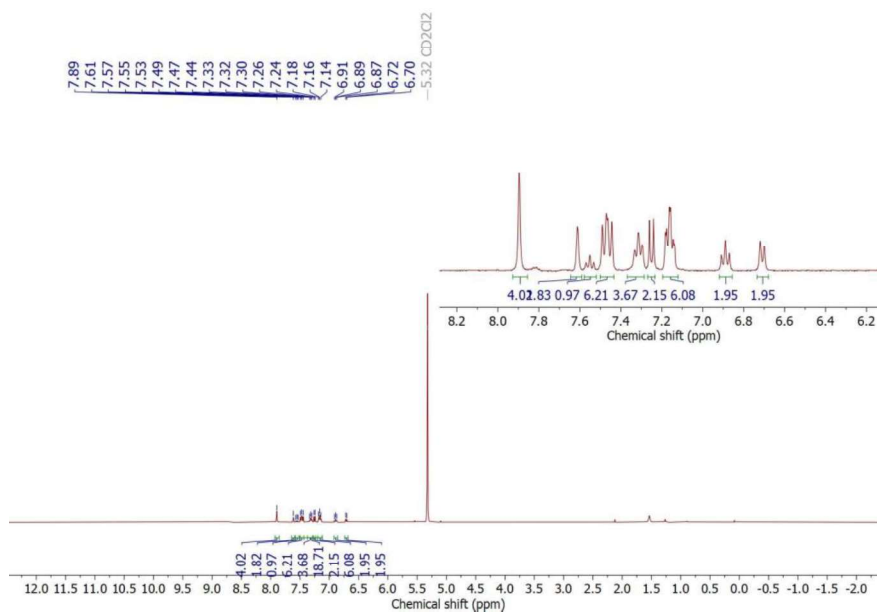
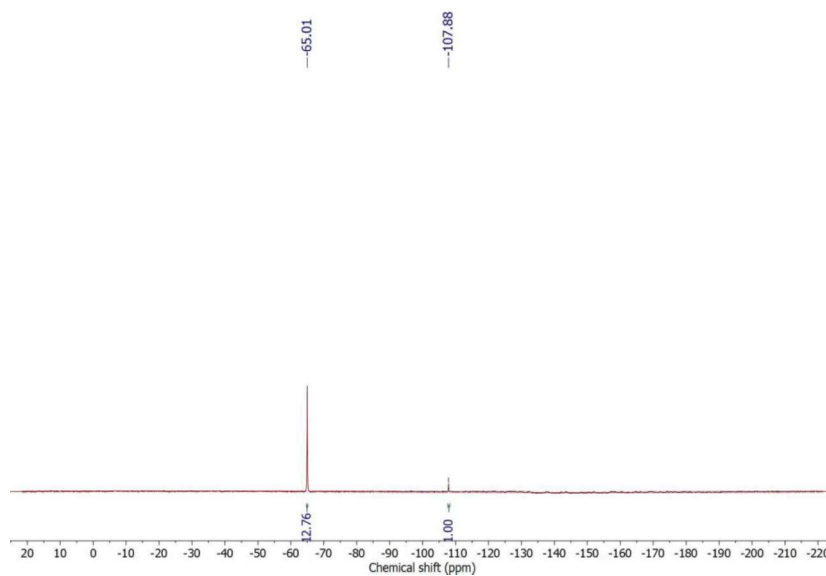


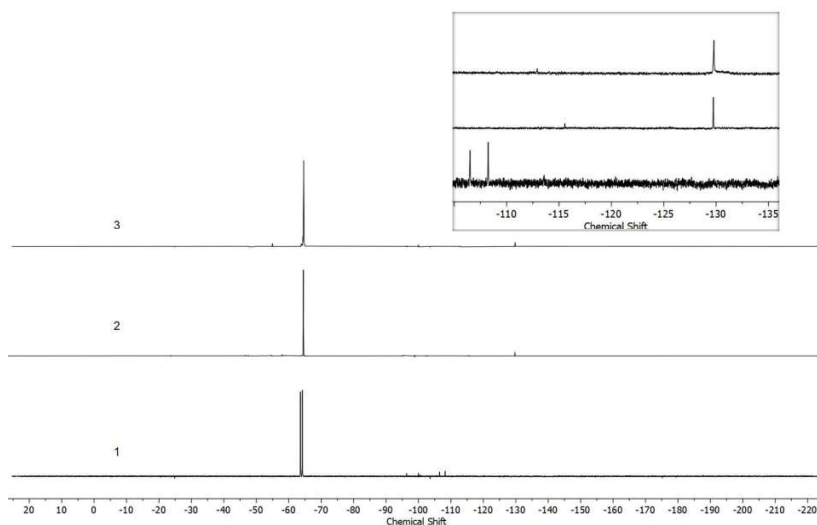
Figure S16: IR (KBr) spectrum of *trans,mer*-[Tc(NPh)(CNAr<sup>Tripp2</sup>)Cl<sub>3</sub>] (**4b**).



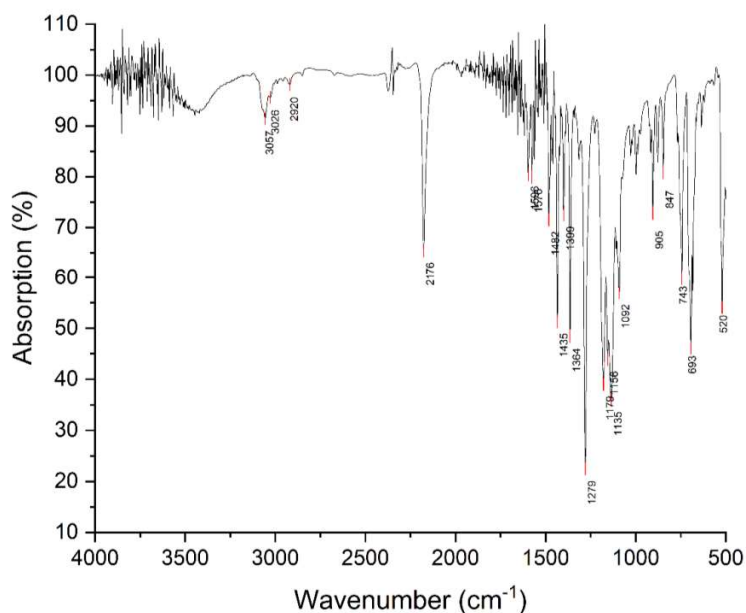
**Figure S17:**  $^1\text{H}$  NMR spectrum of *fac*-[Tc(NPh)Cl<sub>3</sub>(PPh<sub>3</sub>)(CNp-FAR<sup>DarF2</sup>)] (**5**) in CD<sub>2</sub>Cl<sub>2</sub>.



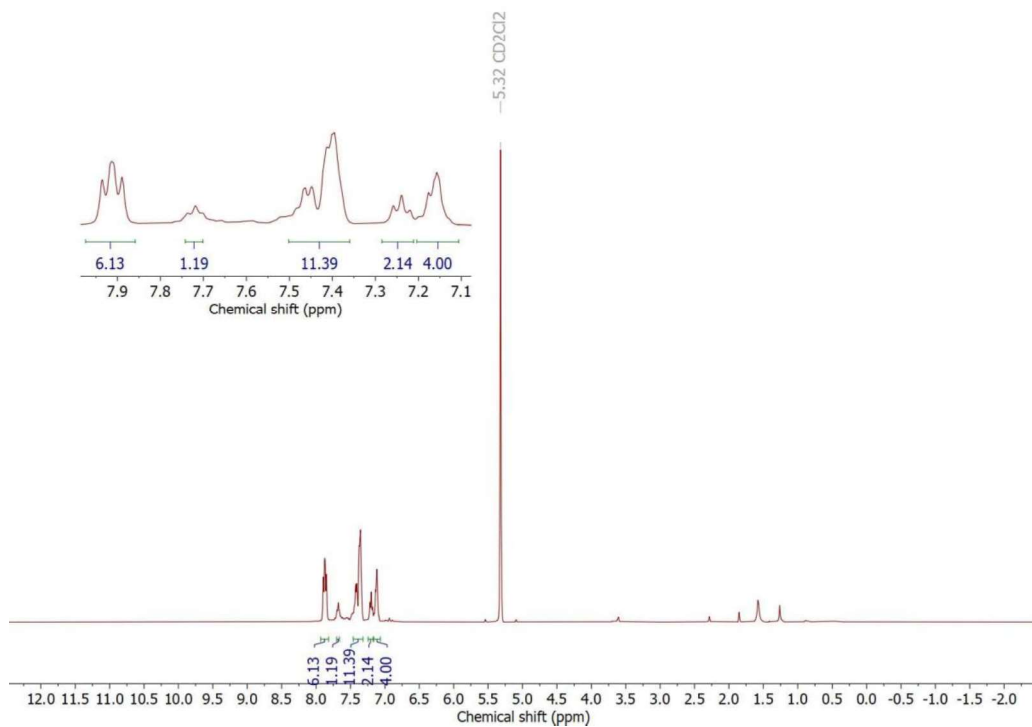
**Figure S18:**  $^{19}\text{F}$  NMR spectrum of *fac*-[Tc(NPh)Cl<sub>3</sub>(PPh<sub>3</sub>)(CNp-FAR<sup>DarF2</sup>)] (**5**) in CD<sub>2</sub>Cl<sub>2</sub>.



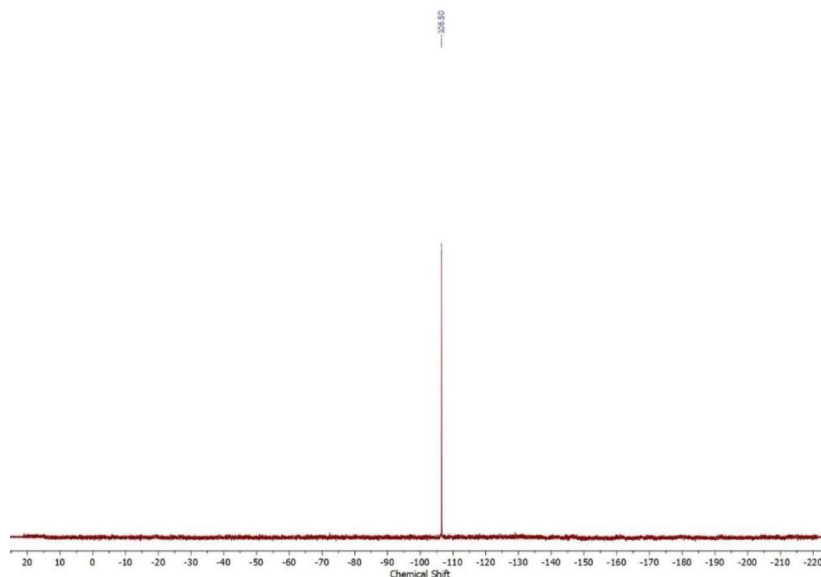
**Figure S19:**  $^{19}\text{F}$  NMR spectra recorded during the reaction of *fac*-[Tc(NPh)Cl<sub>3</sub>(PPh<sub>3</sub>)(CNp-FAr<sup>DarF2</sup>)] (**5**) with CNp-FAr<sup>DarF2</sup> in THF. Spectrum 1 was recorded after the addition of one equivalent of CNp-FAr<sup>DarF2</sup> to **5**. Spectrum 2 was recorded after heating the previously obtained solution for 10 min in boiling THF. Spectrum 3 was recorded after heating a solution of complex **5** for 10 min in boiling THF.



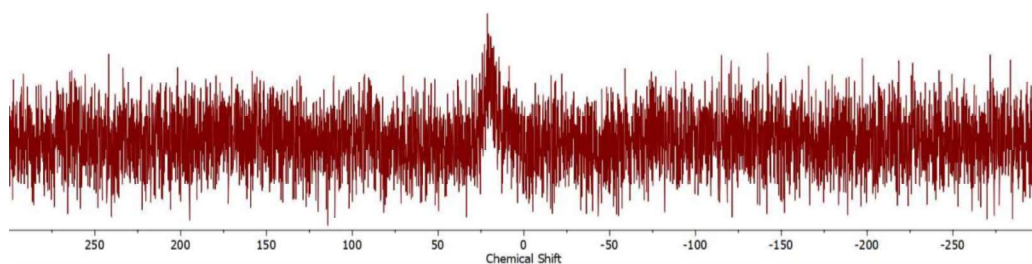
**Figure S20:** IR (KBr) spectrum of *fac*-[Tc(NPh)Cl<sub>3</sub>(PPh<sub>3</sub>)(CNp-FAr<sup>DarF2</sup>)] (**5**).



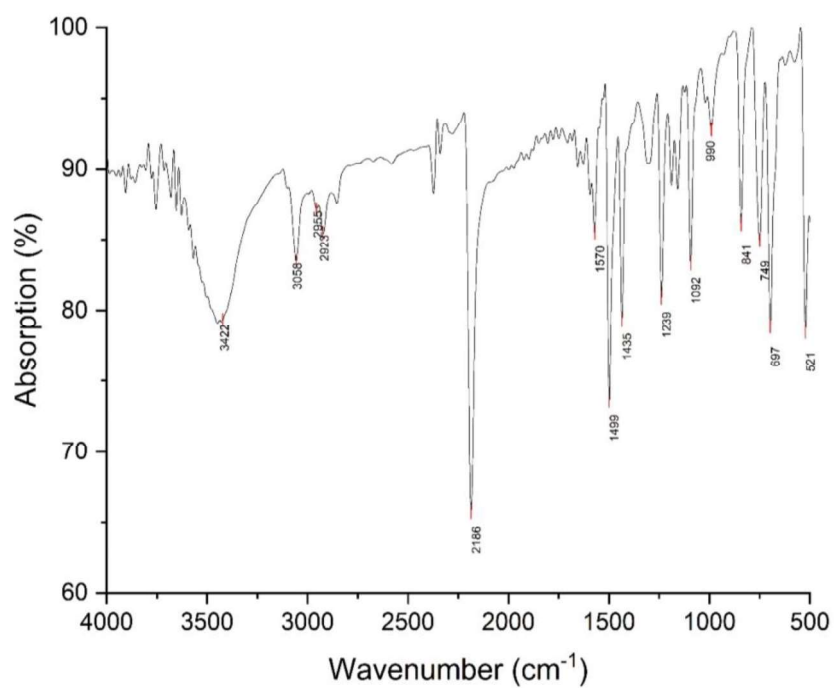
**Figure S21:**  $^1\text{H}$  NMR spectrum of  $\text{fac-}[\text{Tc}(\text{NPh})\text{Cl}_3(\text{PPh}_3)(\text{CNPh}^{\text{pF}})]$  (**6**) in  $\text{CD}_2\text{Cl}_2$ .



**Figure S22:**  $^{19}\text{F}$  NMR spectrum of  $\text{fac-}[\text{Tc}(\text{NPh})\text{Cl}_3(\text{PPh}_3)(\text{CNPh}^{\text{pF}})]$  (**6**) in  $\text{CD}_2\text{Cl}_2$ .

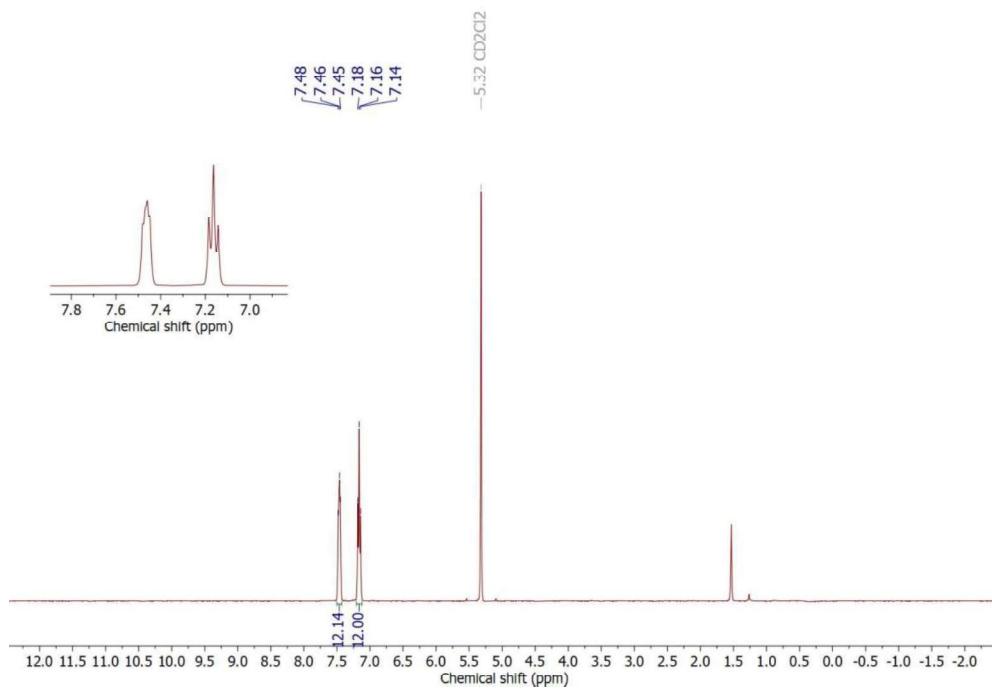


**Figure S23:**  $^{31}\text{P}\{^1\text{H}\}$  NMR spectrum of *fac*-[Tc(NPh)Cl<sub>3</sub>(PPh<sub>3</sub>)(CNPh<sup>PF</sup>)] (**6**) in CD<sub>2</sub>Cl<sub>2</sub>.

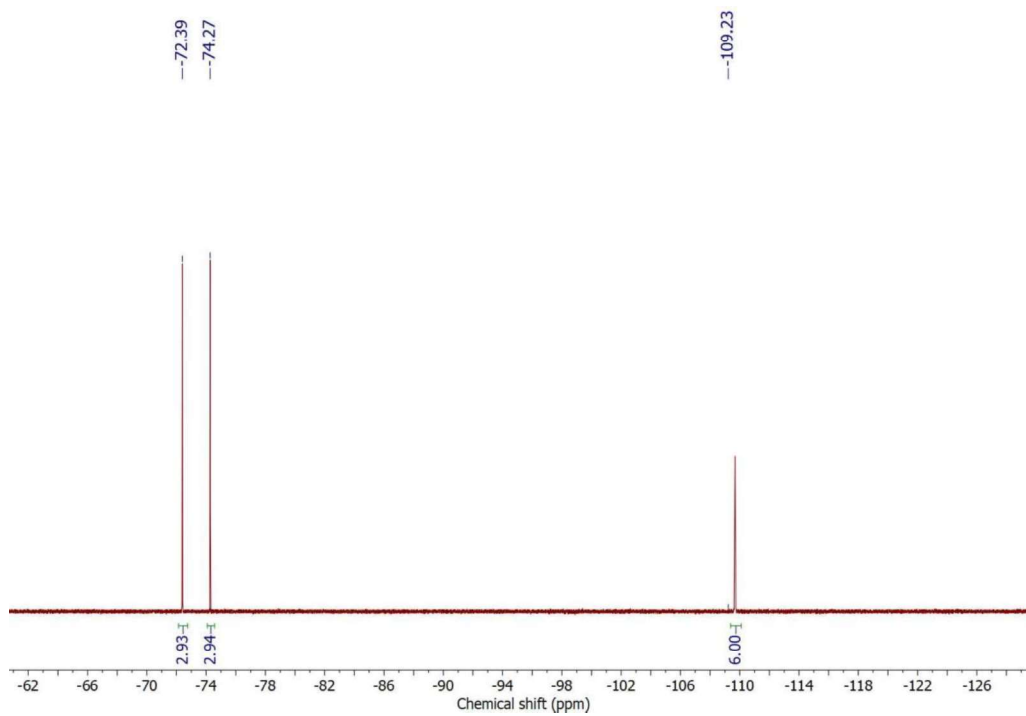


**Figure S24:** IR (KBr) spectrum of *fac*-[Tc(NPh)Cl<sub>3</sub>(PPh<sub>3</sub>)(CNPh<sup>PF</sup>)] (**6**).

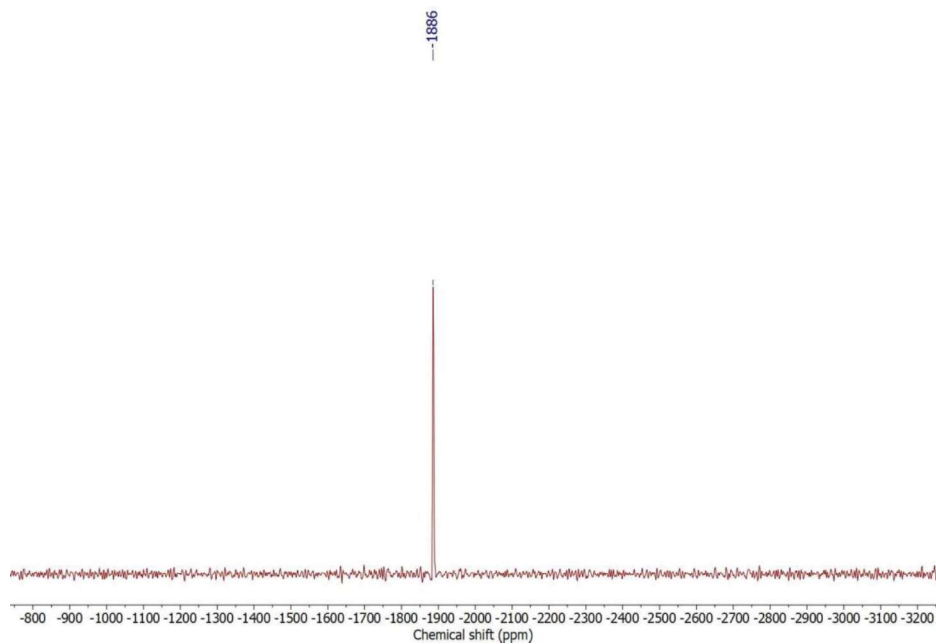




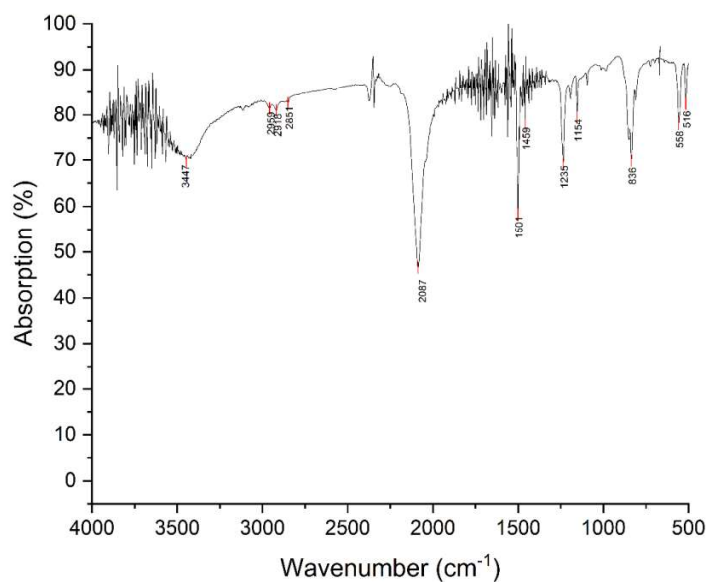
**Figure S25:**  $^1\text{H}$  NMR spectrum of *fac*-[Tc(CNPh<sup>pF</sup>)<sub>6</sub>][PF<sub>6</sub>] (**7**) in CD<sub>2</sub>Cl<sub>2</sub>.



**Figure S26:**  $^{19}\text{F}$  NMR spectrum of [Tc(CNPh<sup>pF</sup>)<sub>6</sub>][PF<sub>6</sub>] (**7**) in CD<sub>2</sub>Cl<sub>2</sub>.



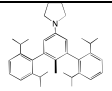


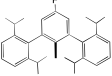

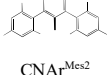
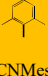
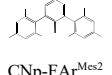
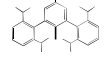
**Figure S27:**  $^{99}\text{Tc}$  NMR spectrum of  $[\text{Tc}(\text{CNPh}^{\text{PF}})_6][\text{PF}_6]$  (**7**) in  $\text{CD}_2\text{Cl}_2$ .


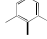


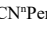

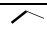

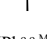

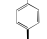
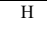
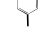
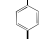



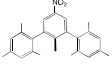
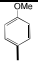

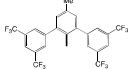
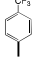
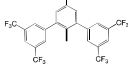
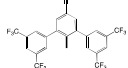

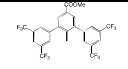
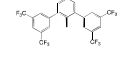
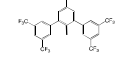
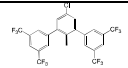
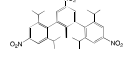
**Figure S28:** IR (KBr) spectrum of  $[\text{Tc}(\text{CNPh}^{\text{PF}})_6][\text{PF}_6]$  (**7**).

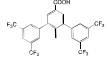
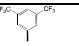
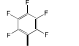
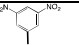
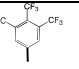
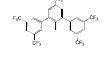
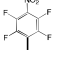
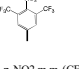
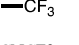
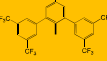
## DFT Calculations

**Table S8.** Calculated electrostatic potential surface properties of the isocyanide carbon atom at the Van der Waals (VdW) boundary for structures optimized at the B3LYP/6-311++G\*\* level. Surface properties were evaluated at  $\rho = 0.001$  level using an electrostatic potential map basis with a grid-point spacing of 0.25. The last column contains the Surface-Averaged Donor Atom Potential SADAP =  $(EP_{\min} + EP_{\max} + AP)/(ES_{\text{pos}} + ES_{\text{neg}})$  as a combined descriptor of steric and electrostatic properties of the potential ligands, which allows an estimation of their reactivity.

CN-R	Exposed VdW surface, ES (Å <sup>2</sup> )		Extrema for potential energies at VdW surface, EP (kcal/mol)		Average potential energies at VdW surface, AP (kcal/mol)	Surface-averaged donor atom potential SADAP, (kcal/mol Å <sup>2</sup> )
	ES <sub>pos</sub>	ES <sub>neg</sub>	EP <sub>min</sub>	EP <sub>max</sub>	$\bar{\phi}_{\text{overall}}$	SADAP
 CNAr <sup>Dipp</sup> NC4H8	0.00	21.81	-42.74	-15.96	-31.70	-4.15
 TRIP	0.00	22.23	-38.01	-9.31	-26.65	-3.33
 CNAr <sup>Dipp2</sup>	0.00	22.13	-37.64	-8.87	-26.04	-3.28
 CNp-FAr <sup>Dipp2</sup>	0.00	22.14	-36.22	-7.19	-24.42	-3.06
 CNPh <sup>i-prop2</sup>	0.00	25.99	-35.47	-5.16	-21.20	-2.38
 CNAr <sup>Mes2</sup>	0.00	30.10	-39.20	-7.01	-25.11	-2.37
 CNMes	0.00	28.89	-36.79	-6.83	-21.68	-2.26
 CNp-FAr <sup>Mes2</sup>	0.00	30.13	-37.67	-5.04	-23.31	-2.19
 CNp-NO <sub>2</sub> Ar <sup>Dipp2</sup>	0.01	22.81	-31.40	0.48	-18.83	-2.18

	CN <sup>t</sup> Bu	0.00	31.43	-39.63	-5.86	-22.00	-2.15
	CNPh <sup>o,o-Me2</sup>	0.00	28.80	-35.60	-5.35	-20.34	-2.13
	CNCy	0.00	31.61	-39.23	-5.09	-21.81	-2.09
	CN <sup>n</sup> Hex	0.00	31.61	-38.62	-5.69	-21.48	-2.08
	CN <sup>n</sup> Pent	0.00	31.58	-38.60	-5.67	-21.45	-2.08
	CN <sup>n</sup> Bu	0.00	31.58	-38.51	-5.52	-21.36	-2.07
	CN <sup>n</sup> Pr	0.00	31.57	-38.37	-5.51	-21.23	-2.06
	CNEt	0.00	31.62	-38.06	-5.17	-20.98	-2.03
	CNMe	0.00	31.52	-37.41	-6.01	-20.50	-2.03
	CNPh <sup>o,o-Me2,p-F</sup>	0.00	28.79	-33.68	-2.45	-18.02	-1.88
	MIBI	0.02	29.07	-35.96	2.30	-18.65	-1.80
	CNPh <sup>p-Me</sup>	0.01	31.24	-35.69	0.94	-18.57	-1.71
H	CNH	0.00	31.12	-31.48	-4.62	-16.42	-1.69
	CNPh <sup>p-NMe2</sup>	0.16	31.28	-36.06	2.15	-18.61	-1.67
	CNPh <sup>p-CCH</sup>	0.15	30.08	-34.98	1.79	-17.21	-1.67
	CNPh	0.05	31.28	-35.20	1.72	-18.01	-1.64

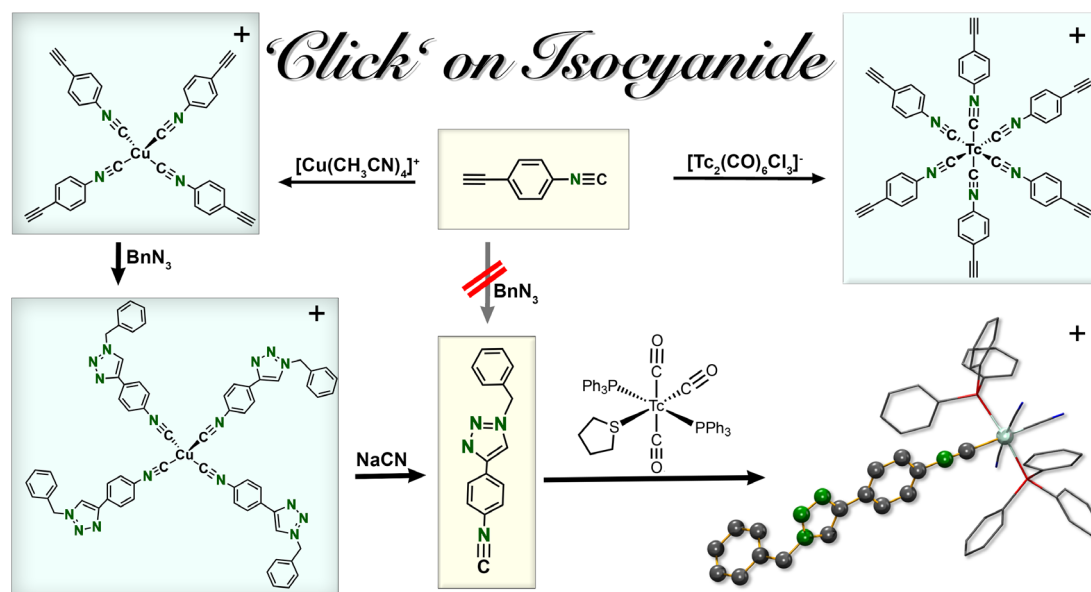
	0.17	29.91	-32.56	2.46	-17.50	-1.58
	0.43	30.95	-34.17	4.50	-16.60	-1.47
	1.67	29.53	-32.02	7.05	-14.10	-1.25
	1.87	26.11	-30.32	9.17	-13.34	-1.23
	1.86	29.19	-31.18	6.80	-13.37	-1.22
	3.43	24.42	-29.04	10.22	-11.95	-1.10
	4.52	23.37	-28.26	11.17	-11.03	-1.01
	6.15	24.86	-28.59	9.44	-10.27	-0.95
	5.45	22.34	-27.45	12.53	-10.13	-0.90
	5.61	22.28	-27.38	12.50	-10.03	-0.89
	5.61	22.34	-27.42	12.53	-10.04	-0.89
	5.74	22.15	-27.30	12.92	-9.96	-0.87
	4.92	18.14	-23.28	12.74	-8.26	-0.81

	6.74	21.13	-26.39	14.75	-8.89	-0.74
	8.23	22.96	-27.55	14.48	-8.68	-0.70
	9.36	21.48	-25.27	14.24	-7.07	-0.59
	12.09	19.09	-23.33	14.43	-4.67	-0.44
	11.49	19.44	-24.62	17.89	-5.28	-0.39
	10.54	17.20	-22.73	18.30	-4.73	-0.33
	12.46	18.27	-22.28	18.10	-3.77	-0.26
	14.33	17.03	-21.39	17.29	-2.32	-0.20
	15.06	15.57	-19.94	16.88	-0.94	-0.13
CO	19.29	10.31	-12.49	12.42	3.35	0.11
	20.50	6.74	-11.49	69.07	16.88	2.73

**Table S9.**  $LP_C/\pi^*_{CN}$  properties of some representative, free isocyanides, number of donated  $\sigma_{CTC}$  electrons ( $\#e^-$ ;  $LP_C \rightarrow LP^*_{TC}$ ) and second order perturbation parameters (interaction energy  $E$ ; energy difference between the two orbitals  $E_i - E_j$ ; overlap parameter  $A$ ) for  $LP_{TC} \rightarrow \pi^*_{CN}$  in the model complexes  $[TcO_3(CO/CNR)]^+$  and  $[Tc(CO)_5(CO/CNR)]^+$  ( $R = Ph^{F5}, Ph^{p-F}, Ph, ^tBu, Ar^{DArF2}$ ).

L	$\pi^*_{CN}$	$LP_C$	$\Delta(\pi^*_{CN} - LP_C)$	[TcO <sub>3</sub> (L)] <sup>+</sup>		[Tc(CO) <sub>5</sub> (L)] <sup>+</sup>		
				$\#e^-/\sigma_{CTC}$	$\#e^-/\sigma_{CTC}$	$E(LP_{TC} \rightarrow \pi^*_{CN})$ [kJ/mol]	$E_i - E_j$ [a.u.]	$A$
CNAI <sup>Dipp2</sup>	-1.53	-8.48	6.95					
CN <sup>t</sup> Bu	2.74	-11.15	13.89	1.9029	1.8910	8.37/8.37	0.32/0.32	0.049/0.049
CNPh	2.20	-11.59	13.80	1.9033	1.8923	9.00/9.06	0.31/0.31	0.050/0.049
CNPh <sup>p-F</sup>	2.04	-11.72	13.76	1.9035	1.8927	9.13/9.17	0.31/0.31	0.050/0.051
CNPh <sup>F5</sup>	1.48	-12.36	13.84	1.9076	1.8947	10.64/10.62	0.30/0.30	0.054/0.052
CNAI <sup>DArF2</sup>	103.58	-12.18	115.76	1.9022	1.8919	9.49/9.55	0.31/0.31	0.052/0.050
CO	-1.16	-10.55	9.39	1.9364	1.9111	13.81/13.81	0.28/0.28	0.059/0.059

## 5.5. Technetium Complexes with an Isocyano-Alkyne Ligand and its Reaction Products



Claude, G.; Puccio, D.; Roca Jungfer, M; Hagenbach, A.; Spreckelmeyer, S.; Abram, U. *Inorg. Chem.*, **2023**, *submitted*.

This document is the unedited Author's version of a Submitted Work that was subsequently accepted for publication in *Inorg. Chem.*, copyright © 2023 American Chemical Society after peer review. To access the final edited and published work see [10.1021/acs.inorgchem.3c01638](https://doi.org/10.1021/acs.inorgchem.3c01638).

### Author Contributions:

Guilhem Claude, Ulrich Abram designed the project. Guilhem Claude performed the synthesis and characterization of the compounds and wrote a draft of the manuscript. Maximilian Roca Jungfer performed DFT calculations. Guilhem Claude and Adelheid Hagenbach calculated the X-ray structures. Sarah Spreckelmeyer performed experiments with  $^{99\text{m}}\text{Tc}$ . Denis Puccio performed some of the experiments during a research internship under the supervision of Guilhem Claude. Ulrich Abram wrote the final draft, supervised the project, provided scientific guidance and suggestions.



# Tchnetium complexes with an isocyano-alkyne ligand and its reaction products

Guilhem Claude,<sup>§</sup> Denis Puccio,<sup>§</sup> Maximilian Roca Jungfer,<sup>§</sup> Adelheid Hagenbach,<sup>§</sup> Sarah Spreckelmeyer<sup>†</sup> and Ulrich Abram<sup>§\*</sup>

<sup>§</sup> Freie Universität Berlin, Institute of Chemistry and Biochemistry, Fabeckstr. 34/36, 14195 Berlin, Germany

<sup>†</sup> Charité - Universitätsmedizin Berlin, corporate member of Freie Universität Berlin, Humboldt-Universität zu Berlin, and Berlin Institute of Health, Department of Nuclear Medicine, Augustenburger Platz 1, 13353, Berlin

\*Corresponding author

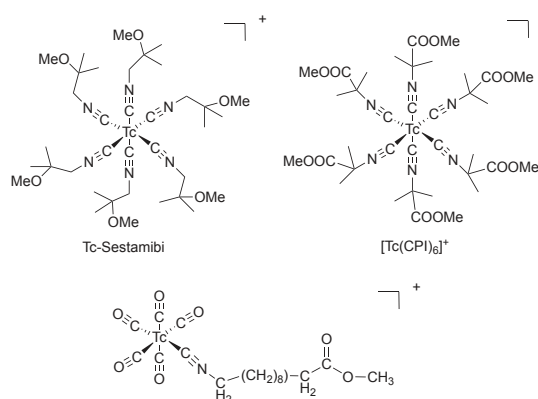
## Supporting Information Placeholder

**ABSTRACT.** The attachment of an ethyne substituent in *para* position of phenylisocyanide,  $\text{CNPh}^{\text{pC}\equiv\text{CH}}$ , enables the isocyanide to replace carbonyl ligands in the coordination sphere of common technetium(I) starting materials such as  $(\text{NBU}_3)[\text{Tc}_2(\mu\text{-Cl})_3(\text{CO})_6]$ . The ligand exchange proceeds under thermal conditions and finally forms the corresponding hexakis(isocyanide)technetium(I) complex. The product undergoes a copper-catalyzed cycloaddition ('Click' reaction), e.g. with benzyl azide, which gives the  $[\text{Tc}(\text{CNPh}^{\text{azole}})_6]^+$  cation. The free, uncoordinated 'Click' product is obtained from a reaction of the corresponding tetrakis( $\text{CNPh}^{\text{azole}}$ )copper(I) complex and  $\text{NaCN}$ . It readily reacts with *mer*- $[\text{Tc}(\text{CO})_3(\text{tht})(\text{PPh}_3)_2](\text{BF}_4)$  (*tht* = tetrahydrothiophene) under exchange of the thioether ligand. Alternatively,  $[\text{Cu}(\text{CNPh}^{\text{azole}})_4]^+$  can be used as a transmetalation reagent for the synthesis of the hexakis(isocyanide)technetium(I) complex, which is the preferable approach for the synthesis of the technetium complex with the short-lived isotope  $^{99\text{m}}\text{Tc}$  and a corresponding protocol for  $[\text{Tc}(\text{CNPh}^{\text{azole}})_6]^+$  is reported. The  $^{99}\text{Tc}$  and copper complexes have been studied by single-crystal X-ray diffraction and/or spectroscopic methods including IR and multinuclear NMR spectroscopy.

## INTRODUCTION

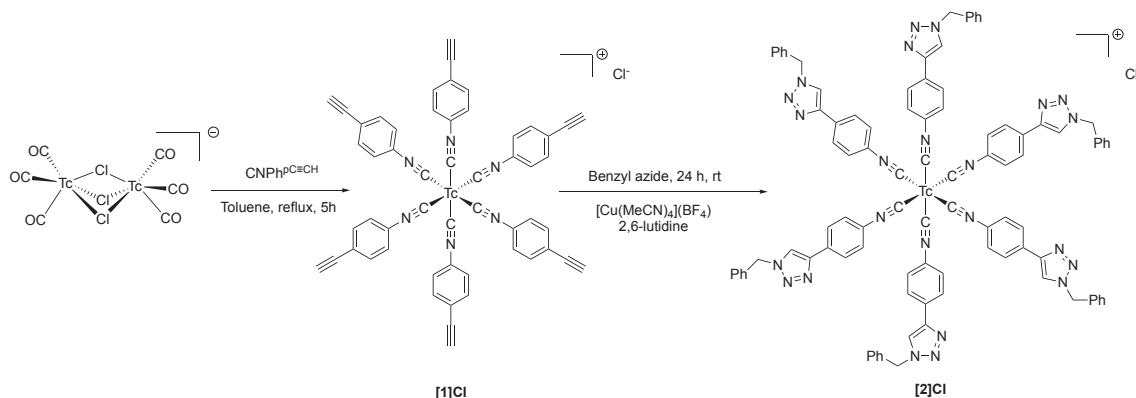
(Hexakis)isocyanide complexes of technetium(I) are known for their remarkable inertness thanks to their  $d^6$  electronic configuration.<sup>1</sup> Corresponding compounds with the long-lived isotope  $^{99}\text{Tc}$  (weak  $\beta^-$  emitter, half-life approximately  $2 \times 10^5$  years) can be synthesized by a ligand-exchange procedure starting from  $[\text{Tc}(\text{thiourea})_6]\text{Cl}_3$  or from  $(\text{NH}_4)[\text{TcO}_4]$ .<sup>1,2</sup> The latter procedure is also suitable for the short-lived  $\gamma$  emitter  $^{99\text{m}}\text{Tc}$  (half-life 6 h) and  $^{99\text{m}}\text{Tc}$ -Sestamibi (trade name Cardiolite<sup>®</sup>), which contains the homoleptic hexakis(2-methoxy-2-methylpropylisocyanide)technetium(I) cation (Chart 1), has become the workhorse of diagnostic nuclear medicine.<sup>3,4</sup> Although developed for myocardial imaging,  $^{99\text{m}}\text{Tc}$ -Sestamibi has found a number of other applications without any changes of the molecular setup or the kit formulation, e.g. in the parathyroid diagnostics, scintimammography or oncology.<sup>5,6</sup> The uptake of this drug in tissues with a large number of mitochondria and negative plasma membrane potentials is provided by its cationic charge, a well-balanced lipophilicity and the retention in the tissue by a (partial) hydrolysis of the methoxy groups in its molecular periphery. The highly stable central metal-carbon bonds in such compounds make it desirable to expand the scope of applications by the attachment of bio-targeting groups in the outer sphere. The complexity of the synthesis of appropriate isocyanides sets narrow limits to such efforts and to the best of our knowledge there are only a few reports about technetium complexes with specifically substituted isocyanides. Such compounds with ester-

functionalization have been introduced in the context of the search for myocardial imaging agents ( $[\text{Tc}(\text{CPI})_6]^+$ , Chart 1) or as mimic for  $\omega$ -fatty acids (e.g.  $[\text{Tc}(\text{CO})_5(\text{CN}(\text{CH}_2)_{10}\text{COOMe})]^+$ , Chart 1).<sup>7,8</sup> Corresponding complexes with chemically more flexible isocyanides are practically unknown.

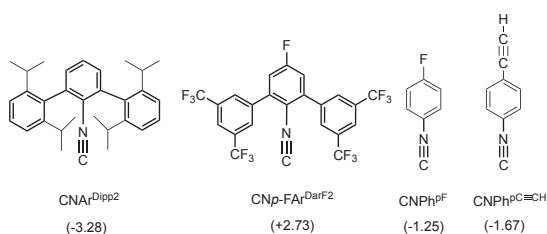


**Chart 1.** Technetium(I) complexes with functionalized isocyanides.

Recently, we studied reactions of carbonyltechnetium(I) complexes with sterically highly encumbered *m*-terphenyl iso-



**Scheme 1.** Synthesis of  $[\text{Tc}(\text{CNPh}^{\text{pC}\equiv\text{CH}})_6]\text{Cl}$  (**[1]Cl**) and its reaction with benzyl azide under formation of  $[\text{Tc}(\text{CNPh}^{\text{azole}})_6]\text{Cl}$  (**[2]Cl**).



**Chart 2.** Sterically encumbered isocyanides ( $\text{CNAr}^{\text{Dipp}2}$  and  $\text{CNp-FAr}^{\text{DarF}2}$ ) and isocyanides with enhanced reactivity ( $\text{CNPh}^{\text{pF}}$  and  $\text{CNPh}^{\text{pC}\equiv\text{CH}}$ ) together with their SADAP parameters (in parenthesis, values in  $\text{kcal mol}^{-1} \text{\AA}^{-2}$ )<sup>11</sup>.

cyanides (Chart 2) and could show that the substituents on isocyanide ligands profoundly change their reactivity.<sup>9-13</sup> This concerns steric factors due to the bulky residues, but also electronic effects seem to play a decisive role. It became apparent that there seems to be a rational relationship between the reactivity of the isocyanides and their organic residues. This became particularly evident when fluorine or related residues were found in *para* position in (substituted) arylisocyanides. Such ligands ( $\text{CNp-FAr}^{\text{DarF}2}$  or  $\text{CNPh}^{\text{pF}}$ , Chart 2) readily replace carbonyl ligands in the coordination sphere of technetium under thermal conditions,<sup>10,11</sup> which is commonly not observed for alkyl isocyanides.<sup>14-17</sup> A DFT-based empirical parameter, which combines the substituent-dependent electron potential at the surface of the carbon donor atom with the size of the accessible surface allows to classify isocyanides depending on their substituents. The resulting Surface-Averaged Donor-Acceptor Potential (SADAP) parameters were found to correlate well with the experimentally observed reactivity of the corresponding isocyanides.<sup>11</sup> Electron-deficient isocyanides with less negative or even positive SADAP parameters (Chart 2) can replace carbonyl ligands under thermal conditions and even form (hexakis)isocyanide complexes, while those with clearly negative SADAP values are not able to replace carbonyls from  $\text{fac-}\{\text{Tc}(\text{CO})_3\}^+$  units. Thus,  $[\text{Tc}(\text{CNPh}^{\text{pF}})_6]^+$  was obtained from  $(\text{NBu}_4)[\text{Tc}_2(\mu\text{-Cl})_3(\text{CO})_6]$  and the fluorinated ligand  $\text{CNPh}^{\text{pF}}$  in good yields.<sup>11</sup>

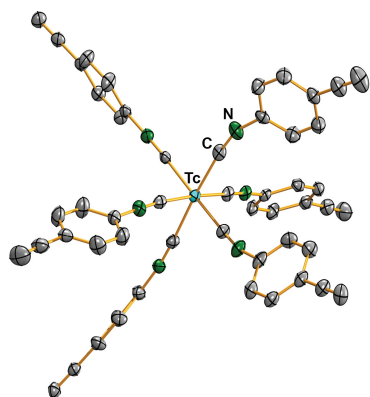
Interestingly, the calculated SADAP parameters for *para*-alkyne aryl isocyanides are similar to those of  $\text{CNPh}^{\text{pF}}$  and predict that the reaction of  $\text{CNPh}^{\text{pC}\equiv\text{CH}}$  with  $\text{fac-}\{\text{Tc}(\text{CO})_3\}^+$  starting materials should lead to a (hexakis)isocyanide complex with six reactive alkyne residues in its periphery. Such a compound may represent an appropriate platform for subsequent copper-catalyzed cycloaddition ('Click') reactions with a variety of biologically interesting azides since the resulting 1,4-triazole linker is known to be remarkably stable under biological conditions.<sup>18</sup>

## RESULTS AND DISCUSSION

The reaction of an excess of  $\text{CNPh}^{\text{pC}\equiv\text{CH}}$  with  $(\text{NBu}_4)[\text{Tc}_2(\mu\text{-Cl})_3(\text{CO})_6]$  in dry toluene gives a pale beige solid of  $[\text{Tc}^{\text{I}}(\text{CNPh}^{\text{pC}\equiv\text{CH}})_6]\text{Cl}$ , which was isolated and subsequently washed with water, toluene and *n*-pentane (Scheme 1). The ligand exchange behavior of  $\text{CNPh}^{\text{pC}\equiv\text{CH}}$  is similar to that of  $\text{CNPh}^{\text{pF}}$ , which also replaces carbonyl ligands under thermal conditions. The required reaction time with  $\text{CNPh}^{\text{pC}\equiv\text{CH}}$ , however, is slightly longer than with  $\text{CNPh}^{\text{pF}}$ , which nicely correlates with its slightly more negative SADAP parameter (Chart 2).  $[\text{Tc}(\text{CNPh}^{\text{pC}\equiv\text{CH}})_6]\text{Cl}$  is well-soluble in methanol but attempts to isolate a crystalline solid from such solutions failed. Thus, an aqueous solution of  $(\text{NH}_4)(\text{PF}_6)$  was added, which resulted in the precipitation of the corresponding hexafluorophosphate salt.  $[\text{Tc}(\text{CNPh}^{\text{pC}\equiv\text{CH}})_6](\text{PF}_6)$  (**[1](PF<sub>6</sub>)**) is soluble in nonpolar solvents such as dichloromethane. Slow evaporation of a dichloromethane/toluene solution gave single crystals suitable for X-ray diffraction (see Fig. 1).

The coordination environment of the technetium atom is a slightly distorted octahedron with *cis*-C-Tc-C angles between 82.9(2) and 95.3(2)°. The Tc-C-N angles are slightly bent (maximum deviation from linearity: 8.6°). One C-N-C angle at 159.6(6)° deviates markedly from the ideal 180°. As all ligands are similar and only one set of resonances can be observed in the <sup>1</sup>H NMR spectrum, it can be reasonably assumed that the distortion is due to the crystal packing. The Tc-C bond lengths range from 2.015(6) Å to 2.040(6) Å. The isocyanide C-N bond lengths range from 1.158(7) Å to 1.179(7) Å. Both Tc-C and C-N bonds are in the same range we observed previously

for  $[\text{Tc}(\text{CNPh}^{\text{PF}})_6][\text{PF}_6]$ .<sup>11</sup> Details about individual bond lengths and angles are contained in the Supporting Information.

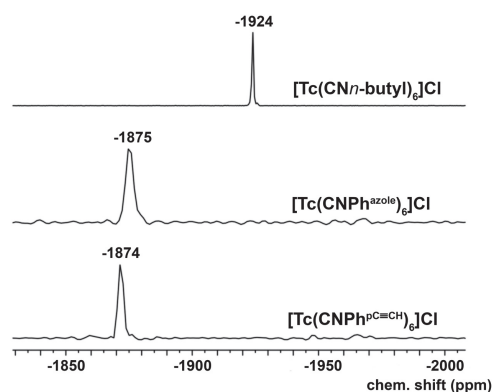


**Figure 1.** Structure of the complex cation of  $[1](\text{PF}_6)$ .

As described for other hexakis(isocyanide) complexes of technetium(I),<sup>1,11</sup> the  $\nu(\text{C}\equiv\text{N})$  stretch in the IR spectrum of  $[1](\text{PF}_6)$  is bathochromically shifted against the value in the uncoordinated isocyanide ( $2134\text{ cm}^{-1}$  to  $2081\text{ cm}^{-1}$ ). This indicates a considerable back-donation of electron density from the  $d^6$  metal ion into antibonding orbitals of the isocyanide ligands. This observation should not be remarkable considering that isocyanides are frequently cited as textbook examples for  $\pi$ -acceptor ligands. On the other hand, we had to note that the degree of back-donation to isocyanides depends on the presence or absence of other (competing)  $\pi$ -acceptor ligands and the oxidation state of the metal. Thus, we found the  $\nu(\text{CN})$  bands in mixed tricarbonyl/isocyanide complexes generally at higher frequencies than in the uncoordinated isocyanides indicating that back-donation is preferably established into the  $\pi^*$  orbitals of the ‘better’ acceptor (here CO).<sup>9,11,16,17</sup> With decreasing number of carbonyl ligands, however, also the isocyanides contribute to the back-donation as has been found for a series of  $[\text{M}(\text{CO})\text{X}(\text{L})_4]$  complexes ( $\text{M} = \text{Tc}$  or  $\text{Re}$ ;  $\text{X} = \text{Cl}$  or  $\text{Br}$ ;  $\text{CNp-FAr}^{\text{DarF2}}$  or  $\text{CNPh}^{\text{PF}}$ ).<sup>10-13,18</sup> The influence of the electron density located at the metal ions has nicely been demonstrated for a series of the structurally similar rhenium complexes  $[\text{Re}^-(\text{CO})(\text{CNp-FAr}^{\text{DarF2}})_4]^-$ ,  $[\text{Re}^0(\text{CO})(\text{CNp-FAr}^{\text{DarF2}})_4]$ , and  $[\text{Re}^{+1}\text{Br}(\text{CO})(\text{CNp-FAr}^{\text{DarF2}})_4]^+$ , representing species with 18, 17 and 16 valence electrons and show the corresponding  $\nu(\text{CN})$  frequencies at  $1886$ ,  $1975$  and  $2051\text{ cm}^{-1}$  (value for the uncoordinated isocyanide:  $2119\text{ cm}^{-1}$ ).<sup>12</sup>

<sup>99</sup>Tc NMR spectroscopy is an instructive method for the characterization of technetium(I) compounds.<sup>19</sup> Particularly highly symmetric compounds such as the tetrahedral pertechnetate or the octahedral hexakis(isocyanide) complexes give narrow signals,<sup>1,11,20</sup> while the large quadrupole moment of <sup>99</sup>Tc results in significant line-broadenings when the local symmetry around the technetium nucleus decreases.<sup>11,19</sup> <sup>99</sup>Tc NMR signals of technetium(I) compounds span an extremely large chemical shift range from approximately  $+2000$  to  $-3500\text{ ppm}$ .<sup>21</sup> Thus, it allows the detection of even minor changes in the coordination sphere of the metal. This is also evident for the compounds of the present study. The resonance of  $[1]\text{Cl}$  appears at  $-1874\text{ ppm}$  (Fig. 2), which corresponds to a

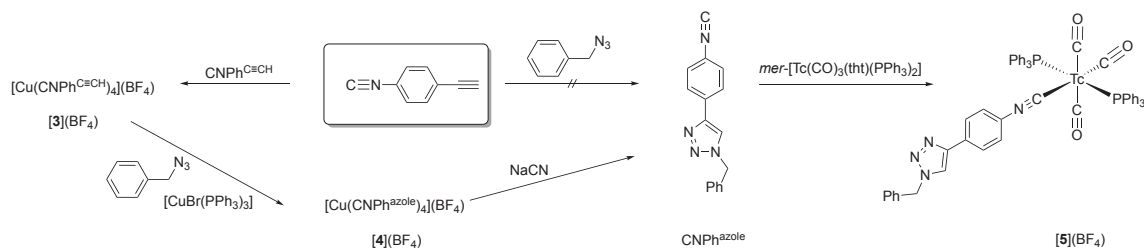
significantly more deshielded nucleus than in hexakis-(alkylisocyanide)technetium(I) complexes, the signals of which are observed between  $-1914$  and  $-1964\text{ ppm}$ .<sup>20</sup> Similar observations have been made before for corresponding complexes with phenyl or tolyl isocyanides as well as with  $\text{CNPh}^{\text{PF}}$ ,<sup>11,20</sup> indicating also by this parameter that the electronic situation at the metal might be slightly different between complexes with alkyl- or aryl-substituted isocyanides and might also have implications for the reactivity of the respective ligands. Some serious hints regarding this point have recently been given by Mizuno and co-workers.<sup>22-24</sup>



**Figure 2.** <sup>99</sup>Tc NMR spectra of  $[1]\text{Cl}$ ,  $[2]\text{Cl}$  and  $[\text{Tc}(\text{CNn-butyl})_6]\text{Cl}$  in methanol.

The alkyne substituents of complex  $[1]\text{Cl}$  can be reacted with benzyl azide in a copper-catalyzed cycloaddition under formation of the corresponding triazole. The reaction proceeds in acetonitrile using  $[\text{Cu}(\text{MeCN})_4][\text{BF}_4]$  as catalyst with 2,6-lutidine as an additive.<sup>25</sup> The starting material is only partially soluble in acetonitrile but the mixture becomes gradually homogeneous indicating the progress of the reaction. A beige powder was isolated upon removal of the volatiles. It was washed with methanol and n-pentane giving  $[\text{Tc}(\text{CNPh}^{\text{azole}})_6]\text{Cl}$ ,  $[2]\text{Cl}$ , (see Scheme 1). The success of the ‘Click’ reaction on the coordinated alkyne could be verified by the proton and <sup>99</sup>Tc NMR spectra of the product. The <sup>1</sup>H spectrum shows the signals of the formed triazole with the expected coupling patterns and intensities and the <sup>99</sup>Tc spectrum confirms the presence of only one technetium species. Although the signals of the starting material  $[1]\text{Cl}$  ( $-1874\text{ ppm}$ ) and the ‘Click’ product  $[2]\text{Cl}$  ( $-1875\text{ ppm}$ ) appear close together, the resolution of the method would be good enough to separate them when they appear in the same spectrum. This has been demonstrated recently by the parallel detection of  $[\text{Tc}(\text{CNn-butyl})_{6-n}(\text{CNt-butyl})_n]^+$  ( $n = 0 - 6$ ) mixed-ligand complexes.<sup>11</sup> Additional proof for a successful cycloaddition is given by the disappearance of the  $\nu(\text{C-H})$  IR band of the terminal alkyne at  $3289\text{ cm}^{-1}$ .

Uncoordinated  $\text{CNPh}^{\text{azole}}$  can be isolated following a reaction sequence via its copper(I) complex as is shown in Scheme 2. The use of copper compounds for this purpose is obvious, since both intermediates are interesting as potential transmetalation agents for the syntheses of corresponding <sup>99m</sup>Tc complexes.

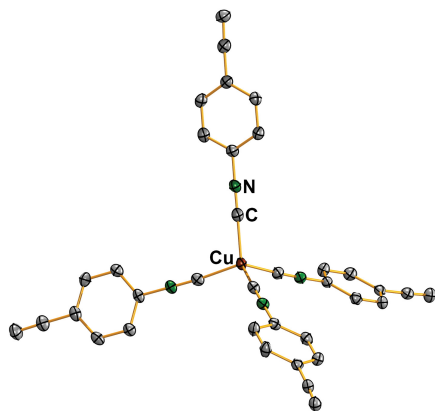


**Scheme 2.** Synthesis of  $\text{CNPh}^{\text{azole}}$  via copper(I) complexes and its reaction with  $\text{mer-}[\text{Tc}(\text{CO})_3(\text{tht})(\text{PPh}_3)_2]$  (tht = tetrahydrothiophene).

The subsequent syntheses of  $[\text{Cu}(\text{CNPh}^{\text{P}^{\text{C}=\text{CH}}})_4](\text{BF}_4)$  (**[3](BF<sub>4</sub>)**) and  $[\text{Cu}(\text{CNPh}^{\text{azole}})_4](\text{BF}_4)$  (**[4](BF<sub>4</sub>)**) are straightforward. No reactions on the  $\text{C}\equiv\text{N}$  triple bond were observed under the conditions applied. The convenient and fast formation of isocyanide copper(I) complexes has been reported with three or four ligands around the metal center depending on the amount of added isocyanide.<sup>26,27</sup>

During the synthesis, the corresponding tetrakis complexes must be obtained selectively as contamination with the tris complexes leads to insoluble polymeric materials during subsequent reactions.

Compound **[3](BF<sub>4</sub>)** can be obtained by adding a solution with one equivalent of  $[\text{Cu}(\text{MeCN})_4][\text{BF}_4]$  to a solution containing four equivalents of  $\text{CNPh}^{\text{P}^{\text{C}=\text{CH}}}$  (Scheme 2). This avoids the formation of the tris complex. A downfield shift of all proton NMR resonances as well as a significant hypsochromic shift of the  $\nu(\text{CN})$  IR band of  $32\text{ cm}^{-1}$  indicate a preferably  $\sigma$ -donating behavior of the isocyanide ligand in the product. The structure of the complex cation (Fig. 3) shows that the ligands form a slightly distorted tetrahedral arrangement around the copper ion. The C-Cu-C angles in **[3](BF<sub>4</sub>)** range from  $106.33(9)$  to  $114.98(9)^\circ$  and the Cu-C bonds lengths are found between  $1.945(2)$  and  $1.955(2)\text{ \AA}$ . The C-N bonds are clearly in the range of carbon-nitrogen triple bonds ( $1.148(3)\text{ \AA}$  to  $1.152\text{ \AA}$ ). These bonding features are very similar to the values found for other (tetrakis)isocyanide copper complexes.<sup>28</sup> More details about individual bond lengths and angles are contained in the Supporting Information.



**Figure 3:** Structure of the  $[\text{Cu}(\text{CNPh}^{\text{P}^{\text{C}=\text{CH}}})_4]^+$  cation in **[3](BF<sub>4</sub>)**.

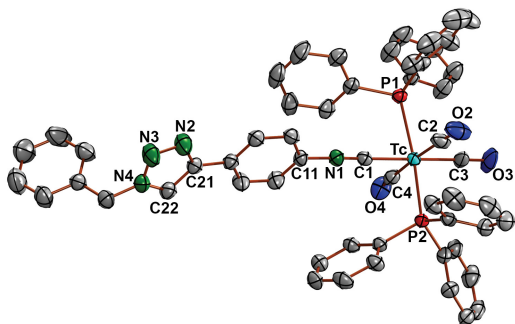
Although a gradual decomposition of **[3](BF<sub>4</sub>)** is observed in solution, freshly prepared solutions of this compound are suitable for cycloadditions with organic azides. This is not least demonstrated by the fact that additional copper ions must be added as catalyst, while the Cu(I) ions in **[3](BF<sub>4</sub>)** are perfectly shielded by the coordination of the isocyanide ligands and preclude an autocatalysis.<sup>27</sup>

We screened several copper catalysts and monitored the reaction by  $^1\text{H}$  NMR. No reactivity was observed under the canonical conditions of copper(I)-catalyzed azide-alkyne cycloaddition with  $\text{CuSO}_4/\text{ascorbate}$ .<sup>25</sup> However, other Cu(I) catalysts described in the literature with either phosphine or chelating nitrogen ligands e.g. (tris(benzyltriazolylmethyl)amine) were found to be suitable for this reaction.<sup>29,30</sup> Finally the use of  $[\text{CuBr}(\text{PPh}_3)_2]$  gave the best results. As previously observed in the literature and with technetium (*vide supra*), the reaction was only possible when the isocyanide moiety was coordinated to a metal center to prevent a coordination on the catalyst.<sup>31</sup> The use of an isocyanide-alkyne system allows the synthesis of C-bonded isocyanide triazole and avoids the use of very reactive and frequently explosive isocyanide-azide ligands.<sup>32</sup>

Once the ‘Click’ reaction of Scheme 2 is completed, the obtained isocyanide-triazole copper complex **[4](BF<sub>4</sub>)** can be cleaved using an excess of aqueous sodium cyanide within minutes. The IR frequency of the isocyanide moiety shows a pronounced bathochromic shift upon cleavage from  $2165\text{ cm}^{-1}$  to  $2124\text{ cm}^{-1}$ . The obtained  $\text{CNPh}^{\text{azole}}$  isocyanide is a potential synthon for multi-component reactions and is to the best of our knowledge the first uncoordinated C-bonded triazole isocyanide.<sup>31</sup>

The reactivity of  $\text{CNPh}^{\text{azole}}$  was tested in a reaction with the technetium(I) complex  $\text{mer-}[\text{Tc}(\text{CO})_3(\text{tht})(\text{PPh}_3)_2](\text{BF}_4)$  (tht = tetrahydrothiophene), which is known for the ready release of its thioether ligand.<sup>33</sup> Expectedly,  $\text{mer-}[\text{Tc}(\text{CO})_3(\text{CNPh}^{\text{azole}})(\text{PPh}_3)_2](\text{BF}_4)$  (**[5](BF<sub>4</sub>)**) was formed (Scheme 2). It could be isolated as a colorless, crystalline solid in good yields. The  $\nu(\text{CN})$  stretch is observed at  $2164\text{ cm}^{-1}$ , which corresponds to a hypsochromic shift with respect to the uncoordinated ligand and indicates that back-donation is preferably observed into the  $\pi^*$  orbitals of the carbonyl ligands as has been discussed for other tricarbonyl complexes of technetium(I) *vide supra*. In contrast to the narrow  $^{99}\text{Tc}$  NMR signals of the hexakis(isocyanide)-technetium(I) cations shown in Fig. 2 with line widths  $\nu_{1/2}$  between 60 and 378 Hz, the signal for **[5](BF<sub>4</sub>)** is extremely broad ( $\nu_{1/2} \approx 5550\text{ Hz}$ ). A comparison of the three signals in the same scale is shown in the Supporting Information. The

resonance of  $[5](BF_4)$  appears at  $-1907$  ppm, which is the range, where also the signals for other  $mer-[Tc(CO)_3-(CNR)(PPh_3)_2]^+$  complexes ( $R = t$ -butyl, phenyl) with similarly large line widths were observed.<sup>34</sup>



**Figure 4.** Structure of the complex cation of  $mer-[Tc(CO)_3-(CNPh^{azole})(PPh_3)_2](BF_4)$  ( $[5](BF_4)$ ).

The single crystals obtained for  $[5](BF_4)$  were of sufficient quality for X-ray diffraction and Figure 4 depicts the molecular structure of the compound confirming that the  $CNPh^{azole}$  ligand is C-bonded. Thus, the structure of the products is similar to those of the  $mer-[Tc(CO)_3(CNPh)(PPh_3)_2](BF_4)$  and  $mer-[Tc(CO)_3(CNtbutyl)(PPh_3)_2](BF_4)$ . Some selected bond lengths and angles are summarized in Table 1. The Tc-C1 (isocyanide) bond is expectedly clearly longer than those to the carbonyl ligands. The shortest Tc-C bond is that to C3, which indicates that the *trans*-labilization effect due to CO ligands is clearly larger than that due to  $CNPh^{azole}$ . The isocyanide ligand in  $[5](BF_4)$  is linearly bonded. More bond lengths and angles are given as Supporting Information.

**Table 1.** Selected bond lengths (Å) and angles (°) in  $[5](BF_4)$ .

Tc-C1	2.077(3)	Tc-C2	1.996(4)
Tc-C3	1.944(3)	Tc-C4	1.975(4)
C1-N1	1.150(4)	C21-N2	1.362(4)
N2-N3	1.312(4)	N3-N4	1.333(4)
N4-C22	1.349(4)	C21-C22	1.366(5)
Tc-C1-N1	176.7(3)	C1-N1-C11	174.3(3)

The choice of copper compounds for the synthesis of the substituted isocyanide complexes of the present study was of course not inadvertently, but clearly inspired by the use of  $[Cu(MIBI)_4](BF_4)$  as the isocyanide source in the commercially used  $^{99m}Tc$ -Sestamibi kits.<sup>3</sup> Since we regard ‘Click’ reactions on the copper complex  $[3](BF_4)$  with organic azides bonded to a variety of biological vectors as a promising platform for the development of prospective  $^{99m}Tc$ -based radiopharmaceuticals, we undertook some initial experiments with  $^{99m}Tc$ . For this, we treated an aqueous solution of  $[4](BF_4)$  with  $^{99m}TcO_4^-$  and tin chloride as reductant. Although the reactions conditions were not at all optimized, the corresponding  $[^{99m}Tc(CNPh^{azole})_4]^+$  cation was formed in a reasonable yield and could readily be

purified by a simple chromatographic procedure. A continuation of these initial  $^{99m}Tc$  experiments with biologically more relevant azides is scheduled for the future. They shall also answer the question if the novel access to hexakis(isocyanide)technetium(I) cations via carbonyl precursors has potential in the clinical  $^{99m}Tc$  chemistry.

## CONCLUSIONS

The use of activated isocyanides such as  $CNPh^{PF}$  or  $CNPh^{C=CH}$  allows the synthesis of hexakis(isocyanide)technetium(I) complexes starting from technetium carbonyls. Complexes (here Tc(I) and Cu(I) compounds) with the alkyne-substituted ligand can be involved in ‘Click’ reactions with organic azides. The resulting triazole-substituted isocyanide can be released from the copper complex by treatment with  $CN^-$  and subsequently be employed directly as a reactant for ongoing complex formations. Alternatively, the Cu(I) compound is suitable as transmetalation reagent, e.g. for the synthesis of corresponding  $^{99m}Tc$  complexes

## EXPERIMENTAL SECTION

**General Considerations.** Unless otherwise stated, reagent-grade starting materials were purchased from commercial sources and either used as received or purified by standard procedures. Solvents were dried and deoxygenated according to standard procedures.  $(NBu_4)[Tc_2(\mu-Cl)_3(CO)_6]$ ,  $CNPh^{C=CH}$ ,  $[Cu(MeCN)_4](BF_4)$ ,  $[Tc(CO)_3(tht)(PPh_3)_2](BF_4)$  and  $[CuBr(PPh_3)_3]$  were prepared according to literature procedures.<sup>33,35-37</sup>  $^{99m}TcO_4^-$  solution was eluted from a  $^{99}Mo/^{99m}Tc$  generator (Ultra Technekow, GE Healthcare).

**Physical Measurements.** NMR spectra were recorded with JEOL 400 MHz ECS or ECZ or JEOL ECZ 600 or Bruker AV700 multinuclear spectrometers. IR spectra were recorded with a Shimadzu FTIR 8300 spectrometer as KBr pellets (Tc complexes) or a Nicolet iS10, Thermo Scientific an ATR spectrometer (non-radioactive compounds). Intensities are classified as vs = very strong, s = strong, m = medium, w = weak, vw = very weak, sh = shoulder. Electrospray ionization mass spectrometry (ESI MS) was carried out with the ESI MSD time-of-flight (TOF) unit of an Agilent 6210 TOF liquid chromatography/mass spectrometry system. Elemental analyses of carefully dried samples of the bulk were performed using a Vario MICRO cube CHNS elemental analyser. Activity counting was performed using a borehole counter (Nuklear-Medizintechnik Dresden GmbH, Germany).

**X-Ray Crystallography.** The intensities for the X-ray determinations were collected on STOE IPDS II or Bruker D8 Venture instruments with Mo  $K\alpha$  radiation. The space groups were determined by the detection of systematic absences. Absorption corrections were carried out by the multi scan method.<sup>38,39</sup> Structure solution and refinement were performed with the SHELX program package using OLEX 2.<sup>40-42</sup> Hydrogen atoms were derived from the final Fourier maps and refined or placed at calculated positions and treated with the ‘riding model’ option of SHELXL. The representation of molecular structures was done using the program DIAMOND 4.2.2.<sup>43</sup> Additional information on the structure determinations is contained in the Supporting Information and has been deposited with the Cambridge Crystallographic Data Centre.

**Radiation Precautions.**  $^{99}\text{Tc}$  is a long-lived, weak  $\beta^-$  emitter ( $E_{\text{max}} = 0.292$  MeV). Normal glassware provides adequate protection against the weak beta radiation when milligram amounts are used. Secondary X-rays (bremsstrahlung) play a significant role only when larger amounts of  $^{99}\text{Tc}$  are handled. All manipulations were done in a laboratory approved for the handling of radioactive materials.

**Syntheses.**  $[\text{Tc}(\text{CNPh}^{\text{C}=\text{CH}})_6]\text{Cl}$  ( $[\text{I}]\text{Cl}$ ).  $(\text{NBu}_4)[\text{Tc}_2(\mu\text{-Cl})_3(\text{CO})_6]$  (71 mg, 0.1 mmol) was suspended in dry, degassed toluene (3 mL) and  $\text{CNPh}^{\text{C}=\text{CH}}$  (252 mg, 2.0 mmol) was added. The reaction was performed under a stringent exclusion of air under an argon atmosphere. The mixture was heated under reflux for 5 h. A beige precipitate formed, which was filtered off and washed sequentially with water, toluene and *n*-pentane, and finally dried under reduced pressure. Yield: 134 mg (0.15 mmol, 75%). IR (KBr,  $\text{cm}^{-1}$ ): 3289 (w,  $\nu(\text{C-H})$ ), 3129 (m), 2081 (vs,  $\nu(\text{N}=\text{C})$ ), 1593 (w), 1497 (s), 1406 (w), 1265 (w); 1171 (w), 1101 (w), 837 (s), 677 (m), 546 (s).  $^1\text{H}$  NMR (MeOD- $d_4$ , ppm): 7.56 (m, 24H), 3.75 (s, 6H).  $^{99}\text{Tc}$  NMR (MeOD- $d_4$ , ppm):  $-1874$  ( $\nu_{1/2} = 366$  Hz).

$[\text{Tc}(\text{CNPh}^{\text{C}=\text{CH}})_6](\text{PF}_6)$  ( $[\text{I}](\text{PF}_6)$ ).  $[\text{I}]\text{Cl}$  (0.05 mmol, 45 mg) was dissolved in methanol and a solution of  $\text{NH}_4\text{PF}_6$  (0.5 g in 3 mL methanol) was added dropwise leading to the formation of an off-white precipitate, which was filtered off and washed with water and *n*-pentane. The obtained solid was dissolved in a small amount of  $\text{CH}_2\text{Cl}_2$  and toluene was added. The solution was slowly evaporated at  $5^\circ\text{C}$  leading to the formation of single crystals suitable for X-ray diffraction. They were filtered and washed with *n*-pentane. Yield: 21 mg (0.021 mmol, 40%). IR (KBr,  $\text{cm}^{-1}$ ): 3298 (m,  $\nu(\text{C-H})$ ), 2940 (w), 2095 (vs,  $\nu(\text{N}=\text{C})$ ), 1512 (m), 870 (s), 692 (m), 573 (m).  $^1\text{H}$  NMR ( $\text{CD}_2\text{Cl}_2$ , ppm): 7.57 (d,  $^3J(^1\text{H}, ^1\text{H}) = 8$  Hz, 12H), 7.41 (d,  $^3J(^1\text{H}, ^1\text{H}) = 8$  Hz, 12H), 3.30 (s, 6H).  $^{19}\text{F}$  NMR ( $\text{CD}_2\text{Cl}_2$ , ppm):  $-73.3$  ( $^1J(^{19}\text{F}, ^{31}\text{P}) = 710$  Hz).  $^{99}\text{Tc}$  NMR ( $\text{CD}_2\text{Cl}_2$ , ppm) =  $-1871$  ( $\nu_{1/2} = 240$  Hz).

$[\text{Tc}(\text{CNPh}^{\text{azole}})_6]\text{Cl}$  ( $[\text{2}]\text{Cl}$ ).  $[\text{I}]\text{Cl}$  (20 mg, 0.022 mmol) was suspended in MeCN (2 mL).  $[\text{Cu}(\text{MeCN})_4](\text{BF}_4)$  (1.4 mg, 3 mol%/alkyne, 45  $\mu\text{mol}$ ), benzyl azide (17  $\mu\text{L}$ , 0.134 mmol) and 2,6-lutidine (16  $\mu\text{L}$ , 0.134 mmol) were added. The solution was stirred overnight and became homogeneous. Volatiles were removed under reduced pressure and the obtained beige solid was washed with methanol and *n*-pentane and dried under reduced pressure. Yield: 30 mg (0.018 mmol, 80%). IR (KBr,  $\text{cm}^{-1}$ ): 2920 (w), 2085 (vs,  $\nu(\text{N}=\text{C})$ ), 1491 (m), 1456 (m), 1350 (w), 1227 (w), 1045 (m), 972 (w), 843 (m), 721 (s), 600 (m).  $^1\text{H}$  NMR (acetone- $d_6$ , ppm): 8.53 (s, 6H), 8.01 (d,  $^3J(^1\text{H}, ^1\text{H}) = 8$  Hz, 12H), 7.65 (d,  $^3J(^1\text{H}, ^1\text{H}) = 8$  Hz, 12H), 7.43-7.32 (m, 30H), 5.69 (s, 12H).  $^{99}\text{Tc}$  NMR (acetone- $d_6$ , ppm):  $-1874$  ( $\nu_{1/2} = 378$  Hz).

$[\text{Cu}(\text{CNPh}^{\text{C}=\text{CH}})_4](\text{BF}_4)$  ( $[\text{3}](\text{BF}_4)$ ).  $[\text{Cu}(\text{MeCN})_4](\text{BF}_4)$  (31.4 mg, 0.10 mmol) was suspended in dichloromethane (3 mL) and  $\text{CNPh}^{\text{C}=\text{CH}}$  (0.40 mmol, 51.0 mg) dissolved in dichloromethane (2 mL) was added. After stirring for 5 min., the volatiles were removed under reduced pressure and the crude product was obtained without further purification as a colorless solid. Single crystals suitable for X-Ray diffraction were obtained by overlaying a THF solution with MeOH. The reaction was quantitative. Elemental analysis Calcd for  $\text{C}_{36}\text{H}_{20}\text{BCuF}_4\text{N}_4$ : C, 65.62; H, 3.06; N, 8.50%. Found: C, 65.29; H, 3.09; N, 8.41%. IR (ATR,  $\text{cm}^{-1}$ ): 3284 (m,  $\nu(\text{C-H})$ ), 3097 (w), 2163 (vs,  $\nu(\text{N}=\text{C})$ ), 1499 (m), 1461 (m), 1409 (w), 1274

(w), 1195 (w), 1066 (s), 1012 (m), 841 (s), 661 (m), 599 (m).  $^1\text{H}$  NMR (acetone- $d_6$ , ppm): 7.79 (m, 8H), 7.71 (m, 8H), 4.00 (s, 4H).  $^{13}\text{C}\{^1\text{H}\}$  NMR (acetone- $d_6$ , ppm): 149.30 (br), 134.30, 128.18, 126.34, 125.99, 83.02, 82.45.  $^{19}\text{F}$  NMR (acetone- $d_6$ , ppm):  $-151.36$  ( $^{10}\text{B-F}_4$ ),  $-151.41$  ( $^{11}\text{B-F}_4$ ). ESI $^+$  MS in MeCN (m/z): 317.012 ( $[\text{M}+\text{Cu}]^{2+}$  Calcd 317.013).

$[\text{Cu}(\text{CNPh}^{\text{azole}})_4](\text{BF}_4)$  ( $[\text{4}](\text{BF}_4)$ ).  $[\text{CuBr}(\text{PPh}_3)_3]$  (1 mg, 0.5 mol%/alkyne, 1  $\mu\text{mol}$ ) was added to a solution of freshly prepared  $[\text{3}][\text{BF}_4]$  (0.05 mmol, 16 mg) in benzyl azide (25  $\mu\text{L}$ , 0.2 mmol). The reaction mixture was stirred at room temperature for 5 h and monitored by  $^1\text{H}$  NMR. The initially formed paste slowly became solid during the reaction. The obtained solid was suspended in acetonitrile, filtered, washed with small amounts of acetonitrile and *n*-pentane, and then dried under reduced pressure. The obtained beige residue is sparingly soluble in polar solvents and only slightly more in nonpolar solvents such as  $\text{CH}_2\text{Cl}_2$ . Yield: 48.8 mg, (0.041 mmol, 82%). Elemental analysis Calcd for  $\text{C}_{64}\text{H}_{48}\text{BCuF}_4\text{N}_{16}$ : C, 64.51; H, 4.06; N, 18.81%. Found: C, 64.19; H, 4.09; N, 18.97. IR (ATR,  $\text{cm}^{-1}$ ): 3135 (w), 2165 (vs,  $\nu(\text{N}=\text{C})$ ), 1608 (w), 1496 (w), 1462 (w), 1350 (w), 1231 (w), 1045 (m), 974 (w), 843 (w), 717 (m).  $^1\text{H}$  NMR (acetone- $d_6$ , ppm): 8.57 (s, 1H), 8.09 (d,  $J = 8.6$  Hz, 2H), 7.78 (d,  $J = 8.6$  Hz, 2H), 7.43-7.32 (m, 5H), 5.71 (s, 2H).  $^1\text{H}$  NMR ( $\text{CD}_2\text{Cl}_2$ , ppm): 7.94 (d,  $J = 8.6$  Hz, 2H), 7.89 (s, 1H), 7.58 (d,  $J = 8.6$  Hz, 2H), 7.43 - 7.32 (m, 5H), 5.58 (s, 2H).  $^{13}\text{C}\{^1\text{H}\}$  NMR ( $\text{CD}_2\text{Cl}_2$ , ppm): 146.53, 135.33, 133.89, 129.68, 129.35, 128.72, 127.71, 127.25, 125.42, 121.53, 54.72. The signal of the isocyanide carbon atom could not be observed and is probably very broadened.  $^{19}\text{F}$  NMR ( $\text{CD}_2\text{Cl}_2$ , ppm):  $-151.59$  ( $^{10}\text{B-F}_4$ ),  $-152.64$  ( $^{11}\text{B-F}_4$ ). ESI $^+$  MS in MeCN (m/z): 583.139 ( $[\text{M}+\text{Cu}]^{2+}$  Calcd 583.141).

$\text{CNPh}^{\text{azole}}$ .  $[\text{4}](\text{BF}_4)$  (0.05 mmol, 59.5 mg) was suspended in a biphasic dichloromethane/water mixture (5 mL/1:1). A large excess of NaCN (0.3 mmol, 15 mg) was added and the solid dissolved immediately upon addition. The phases were separated, and the aqueous phase was extracted with dichloromethane (3 x 10 mL). The combined organic phases were then washed with brine (10 mL), dried over  $\text{Na}_2\text{SO}_4$  and filtered (the use of  $\text{MgSO}_4$  as a drying agent reduces the yield significantly). Volatiles were removed leading to an off-white powder that could be used for further reactions without purification or if required dry-loaded on silica and purified by column chromatography (1:2  $\text{CH}_2\text{Cl}_2$ /*n*-hexane) leading to a colorless solid. Yield of the purified compound: 36 mg (0.14 mmol, 70%). Elemental analysis Calcd for  $\text{C}_{16}\text{H}_{12}\text{N}_4$ : C, 73.83; H, 4.65; N, 21.52%. Found: C, 73.90; H, 4.68; N, 21.65. IR (ATR,  $\text{cm}^{-1}$ ): 3082 (w), 2124 (s,  $\nu(\text{N}=\text{C})$ ), 1494 (s), 1416 (m), 1237 (s), 1199 (m), 1072 (m), 1049 (s), 972 (m), 865 (s), 827 (vs), 720 (vs), 693 (m), 586 (s), 562 (s).  $^1\text{H}$  NMR (acetone- $d_6$ , ppm): 8.49 (s, 1H), 8.00 (m, 2H), 7.55 (m, 2H), 7.41-7.34 (m, 5H), 5.70 (s, 2H).  $^{13}\text{C}\{^1\text{H}\}$  NMR (acetone- $d_6$ , ppm): 166.51, 146.70, 136.81, 133.50, 129.76, 129.21, 128.92, 127.79, 127.25, 126.37 (t,  $^1J(^{13}\text{C}-^{14}\text{N}) = 11$  Hz), 122.50, 54.47. ESI $^+$  MS in MeCN (m/z): 283.096 ( $[\text{M}+\text{Na}]^+$  Calcd 283.095), 543.204 ( $[\text{2M}+\text{Na}]^+$  Calcd 543.202).

*mer*- $[\text{Tc}(\text{CO})_3(\text{CNPh}^{\text{azole}})(\text{PPh}_3)_2](\text{BF}_4)$  ( $[\text{5}](\text{BF}_4)$ ).  $\text{CNPh}^{\text{azole}}$  (13 mg, 0.05 mmol) and  $[\text{Tc}(\text{CO})_3(\text{tht})\text{PPh}_3)_2](\text{BF}_4)$  (44 mg, 0.05 mmol) were dissolved in dichloromethane (3 mL) and stirred at room temperature for 5 min. *n*-Hexane was added, which lead to the formation of a precipitate. The solid was

filtered off and washed with n-hexane. Single crystals suitable for X-Ray diffraction were obtained by slow evaporation of a dichloromethane/toluene solution. Yield: 39 mg (0.037 mmol, 74%). IR (KBr,  $\text{cm}^{-1}$ ): 3059 (w), 2929 (w), 2164 ( $\nu(\text{N}\equiv\text{C})$ ), 2073 (m), 1994 (vs), 1481 (w), 1431 (m), 1053 (s), 847 (w), 696 (s), 611 (m), 511 (s).  $^1\text{H}$  NMR ( $\text{CD}_2\text{Cl}_2$ , ppm)  $\delta$  8.06 (s, 1H), 7.79 (d,  $^3J(\text{H}-\text{H})$ , 2H), 7.58-7.47 (m, 30H), 7.40-7.35 (m, 5H), 6.72 (d,  $^3J(\text{H}-\text{H})$ , 2H), 5.58 (s, 2H).  $^{19}\text{F}$  NMR ( $\text{CD}_2\text{Cl}_2$ , ppm): -152.78 ( $^{10}\text{B-F}_4$ ), -152.83 ( $^{11}\text{B-F}_4$ ).  $^{99\text{m}}\text{Tc}$  NMR ( $\text{CD}_2\text{Cl}_2$ , ppm): -1907 ppm ( $\nu_{1/2} \approx 5.5$  kHz).

$[\text{}^{99\text{m}}\text{Tc}(\text{CNPh}^{\text{azole}})_6]\text{Cl}$ :  $[\text{Cu}(\text{CNPh}^{\text{azole}})_4](\text{BF}_4)$  (0.250 mg) was dissolved in 1 mL buffer solution containing 0.5 mg sodium ascorbate, 0.5 mg L-cysteine and 0.1 mg  $\text{SnCl}_2$ .  $^{99\text{m}}\text{Tc}$  pertechnetate solution (0.5 mL eluate taken from a commercial  $^{99}\text{Mo}/^{99\text{m}}\text{Tc}$  generator) containing approximately 1 GBq of  $^{99\text{m}}\text{TcO}_4^-$  was added. The reaction mixture was kept at  $95^\circ\text{C}$  for 15 min. The radiochemical purity was assessed by iTLC. For iTLC, we used iTLC-SG paper strips and either water or methylethylketone as a mobile phase. Purification of the product was done by loading the reaction mixture on a pre-conditioned C18 cartridge. The pure product was eluted with 1 mL ethanol followed by 3 mL 0.9% NaCl and resulted in 98.8 % radiochemical purity with 68% radiochemical yield.

## ASSOCIATED CONTENT

### Supporting Information

The Supporting Information is available free of charge at ...

Crystallographic tables, bond lengths and angles, ellipsoid plots, and spectroscopic data (PDF)

### Accession Codes

CCDC 2262126 - 2262128 contain the supplementary crystallographic data for this paper. These data can be obtained free of charge via [www.ccdc.cam.ac.uk/data\\_request/cif](http://www.ccdc.cam.ac.uk/data_request/cif), or by emailing [data\\_request@ccdc.cam.ac.uk](mailto:data_request@ccdc.cam.ac.uk), or by contacting The Cambridge Crystallographic Data Centre, 12 Union Road, Cambridge CB2 1EZ, UK; fax: +44 1223 336033.

## AUTHOR INFORMATION

### Corresponding Author

Ulrich Abram – *Institute of Chemistry and Biochemistry, Freie Universität Berlin, Fabeckstr, 34/36, D-14195 Berlin, Germany*; <http://orcid.org/0000-0002-1747-7927>; Email: [ulrich.abram@fu-berlin.de](mailto:ulrich.abram@fu-berlin.de); <https://www.bcp.fu-berlin.de/chemie/chemie/forschung/InorgChem/agabram/index.html>

### Authors

Guilhem Claude - *Institute of Chemistry and Biochemistry, Freie Universität Berlin, Fabeckstr, 34/36, D-14195 Berlin, Germany*; <https://orcid.org/0009-0000-0404-7242>.

Denis Puccio - *Institute of Chemistry and Biochemistry, Freie Universität Berlin, Fabeckstr, 34/36, D-14195 Berlin, Germany*

Adelheid Hagenbach - *Institute of Chemistry and Biochemistry, Freie Universität Berlin, Fabeckstr, 34/36, D-14195 Berlin, Germany*

Maximilian Roca-Jungfer - *Institute of Chemistry and Biochemistry, Freie Universität Berlin, Fabeckstr, 34/36, D-14195 Berlin, Germany*

Sarah Spreckelmeyer - *Charité - Universitätsmedizin Berlin, corporate member of Freie Universität Berlin, Humboldt-Universität zu Berlin, and Berlin Institute of Health, Department of Nuclear Medicine, Augustenburger Platz 1, 13353, Berlin*

## Funding

Deutsche Forschungsgemeinschaft (Germany) and Freie Universität Berlin (Germany).

## ACKNOWLEDGMENT

We gratefully acknowledge financial support from the DFG (Deutsche Forschungsgemeinschaft: Graduated School BIOQIC). We acknowledge the assistance of the Core Facility BioSupraMol supported by the DFG. Joshua S. Figueroa of the University of California-San Diego is acknowledged for fruitful scientific discussions.

## REFERENCES

- (1) Abrams, M. J.; Davison, A.; Jones, A. G.; Costello, C. E.; Pang, H. Synthesis and characterization of hexakis(alkylisocyanide) and hexakis(arylisocyanide) complexes of technetium (I). *Inorg. Chem.* **1983**, *22*, 2798-2800.
- (2) Abrams, M. J.; Davison, A.; Faggiani, R.; Jones, A. G.; Lock, C. J. L. Chemistry and structure of hexakis(thiourea-S)technetium(III) trichloride tetrahydrate,  $[\text{Tc}(\text{SC}(\text{NH}_2)_2)_6]\text{Cl}_3 \times 4 \text{H}_2\text{O}$ . *Inorg. Chem.* **1984**, *23*, 3284-3288.
- (3) Kronauge, J. F.; Mindiola, D. J. The Value of Stable Metal-Carbon Bonds in Nuclear Medicine and the Cardiolute Story. *Organometallics* **2016**, *35*, 3432-3435.
- (4) Piwnica-Worms, D.; Kronauge, J. F.; Holman, B. L.; Davison, A.; Jones, A. G. Comparative Myocardial Uptake Characteristics of Hexakis (Alkylisocyanide) Technetium(I) Complexes Effect of Lipophilicity. *Invest. Radiol.* **1989**, *24*, 25-29.
- (5) Boschi, A.; Uccelli, L.; Marvelli, L.; Cittanti, C.; Giganti, M.; Martini, P. Technetium-99m Radiopharmaceuticals for Ideal Myocardial Perfusion Imaging: Lost and Found Opportunities. *Molecules*, **2022**, *27*, 1188.
- (6) Urbano, N.; Scimeca, M.; Bonanno, E.; Schillaci, O.  $^{99\text{m}}\text{Tc}$  sestamibi SPECT: a possible tool for early detection of breast cancer lesions with high bone metastatic potential. *Future Oncology*, **2019**, *15*, 455-457.
- (7) Holman, B. L.; Sporn, V.; Jones, A. G.; Sia, T.; Perez-Balino, N.; Davison, A.; Lister-James, J.; Kronauge, J. F.; Mitta, A. E.; Camin, L. L.; Campbell, S.; Williams, S. J.; Carpenter, A. T. Myocardial Imaging with Technetium-99m CPI: Initial Experience in the Human. *J. Nucl. Med.* **1987**, *28*, 13-18.
- (8) Miroslavov, A. E.; Polotskii, Y. S.; Gurzhiy, V. V.; Ivanov, A. Y.; Lumpov, A. A.; Tyupina, M. Y.; Sidorenko, G. V.; Tolstoy, P. M.; Maltsev, D. A.; Suglobov, D. N. Technetium and Rhenium Pentacarbonyl Complexes with C2 and C11  $\omega$ -Isocyanocarboxylic Acid Esters. *Inorg. Chem.* **2014**, *53*, 7861-7869.
- (9) Claude, G.; Salsi, F.; Hagenbach, A.; Gembicky, M.; Drance, M. J.; Neville, M.; Chan, C.; Figueroa, J. S.; Abram, U. Structural and Redox Variations in Technetium Complexes Supported by *m*-Terphenyl Isocyanides. *Organometallics*, **2020**, *39*, 2287-2294.
- (10) Salsi, F.; Neville, M.; Drance, M.; Hagenbach, A.; Figueroa, J. S.; Abram, U.  $\{M^I(\text{CO})X(\text{CNAr}^{\text{DArF}2})_4\}$  (DArF = 3,5-(CF<sub>3</sub>)<sub>2</sub>C<sub>6</sub>H<sub>3</sub>; M = Re, Tc; X = Br, Cl) Complexes: Convenient Platforms for the Synthesis of Low-valent Rhenium and Technetium Compounds. *Organometallics*. **2021**, *40*, 1336-1343.

- (11) Claude, G.; Genz, J.; Weh, D.; Roca Jungfer, M.; Hagenbach, A.; Gembicky, M.; Figueroa, J. S.; Abram, U. Mixed-Isocyanide Complexes of Technetium under Steric and Electronic Control. *Inorg. Chem.* **2022**, *61*, 16163-16176.
- (12) Salsi, F.; Wang, S.; Teutloff, C.; Busse, M.; Neville, M.; Hagenbach, A.; Bittl, R.; Figueroa, J. S.; Abram, U. A Complete Triad of Zero-Valent 17-Electron Monoradicals of Group 7 Elements Stabilized by *m*-Terphenyl Isocyanides. *Angew. Chem. Int. Ed.*, **2023**, *62*, e202300254.
- (13) Salsi, F.; Hagenbach, A.; Figueroa, J. S.; Abram, U. Na[Tc(CO)(CNp-F-Ar<sup>DArF2</sup>)<sub>4</sub>]: an isocyanide analogue of the elusive Na[Tc(CO)<sub>5</sub>]. *Chem. Commun.* **2023**, *59*, 4028-4031.
- (14) Hieber, W.; Lux, F.; Herget, C. Über Kohlenoxidverbindungen des Technetiums. *Z. Naturforsch.* **1965**, *20b*, 1159-1165.
- (15) Lorenz, B.; Findeisen, M.; Olk, B.; Schmidt, K. Technetium(I) Complexes Tc(CO)<sub>3</sub>BrL<sub>2</sub> (L = Phosphine, Pyridine, Isocyanide). *Z. Anorg. Allg. Chem.* **1988**, *566*, 160-168.
- (16) Alberto, R.; Schibli, R.; Egli, A.; Hermann, W. A.; Artus, G.; Abram, U.; Kaden, T. A. Metal carbonyl syntheses. XXII. Low-pressure carbonylation of [MOCl<sub>4</sub>] and [MO<sub>4</sub>]. The technetium(I) and rhenium(I) complexes [NEt<sub>4</sub>]<sub>2</sub>[MCl<sub>3</sub>(CO)<sub>3</sub>]. *J. Organomet. Chem.* **1995**, *492*, 217-224.
- (17) Alberto, R.; Schibli, R.; August Schubiger, P. A.; Abram, U.; Kaden, T. A. Reactions with the technetium and rhenium carbonyl complexes (NEt<sub>4</sub>)<sub>2</sub>[MX<sub>3</sub>(CO)<sub>3</sub>]. Synthesis and structures of [Tc(CNBut)<sub>3</sub>(CO)<sub>3</sub>](NO<sub>3</sub>) and (NEt<sub>4</sub>)[Tc<sub>2</sub>(μ-SCH<sub>2</sub>CH<sub>2</sub>OH)<sub>2</sub>(CO)<sub>6</sub>]. *Polyhedron*, **1996**, *15*, 1079-1089.
- (18) Rečnik, L.-M.; Kandioller, W.; Mindt, T. L. 1,4-Disubstituted 1,2,3-Triazoles as Amide Bond Surrogates for the Stabilisation of Linear Peptides with Biological Activity. *Molecules* **2020**, *25*, 3576.
- (19) Mikhalev, V. A. <sup>99</sup>Tc NMR Spectroscopy. *Radiochemistry*, **2005**, *47*, 319-333.
- (20) O'Connell, L. A.; Pearlstein, R. M.; Davison, A.; Thornback, J. R.; Kronauge, J. F.; Jones, A. G. Technetium-99 NMR spectroscopy: chemical shift trends and long range coupling effects. *Inorg. Chim. Acta* **1989**, *161*, 39-43.
- (21) Balasekaran, S. M.; Hagenbach, A.; Drees, M.; Abram, U. [Tc<sup>II</sup>(NO)(trifluoroacetate)<sub>4</sub>F]<sup>2-</sup> - synthesis and reactions. *Dalton Trans.* **2017**, *46*, 13544-13555.
- (22) Mizuno, Y.; Uehara, T.; Hanaoka, H.; Endo, Y.; Jen, C.-W.; Arano, Y. Purification-Free Method for Preparing Technetium-99m Labeled Multivalent Probes for Enhanced in Vivo Imaging of Saturable Systems. *J. Med. Chem.*, **2016**, *59*, 3331-3339.
- (23) Mizuno, Y.; Uehara, T.; Jen, C.-W.; Akizawa, H.; Arano, Y. The synthesis of a <sup>99m</sup>Tc-labeled tetravalent targeting probe upon isonitrile coordination to <sup>99m</sup>Tc(I) for enhanced target uptake in saturable systems. *RSC Adv.*, **2019**, *9*, 26126-26135.
- (24) Mizuno, Y.; Komatsu, N.; Uehara, T.; Shimoda, Y.; Kimura, K.; Arano, Y.; Akizawa, H. Aryl isocyanide derivative for one-pot synthesis of purification-free <sup>99m</sup>Tc-labeled hexavalent targeting probe. *Nucl. Med. Biol.* **2020**, *86-87*, 30-36.
- (25) Rostovtsev, V. V.; Green, L. G.; Fokin, V. V.; Sharpless, K. B. A Stepwise Huisgen Cycloaddition Process: Copper(I)-Catalyzed Regioselective "Ligation" of Azides and Terminal Alkynes. *Angew. Chem. Int. Ed.* **2002**, *41*, 2596-2599.
- (26) Ferraro, V.; Sole, R.; Bortoluzzi, M.; Beghetto, V.; Castro, J. Tris-isocyanide copper(I) complex enabling copper azide-alkyne cycloaddition in neat conditions. *Appl. Organomet. Chem.* **2021**, e6401.
- (27) Bell, A.; Walton, R.; Edwards, D.; Poulter, M. Cationic copper (I) isocyanide complexes, [Cu(CNR)<sub>4</sub>]<sup>+</sup> (R = CH<sub>3</sub>, C(CH<sub>3</sub>)<sub>3</sub> and 2,6-(CH<sub>3</sub>)<sub>2</sub>-C<sub>6</sub>H<sub>3</sub>): Preparations, spectroscopic properties and reactions with neutral ligands. A comparison of the vibrational spectra of [Cu(CNCH<sub>3</sub>)<sub>4</sub>]<sup>+</sup>, [Cu(NCCCH<sub>3</sub>)<sub>4</sub>]<sup>+</sup> and [Cu(NCCD<sub>3</sub>)<sub>4</sub>]<sup>+</sup>. *Inorg. Chim. Acta* **1985**, *104*, 171-178.
- (28) Deicas, B.; Gambino, D.; Kremer, C.; Kremer, E.; Mombrú, A.; Suescun, L.; Mariezcurrena, R.; González, O.; Rey, A.; Mallo, L.; et al. Synthesis, characterization and spectroscopic properties of [Cu(alkylisocyanide)<sub>4</sub>]BF<sub>4</sub> complexes. X-ray crystal structures of [Cu(MIBI)<sub>4</sub>]BF<sub>4</sub> and [Cu(CPI)<sub>4</sub>]BF<sub>4</sub>. *Polyhedron* **1997**, *16* (14), 2397-2403.
- (29) Lal, S.; Diez-Gonzalez, S. [CuBr(PPh<sub>3</sub>)<sub>3</sub>] for azide-alkyne cycloaddition reactions under strict Click conditions. *J. Org. Chem.* **2011**, *76*, 2367-2373.
- (30) Chan, T. R.; Hilgraf, R.; Sharpless, K. B.; Fokin, V. V. Polytriazoles as Copper(I)-Stabilizing Ligands in Catalysis. *Org. Lett.* **2004**, *6*, 2853-2855.
- (31) Nickisch, R.; Gabrielsen, S. M.; Meier, M. A. R. Novel Access to Known and Unknown Thiourea Catalyst via a Multicomponent-Reaction Approach. *ChemistrySelect*, **2020**, *5*, 11915-11920.
- (32) Nenajdenko, V. G.; Gulevich, A. V.; Sokolova, N. V.; Mironov, A. V.; Balenkova, E. S. Chiral Isocyanazides: Efficient Bifunctional Reagents for Bioconjugation. *Eur. J. Org. Chem.* **2010**, *2010*, 1445-1449.
- (33) Roca Jungfer, M.; Abram, U. [Tc(OH<sub>2</sub>)(CO)<sub>3</sub>(PPh<sub>3</sub>)<sub>2</sub>]<sup>+</sup>: A Synthron for Tc(I) Complexes and Its Reactions with Neutral Ligands. *Inorg. Chem.* **2021**, *60*, 16734-16753.
- (34) Roca Jungfer, M.; Abram, U. Unlocking Air- and Water-Stable Technetium Acetylides and Other Organometallic Complexes. *Inorg. Chem.* **2022**, *61*, 7765-7779.
- (35) Škoch, K.; Cisařová, I.; Štěpnička, P. Selective Gold-Catalysed Synthesis of Cyanamides and 1-Substituted 1H-Tetrazol-5-Amines from Isocyanides. *Chemistry—A European Journal* **2018**, *24*, 13788-13791.
- (36) Kubas, G.; Monzyk, B.; Crumblis, A. Tetrakis (Acetonitrile) Copper(I+) Hexafluorophosphate(1-). *Inorganic Syntheses: Reagents for Transition Metal Complex and Organometallic Syntheses* **1990**, *28*, 68-70.
- (37) Gujadhur, R.; Venkataraman, D.; Kintigh, J. T. Formation of aryl nitrogen bonds using a soluble copper (I) catalyst. *Tetrahedron Lett.* **2001**, *42*, 4791-4793.
- (38) Sheldrick, G. SADABS, SHELXS-2008, SHELXL-2014. University of Göttingen: Göttingen, Germany: 2014.
- (39) Coppens, P. The Evaluation of Absorption and Extinction in Single-Crystal Structure Analysis. *Crystallographic Computing*. Copenhagen, Muksgaard: 1979.
- (40) Sheldrick, G. M. A short history of SHELX. *Acta Crystallogr. Sect. A: Found. Crystallogr.* **2008**, *64*, 112-122.
- (41) Sheldrick, G. M. Crystal structure refinement with SHELXL. *Acta Crystallographica Section C: Structural Chemistry* **2015**, *71*, 3-8.
- (42) Dolomanov, O. V.; Bourhis, L. J.; Gildea, R. J.; Howard, J. A.; Puschmann, H. OLEX2: a complete structure solution, refinement and analysis program. *J. Appl. Crystallogr.* **2009**, *42*, 339-341.
- (43) Diamond - Crystal and Molecular Structure Visualization Crystal Impact; Dr. H. Putz & Dr. K. Brandenburg GbR: Bonn, Germany.



Supporting information for the paper entitled:

## Reactivity of an isocyano-alkyne ligand

*Guilhem Claude,<sup>§</sup> Denis Puccio,<sup>§</sup> Maximilian Roca Jungfer,<sup>§</sup> Adelheid Hagenbach<sup>§</sup>, Sarah Spreckelmeyer<sup>†</sup> and Ulrich Abram<sup>§\*</sup>*

<sup>§</sup>Freie Universität Berlin, Institute of Chemistry and Biochemistry, Fabeckstr. 34–36, 14195 Berlin, Germany

<sup>†</sup> Department of Nuclear Medicine, Charité - Universitätsmedizin Berlin, Augustenburger Platz 1, 13353, Berlin, Germany

\*Corresponding author: [ulrich.abram@fu-berlin.de](mailto:ulrich.abram@fu-berlin.de)

## Table of content

Crystallographic data.....	4
<b>Table S1:</b> Crystallographic data and data collection parameters.....	4
<b>Figure S1:</b> Ellipsoid representation of [Tc(CNPh <sup>pC≡CH</sup> ) <sub>6</sub> ][PF <sub>6</sub> ] <sub>2</sub> ·2.5 toluene ([ <b>1</b> ][PF <sub>6</sub> ]) <sub>2</sub> ·2.5 toluene. The thermal ellipsoids are set at a 50% probability level. Hydrogen atoms are omitted for clarity. ....	5
<b>Table S2:</b> Selected bond lengths (Å) and angles (°) in [Tc(CNPh <sup>pC≡CH</sup> ) <sub>6</sub> ][PF <sub>6</sub> ] <sub>2</sub> ·2.5 toluene ([ <b>1</b> ][PF <sub>6</sub> ]) <sub>2</sub> ·2.5 toluene. ....	5
<b>Figure S2:</b> Ellipsoid representation of [Cu(CNPh <sup>pC≡CH</sup> ) <sub>4</sub> ][BF <sub>4</sub> ] <sub>0.5</sub> CH <sub>2</sub> Cl <sub>2</sub> ([ <b>2</b> ][BF <sub>4</sub> ]) <sub>0.5</sub> CH <sub>2</sub> Cl <sub>2</sub> . The thermal ellipsoids are set at a 50% probability level. Hydrogen atoms are omitted for clarity. ....	7
<b>Table S3:</b> Selected bond lengths (Å) and angles (°) in [Cu(CNPh <sup>pC≡CH</sup> ) <sub>4</sub> ][BF <sub>4</sub> ] <sub>0.5</sub> CH <sub>2</sub> Cl <sub>2</sub> ([ <b>2</b> ][BF <sub>4</sub> ]) <sub>0.5</sub> CH <sub>2</sub> Cl <sub>2</sub> . ....	7
<b>Figure S3:</b> Ellipsoid representation of <i>mer,trans</i> -[Tc(CO) <sub>3</sub> (PPh <sub>3</sub> ) <sub>2</sub> (CNPh <sup>azole</sup> )][BF <sub>4</sub> ] <sub>0.5</sub> toluene ([ <b>6</b> ][BF <sub>4</sub> ]) <sub>0.5</sub> toluene. The thermal ellipsoids are set at a 50% probability level. Hydrogen atoms are omitted for clarity. ....	8
<b>Table S4:</b> Selected bond lengths (Å) and angles (°) in <i>mer,trans</i> -[Tc(CO) <sub>3</sub> (PPh <sub>3</sub> ) <sub>2</sub> (CNPh <sup>azole</sup> )][BF <sub>4</sub> ] <sub>0.5</sub> toluene ([ <b>6</b> ][BF <sub>4</sub> ]) <sub>0.5</sub> toluene. ....	8
Spectroscopic and mass spectrometric data.....	9
<b>Figure S4:</b> IR (KBr) spectrum of [Tc(CNPh <sup>pC≡CH</sup> ) <sub>6</sub> Cl] ([ <b>1</b> ]Cl). ....	9
<b>Figure S5:</b> <sup>1</sup> H NMR spectrum of [Tc(CNPh <sup>pC≡CH</sup> ) <sub>6</sub> Cl] ([ <b>1</b> ]Cl) in MeOD-d <sub>4</sub> . ....	9
<b>Figure S6:</b> <sup>99</sup> Tc NMR spectrum of [Tc(CNPh <sup>pC≡CH</sup> ) <sub>6</sub> Cl] ([ <b>1</b> ]Cl) in MeOD-d <sub>4</sub> . ....	10
<b>Figure S7:</b> IR (KBr) spectrum of [Tc(CNPh <sup>pC≡CH</sup> ) <sub>6</sub> ][PF <sub>6</sub> ] ([ <b>1</b> ][PF <sub>6</sub> ]). ....	10
<b>Figure S8:</b> <sup>1</sup> H NMR spectrum of [Tc(CNPh <sup>pC≡CH</sup> ) <sub>6</sub> ][PF <sub>6</sub> ] ([ <b>1</b> ][PF <sub>6</sub> ]) in CD <sub>2</sub> Cl <sub>2</sub> . ....	11
<b>Figure S9:</b> <sup>19</sup> F NMR spectrum of [Tc(CNPh <sup>pC≡CH</sup> ) <sub>6</sub> ][PF <sub>6</sub> ] ([ <b>1</b> ][PF <sub>6</sub> ]) in CD <sub>2</sub> Cl <sub>2</sub> . ....	11
<b>Figure S10:</b> <sup>99</sup> Tc NMR spectrum of [Tc(CNPh <sup>pC≡CH</sup> ) <sub>6</sub> ][PF <sub>6</sub> ] ([ <b>1</b> ][PF <sub>6</sub> ]) in CD <sub>2</sub> Cl <sub>2</sub> . ....	12
<b>Figure S11:</b> IR (KBr) spectrum of [Tc(CNPh <sup>azole</sup> ) <sub>6</sub> Cl] ([ <b>2</b> ]Cl). ....	12
<b>Figure S12:</b> <sup>1</sup> H NMR spectrum of [Tc(CNPh <sup>azole</sup> ) <sub>6</sub> Cl] ([ <b>2</b> ]Cl) in acetone-d <sub>6</sub> . ....	13
<b>Figure S13:</b> <sup>99</sup> Tc NMR spectrum of [Tc(CNPh <sup>azole</sup> ) <sub>6</sub> Cl] ([ <b>2</b> ]Cl) in acetone-d <sub>6</sub> . ....	13
<b>Figure S14:</b> IR (ATR) spectrum of [Cu(CNPh <sup>pC≡CH</sup> ) <sub>4</sub> ][BF <sub>4</sub> ] ([ <b>3</b> ][BF <sub>4</sub> ]). ....	14
<b>Figure S15:</b> <sup>1</sup> H NMR spectrum of [Cu(CNPh <sup>pC≡CH</sup> ) <sub>4</sub> ][BF <sub>4</sub> ] ([ <b>3</b> ][BF <sub>4</sub> ]) in acetone-d <sub>6</sub> . ....	14
<b>Figure S16:</b> <sup>13</sup> C{ <sup>1</sup> H} NMR spectrum of [Cu(CNPh <sup>pC≡CH</sup> ) <sub>4</sub> ][BF <sub>4</sub> ] ([ <b>3</b> ][BF <sub>4</sub> ]) in acetone-d <sub>6</sub> . ....	15
<b>Figure S17:</b> <sup>19</sup> F NMR spectrum of [Cu(CNPh <sup>pC≡CH</sup> ) <sub>4</sub> ][BF <sub>4</sub> ] ([ <b>3</b> ][BF <sub>4</sub> ]) in acetone-d <sub>6</sub> . ....	15
<b>Figure S18:</b> ESI+ mass spectrum of [Cu(CNPh <sup>pC≡CH</sup> ) <sub>4</sub> ][BF <sub>4</sub> ] ([ <b>3</b> ][BF <sub>4</sub> ]) in acetone-d <sub>6</sub> . ....	16
<b>Figure S19:</b> IR (ATR) spectrum of [Cu(CNPh <sup>azole</sup> ) <sub>4</sub> ][BF <sub>4</sub> ] ([ <b>4</b> ][BF <sub>4</sub> ]). ....	16
<b>Figure S20:</b> <sup>1</sup> H NMR spectrum with assignment of [Cu(CNPh <sup>azole</sup> ) <sub>4</sub> ][BF <sub>4</sub> ] ([ <b>4</b> ][BF <sub>4</sub> ]) in acetone-d <sub>6</sub> . ....	17
<b>Figure S21:</b> <sup>1</sup> H NMR spectrum of [Cu(CNPh <sup>azole</sup> ) <sub>4</sub> ][BF <sub>4</sub> ] ([ <b>4</b> ][BF <sub>4</sub> ]) in CD <sub>2</sub> Cl <sub>2</sub> . ....	17
<b>Figure S22:</b> <sup>13</sup> C{ <sup>1</sup> H} NMR spectrum of [Cu(CNPh <sup>azole</sup> ) <sub>4</sub> ][BF <sub>4</sub> ] ([ <b>4</b> ][BF <sub>4</sub> ]) in CD <sub>2</sub> Cl <sub>2</sub> . ....	18

<b>Figure S23:</b> $^{19}\text{F}$ NMR spectrum of $[\text{Cu}(\text{CNPh}^{\text{azole}})_4][\text{BF}_4]$ ( <b>4</b> ) in $\text{CD}_2\text{Cl}_2$ .	18
<b>Figure S24:</b> ESI+ mass spectrum of $[\text{Cu}(\text{CNPh}^{\text{azole}})_4][\text{BF}_4]$ ( <b>4</b> ) in MeCN.	19
<b>Figure S25:</b> IR (ATR) spectrum of $\text{CNPh}^{\text{azole}}$ ( <b>5</b> ).	19
<b>Figure S26:</b> $^1\text{H}$ NMR spectrum of $\text{CNPh}^{\text{azole}}$ ( <b>5</b> ) in acetone- $d_6$ .	20
<b>Figure S27:</b> $^{13}\text{C}\{^1\text{H}\}$ NMR spectrum of $\text{CNPh}^{\text{azole}}$ ( <b>5</b> ) in acetone- $d_6$ . The full spectrum with the solvent signals is depicted in the box.	20
<b>Figure S28:</b> ESI+ mass spectrum of $\text{CNPh}^{\text{azole}}$ ( <b>5</b> ) in MeCN.	21
<b>Figure S29:</b> IR (KBr) spectrum of <i>mer,trans</i> - $[\text{Tc}(\text{CO})_3(\text{PPh}_3)_2(\text{CNPh}^{\text{azole}})][\text{BF}_4]$ ( <b>6</b> ).	21
<b>Figure S30:</b> $^1\text{H}$ NMR spectrum of <i>mer,trans</i> - $[\text{Tc}(\text{CO})_3(\text{PPh}_3)_2(\text{CNPh}^{\text{azole}})][\text{BF}_4]$ ( <b>6</b> ) in $\text{CD}_2\text{Cl}_2$ .	22
<b>Figure S31:</b> $^{19}\text{F}$ NMR spectrum of <i>mer,trans</i> - $[\text{Tc}(\text{CO})_3(\text{PPh}_3)_2(\text{CNPh}^{\text{azole}})][\text{BF}_4]$ ( <b>6</b> ) in acetone- $d_6$ .	22
<b>Figure S32:</b> $^{99}\text{Tc}$ NMR spectrum of <i>mer,trans</i> - $[\text{Tc}(\text{CO})_3(\text{PPh}_3)_2(\text{CNPh}^{\text{azole}})][\text{BF}_4]$ ( <b>6</b> ) in $\text{CD}_2\text{Cl}_2$ .	23
<b>Figure S33:</b> $^{99}\text{Tc}$ NMR spectra of (from top to bottom) $[\text{Tc}(\text{CN}^n\text{Bu})_6]$ , <b>6</b> , <b>2</b> and <b>1</b> .	23
<b>Figure S34:</b> iTLC of $^{99\text{m}}\text{Tc}$ reaction mixture of $[\text{Cu}(\text{CNPh}^{\text{azole}})_4][\text{BF}_4]$ ( <b>4</b> ) and $[\text{C}^{99\text{m}}\text{TcO}_4]^-$ (see experimental for exact conditions) with $\text{H}_2\text{O}$ as a mobile phase. The green area corresponds to a lipophilic compound or $\text{TcO}_2$ . $[\text{C}^{99\text{m}}\text{TcO}_4]^-$ elutes with a $R_f \approx 1,0$ under those conditions, thus the presence of unreacted $[\text{C}^{99\text{m}}\text{TcO}_4]^-$ could be excluded...	24
<b>Figure S35:</b> iTLC of $^{99\text{m}}\text{Tc}$ reaction mixture with $[\text{Cu}(\text{CNPh}^{\text{azole}})_4][\text{BF}_4]$ ( <b>4</b> ) and $[\text{C}^{99\text{m}}\text{TcO}_4]^-$ (see experimental for exact conditions) with methyl-ethylketone (MEK) as a mobile phase. Under those conditions both $[\text{TcO}_4]^-$ , which is not present in this mixture ( <i>vide supra</i> ) elutes with a $R_f \approx 1,0$ . Thus the area in red corresponds to a lipophilic specie which could be eluted with a $R_f \approx 1,0$ using MEK. Colloidal technetium does not elute and thus the area in green can be attributed to it.	24
<b>Figure S36:</b> iTLC of $^{99\text{m}}\text{Tc}$ reaction mixture with $[\text{Cu}(\text{CNPh}^{\text{azole}})_4][\text{BF}_4]$ ( <b>4</b> ) and $[\text{C}^{99\text{m}}\text{TcO}_4]^-$ (see experimental for exact conditions) after purification on a C-18 cartridge. with methyl-ethylketone (MEK) as a mobile phase. Colloidal technetium could be removed almost quantitatively.	25
References	26

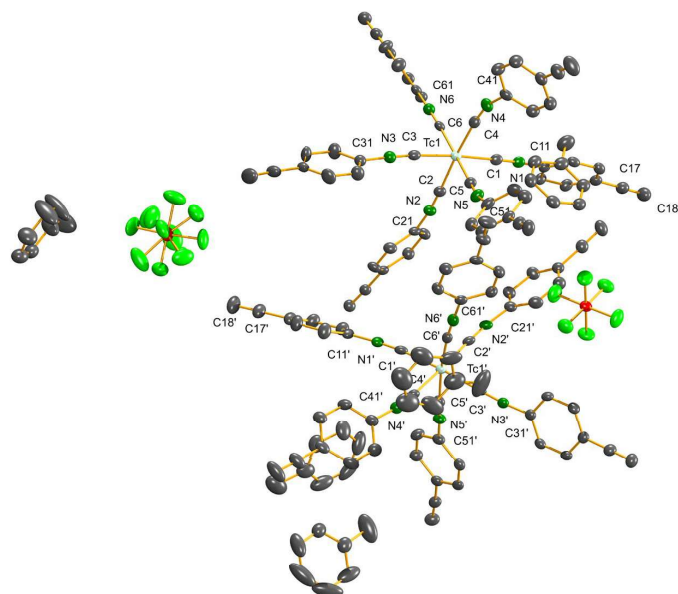
## Crystallographic data

The intensities for the X-ray determinations were collected on STOE IPDS II or Bruker D8 Venture instruments with Mo K $\alpha$  radiation. The space groups were determined by the detection of systematic absences. Absorption corrections were carried out by a multi scan methods.<sup>1,2</sup> Structure solution and refinement were performed with the SHELX program package using OLEX 2.<sup>3-5</sup> Hydrogen atoms were derived from the final Fourier maps and refined or placed at calculated positions and treated with the 'riding model' option of SHELXL. The representation of molecular structures was done using the program DIAMOND 4.2.2.<sup>6</sup>

Additional information on the structure determinations is contained in the Supporting Information and has been deposited with the Cambridge Crystallographic Data Centre.

**Table S1:** Crystallographic data and data collection parameters

	[Tc(CNPh <sup>pC≡CH</sup> ) <sub>6</sub> ][PF <sub>6</sub> ]	[Cu(CNPh <sup>pC≡CH</sup> ) <sub>4</sub> ][BF <sub>4</sub> ]	[Tc(CO) <sub>3</sub> (PPh <sub>3</sub> ) <sub>2</sub> L <sub>1</sub> ][BF <sub>4</sub> ]
	2.5 toluene ([1][PF <sub>6</sub> ]) 2.5 toluene	0.5 CH <sub>2</sub> Cl <sub>2</sub> ([2][BF <sub>4</sub> ])·0.5 CH <sub>2</sub> Cl <sub>2</sub>	0.5 toluene ([6][BF <sub>4</sub> ])·0.5 toluene
Empirical formula	TcPN <sub>6</sub> FeC <sub>71.5</sub> H <sub>50</sub>	CuClBF <sub>4</sub> N <sub>4</sub> C <sub>36.5</sub> H <sub>21</sub>	C <sub>58.5</sub> H <sub>46</sub> BF <sub>4</sub> N <sub>4</sub> O <sub>3</sub> P <sub>2</sub> Tc
Formula weight	1236.14	701.37	1099.74
Temperature/K	100.0	155.00	293(2)
Crystal system	triclinic	triclinic	monoclinic
Space group	P-1	P-1	P2 <sub>1</sub> /c
a/Å	17.442(8)	11.9358(6)	9.3499(5)
b/Å	18.390(5)	13.7785(8)	24.3874(2)
c/Å	20.936(8)	21.6979(13)	23.0136(1)
$\alpha$ /°	85.902(14)	74.776(2)	90
$\beta$ /°	89.617(6)	79.430(2)	99.108(4)
$\gamma$ /°	67.117(6)	87.986(2)	90
Volume/Å <sup>3</sup>	6169(4)	3384.4(3)	5181.4(5)
Z	4	4	4
$\rho_{\text{calc}}$ / cm <sup>3</sup>	1.331	1.376	1.410
$\mu$ / mm <sup>-1</sup>	0.325	0.778	0.404
F(000)	2532.0	1420.0	2252.0
Crystal size / mm <sup>3</sup>	0.38 × 0.13 × 0.045	0.276 × 0.249 × 0.246	0.6 × 0.12 × 0.12
Radiation	MoK $\alpha$ ( $\lambda$ = 0.71073)	MoK $\alpha$ ( $\lambda$ = 0.71073)	Mo K $\alpha$ ( $\lambda$ = 0.71073)
2 $\theta$ range for data collection/°	3.902 to 51.996	3.956 to 54.238	6.678 to 53.998
Index ranges	-21 ≤ h ≤ 21, -22 ≤ k ≤ 22, -25 ≤ l ≤ 25	-14 ≤ h ≤ 15, -17 ≤ k ≤ 17, -27 ≤ l ≤ 27	-11 ≤ h ≤ 10, -31 ≤ k ≤ 29
Reflections collected	157402	122870	34973
Independent reflections	23910 [R <sub>int</sub> = 0.1383, R <sub>sigma</sub> = 0.0845]	14878 [R <sub>int</sub> = 0.0313, R <sub>sigma</sub> = 0.0171]	11270 [R <sub>int</sub> = 0.1156, R <sub>sigma</sub> = 0.1113]
Data/restraints/parameters	23910/1806/1594	14878/4/893	11270/0/680
Goodness-of-fit on F <sup>2</sup>	1.235	1.043	0.837
Final R indexes [ $I \geq 2\sigma(I)$ ]	R <sub>1</sub> = 0.0935, wR <sub>2</sub> = 0.1578	R <sub>1</sub> = 0.0398, wR <sub>2</sub> = 0.1072	R <sub>1</sub> = 0.0430, wR <sub>2</sub> = 0.0838
Final R indexes [all data]	R <sub>1</sub> = 0.1221, wR <sub>2</sub> = 0.1673	R <sub>1</sub> = 0.0452, wR <sub>2</sub> = 0.1122	R <sub>1</sub> = 0.0847, wR <sub>2</sub> = 0.0929
Largest diff. peak/hole / e Å <sup>-3</sup>	1.48/-0.81	1.95/-1.67	0.60/-0.64
Diffractometer	D8 Venture	D8 Venture	IPDS 2T
CCDC access code			

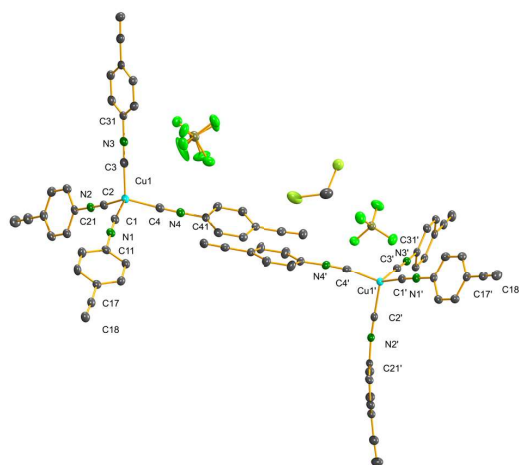


**Figure S1:** Ellipsoid representation of  $[\text{Tc}(\text{CNPh}^{\text{pC}\equiv\text{CH}})][\text{PF}_6]\cdot 2.5$  toluene ( $[\mathbf{1}][\text{PF}_6]\cdot 2.5$  toluene). The thermal ellipsoids are set at a 50% probability level. Hydrogen atoms are omitted for clarity.

**Table S2:** Selected bond lengths (Å) and angles (°) in  $[\text{Tc}(\text{CNPh}^{\text{pC}\equiv\text{CH}})][\text{PF}_6]\cdot 2.5$  toluene ( $[\mathbf{1}][\text{PF}_6]\cdot 2.5$  toluene).

Tc1-C2	2.040(6)	C2-N2	1.160(7)	C27'-C28'	1.179(8)
Tc1-C5	2.021(5)	C5-N5	1.169(7)	C47-C48	1.177(9)
Tc1-C1	2.020(6)	C21-N2	1.394(7)	C17'-C18'	1.176(9)
Tc1-C6	2.029(5)	C4-N4	1.169(7)	C47'-C48'	1.156(9)
Tc1-C3	2.022(6)	C41-N4	1.407(7)	C37-C38	1.176(9)
Tc1-C4	2.015(6)	C51-N5	1.407(7)		
Tc1'-C2'	2.052(6)	C31-N3	1.406(7)		
Tc1'-C3'	2.034(6)	N1'-C11'	1.399(7)		
Tc1'-C4'	2.016(6)	N5'-C51'	1.398(7)		
Tc1'-C6'	2.033(6)	N5'-C5'	1.155(7)		
Tc1'-C1'	2.044(6)	N4'-C4'	1.162(7)		
Tc1'-C5'	2.030(6)	N4'-C41'	1.402(7)		
N1-C1	1.179(7)	N6'-C61'	1.399(7)		
N1-C11	1.393(7)	N6'-C6'	1.166(7)		
N2'-C2'	1.154(7)	C68-C67	1.174(8)		
N2'-C21'	1.396(7)	C27-C28	1.182(8)		
N6-C61	1.398(7)	C57'-C58'	1.184(8)		
N6-C6	1.164(7)	C38'-C37'	1.181(8)		
N3'-C31'	1.402(7)	C17-C18	1.181(9)		
N3'-C3'	1.159(7)	C57-C58	1.179(8)		
N1'-C1'	1.157(7)	C67'-C68'	1.178(9)		

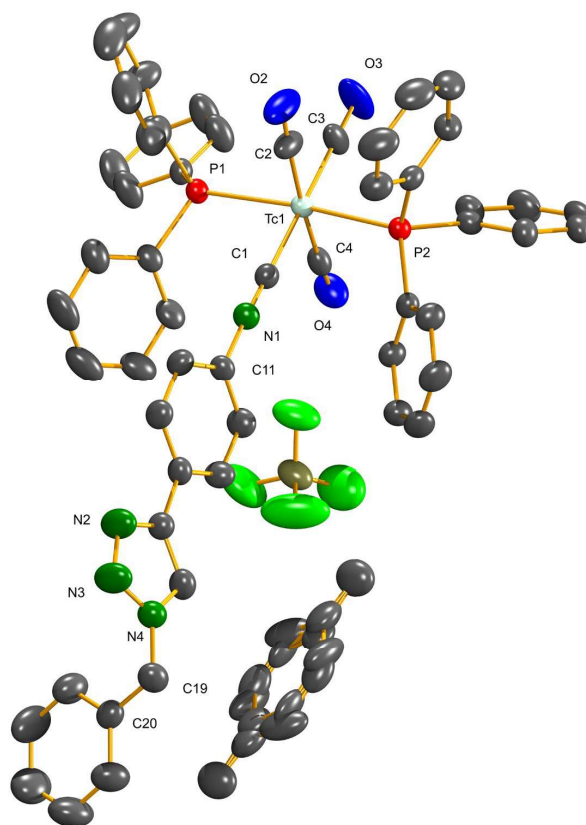
C5-Tc1-C2	94.5(2)	C1-N1-C11	175.7(5)	C18'-C17'-C14'	178.0(8)
C5-Tc1-C3	86.7(2)	C6-N6-C61	177.3(6)	C48'-C47'-C44'	178.7(8)
C1-Tc1-C2	87.6(2)	C3'-N3'-C31'	171.4(6)	C38-C37-C34	177.3(8)
C1-Tc1-C5	93.4(2)	C1'-N1'-C11'	175.5(6)	C58'-C57'-C54'	177.0(6)
C1-Tc1-C6	90.5(2)	C5'-N5'-C51'	176.9(6)	C68-C67-C64	179.4(6)
C1-Tc1-C3	175.0(2)	C4'-N4'-C41'	170.0(6)	C28-C27-C24	176.5(6)
C6-Tc1-C2	88.9(2)	C6'-N6'-C61'	177.4(6)		
C3-Tc1-C2	87.4(2)	N2-C2-Tc1	176.3(5)		
C3-Tc1-C6	89.7(2)	N5-C5-Tc1	171.4(5)		
C4-Tc1-C2	176.2(2)	N2'-C2'-Tc1'	174.4(5)		
C4-Tc1-C5	82.9(2)	N1-C1-Tc1	175.3(4)		
C4-Tc1-C1	89.7(2)	N6-C6-Tc1	177.1(5)		
C4-Tc1-C6	93.8(2)	N3-C3-Tc1	174.3(5)		
C4-Tc1-C3	95.3(2)	N3'-C3'-Tc1'	177.5(5)		
C3'-Tc1'-C2'	87.5(2)	N4'-C4'-Tc1'	176.5(5)		
C3'-Tc1'-C1'	175.4(2)	N6'-C6'-Tc1'	174.8(5)		
C4'-Tc1'-C2'	176.2(2)	N4-C4-Tc1	172.2(5)		
C4'-Tc1'-C3'	93.3(2)	C46-C41-N4	119.3(5)		
C4'-Tc1'-C6'	89.7(2)	C42-C41-N4	120.7(5)		
C4'-Tc1'-C1'	86.1(2)	N1'-C1'-Tc1'	174.2(5)		
C4'-Tc1'-C5'	92.8(2)	N5'-C5'-Tc1'	177.6(5)		
C6'-Tc1'-C2'	86.6(2)	C3-N3-C31	178.1(6)		
C6'-Tc1'-C3'	88.4(2)	C4-N4-C41	159.6(6)		
C6'-Tc1'-C1'	96.2(2)	C2-N2-C21	173.2(6)		
C1'-Tc1'-C2'	93.4(2)	C38'-C37'-C34'	178.4(6)		
C5'-Tc1'-C2'	91.0(2)	C18-C17-C14	178.5(7)		
C5'-Tc1'-C3'	86.6(2)	C58-C57-C54	178.6(7)		
C5'-Tc1'-C6'	174.6(2)	C68'-C67'-C64'	176.6(7)		
C5'-Tc1'-C1'	88.8(2)	C28'-C27'-C24'	178.1(7)		
C5-N5-C51	165.6(6)	C48-C47-C44	179.5(9)		



**Figure S2:** Ellipsoid representation of  $[\text{Cu}(\text{CNPh}^{\text{pC}\equiv\text{CH}})_4][\text{BF}_4] \cdot 0.5 \text{CH}_2\text{Cl}_2$  ( $[\mathbf{2}][\text{BF}_4] \cdot 0.5 \text{CH}_2\text{Cl}_2$ ). The thermal ellipsoids are set at a 50% probability level. Hydrogen atoms are omitted for clarity.

**Table S3:** Selected bond lengths (Å) and angles (°) in  $[\text{Cu}(\text{CNPh}^{\text{pC}\equiv\text{CH}})_4][\text{BF}_4] \cdot 0.5 \text{CH}_2\text{Cl}_2$  ( $[\mathbf{2}][\text{BF}_4] \cdot 0.5 \text{CH}_2\text{Cl}_2$ ).

Cu1'-C3'	1.952(2)	C37'-C38'	1.191(3)	C1-Cu1-C3	114.98(9)
Cu1'-C2'	1.955(2)	C17-C18	1.184(3)	C1-Cu1-C4	104.78(9)
Cu1'-C1'	1.951(2)	C37-C38	1.188(3)	C2-Cu1-C1	110.29(8)
Cu1'-C4'	1.952(2)	C27'-C28'	1.187(3)	C2-Cu1-C3	106.33(9)
Cu1-C1	1.948(2)	C47-C48	1.187(3)	C2-Cu1-C4	112.81(9)
Cu1-C2	1.945(2)	C17'-C18'	1.184(3)	C4-Cu1-C3	107.78(9)
Cu1-C3	1.951(2)	C47'-C48'	1.176(3)	C2-N2-C21	179.3(2)
Cu1-C4	1.950(2)	C27-C28	1.182(3)	C1'-N1'-C11'	178.9(2)
N2-C21	1.399(3)	N3'-C31'	1.404(2)	C1-N1-C11	178.7(2)
N2-C2	1.152(3)	N4'-C41'	1.404(3)	C2'-N2'-C21'	173.9(2)
N1'-C11'	1.397(3)	N4'-C4'	1.151(3)	C3-N3-C31	178.1(2)
N1'-C1'	1.152(3)	N4-C41	1.399(3)	C3'-N3'-C31'	176.0(2)
N1-C1	1.148(3)	N4-C4	1.149(3)	C4'-N4'-C41'	176.4(2)
N1-C11	1.399(3)	C3'-Cu1'-C2'	106.77(8)	C4-N4-C41	178.0(2)
N2'-C21'	1.401(3)	C3'-Cu1'-C4'	113.76(8)	N3'-C3'-Cu1'	176.32(18)
N2'-C2'	1.151(3)	C1'-Cu1'-C3'	108.36(8)	N2'-C2'-Cu1'	179.27(18)
N3-C31	1.402(3)	C1'-Cu1'-C2'	110.03(8)	N1'-C1'-Cu1'	174.58(18)
N3-C3	1.149(3)	C1'-Cu1'-C4'	113.73(8)	N1-C1-Cu1	172.85(19)
N3'-C3'	1.148(3)	C4'-Cu1'-C2'	103.88(8)	N2-C2-Cu1	175.81(19)
N3-C3-Cu1	177.13(18)	C28-C27'-C24'	179.0(3)	C28'-C27'-C24'	177.0(3)
N4'-C4'-Cu1'	170.03(18)	C18'-C17'-C14'	178.9(3)	C38-C37-C34	177.8(2)
N4-C4-Cu1	177.38(19)	C48-C47'-C44'	177.8(2)	C18-C17-C14	176.3(2)
C38'-C37'-C34'	178.0(2)	C48'-C47'-C44'	179.4(3)		



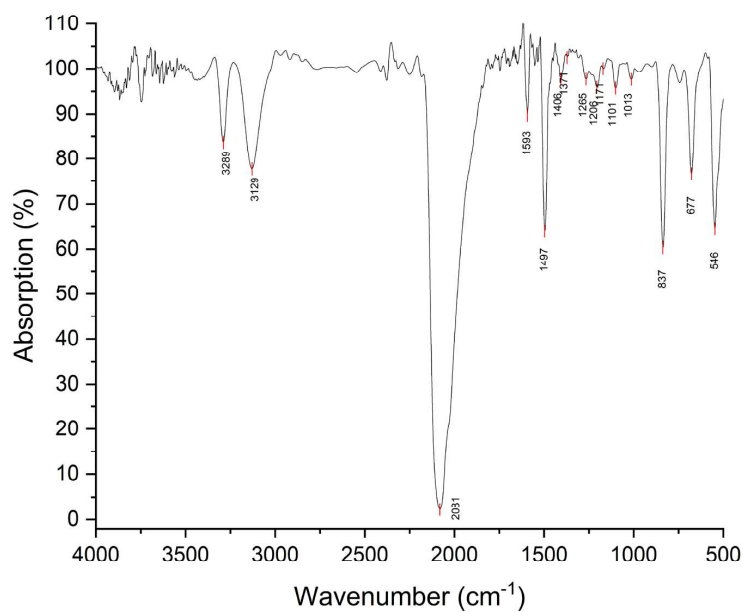
**Figure S3:** Ellipsoid representation of *mer,trans*-[Tc(CO)<sub>3</sub>(PPh<sub>3</sub>)<sub>2</sub>(CNPh<sup>azole</sup>)] [BF<sub>4</sub>] 0.5 toluene ([**6**][BF<sub>4</sub>]) 0.5 toluene. The thermal ellipsoids are set at a 50% probability level. Hydrogen atoms are omitted for clarity.

**Table S4:** Selected bond lengths (Å) and angles (°) in *mer,trans*-[Tc(CO)<sub>3</sub>(PPh<sub>3</sub>)<sub>2</sub>(CNPh<sup>azole</sup>)] [BF<sub>4</sub>] 0.5 toluene ([**6**][BF<sub>4</sub>]) 0.5 toluene.

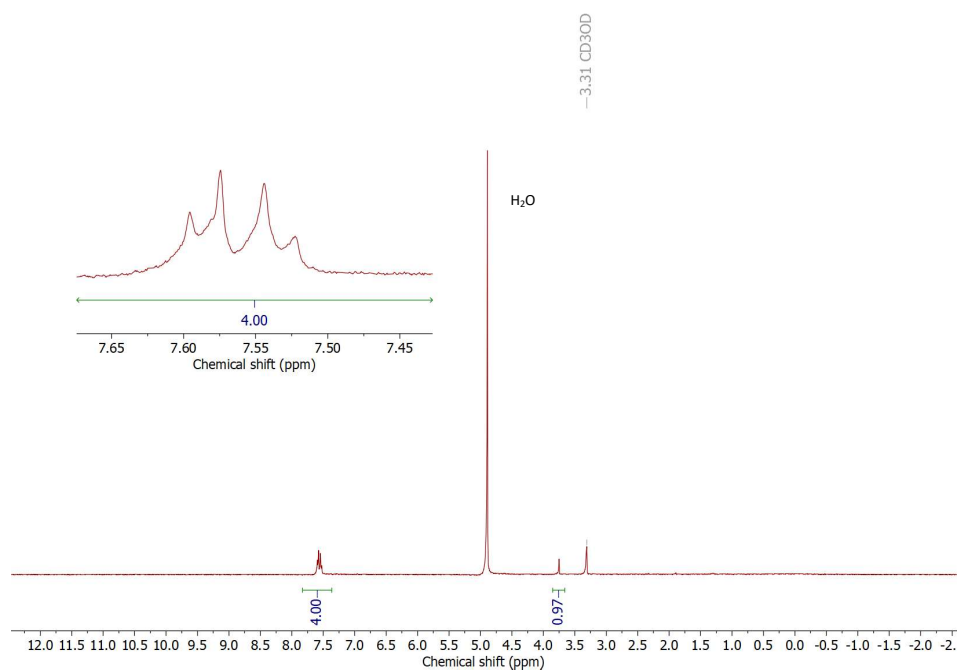
Tc1-C1	2.077(3)	Tc1-C2	1.996(4)	Tc1-C3	1.944(3)
Tc1-C4	1.975(4)	Tc1-P1	2.4661(8)	Tc1-P2	2.4482(8)
C1-N1	1.150(4)	C2-O2	1.139(4)	C3-O3	1.142(4)
C4-O4	1.144(4)	N1-C11	1.402(4)	Tc1-C1-N1	176.7(3)
Tc1-C2-O2	175.4(4)	Tc1-C3-O3	178.7(4)	C1-Tc1-P1	85.39(8)
C1-Tc1-P2	86.86(8)	C1-Tc1-C3	177.46(2)	C1-Tc1-C2	92.70(2)
C1-N1-C11	174.3(3)	N4-C19-C20	113.3(3)		



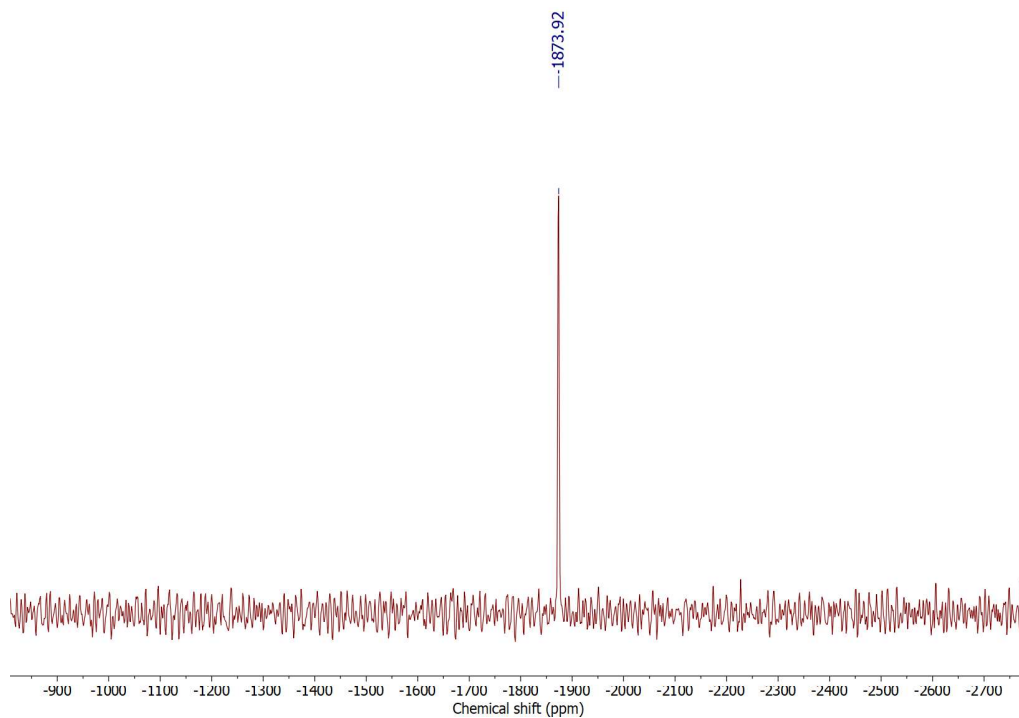
## Spectroscopic and mass spectrometric data



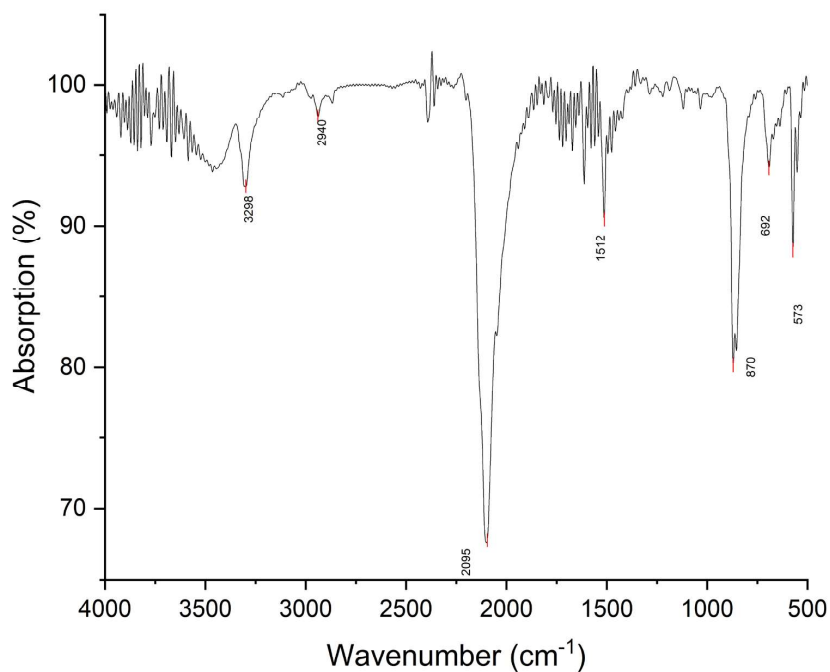
**Figure S4:** IR (KBr) spectrum of  $[\text{Tc}(\text{CNPh}^{\text{pC}\equiv\text{CH}})_6]\text{Cl}$  (**[1]Cl**).



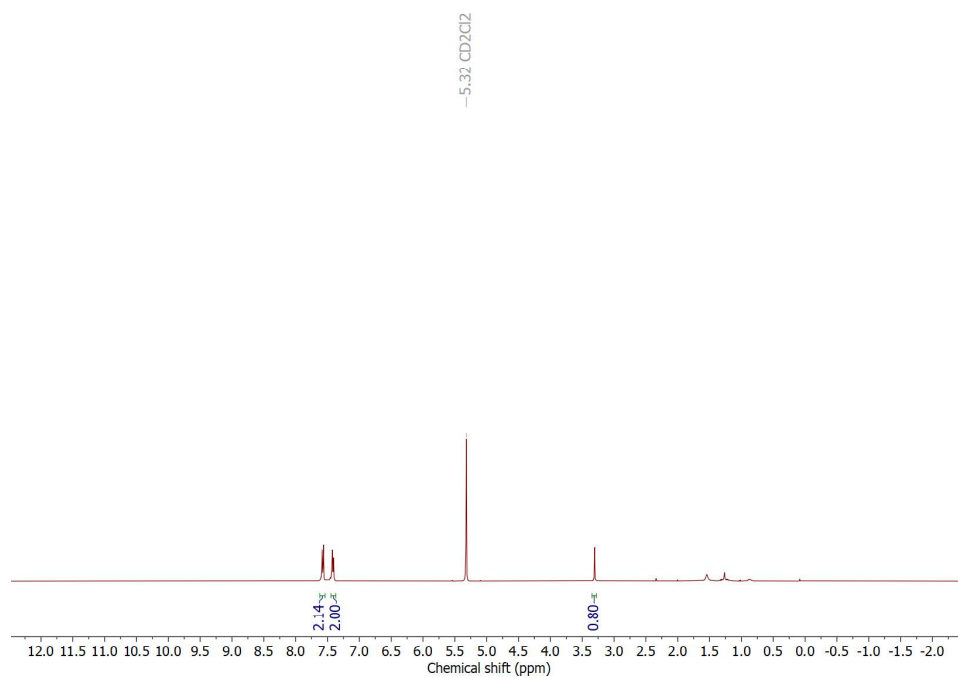
**Figure S5:**  $^1\text{H}$  NMR spectrum of  $[\text{Tc}(\text{CNPh}^{\text{pC}\equiv\text{CH}})_6]\text{Cl}$  (**[1]Cl**) in  $\text{MeOD-d}_4$ .



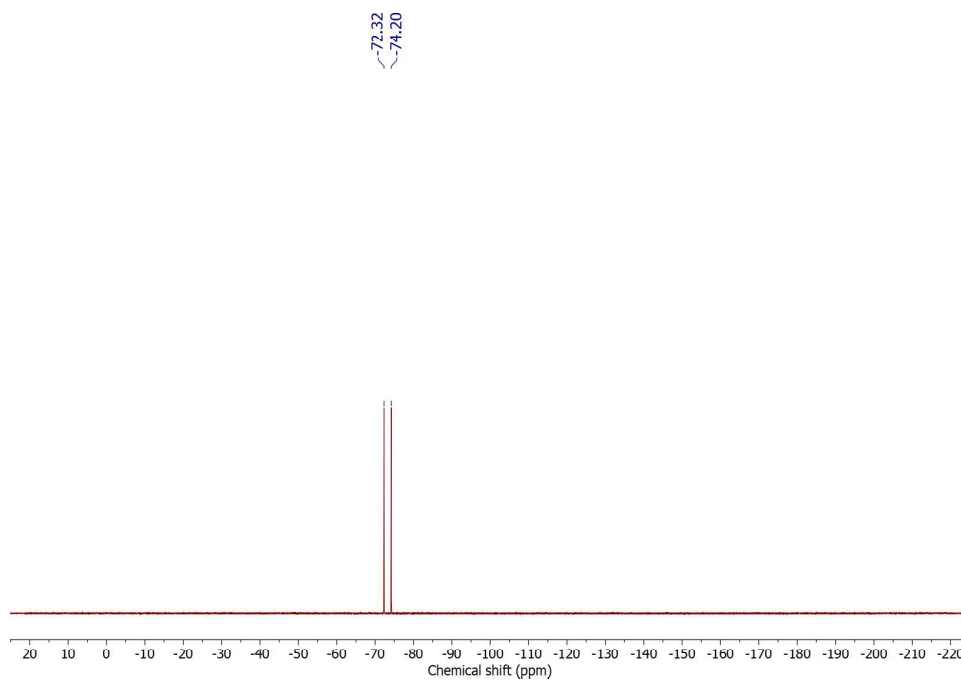
**Figure S6:**  $^{99}\text{Tc}$  NMR spectrum of  $[\text{Tc}(\text{CNPh}^{\text{pC}\equiv\text{CH}})_6]\text{Cl}$  (**[1]Cl**) in  $\text{MeOD-d}_4$ .



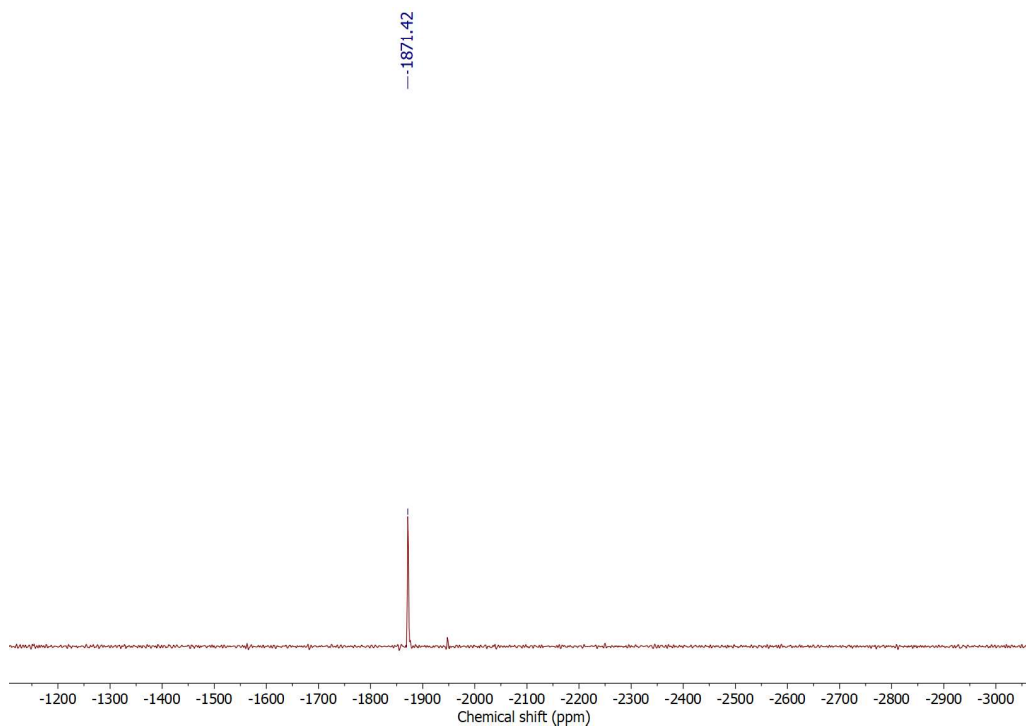
**Figure S7:** IR (KBr) spectrum of  $[\text{Tc}(\text{CNPh}^{\text{pC}\equiv\text{CH}})_6][\text{PF}_6]$  (**[1][PF}\_6]**).



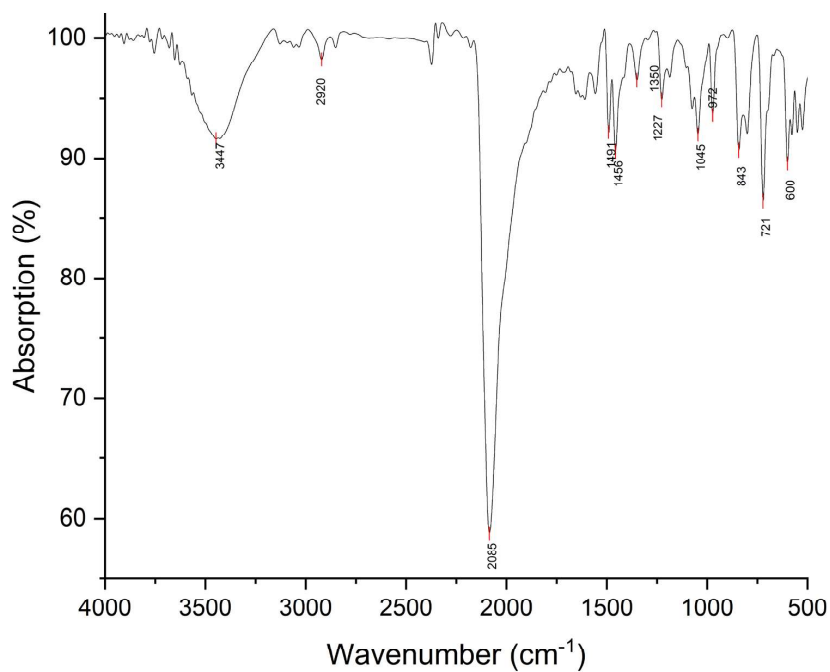
**Figure S8:**  $^1\text{H}$  NMR spectrum of  $[\text{Tc}(\text{CNPh}^{\text{pC}\equiv\text{CH}})_6][\text{PF}_6]$  (**[1]** $[\text{PF}_6]$ ) in  $\text{CD}_2\text{Cl}_2$ .



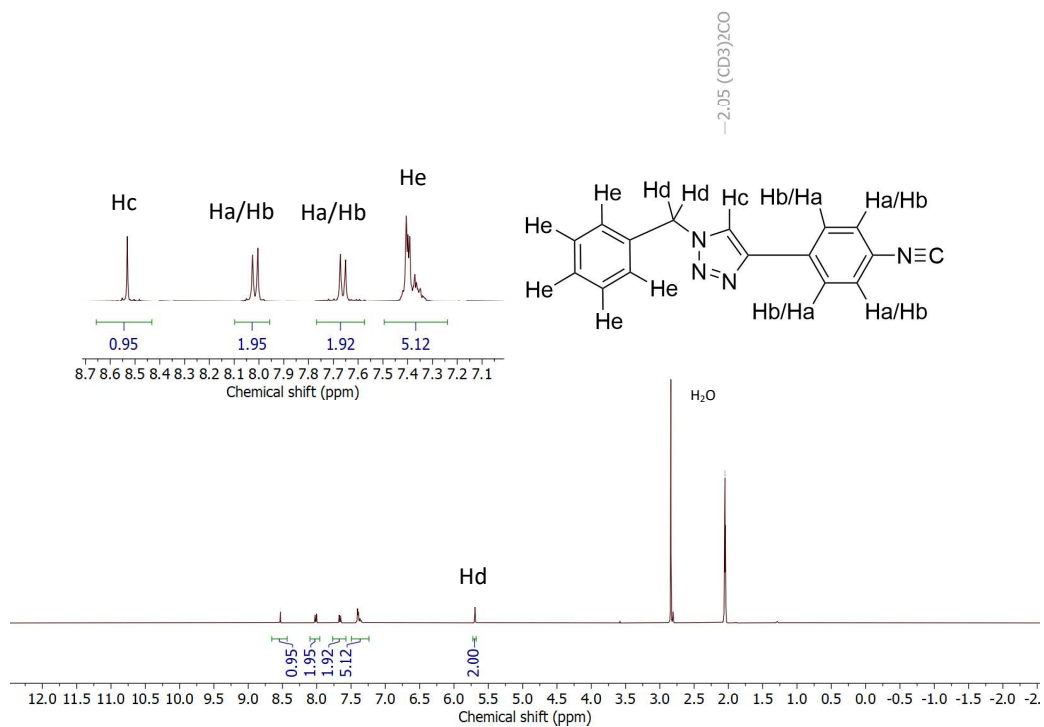
**Figure S9:**  $^{19}\text{F}$  NMR spectrum of  $[\text{Tc}(\text{CNPh}^{\text{pC}\equiv\text{CH}})_6][\text{PF}_6]$  (**[1]** $[\text{PF}_6]$ ) in  $\text{CD}_2\text{Cl}_2$ .



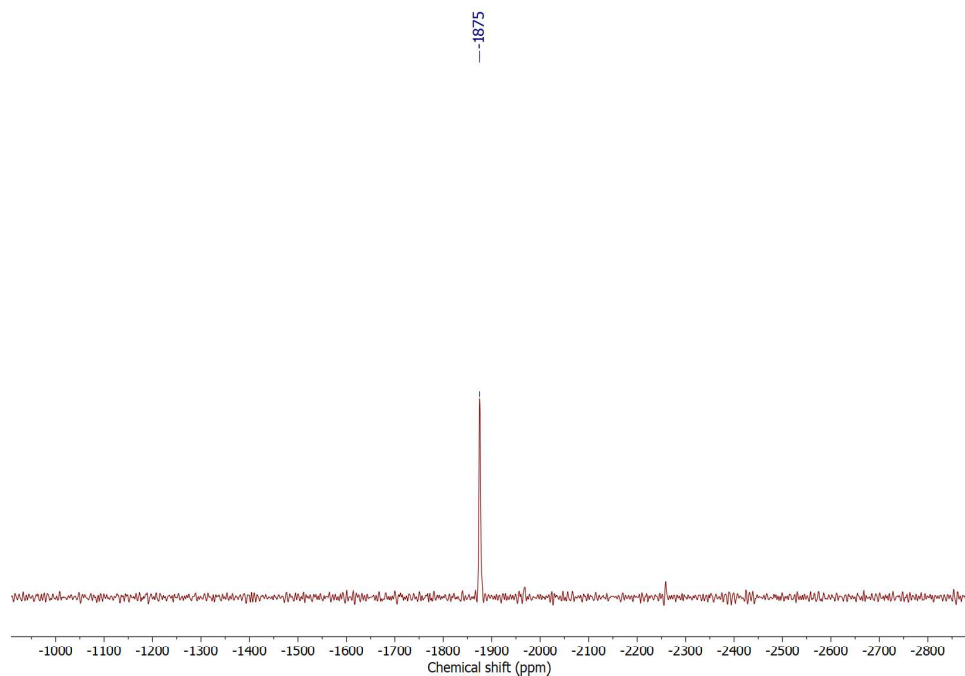
**Figure S10:**  $^{99}\text{Tc}$  NMR spectrum of  $[\text{Tc}(\text{CNPh}^{\text{pC}\equiv\text{CH}})_6][\text{PF}_6]$  (**[1]** $[\text{PF}_6]$ ) in  $\text{CD}_2\text{Cl}_2$ .



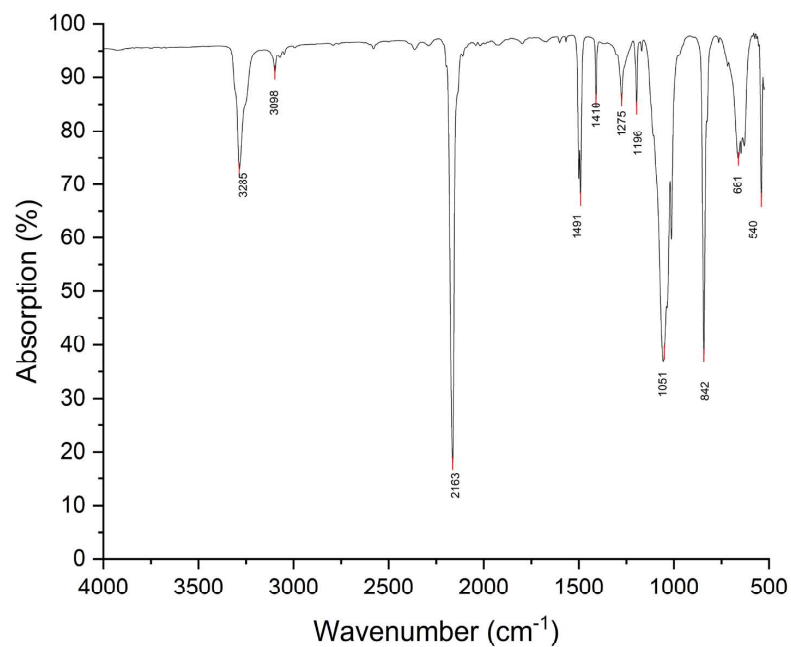
**Figure S11:** IR (KBr) spectrum of  $[\text{Tc}(\text{CNPh}^{\text{azole}})_6]\text{Cl}$  (**[2]** $\text{Cl}$ ).



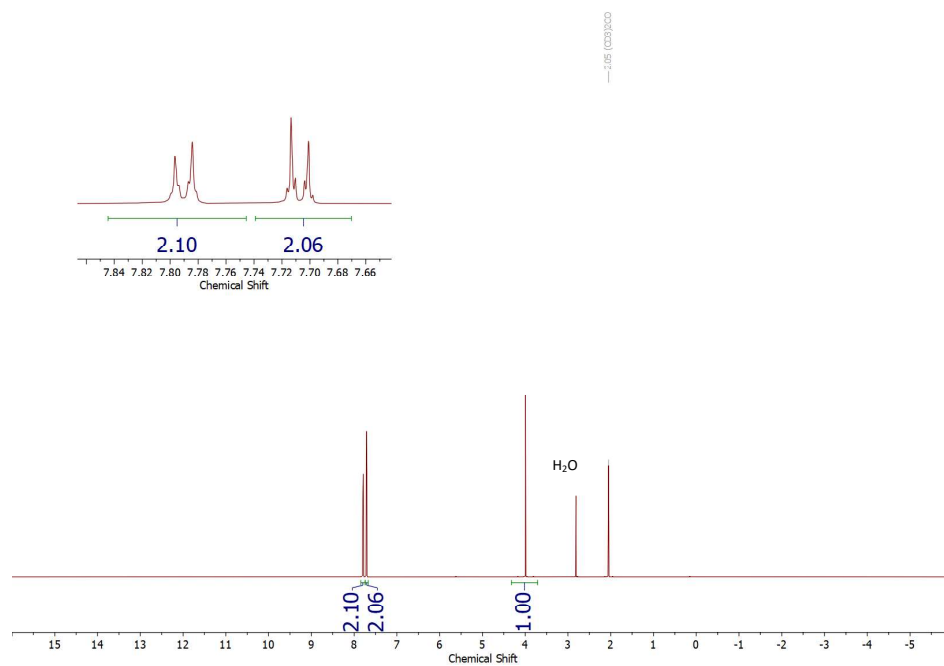
**Figure S12:**  $^1\text{H}$  NMR spectrum of  $[\text{Tc}(\text{CNPh}^{\text{azole}})_6]\text{Cl}$  ( $[2]\text{Cl}$ ) in acetone- $d_6$ .



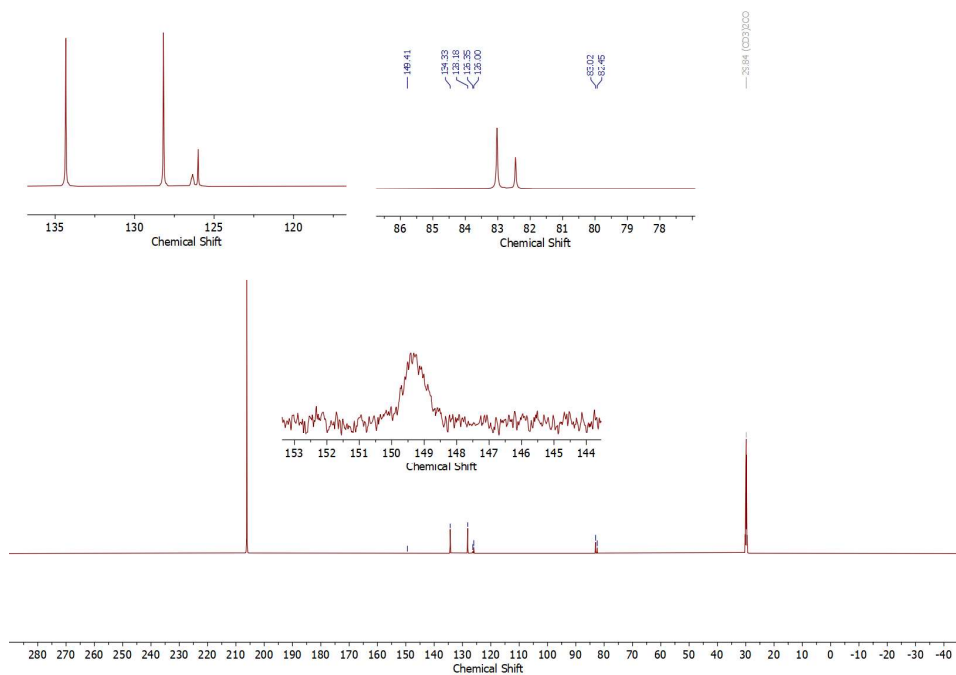
**Figure S13:**  $^{99}\text{Tc}$  NMR spectrum of  $[\text{Tc}(\text{CNPh}^{\text{azole}})_6]\text{Cl}$  ( $[2]\text{Cl}$ ) in acetone- $d_6$ .



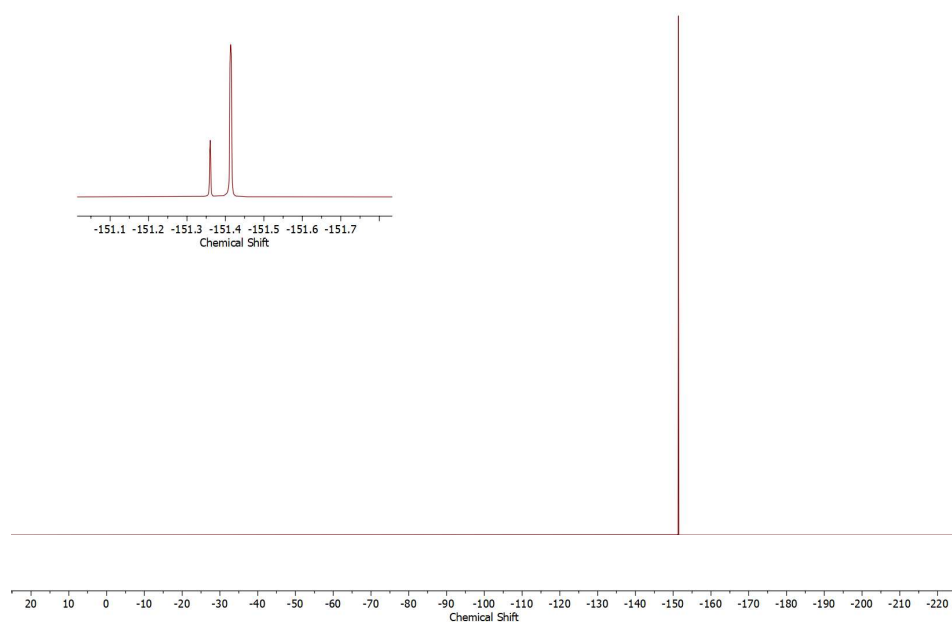
**Figure S14:** IR (ATR) spectrum of  $[\text{Cu}(\text{CNPh}^{\text{pC}\equiv\text{CH}})_4][\text{BF}_4]$  (**[3][BF<sub>4</sub>]**).



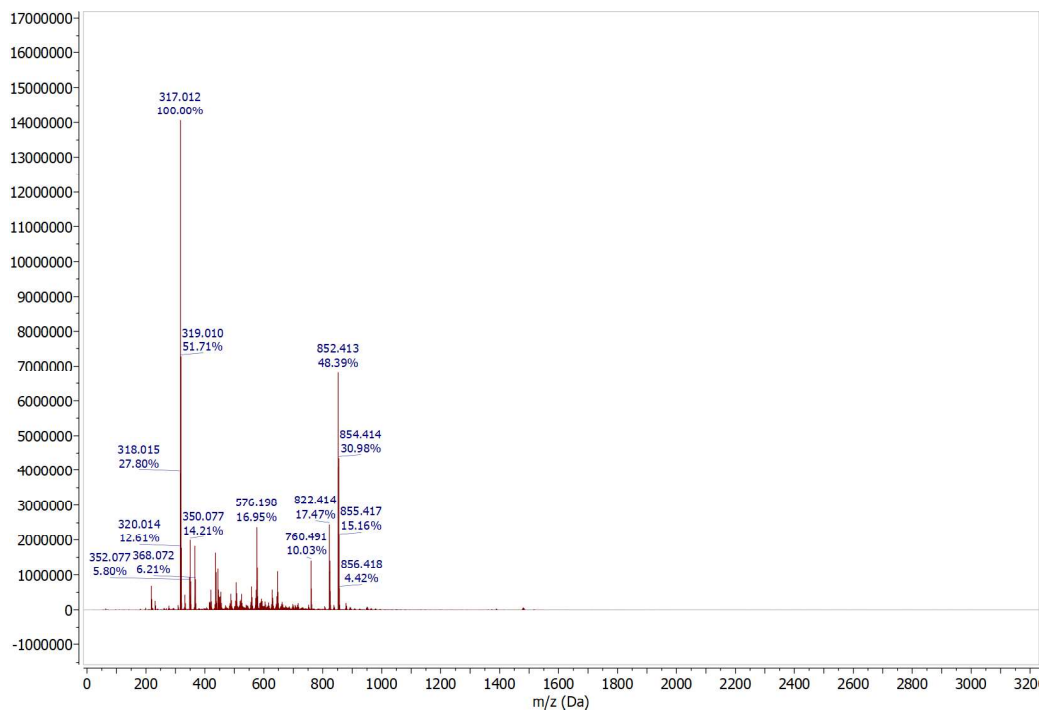
**Figure S15:**  $^1\text{H}$  NMR spectrum of  $[\text{Cu}(\text{CNPh}^{\text{pC}\equiv\text{CH}})_4][\text{BF}_4]$  (**[3][BF<sub>4</sub>]**) in acetone- $\text{d}_6$ .



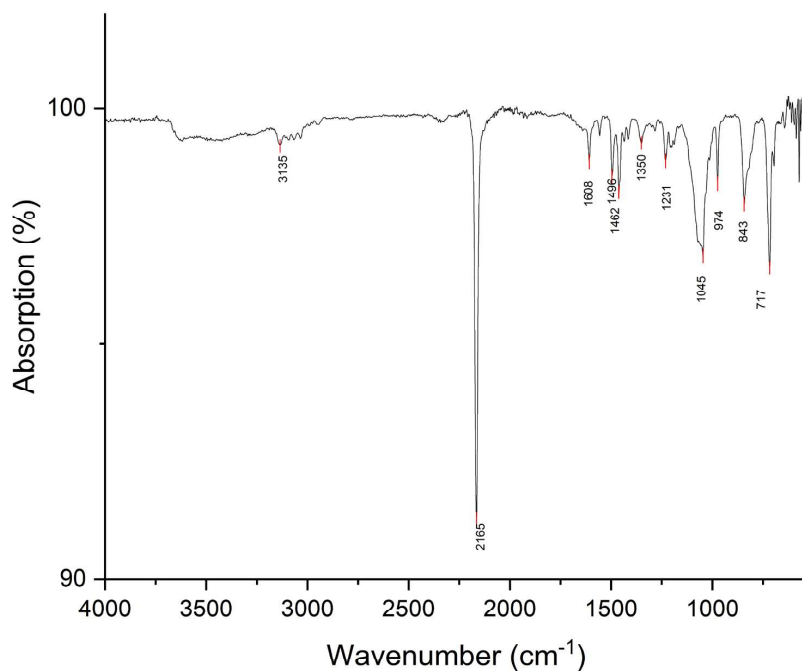
**Figure S16:**  $^{13}\text{C}\{^1\text{H}\}$  NMR spectrum of  $[\text{Cu}(\text{CNPh}^{\text{pC}\equiv\text{CH}})_4][\text{BF}_4]$  (**[3]** $[\text{BF}_4]$ ) in acetone- $\text{d}_6$ .



**Figure S17**  $^{19}\text{F}$  NMR spectrum of  $[\text{Cu}(\text{CNPh}^{\text{pC}\equiv\text{CH}})_4][\text{BF}_4]$  (**[3]** $[\text{BF}_4]$ ) in acetone- $\text{d}_6$ .

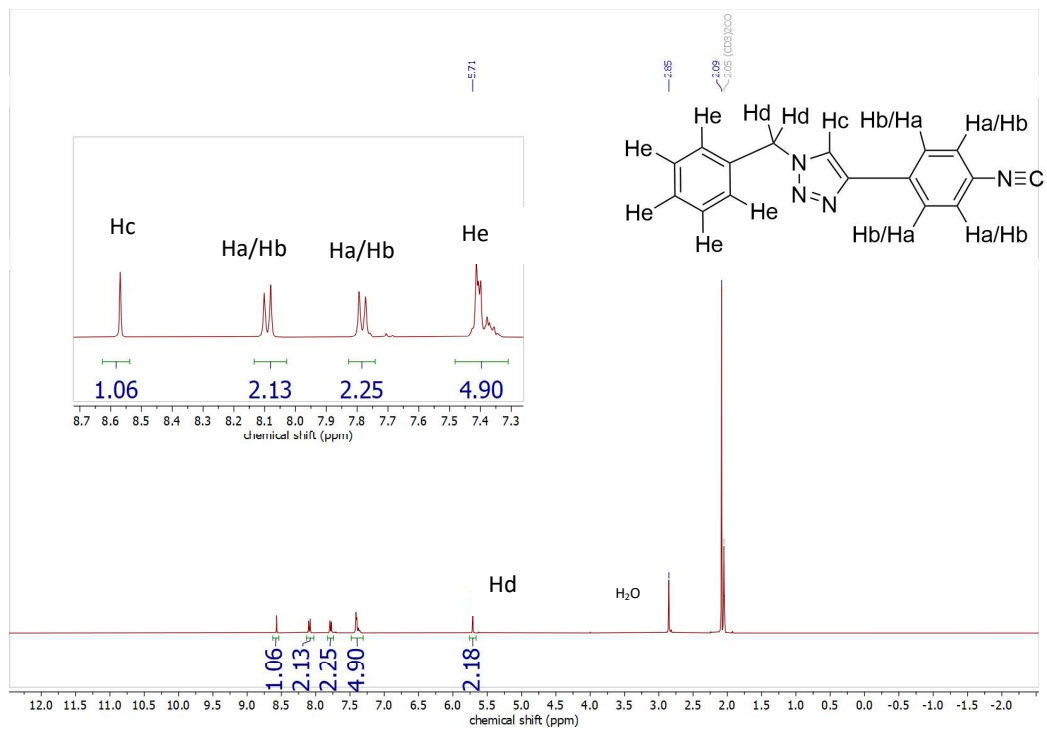


**Figure S18:** ESI+ mass spectrum of  $[\text{Cu}(\text{CNPh}^{\text{pC}\equiv\text{CH}})_4][\text{BF}_4]$  (**[3][BF<sub>4</sub>]**) in acetone-d<sub>6</sub>.

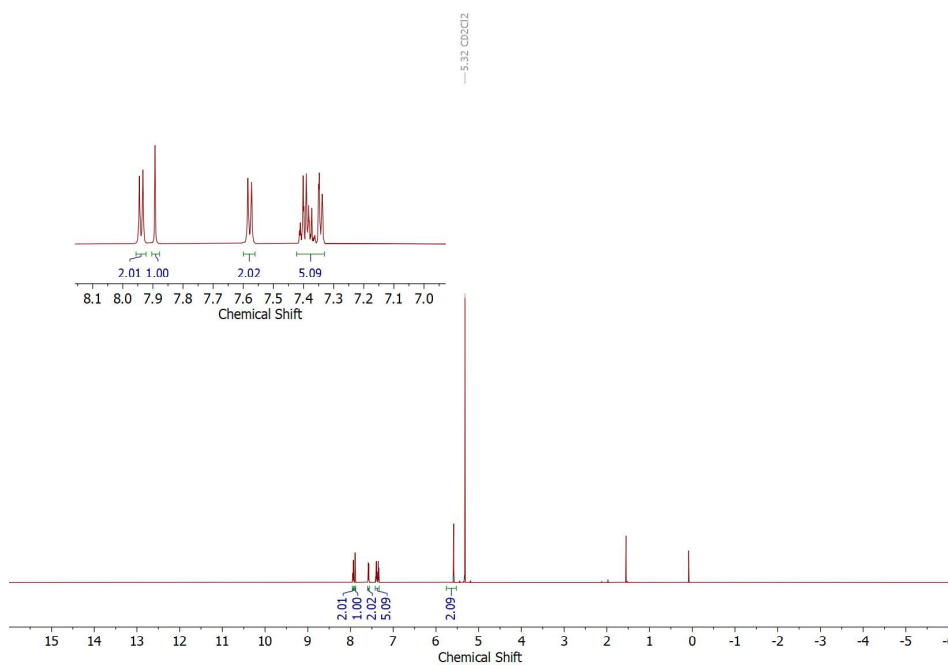


**Figure S19:** IR (ATR) spectrum of  $[\text{Cu}(\text{CNPh}^{\text{azole}})_4][\text{BF}_4]$  (**[4][BF<sub>4</sub>]**).

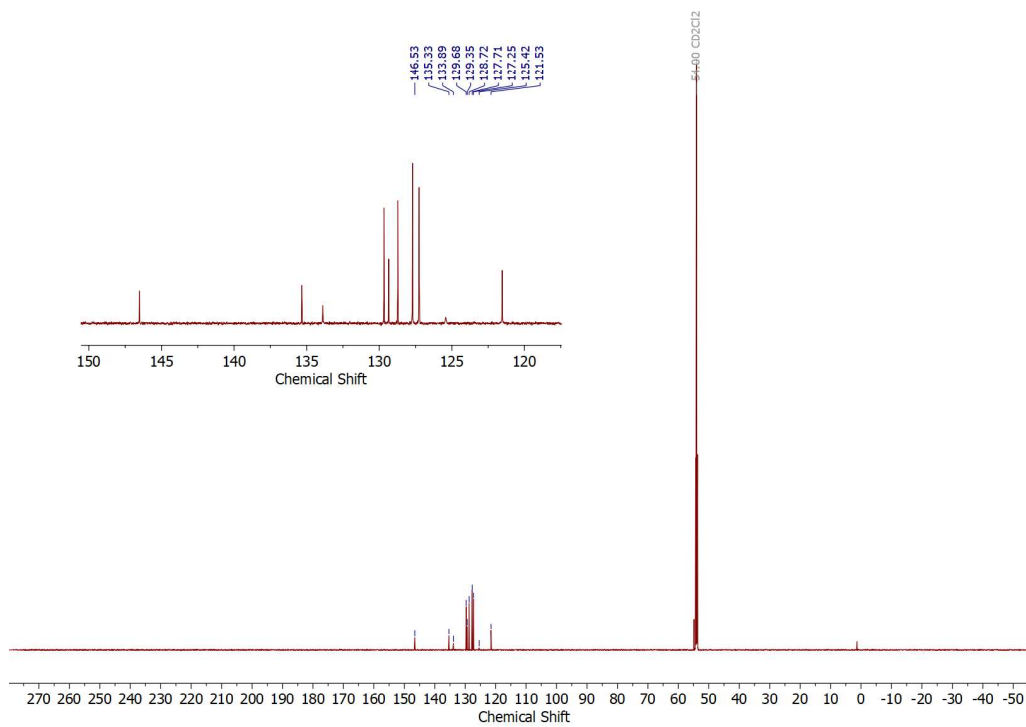




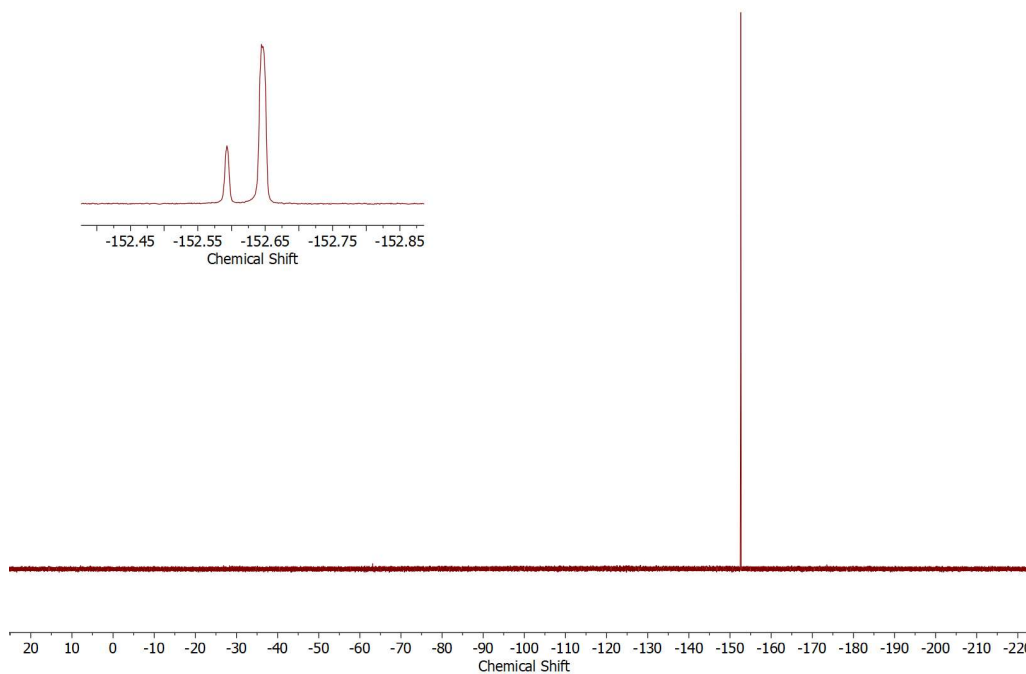
**Figure S20:**  $^1\text{H}$  NMR spectrum with assignment of  $[\text{Cu}(\text{CNPh}^{\text{azole}})_4][\text{BF}_4]$  ( $[\text{I}][\text{BF}_4]$ ) in  $\text{acetone-}d_6$ .



**Figure S21:**  $^1\text{H}$  NMR spectrum of  $[\text{Cu}(\text{CNPh}^{\text{azole}})_4][\text{BF}_4]$  ( $[\text{I}][\text{BF}_4]$ ) in  $\text{CD}_2\text{Cl}_2$ .



**Figure S22:**  $^{13}\text{C}\{^1\text{H}\}$  NMR spectrum of  $[\text{Cu}(\text{CNPh}^{\text{azole}})_4][\text{BF}_4]$  (**[4]** $[\text{BF}_4]$ ) in  $\text{CD}_2\text{Cl}_2$ .



**Figure S23:**  $^{19}\text{F}$  NMR spectrum of  $[\text{Cu}(\text{CNPh}^{\text{azole}})_4][\text{BF}_4]$  (**[4]** $[\text{BF}_4]$ ) in  $\text{CD}_2\text{Cl}_2$ .

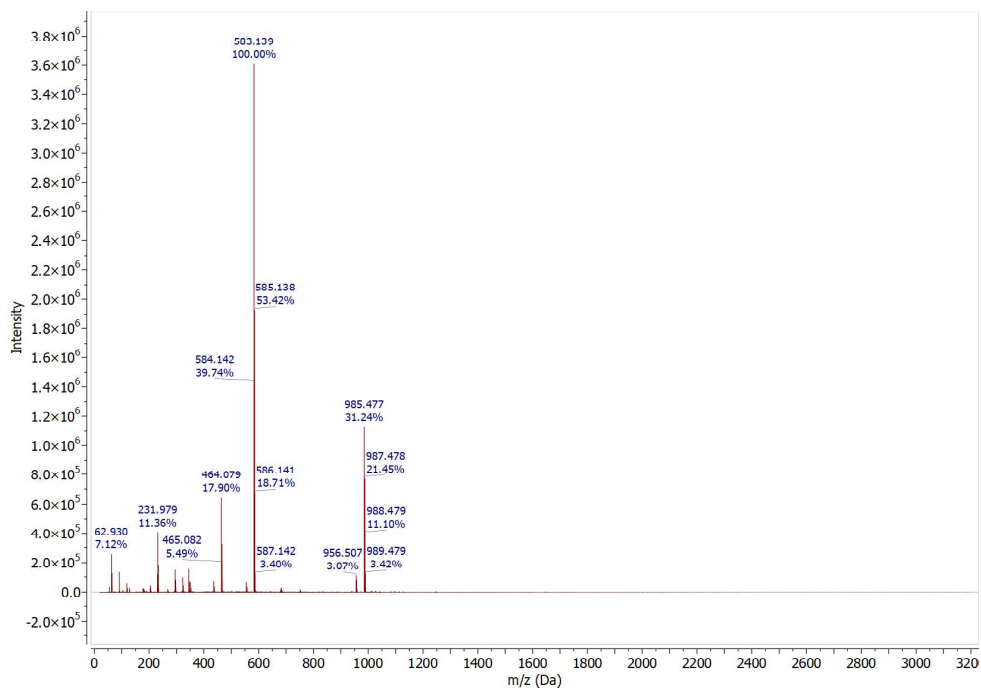


Figure S24: ES+ mass spectrum of  $[\text{Cu}(\text{CNPh}^{\text{azole}})_4][\text{BF}_4]$  ( $[4][\text{BF}_4]$ ) in MeCN.

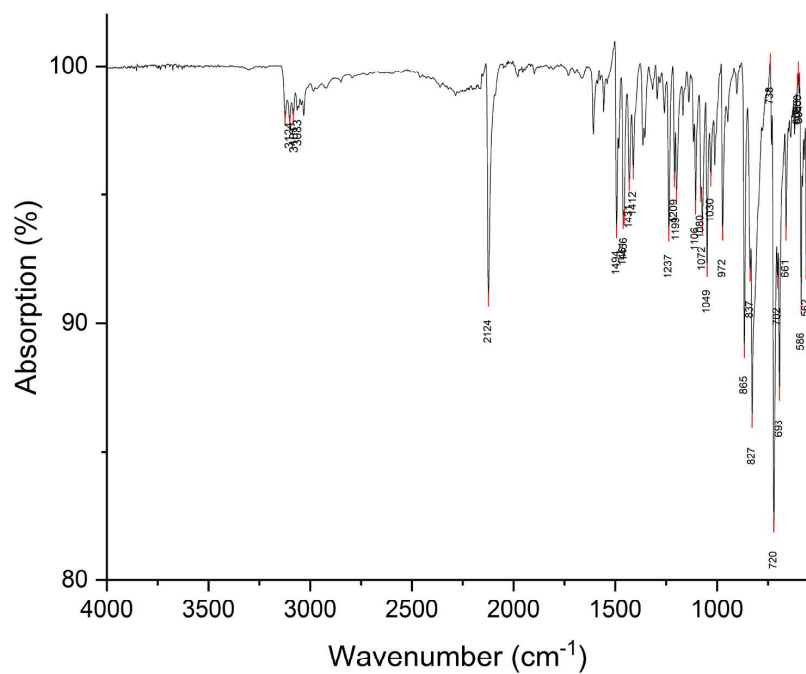
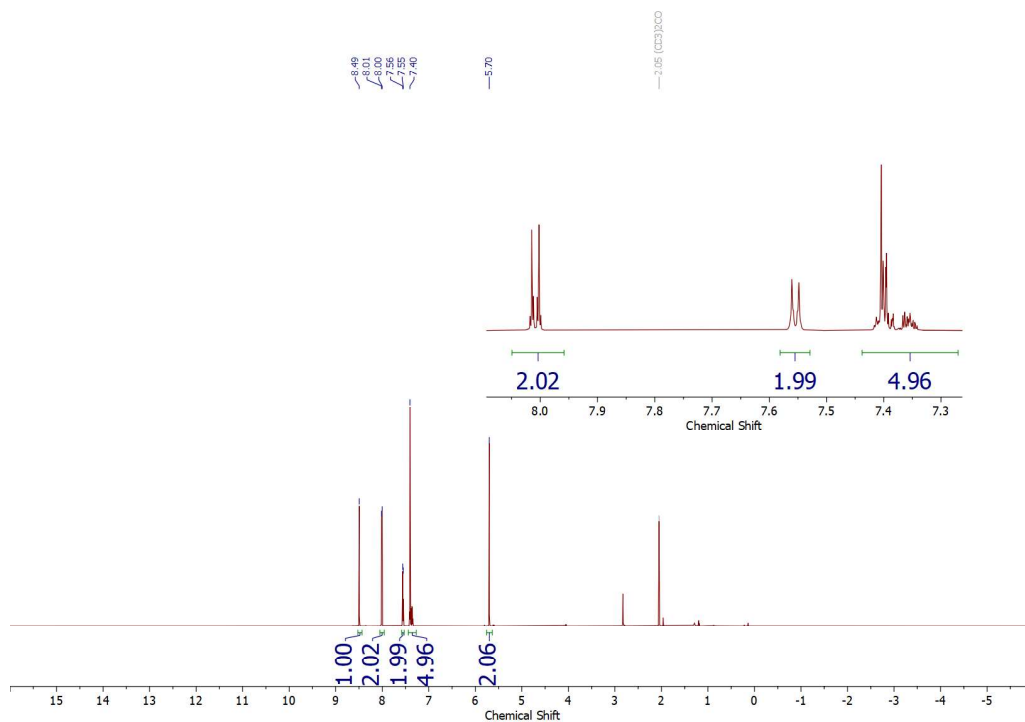
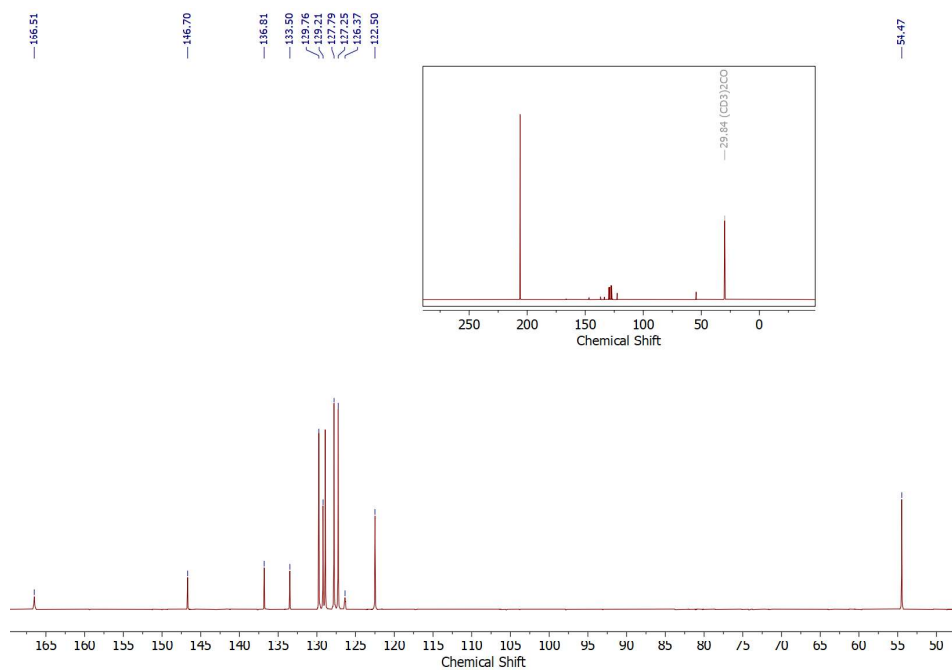


Figure S25: IR (ATR) spectrum of  $\text{CNPh}^{\text{azole}}$  (**5**).



**Figure S26:**  $^1\text{H}$  NMR spectrum of  $\text{CNPh}^{\text{azole}}$  (**5**) in acetone- $\text{d}_6$ .



**Figure S27:**  $^{13}\text{C}\{^1\text{H}\}$  NMR spectrum of  $\text{CNPh}^{\text{azole}}$  (**5**) in acetone- $\text{d}_6$ . The full spectrum with the solvent signals is depicted in the box.

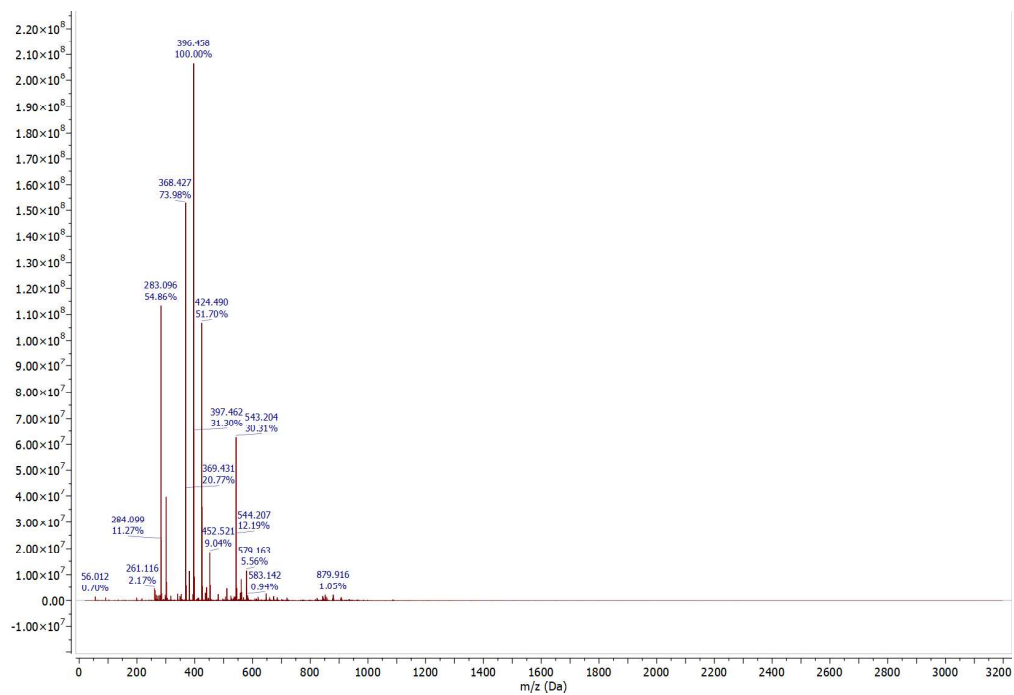


Figure S28: ESI+ mass spectrum of CNPhazole (5) in MeCN.

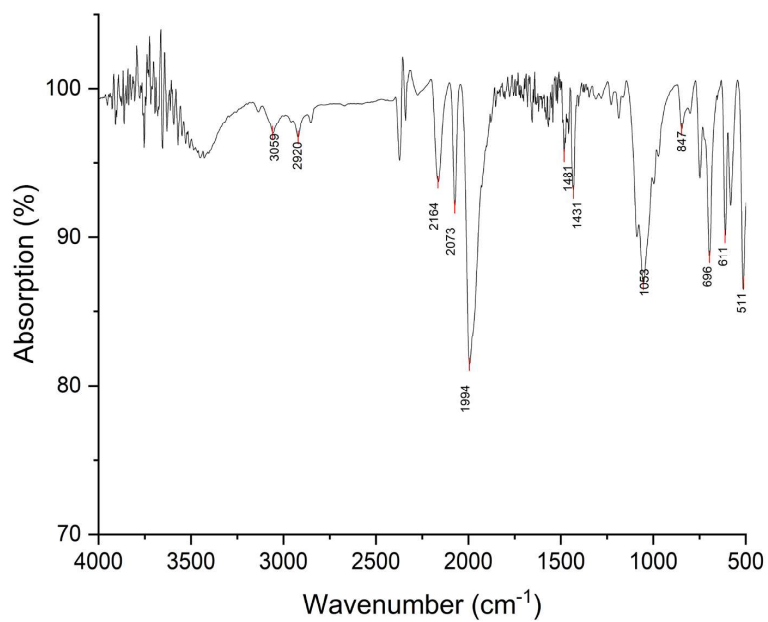
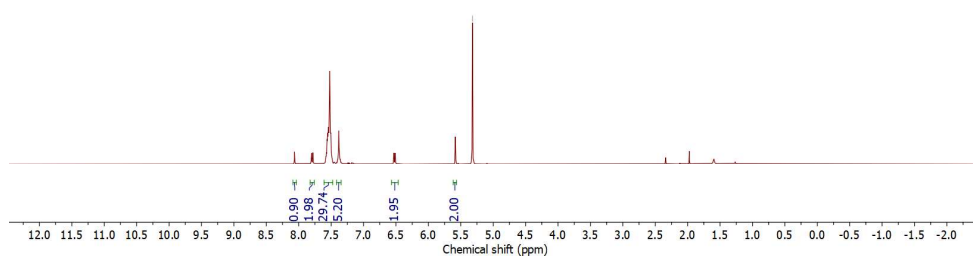
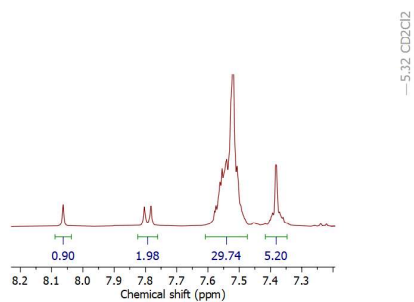
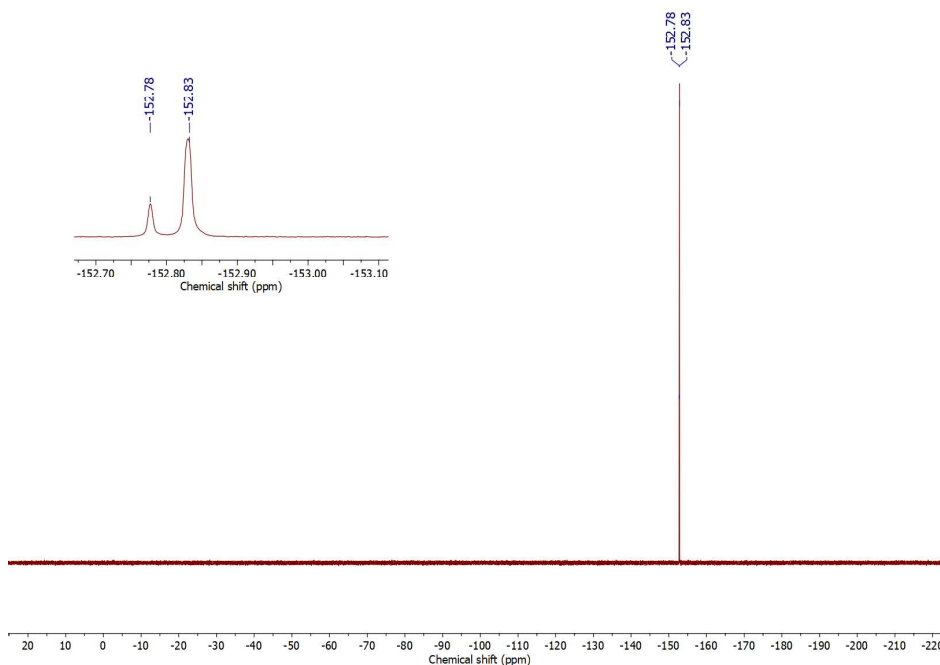


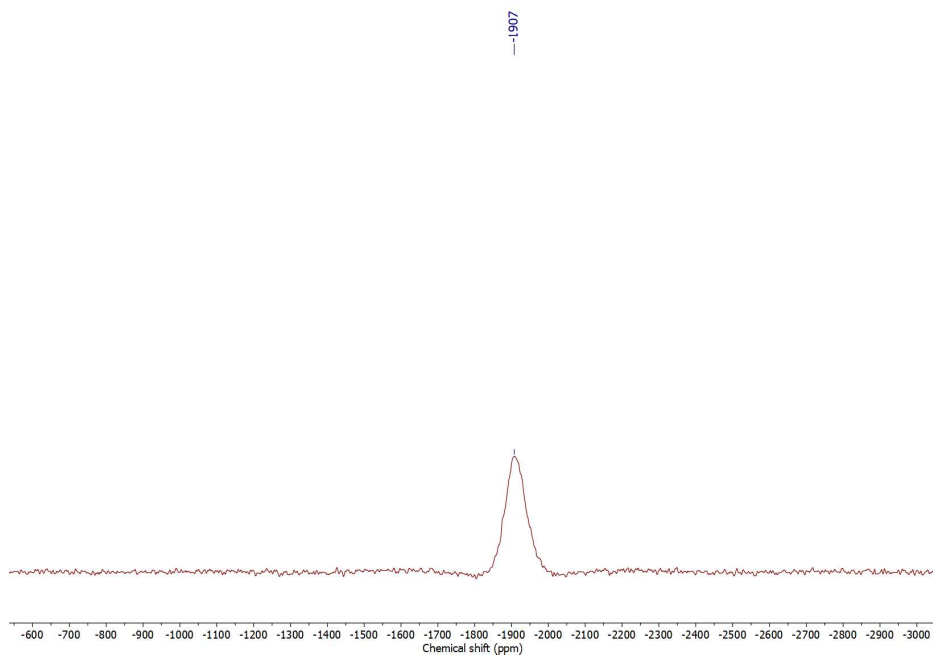
Figure S29: IR (KBr) spectrum of *mer,trans*-[Tc(CO)<sub>3</sub>(PPh<sub>3</sub>)<sub>2</sub>(CNPhazole)][BF<sub>4</sub>] ([6][BF<sub>4</sub>]).



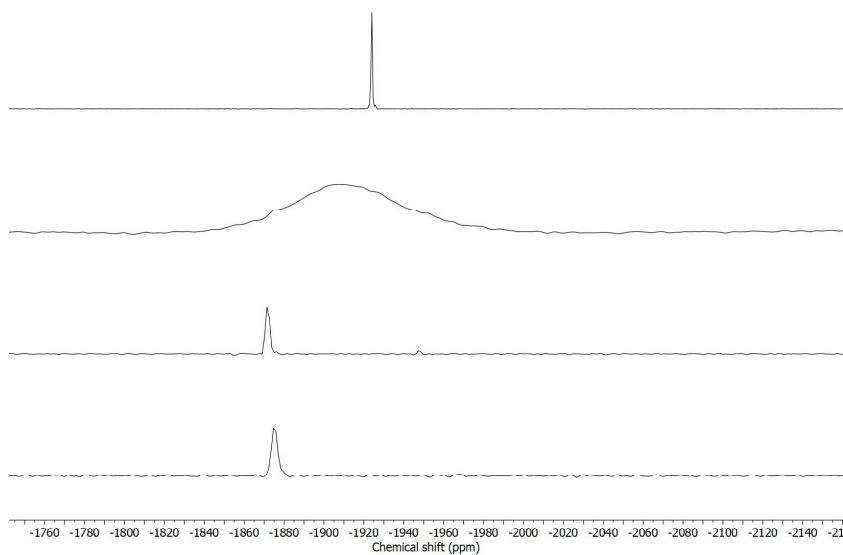
**Figure S30:** <sup>1</sup>H NMR spectrum of *mer,trans*-[Tc(CO)<sub>3</sub>(PPh<sub>3</sub>)<sub>2</sub>(CNPh<sup>azole</sup>)] [BF<sub>4</sub>] ([6] [BF<sub>4</sub>]) in CD<sub>2</sub>Cl<sub>2</sub>.



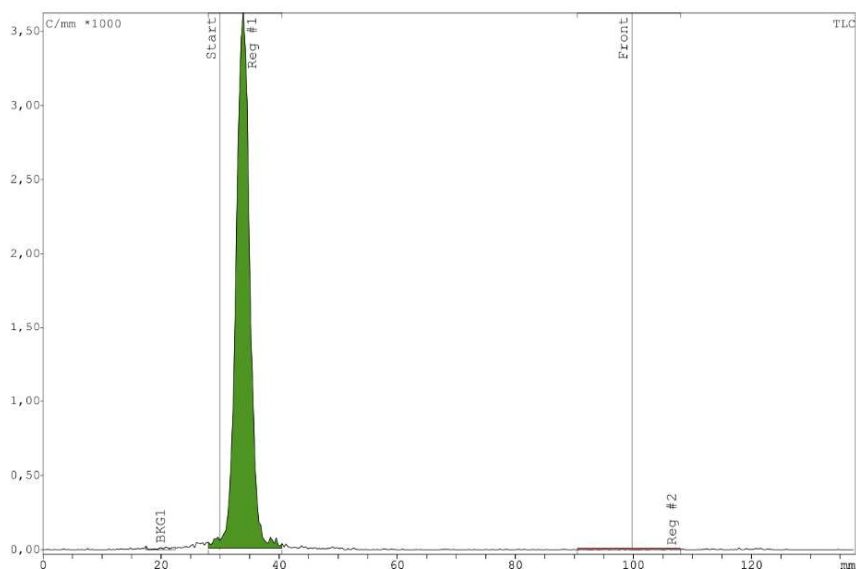
**Figure S31:** <sup>19</sup>F NMR spectrum of *mer,trans*-[Tc(CO)<sub>3</sub>(PPh<sub>3</sub>)<sub>2</sub>(CNPh<sup>azole</sup>)] [BF<sub>4</sub>] ([6] [BF<sub>4</sub>]) in acetone-d<sub>6</sub>.



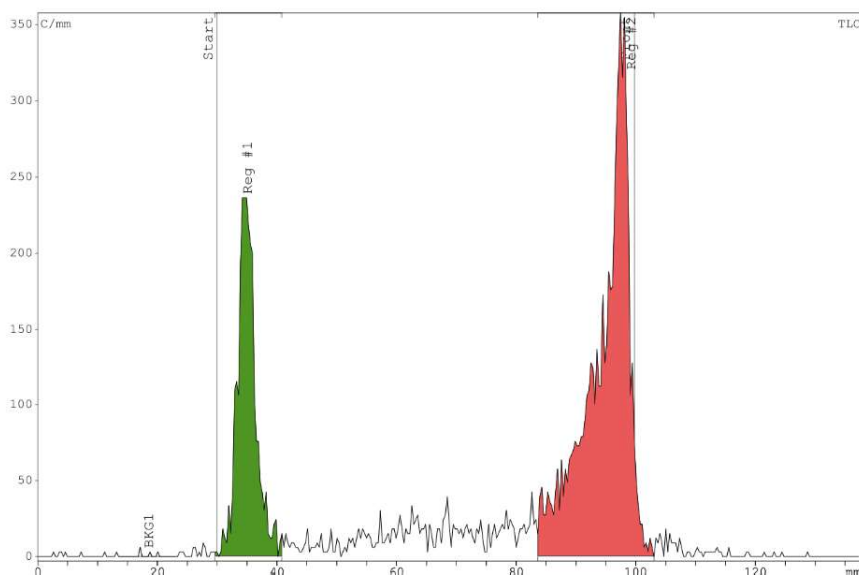
**Figure S32:**  $^{99}\text{Tc}$  NMR spectrum of *mer,trans*- $[\text{Tc}(\text{CO})_3(\text{PPh}_3)_2(\text{CNPh}^{\text{azole}})][\text{BF}_4]$  (**6**)[ $\text{BF}_4$ ] in  $\text{CD}_2\text{Cl}_2$ .



**Figure S33:**  $^{99}\text{Tc}$  NMR spectra of (from top to bottom)  $[\text{Tc}(\text{CN}^n\text{Bu})_6]$ , **6**, **2** and **1**.

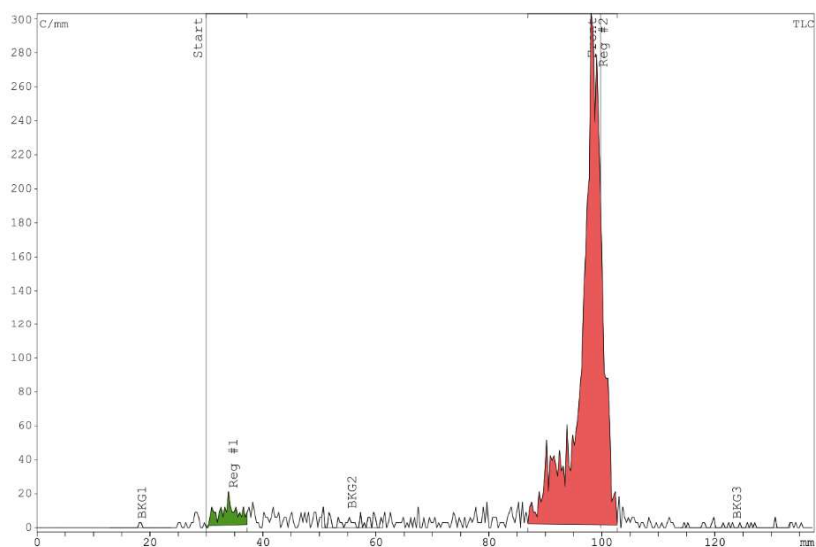


**Figure S34:** iTLC of  $^{99m}\text{Tc}$  reaction mixture of  $[\text{Cu}(\text{CNPh}^{\text{azole}})_4][\text{BF}_4]$  (**4** $[\text{BF}_4]$ ) and  $[\text{99mTcO}_4]^-$  (see experimental for exact conditions) with  $\text{H}_2\text{O}$  as a mobile phase. The green area corresponds to a lipophilic compound or  $\text{TcO}_2$ .  $[\text{99mTcO}_4]^-$  elutes with a  $R_f \approx 1,0$  under those conditions, thus the presence of unreacted  $[\text{99mTcO}_4]^-$  could be excluded.



**Figure S35:** iTLC of  $^{99m}\text{Tc}$  reaction mixture with  $[\text{Cu}(\text{CNPh}^{\text{azole}})_4][\text{BF}_4]$  (**4** $[\text{BF}_4]$ ) and  $[\text{99mTcO}_4]^-$  (see experimental for exact conditions) with methyl-ethylketone (MEK) as a mobile phase. Under those conditions both  $[\text{TcO}_4]^-$ , which is not present in this mixture (*vide supra*) elutes with a  $R_f \approx 1,0$ . Thus the area in red corresponds to a lipophilic specie which could be eluted with a  $R_f \approx 1,0$  using MEK. Colloidal technetium does not elute and thus the area in green can be attributed to it.





**Figure S36:** iTLC of  $^{99m}\text{Tc}$  reaction mixture with  $[\text{Cu}(\text{CNPh}^{\text{azole}})_4][\text{BF}_4]$  (**4** $[\text{BF}_4]$ ) and  $[\text{}^{99m}\text{TcO}_4]^-$  (see experimental for exact conditions) after purification on a C-18 cartridge, with methyl-ethylketone (MEK) as a mobile phase. Colloidal technetium could be removed almost quantitatively.

## References

- (1) Sheldrick, G. SADABS, SHELXS-2008, SHELXL-2014. University of Göttingen: Göttingen, Germany: 2014.
- (2) Coppens, P. The Evaluation of Absorption and Extinction in Single-Crystal Structure Analysis. Crystallographic Computing. Copenhagen, Muksgaard: 1979.
- (3) Sheldrick, G. M. A short history of SHELX. *Acta Crystallogr. Sect. A: Found. Crystallogr.* **2008**, *64* (1), 112-122.
- (4) Sheldrick, G. M. Crystal structure refinement with SHELXL. *Acta Crystallographica Section C: Structural Chemistry* **2015**, *71* (1), 3-8.
- (5) Dolomanov, O. V.; Bourhis, L. J.; Gildea, R. J.; Howard, J. A.; Puschmann, H. OLEX2: a complete structure solution, refinement and analysis program. *J. Appl. Crystallogr.* **2009**, *42* (2), 339-341.
- (6) *Diamond - Crystal and Molecular Structure Visualization*;  
<http://www.crystalimpact.com/diamond>.



## 6. List of all Publications

### 6.1. Full Papers and Communications

- (1) Claude, G.; Salsi, F.; Hagenbach, A.; Gembicky, M.; Neville, M.; Chan, C.; Figueroa, J. S.; Abram, U. Structural and Redox Variations in Technetium Complexes Supported by m-Terphenyl Isocyanides. *Organometallics* **2020**, *39*, 2287-2294.
- (2) Bhol, M.; Claude, G.; Jungfer, M. R.; Abram, U.; Sathiyendiran, M. Calix[4]arene-Analogous Technetium Supramolecules. *Inorg. Chem.* **2022**, *61*, 5173-5177.
- (3) Claude, G.; Genz, J.; Weh, D.; Roca Jungfer, M.; Hagenbach, A.; Gembicky, M.; Figueroa, J. S.; Abram, U. Mixed-Isocyanide Complexes of Technetium under Steric and Electronic Control. *Inorg. Chem.* **2022**, *61*, 16163-16176.
- (4) Claude, G.; Weh, D.; Hagenbach, A.; Figueroa, J. S.; Abram, U. Rhenium Complexes with p-Fluorophenylisocyanide. *Z. Anorg. Allg. Chem.* **2022**, *649*, e202200320.
- (5) Claude, G.; Zeh, L.; Roca Jungfer, M.; Hagenbach, A.; Figueroa, J. S.; Abram, U. The Chemistry of Phenylimidotechnetium(V) Complexes with Isocyanides: Steric and Electronic Factors. *Molecules* **2022**, *27*, 8546.
- (6) Claude, G.; Kultzki, E.; Hagenbach, A.; Roca Jungfer, M.; Figueroa, J. S.; Abram, U. Phenylimido Complexes of Rhenium: Fluorine Substituents Provide Protection, Reactivity and Solubility. *Dalton Trans.* **2023**, 4768-4778.
- (7) Claude, G.; Puccio, D.; Roca Jungfer, M.; Hagenbach, A.; Spreckelmeyer, S.; Abram, U. *Inorg. Chem.*, **2023**, submitted.

### 6.2. Contribution to Conferences

- (9) Poster at the Kongress der Deutschen Gesellschaft für Nuklearmedizin in Leipzig (27/04/2022 to 30/04/2022). Abstract published under : Claude, G.; Abram, U.; Brenner, W.; Spreckelmeyer, S. Modifizierbare Tc-Isonitril-Komplexe mit triazolgebundenen Biovektoren. *Nuklearmedizin-NuclearMedicine* **2022**, *61*, P9.
- (10) Oral presentation at the iSRS conference of the Society of Radiochemical Sciences in Nantes (29/05/2022 to 02/05/2022). Abstract published under : Claude, G.; Spreckelmeyer, S.; Brenner, W.; Abram, U. O-10 - Towards bifunctional technetium isonitrile complexes. *Nuclear Medicine and Biology* **2022**, *108-109*, S9-S10.

(11) Poster at the Terachem conference of the Society of Radiochemical Sciences (14/09/2022 bis 17/09/2022). Abstract published under : Claude, G.; Spreckelmeyer, S.; Abram, U.; Brenner, W.; Figueroa, J.; Jungfer, M. R. P-04 - Towards bifunctional and heteroleptic technetium isocyanide complexes. *Nuclear Medicine and Biology* **2022**, 114-115, S33-S34.